TITANIUM DIOXIDE NANOMATERIALS, SYNTHESIS, STABILITY AND MOBILITY IN NATURAL AND SYNTHETIC POROUS MEDIA

by

Ghulam Raza

A Thesis submitted to

The University of Birmingham

for the degree of

DOCTOR OF PHILOSOPHY

School of Geography, Earth and Environmental Sciences

The University of Birmingham

December 2016

Abstract

Titanium oxide (TiO_2) nanomaterials (NMs) improve potential value to commercial products like sun creams, cosmetics, paints, self-cleaning products, textiles, sports equipment etc. Research on the fabrication of NMs to develop or invent probable new methods and functionalities is an ongoing process. Stabilization of these NMs to retain their nanometric scale is a major issue: and to accomplish this goal, different surfactants and coating agents are used to modify NMs properties. Synthesis of highly ordered, stable, reproducible and cost effective TiO_2 NMs remains a challenge. A need of further research still exists in order to develop an in depth understanding of synthesis, aggregation kinetics and transport through porous media, and to determine the ultimate fate and interactions of these NMs with environmental constituents after their release in the natural ecosystem.

This research work was typically divided into three phases; synthesis, stabilization and transport. Synthesis was accomplished with sol-gel, hydrothermal and a mix of both methods. The effects of pH, precursors, temperature and different alcohol concentrations were studied in detail. Stability was achieved after extensive research on different surfactants including polyethylene glycol (PEG), Polyvinylpyrrolidone (PVP), Sodium citrate, Sodium Dodecyl Sulfate (SDS), Suwannee River fulvic acid (SRFA). Aggregation kinetics of stabilized NMs was evaluated in detail in the presence of mono and divalent electrolytes ($NaNO_3$, NaCl, CaN_2O_6, $CaCl_2$). Two different types of morphologies of TiO_2 NMs were used during these studies i.e. round anatase NPs and rutile ellipsoids. The stabilized NMs were checked for their mobility through different natural and synthetic porous media (sandstone and glass bead columns) in the third and final phase of this research work.

Different forms of Titanium dioxide nanomaterials including nano-powders and stabilized suspensions were synthesized. The effect of pH, precursors, temperature and zeta potential on nanoparticles nucleation, agglomeration, shape, size, and phase transformation was investigated. Initially the variation of pH from 1 to 11 was systematically studied at different temperatures (25-700^{o}C). The morphological differences as a function of pH were studied in detail. A temperature of 400^{o}C was considered best for crystalline growth while a pH value of 4 gave round and well dispersed TiO_2 with a shape factor of >0.9. From the data generated it is obvious that with an increase in pH there is a decrease in agglomeration and increase in dispersion and vice versa. Stable titania suspensions were fabricated by controlling the synthesis solution chemistry. Titanium trichloride and tetrachloride were used to fabricate NPs at room or near room temperature. Different alcohols and alcohol water ratios helped to control the NPs morphology at room or very low temperatures. $TiCl_4$ was evaluated as the best precursor in controlling shape and size in low temperature synthesis processes. Various shapes of TiO_2 including spherical NPs with shape factor of 0.9 or more, nanocubes, nanorods and ellipsoids were synthesised with different alcohols and water mixture ratios.

In the next phase a couple of synthesized NPs were checked for their stability with 5 different surfactants; PEG, PVP, SDS, SRFA and sodium citrate. The stability of anatase spherical attenuated as sodium citrate, SRFA, PVP, PEG and SDS while this attenuation was SRFA, sodium citrate, PEG, SDS and PVP for rutile ellipsoids. SRFA and sodium citrate at 0.3% weight concentration proved to be the best stabilising agents without any change in the hydrodynamic diameter over a period of 2 weeks. These two types of NPs stabilized with two different types of surfactants i.e. SRFA and sodium citrate were further used for aggregation kinetics and transport studies through natural and artificial porous media. The aggregation kinetic studies showed that rutile ellipsoids behaved well against different mono and divalent

cations. The critical coagulation concentrations (CCC's) observed for sodium citrate stabilized NMs were significantly higher than SRFA stabilized NMs, showing that sodium citrate is a better stabilizing agent than SRFA. TEM analysis of aggregated samples in slow and fast regime of aggregation showed different morphologies of aggregates which were analysed with fractal dimension analysis. Most of the aggregating salts gave a fractal dimension of more than 1.5 which means presence of consolidated aggregates after addition of different salts.

In the last phase the stabilized NMs with SRFA and sodium citrate were studied for porous media column transport by using glass bead as an artificial and sandstone as more complex natural environmental media. The transport of the rutile ellipsoids is greater than spherical anatase. Bare anatase NPs gave no breakthrough and the NPs clogged both the sandstone and glass bead columns; while bare rutile ellipsoids gave nearly 100% breakthrough curves. In most of the cases for glass beads the C'/C_o values remained above 80% and after retention NPs release gave more than 80% of retained NPs. Only 40% or less NPs were released from sandstone columns and rest of injected NPs were retained within the columns. For both sandstone and glass bead media SRFA proved a better flushing agent than sodium citrate. Stabilized anatase showed no difference in mobility as compared to stabilized rutile but bare rutile NPs behaved entirely different from bare anatase. Bare anatase showed difficulty in movement through both sandstone and glass bead media. Both stabilizers i.e. have different effects on mobility of nanomaterials as SRFA gave steric while sodium citrate gave electrostatic stabilization. Tailing was seen in all runs and it is more physical in glass bead followed by sandstone columns while a little tailing is seen in fluorescein. This tailing behaviour shows probably a non-equilibrium attachment process which suggests that colloid filtration theory (CFT) not likely to be correct. The total release in case of glass bead columns was nearly 100% which was much greater than the total release from sandstone columns. Only

40% or less NPs were released from sandstone columns and rest of injected NPs were retained within the columns. From overall experimental results it is concluded that glass bead columns are analogous to sandstone columns, in style, though not in degree. So it is encouraging for laboratory experimentation. More release of NPs with SRFA flush is also important as it reflects the ultimate fate and behaviour of TiO_2 NPs in natural environment which is rich in humic substances.

I DEDICATE THIS STUDY TO MY SON, MUHAMMAD HASSAN RAZA AND MY DAUGHTER, PAKIZA RAZA

Acknowledgements

I would like to take this opportunity to acknowledge the people who have been tremendously helpful, patient and kind during this exciting journey of my second PhD.

To my advisors, Professor Jamie Lead and Eva Valsami Jones, I would like to express my sincerest thanks for their unwavering support: this thesis would simply not have been possible without their assistance.

A special thank you is due to my co-supervisors, Professor John Tellam and Dr Mohammed Baalousha, for their guidance and technical support during my laboratory work and the writing up of this dissertation.

Thank you to my colleagues, Dr. Yusuf Nur, Dr. Mila Tejamaya, Indrani Mahapatra, Inder Kaur, Dr. Auwal Farouk Abdussalam and Isaac Aidoo for their help, moral support, and above all, friendship.

To Hasan Shikoh, I extend my most sincere gratitude for being there for me when I needed it most: his kind words and constructive criticism will forever be appreciated.

I am grateful to the National Environmental Research Council (NERC), United Kingdom and Natural History Museum (NHM) London, for funding my PhD research project.

I would like to thank my extended family, especially my parents, for continuously reminding me that the journey towards my PhD was indeed worth it. I pray for their good health and long

life because the foundations of my achievements to date are a direct result of their ardent prayers and guidance.

Finally, I would like to thank my beloved wife, Sobia Raza, my son, Muhammad Hassan Raza, and daughter, Pakiza Raza, for their unconditional love and support. I could not possibly have reached this landmark without their continuous patience and encouragement throughout my research. On occasions, when I felt it was too difficult to continue, it was only their love and the sparkle in their eyes which helped me carry on with renewed zest to achieve this success.

Table of Contents

List of abbreviations

A	Anatase
AAS	Atomic absorption spectrometer
AES	Auger electron spectroscopy
AFM	Atomic force microscopy
AgNPs	Silver nanoparticles
BET	Brunauer-Emmett-Teller
BPA	Bisphenol A
BSA	Bovine Serum Albumin
BTCs	Breakthrough curves
CCC	Critical coagulation concentration
CFT	Colloid Filtration Theory
CNTs	Carbon Nanotubes
CTAB	Cetyltrimethyl Ammonium Bromide
DDA	Dodecylamine
DI	Deionized water
DLS	Dynamic light scattering
DLVO	Derjaguin–Landau–Verwey–Overbeek
DNA	Deoxyribonucleic Acid
DOC	Dissolved organic carbon
DRS	Diffused reflectance spectroscopy
EBE	Electron-beam evaporation

EDTA	Eethylenediammine tetra-acetate
EDX	Energy dispersive X-ray
FBS	Fetal bovine serum
FE-SEM	Field emission-scanning electron microscopy
FFF	Field flow fractionation
FTIR	Fourier Transform Infrared
GB	Glass bead column
GIXRD	Glancing incidence x-ray diffraction
H	Horizontal
HR-TEM	High Resolution Transmission Electron Microscopy
ICP_MS	Inductively coupled plasma mass spectrometery
ICP_OES	Inductively coupled plasma optical emission spectrometer
IHSS	International Humic Substances Society
MB	Methylene blue
MBSL	Multibubble sonoluminescence
MWCNT	Multi-Walled Carbon Nanotubes
NMs	Nanomaterials
NNI	National Nanotechnology Initiative
NOM	Natural organic matter
NPs	Nanoparticles
OCDD	Octachlorodibenzo-*p*-dioxin
PCS	Photon Correlation Spectroscopy
PD	Photodeposition

PEG	Polyethylene glycol
PEO	Poly-ethylene oxide
pH_{pzc}	pH point of zero charge
ppb	Parts per billion
ppm	Parts per million
ppt	Parts per trillion
PVA	Poly-vinyl alcohol
PVP	Polyvinylpyrrolidone
PZC	Point of zero charge
QELS	Quasi-Elastic Light Scattering
R	Rutile
RF	Radio frequency
SCR	Soft chemical reduction
SDS	Sodium dodecyl sulfate
SEM	Scanning Electron Microscopy
SGD	Sol-gel dip-coating
SRFA	Suwannee River Fulvic Acid
SRHA	Suwannee River Humic Acid
SS-EFM	Single Surface Electroosmotic Flow Mapping
Sst	Sandstone column
TBT	Tetrabutyl titanate
TCE	Trichloroethylene
TEM	Transmission Electron Microscopy

TGA	Thermogravimetric analysis
TS	Titanyl sulphate
TTIP	Titanium tetra isopropoxide
UV	Ultra violet
V	Vertical
VDWL	van der Waals London forces
XPS	X-ray photoelectron spectroscopy
XRD	X-Ray Diffraction
Z_{AVG}	Hydrodynamic Diameter

List of Figures

List of tables

Chapter 1

INTRODUCTION

1.1 Justification

TiO_2 NMs add potential value to products such as sun creams, cosmetics, paints, self-cleaning, textiles, sports equipment, solar cells, water splitting, and waste water treatment (Gottschalk et al., 2009). Since TiO_2 particle size plays an important role in different applications. Research on the fabrication of NMs with different methods, in order to improve the understanding of synthesis processes and their probable new functionalities or properties, has been conducted by many scientists. Stabilization of NMs is another issue: to accomplish the stability of NPs, different surfactants and coating agents were applied to modify their properties. However, fabrication of highly ordered, reproducible and cost effective TiO_2 NMs remains a challenge. Further research investigation is needed in order to develop an in-depth understanding of aggregation kinetics and transport through porous media, and to determine the ultimate fortune and interactions of these NMs with environmental constituents after their release in natural ecosystem.

1.2 Research Background

The NMs are defined as “a natural, incidental or manufactured material containing particles, in an unbound state or as an aggregate or as an agglomerate and where, for 50 % or more of the particles in the number size distribution, one or more external dimensions is in the size range 1 nm-100 nm” (EU, 2011). Whereas the application nanotechnology is the synthesis and handling of very small particles with nanometric dimensions which are smaller than 100 nm when at least 50 % of the particles possess these properties. As defined by the National

Nanotechnology Initiative: “Nanotechnology is science, engineering, and technology conducted at the nanoscale, which is about 1 to 100 nanometers”(NNI, 2013).

There are two main approaches of NMs synthesis as these can be synthesized from bottom up with building the groups of atoms and molecules or by top-down process by breaking big macroscopic materials to small nanometric level (Aitken et al., 2004). Being a multidisciplinary science, nanotechnology involves disciplines like physics, materials science, biology, chemistry, environmental science and engineering, electronics etc. all together. To understand nanometric length scale, a comparison of different sizes scale is presented in Figure 1.0.1 (Li and Elimelech, 2006).

Figure 1.0.1 shows that the thickness of human hair is approximately 80,000 to 100,000 nm, DNA 2.5 nm and gold item is one-third part of single nanometer, while the thickness of a sheet of paper is 100,000 nm.

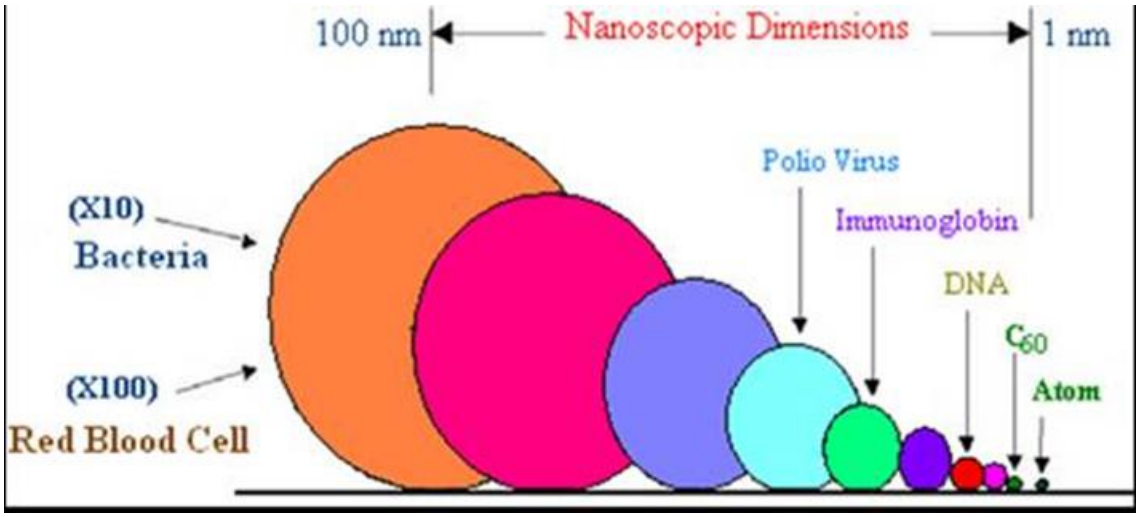

Figure 1.0.1: Nanoscopic dimensions a comparison with bacteria, viruses, DNA and molecules; picture idea from (Tufenkji and Elimelech, 2004)

Currently nanotechnology has been presenting exciting solutions to overwhelm the needs of energy, electronic, medical and the environmental sectors. As compared to bulk materials, nanomaterials have many properties which make them unique entity. These properties include;

small comparative size, high chemical reactivity, larger surface area and surface to volume ratio etc. Such properties make the nanomaterials highly effective as compared to bulk material in terms of catalysis, drug delivery and surface reactivity (Buzea et al., 2007a). Moreover, such materials are less brittle than bulk materials because of their high surface tension and local electromagnetic properties (Lue, 2007). Because of all the unique properties of NM, there is a need to understand the synthesis behaviour to engineer NMs morphology. For certain applications, a control in nanoparticles size and shape is a prerequisite.

Nanostructured TiO_2 has been extensively studied for its different uses (Zhang et al., 1998, Wang et al., 2000, Liu et al., 2011a) like pigments, exploiting its brilliant whiteness and color-occluding properties in paints, coffee whitener, toothpaste, sun screens, cosmetics etc. Unusual properties of titanium dioxide arise because of quantum confinement, residual oxygen specie (ROS) and larger surface area.

It is size and shape properties which effect the overall behaviour of titania materials otherwise bulk TiO_2 is being extensively used and investigated for different photocatalytic properties since 1970s (Verwey, 1947, Franchi and O'Melia, 2003). Extensive laboratory and commercial use of TiO_2 was started with a discovery of photocatalytic splitting of water with use of TiO_2 electrodes (Fujishima, 1972). Nanocrystalline TiO_2 is an important material in all disciplines of science including material engineering and biomaterials (Ranade et al., 2002).

As titania morphology is important to enhance its properties, a controlled nanocrystalline titanium dioxide synthesis is important. There is a strong need to understand the synthesis methodologies where we can synthesize engineered NM's with ease and with a set recipe. Keeping in view the knowledge gap after reviewing the background of research conducted on TiO_2, following three type of areas are selected for further investigation.

1.2.1 Synthesis of TiO_2

In depth knowledge of individual particles and their interaction with other constituents of the system is prerequisite to understand the physico-chemical characteristics of materials. Desired material should have controlled properties with all aspects of size, shape, phase and population control. TiO_2 powder in bulk is synthesized by two processes: sulfate process or chloride process. Sulfate process where TiO_2 powder is synthesized in the presence of H_2SO_4 to hydrolyse ilmenite at 95°C followed by calcination above 800°C and pulverization. $TiCl_4$ is a by-product of chloride process when HCl reacts with natural rutile ore with HCl gas at very high temperatures. The produced $TiCl_4$ reacts with highly reactive oxygen gas at 1000°C to produce highly pure rutile structures. The properties for this TiO_2 powder are very limited as this process does not guarantee the control over particle size, shape or distribution (Matijevic, 1985, Masala and Seshadri, 2004, Akhtar et al., 1994, Akhtar et al., 1992, Levchenko et al., 2006).

Sol-gel and hydrothermal processes were used to synthesize the TiO_2 NPs. In sol-gel process as name implies, a sol is derived from the hydrolysis of alkoxide precursor, is used to produce a gel after hydrolytic polycondensation. Precursors involved in fabrication of metal oxide nanoparticles are called metal alkoxides and metal chlorides. Low processing temperatures, relatively low cost and ease of handling of certain alkoxides allow a good control over shape and size (Brinker, 1990). Sol-gel synthesized fine spherical particles of less than 1μm proved to be heavily hydrated and not in contact with each other (Hu et al., 2003). Yang and co-workers observed that strong agglomeration deteriorated the properties of sol-gel synthesized powder (Yang et al., 2005, Yang et al., 2001).

The nucleation of titania nanocrystals is dependent on pH value and sintering temperature as claimed by Hu et al. (2003). They revealed that pH was the main reason of

agglomeration and hence decrease of specific surface area. Synthesis pH also affects the size, anatase-rutile transformation and amount of brookite phases. Sugimoto and Zhou (2002) studied that the gel-sol pH alterations can give even sized anatase TiO_2 particles and it depends on adsorption and desorption of H^+ ions.

Burnside's group (Burnside et al., 1998) studied the temperature dependent crystallite size, shape and self-assembly of TiO_2. The crystals in the colloidal suspension were allowed to grow in an autoclave at temperatures ranging from 190-270ºC. The growth of the crystallites under hydrothermal conditions is a result of Ostwald Ripening (Burnside et al., 1998).

1.2.2 Colloidal Stability of Nanoparticles

Different synthesis processes may give aggregate structures of NMs. Sometimes due to the strong bonding forces between primary particles make unbreakable sinters along with the action of temperature. But while weak physical forces like van der Waals forces give rise to agglomerates, which can be separated by sample preparation methods (Grass et al., 2006, Mandzy et al., 2005, Teleki et al., 2008). Aggregation of NPs is the biggest issue under discussion these days as it alters the fundamental properties of NMs. So the NMs should be stable enough to maintain their NM properties. Stability of colloids is always in scientific discussions with a significant amount of research data so far.

The colloid stability depends on a theory which guides about two opposite forces in a suspension; one being the electrostatic repulsion and second van der Waals forces. The first force favours stability and second promotes the aggregation. The theory is called the DLVO theory after the name of Deryaguin, Landau, Verwey and Overbeek (DLVO), four eminent scientists, who firstly gave this idea of opposite forces in a suspension. As explained by the DLVO theory, particle stability depends on particle to particle and surface to particle

interactions. Most of the assumptions from DLVO theory don't support the NMs with dissimilar structures and large surface to volume ratios. In NMs high surface area is much more important than for the larger colloids in determination of their stability. The classic DLVO theory doesn't consider all these factors, which make the assessment of NM's stability more interesting and rather challenging. So it is need of the time to do some research on a better understanding of the interactions of; the NP to NP and NPs to surface. Influence of surface heterogeneity on the stability of NMs necessarily needs an explanation to increase the capability of DLVO theory for the prediction of NM's stability. As in spite of DLVO theory's pronounced achievements, there are many reports which illustrate its deviations; mentioning many draw backs. Most of the reported cases are usually credited to surface heterogeneity and interfacial forces; without taking into account the in depth factors like roughness, chemical or structural heterogeneity (Taboada-Serrano et al., 2005, Duval et al., 2004, Elimelech et al., 2003, Tufenkji and Elimelech, 2005).

1.2.3 Mobility of Nanomaterials

Due to interaction with environmental constituents, NPs are presumed to be in agglomerated state when released into the environment. With progress of time and with effect of the fluctuations in temperature and pH, these agglomerates either become stronger aggregates or rather loose agglomerates which further torn apart into smaller and individual NPs. Such structural arrangements and their effects on the stability and mobility of NMs were never studied to any significant level with respect to natural or artificial environmental conditions. Only very limited research is reported on the mobility of titania NPs in aqueous environments (Chen et al., 2011a, Fang et al., 2009a). From these studies it is obvious that titania mobility in saturated porous media is affected by chemical properties of solution like ionic strength, pH, flow velocity, stabilizing agents and humic substances (Chen et al., 2012,

Chowdhury et al., 2012, Godinez and Darnault, 2011a). It was observed that increase in pH promoted mobility of titania NPs while ionic strength increased retention of NPs in the porous media. Reason for retention at higher ionic strength is due to promotion of agglomeration which resulted in greater retention. NOM has induced stability in the system with increased mobility.

1.3 Research Objectives

This research work has following main objectives:

- To synthesize TiO_2 NMs using sol-gel and hydrothermal methods and evaluate the effect of alcohol concentrations and precursors on phase and shape control (Chapter 4).
- To observe the in-depth nucleation, growth and agglomeration of TiO_2 NMs and study the effects of pH and gel drying temperature grain growth, the physicochemical and the structural properties of the same (Chapter 4).
- To optimize the stability of NMs with use of different surfactants to evaluate time resolved aggregation kinetics using different monovalent and divalent cations for stabilized NMs. This objective has been met and is reported in chapter 5.
- To evaluate the mobility and retention of stabilized and bare nanoparticle (NPs) in synthetic and natural porous media and study the behaviour of flow velocity on NPs transport (Chapter 6).
- To review some of the recommendations of Derjaguin–Landau–Verwey–Overbeek (DLVO) theory against different shapes and sizes of NPs; to identify critical issues for NPs retention during their mobility through saturated porous media (Chapter 6).

Different industries are continuously using engineered NMs since many decades. Consequently, these NMs are being released in to the environment with increased concerns of their ultimate fate and behaviour in complex environmental matrix. Research on the presence

of NMs in environmental systems has already been reported by many scientists (Nowack et al., 2012, Gottschalk and Nowack, 2011, Colvin, 2003, Lin et al., 2010). The ongoing research illustrates the presence of NMs in the environment without the in-depth knowledge of their interaction with the environmental constituents. So we are starting to generate this in depth knowledge, but at an early stage, without being able to analyse in environment.

TiO_2 NMs were selected for this research work, because of their agglomeration behaviour, stability and reactive nature with different environmental factors. TiO_2 is continuously being discharged from different products during their life cycle and through industrial processes; significantly increasing its concentrations in environmental systems like sewage treatment plants, surface water or soil ecosystem (Mueller and Nowack, 2008, Kaegi et al., 2008, Boxall et al., 2007).

Chapter 1 gives an inclusive outline of the research on fabrication, stability and mobility of titanium dioxide NMs. The challenges in this area are reviewed along with most significant outcome of this work.

1.4 Thesis Layout

This thesis is comprised of seven chapters: Introduction; Review of Literature; Materials and Methodology; Synthesis of TiO_2 NMs; Stabilization of NPs in Different Media; Transport of NPs through a Porous Medium; and Conclusion.

Chapter One presents an overview to the research project considering the need and objectives of the research. Chapter Two reviews some existing researches on nanotechnology, TiO_2 synthesis, its stability and transport. Chapter Three introduces NP synthesis experiments performed in laboratories[1] along with a brief introduction to the characterization techniques

[1] At the University of Birmingham

employed. This chapter also explains the underlying theories behind the experiments and the experimental layout for stability and mobility studies. Different characterization tools like x-ray diffraction (XRD), high resolution transmission electron microscopy (Garzella et al., 2000) and atomic force microscopy (AFM) have been used to characterize the synthesized NMs.

Chapter Four focuses on the fundamental synthesis aspects of TiO_2 NMs, specifically, pH dependent nanoparticle growth; effect of different alcohols and alcohol water concentration on shape of NPs; effect of temperature on phase; shape and size; and effect of aging on hydrodynamic diameter of NPs. Chapter Five collects all the data on the stability of synthesized NMs and evaluates the time resolved kinetics for NM agglomeration. In this chapter, different batches of synthesized NMs are checked for their stability against different monovalent and divalent salt concentrations. Complete time resolved aggregation kinetics is studied with dynamic light scattering (DLS). Chapter Six presents transport calculations that are employed for the simulation of NMs transport through glass bead and sandstone columns. The results are compared with a pre-developed model for its validity. The model is validated by the experimental data in a rigorous approach. Chapter Seven draws conclusions from all the results and lists the future work plan and suggestions for improvement.

1.5 Approach for Current Research and Motivation

Nanotechnology industry is growing at an uncontrollable pace because of industrial use of NPs in different products. Due to this increased industrial use, nanomaterials are continuously going to the ecosystem with very less measurement and control approaches which are mainly based on chemical control policies. Due to nature of the nanomaterials, these are difficult to quantify in natural environments and can easily pass through traditional filtration methods (Nowack and Bucheli, 2007). So research work on the stability and transport of engineered nanomaterials is need of current era to help the regulatory authorities for proper

legislation. It is a common belief that distinguishing natural NMs from engineered NMs is a complex and challenging task (Agrios and Pichat, 2005). Aggregation of NMs into larger aggregates or agglomerates is another issue in the field of nanotechnology. There is an absolute need to fabricate NMs with more stability in solution form. While released in to the complex environmental media, these NMs may behave differently while reacting with other constituents which are already there. So an understanding of complete aggregation kinetics may help to evaluate the mobility of these NPs in the environment. Overall theme of current research work was to get precise data sets of synthesis, stability and mobility of engineered titania NMs which can help scientist and regulatory authorities in making policy decisions for titania NPs synthesis and their release in natural ecosystem.

Chapter 2

LITERATURE REVIEW

This review chapter is written with the purpose to obtain general understanding of synthesis, characterization, stability, aggregation kinetics and transport of titania NPs. Titanium dioxide mainly occurs as three crystalline polymorphs; anatase, rutile and brookite (Zhao et al., 2008). Anatase and rutile phases are generally used a lot more than brookite in a variety of applications. Literature is also reviewed for the stability, aggregation kinetics and interactions of engineered titania NPs in natural aquatic environments.

2.1 Introduction to Nanomaterials/Nanoparticles

Nanotechnology comprises the handling of materials in the nanometer regime to use these in industry producing enhanced quality products. A nanometer is a billionth part of a meter, or $1/10^9$m. According to the recommendations of European Commission, the NMs are defined as "a natural, incidental or manufactured material containing particles, in an unbound state or as an aggregate or as an agglomerate and where, for 50 % or more of the particles in the number size distribution, one or more external dimensions is in the size range 1 nm-100 nm" (EU, 2011). To provide a measure of the nanoscale, one nanometer (nm) is approximately the width of 10 hydrogen atoms (Saw et al., 2007, Cappelletti et al., 2009). For further elaboration of size concept, a comparison of different biological entities at nanometric scale is illustrated in Table 2-1. NMs as compared to bulk materials, exhibit few remarkable specific characteristics and have better structural integrity as they exhibit distinctive mechanical, chemical, optical, electrical and magnetic properties (Oberdörster et al., 2005, Thomas and Sayre, 2005).

Table 2-1: Size comparison of different biological entities (CARLSON, 2006)

Item	Size
Red ant	5mm
Head of a pin	1mm
Human hair (width)	0.08mm=80,000nm
Most animal cells	10-50**µ**m
Alveular Macrophage	~15um
Red Blood Cell	9um
Nucleus	3-10um
Diameter of a typical bacterium	1,000-10,000nm
Average wavelength of visible light	400-700nm
Lysosomes, peroxisomes	200-500nm
Human immunodeficiency virus	90nm
Wavelength of extreme ultraviolet light	40nm
Cell membrane, Mitochondria	10nm
DNA Alpha Helix	2.0nm
Amino Acid	0.8nm
Water molecule (width)	0.3nm
Hydrogen atoms	0.1nm

NMs are not something new as these are naturally present in the environmental system since beginning of life on this planet. However rapid industrial development increased the overall load of different NMs in the environment. (Klaine et al., 2008a). Aquatic colloids (including sand, silt, clay, microorganisms etc.), the finest desert sand, oil vapours, volcanic dust, forest fire products, humic substances, biological products and air dust are most important types of ancient natural NPs (Ostiguy et al., 2006). NMs are either classified on the basis of their chemical composition; (Handy et al., 2008b, Buzea et al., 2007a) where these are

categorised as carbon based structures, metal NPs, metal oxides or semiconductor crystals (quantum dots); or these are classified on basis of NPs dimensions (Buzea et al., 2007b, Krug and Wick, 2011). Figure 2.1 illustrates the possible sources of natural and engineered NMs.

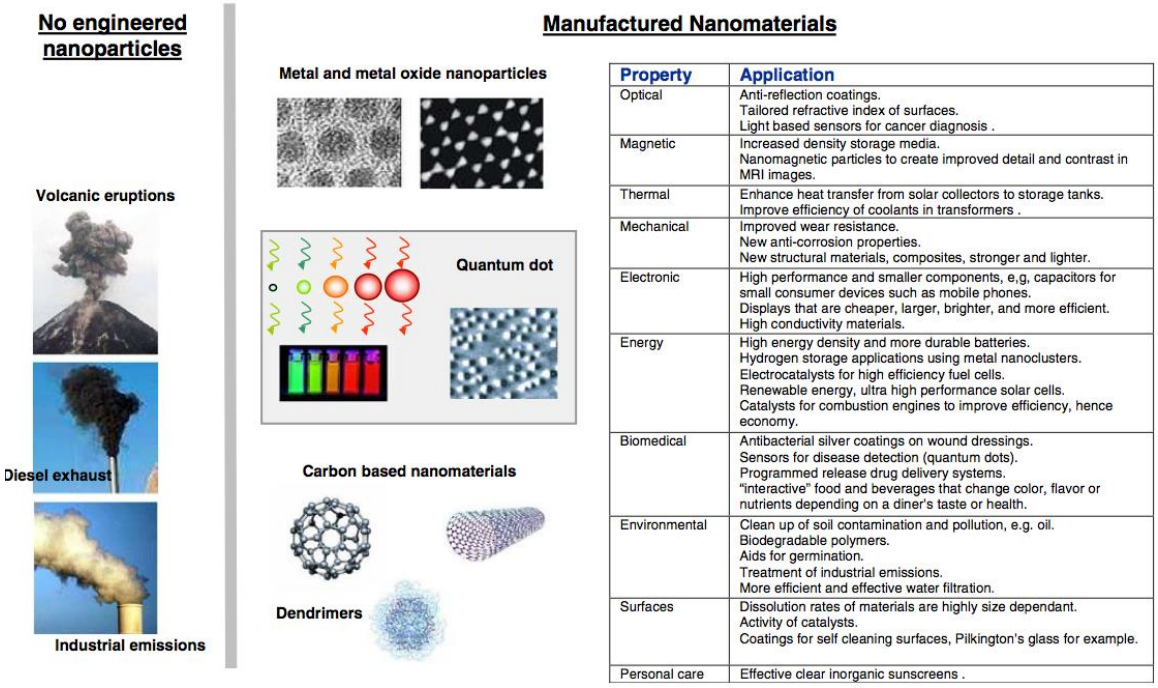

Property	Application
Optical	Anti-reflection coatings. Tailored refractive index of surfaces. Light based sensors for cancer diagnosis .
Magnetic	Increased density storage media. Nanomagnetic particles to create improved detail and contrast in MRI images.
Thermal	Enhance heat transfer from solar collectors to storage tanks. Improve efficiency of coolants in transformers .
Mechanical	Improved wear resistance. New anti-corrosion properties. New structural materials, composites, stronger and lighter.
Electronic	High performance and smaller components, e,g, capacitors for small consumer devices such as mobile phones. Displays that are cheaper, larger, brighter, and more efficient. High conductivity materials.
Energy	High energy density and more durable batteries. Hydrogen storage applications using metal nanoclusters. Electrocatalysts for high efficiency fuel cells. Renewable energy, ultra high performance solar cells. Catalysts for combustion engines to improve efficiency, hence economy.
Biomedical	Antibacterial silver coatings on wound dressings. Sensors for disease detection (quantum dots). Programmed release drug delivery systems. "interactive" food and beverages that change color, flavor or nutrients depending on a diner's taste or health.
Environmental	Clean up of soil contamination and pollution, e.g. oil. Biodegradable polymers. Aids for germination. Treatment of industrial emissions. More efficient and effective water filtration.
Surfaces	Dissolution rates of materials are highly size dependant. Activity of catalysts. Coatings for self cleaning surfaces, Pilkington's glass for example.
Personal care	Effective clear inorganic sunscreens .

Figure 2.1: Sources of natural and engineered nanoscale substances (Farré et al., 2009)

2.1.1 Nanostructured Titanium Dioxide

As compared to bulk material, nanocrystalline TiO_2 has improved properties and it is an important material in all disciplines of science including material engineering and biomaterials (Hearne et al., 2004, Swamy et al., 2005, Chen et al., 2009, Wang et al., 2013, Ranade et al., 2002). NMs show varied physico-chemical characteristics which are significantly dissimilar to the bulk materials (Wang et al., 2013, Martyanov and Klabunde, 2004, Rao et al., 2006). The interest in nanocrystalline titanium dioxide synthesis was grown due to its diverse nature and tremendous applications in catalysis, photocatalysis, paint pigments (Middlemas et al., 2013), sensors (Garzella et al., 2000), cosmetics (Serpone et al., 2007, Popov et al., 2005), medicines (Singh and Nalwa, 2011), water purification (Mills et al.,

1993), photovoltaics (O'regan and Grfitzeli, 1991) and self-cleaning windows (Paz et al., 1995).

Titanium is the simplest of the transition metals having electronic structure $3d^2 4S^2$. It is present in the earth's crust and constitutes 0.6 % of it (Lab, 2013). It is mainly present as ilmenite ($FeTiO_3$) and the binary metal oxides. TiO_2 is the most important material amongst binary metal oxides which has three phases; rutile, anatase and brookite (Liao et al., 2012, Banfield et al., 1993, Ozawa et al., 2005, Reyes-Coronado et al., 2008, Smith et al., 2009). Table 2-2 illustrates the crystal structure properties for all three forms of TiO_2 (Cromer and Herrington, 1955, Mo and Ching, 1995).

Table 2-2: Crystal structure properties of TiO_2 (Cromer and Herrington, 1955, Mo and Ching, 1995)

Properties	**Rutile**	**Anatase**	**Brookite**
Crystal structure	Tetragonal	Tetragonal	Orthorhombic
Ti–O bond length (Å)	1.937(4) 1.965(2)	1.949 (4) 1.980 (2)	1.87–2.04
O–Ti–O bond angle	77.7° 92.6°	81.2° 90.0°	77.0°–105°
Lattice constant (Å)	a = 3.784 c = 9.515	a = 4.5936 c =2.9587	a = 9.184 b = 5.447 c = 5.154
Space group	$I4_1/amd$	$P4_2/mnm$	Pbca
Molecule	2	2	4
Density (g cm^{-3})	3.79	4.13	3.99
Volume/ molecule ($Å^3$)	34.061	31.2160	32.172

Anatase is the major commercial phase of titanium dioxide. Navrotsky and Kleppa (1967) studied that anatase is metastable tetragonal structure as compared to rutile at varying temperature and pressure. It transforms to rutile at very high temperatures (>915ºC). Figure 2.2

shows the tetragonal structure of anatase where Ti-O octahedral shared four corners. This structure has a three dimensional topology of edge-sharing octahedra in all directions, forming a zigzag pattern through the crystal plane.

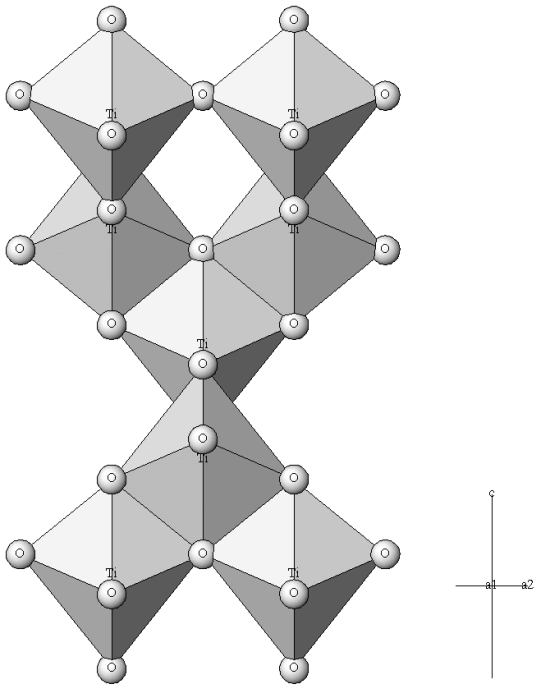

Figure 2.2: Anatase crystal; Tetragonal di-tetragonal di-pyramidal a = 3.7845 Å, c = 9.5143 Å; Z = 4 (Crystal, 2013a)

At high temperatures brookite and anatase transform to rutile, which is the stable and the most studied form of TiO_2 (Haines and Léger, 1993). As shown in Figure 2.3, rutile has rows of edge-sharing octahedra in the *c* direction which are connected by corner sharing in the *a* and *b* directions. (Agrafiotis and Tsetsekou, 2000, Brinker et al., 2002, Kerner, 1993). There is no difference between the crystal structure of rutile and anatase except that, in rutile the octahedra share four edges as compared to four corners in anatase. Such an arrangement give rise to four-folded symmetrical chains (Zhang et al., 2010).

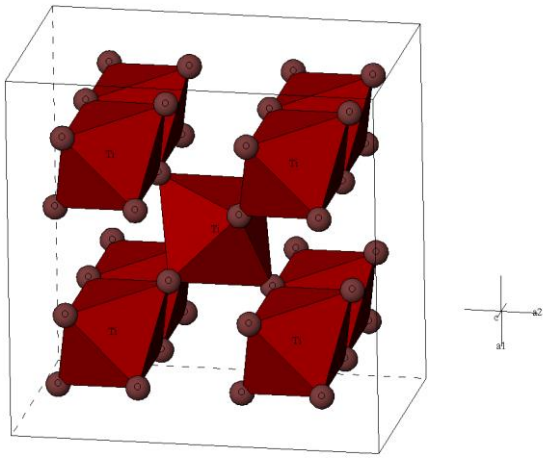

Figure 2.3: Rutile crystal Tetragonal di-tetragonal di-pyramidal a = 4.5937 Å, c = 2.9587 Å; Z = 2 (Crystal, 2013c)

The crystal structures of anatase and rutile as shown in Figure 2.2 and Figure 2.3 reveal that rutile has very dense arrangement of molecules as compared to anatase. Brookite exhibit an orthorhombic crystal structure (Figure 2.4) which reverts to rutile at a temperature of 750^{o}C (McColm, 1995). Brookite has similar mechanical characteristics to rutile but it is not used frequently in the industry.

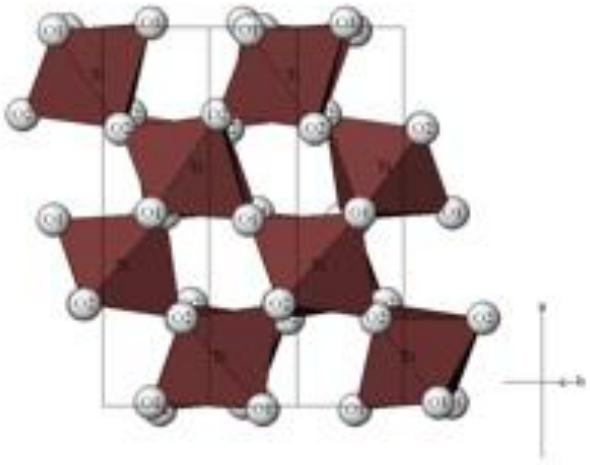

Figure 2.4: Brookite crystal Orthorhombic di-pyramidal Z = 8, a = 5.4558 Å, b = 9.1819 Å, c = 5.1429 Å (Crystal, 2013b)

2.2 Synthesis of Titanium Dioxide Nanoparticles

Fabrication of NPs with a high degree of control over required properties is a complex task. Generally, NMs can be fabricated by numerous diversified approaches. NMs synthesis can be divided into the top-down and bottom-up fabrication approaches (Figure 2.5). As name elaborates, in the bottom-up synthesis, NMs are synthesized starting from atoms or molecules where these are called the NP building units. Materials from bottom up approach can be synthesized by using different methodologies including chemical synthesis, self-assembly and positioning of single NPs (Arnall, 2003, Siegel et al., 1998).

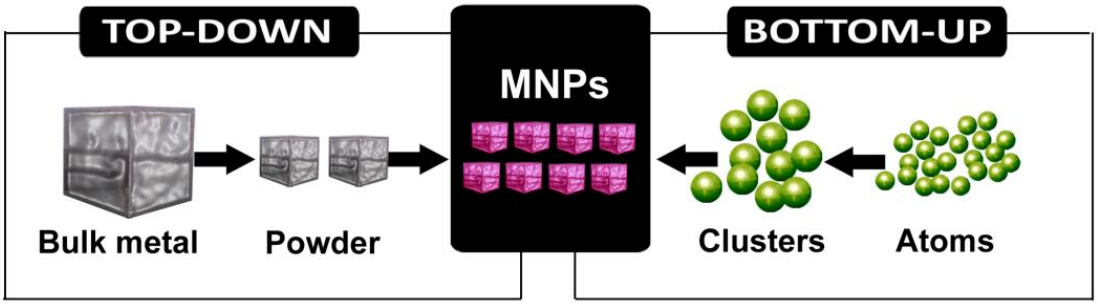

Figure 2.5: Diagram showing the bottom up and top down synthesis approaches (Domènech Garcia et al., 2012)

In top-down synthesis larger structures are broken down to the nanometric dimensions. This approach is just opposite of bottom up synthesis approach of NPs. Usually laser ablation, etching, sputtering and grinding are used to synthesize NPs with top-down synthesis method. Ball milling is a very specific technique to scale down micrometric particles to NPs. Several of these techniques are commonly used in the different sophisticated industries, considering quality control and occupational health and safety regulations (Feigenbaum, 2004). NMs are being used by several industries in their final products, however, only a few use significant quantity (Aitken, 2006). Paint, cosmetics, catalyst and polymer coating industries are few

examples who use NMs in huge quantities as compared to pharmaceutical industry (Aitken, 2006).

NPs can be synthesized considering following approaches which are centred on possible mechanisms of synthesis (Aitken et al., 2004, Siegel et al., 1998, Bergamaschi, 2009):

a. **Condensation Process:** A bottom-up approach where NPs are synthesized with flame pyrolysis which involves nucleation at high-temperature and synthesis occurs in a plasma. Gaseous phase evaporation is main phenomenon.
b. **Vapour Deposition Process:** Another bottom-up approach where NPs are synthesized by evaporation followed by vapour deposition in a cool environment.
c. **Sol-gel Process:** A bottom-up approach consisting of hydrolytic polycondensation of different sols formed by chemical reactions of alkoxides with water. This process involves controlled precipitation phenomena.
d. **Hydrothermal Process:** A process which depends on the solubility of minerals in hot water under high pressure. The crystal growth is performed in an apparatus consisting of a steel pressure vessel called an autoclave, in which a nutrient is supplied along with water.
e. **Mechanical Breakdown Processes:** It is a top-down approach of NPs synthesis where larger molecules are broken down via different techniques.

In this thesis, the sol-gel and hydrothermal approaches are addressed with a specific reference to titanium dioxide NMs. It is well documented that sol-gel synthesis process is used to synthesize titania nano powders at laboratory scale. Nanophase particles formed from aqueous synthesis are heavily hydrated and agglomerated initially (Hu et al., 2003). The nucleation and agglomeration of TiO_2 nanocrystals is dependent on pH value and sintering temperature, as claimed by Hu and co-workers (Hu et al., 2003).

In current research work sol gel and hydro-thermal synthesis methods were chosen to study the effects of pH, temperature, precursor types and alcohol concentrations on morphology of TiO_2 NMs.

2.2.1 Sol gel method of TiO_2 synthesis

In order to synthesize highly controlled NPs characteristics, sol-gel methodology was used. Sol-gel method, as the name implies, comprises of two main parts:

a) Firstly, the precursors form high molecular weight but still soluble oligomeric intermediates, called a sol.

b) Secondly, the intermediates come close together to form a gel.

At laboratory scale the most used process of synthesis is the sol-gel process to synthesize different types of NPs (Livage et al., 1988, Brinker and Dunphy, 2006, Lakshmi et al., 1997). It is wet chemistry based methodology and no high temperature melting of inorganic raw materials is involved. Typically a sol-gel process is based on five processing steps (Fendler, 2008).

i. **Hydrolytic Polycondensation:** Hydrolysis of alkoxide precursors which forms a polymeric or particulate sol containing inorganic materials.
ii. **Formation** of a uniform suspension by deposition of substrate into the sol.
iii. **Solidification** of the gel with solvent and volatile compounds evaporation process.
iv. **Drying** at room temperature to get a condensed inorganic network.
v. **Calcination** where very high temperature is involved to remove of organics and to crystallize the solid material.

In one study Qamar and co-workers (Qamar et al., 2008) obtained titanate nanotubes, with a chemical treatment of 10M NaOH followed by heating in an autoclave at 150^{o}C for

couple of days. They observed a significant effect of sol-gel technique to control different properties including shape and phase. Adan and co-workers also observed significantly different structures and surface characteristics of TiO_2 particles including control over anatase and rutile contents (Adán et al., 2007). The calcination temperature has strong effect on crystal structure, energy band structure, optical adsorption and photocatalysis of the sol-gel fabricated TiO_2 (Behnajady et al., 2013) and Ceria NPs (Sifontes et al., 2013). Calcination temperature is ascribed to the changes in structure and optical property of catalyst such as crystal size, content of rutile, residual NO_3^-, and band-edge position of light adsorption (Behnajady et al., 2013, Sifontes et al., 2013). In sol-gel synthesis of titania NPs, many parameters are important to control the size and shape. Firstly the monodispersity of sol-gel synthesized titania particles were helpful in transferring and separating the photo-generated electrons and holes by reducing the recombination (Yu et al., 2002). Secondly the surface of titania alters the charge compensation depending on pH of the system (Bessekhouad et al., 2004), so pH control is another important parameter. Thirdly doping of titania surface is important for different application as Yang and co-workers (Yang et al., 2004) revealed that absorption edge was extended by Mo^{6+} doped TiO_2 which also decreased the interfacial charge transfer resistance. There was a two-fold increase in the activity of Mo^{6+} doped TiO_2 as compared to pure TiO_2 at 1% optimal concentration. In another study sol–gel synthesized TiO_2 and Au/TiO_2 showed a strong dependence of finalized NPs on functional , composition, structural and morphological properties of the system (Lidia and et al., 2007). Fourthly, calcination temperature is another parameter to control size and shape of NPs. In one important study, high temperature calcinations caused changes in structure and morphology of sol-gel prepared TiO_2 particles supported with flat quartz (SiO_2) (Martyanov and Klabunde, 2004). A temperature of 500^oC anatase phase TiO_2. At 800^oC the SiO_2 helped to retain the anatase form of TiO_2 while bare anatase was transformed into the rutile form. Moreover, TiO_2 modified with SiO_2 did not

change the crystallites at 800^{o}C even their size was increased. Temperature had profound effect on sol-gel dip coating (SGD) and electron beam evaporation (EBE) synthesized transparent TiO_2 thin films which were tested for their photocatalytic activity by Oh et al. (2003). The transmittance of the films was decreased with increased calcination temperature. Growth of particles was observed and refractive index of the films was increased with a 200^{o}C increase in temperature.

Su et al. (2001) prepared the nano-sized TiO_2 photocatalysts by sol-gel method and characterized by FTIR spectroscopy, FT-Raman spectroscopy and diffuse reflectance spectroscopy(DRS). The result showed that calcination temperature has strong effect on crystal structure, energy band structure, optical adsorption and photocatalysis of the TiO_2. It was found that the TiO_2 photocatalyst calcined at 400^{o}C has the best apparent optical adsorption, the biggest band edge position and the highest photoactivity. They revealed that calcination temperature affected the TiO_2 catalysis and ascribed it to the changes in structure and optical property of catalyst such as crystal size, content of rutile, residual NO_3^-, and band-edge position of light adsorption.

Stabilization agents in synthesis are important as Guillard et al. (2002) studied different physicochemical and photocatalytic properties of sol-gel fabricated TiO_2 films. It was noted that the nature of stabilizing agent affects the overall thickness of titania loading and hence the photocatalytic activity. They revealed that the photocatalytic activity was dependent on the nature of titania precursor and stabilising agents. The photocatalytic activity was dependent on the thickness of coating and decrease of coating thickness at high temperature decreased the activity to a significant level.

Keeping in view the research work reported above, it is clear that sol-gel process is a technique which can help in engineering NPs as per requirement if different parameters can be

monitored and controlled during the fabrication process. Obviously the ease of synthesis approach gives sol-gel technique an edge over the other methods.

2.2.2 Hydrothermal Synthesis of TiO_2

Hydrothermal synthesis comprises of multiple synthesis techniques to crystallize substances in solution phase at high temperature and vapor pressure preferably using an autoclave (Wikipedia, 2016). It is a straightforward approach for chemical processing which leads to fabrication of crystallized metal oxides with controlled temperature and pressure (Pookmanee et al., 2004). Spherical titania NMs of small size range can be fabricated when sol-gel precursors are subject to hydrothermal processing. Using this approach Jiang and co-workers (Jiang et al., 2003) synthesized spherical monodispersed NPs by using $TiCl_3$ precursor, modified from $TiCl_4$ with acetyl acetone. Similarly Nian and Teng (Nian and Teng, 2006) fabricated single-crystalline anatase nanorods from the hydrothermal treatment of aqueous titanate nanotubes in acidic system. They mentioned that size of hydrothermally synthesized anatase NPs was dependent on the pH of the suspensions. Moreover Ke et al. (Ke et al., 2008) successfully prepared WO_3/TiO_2 nanocomposite with novel properties with a hydrothermal method where they used cetyl trimethyl ammonium bromide (CTAB) as stabilizing agent.

In another study titanate nanotubes were fabricated by a method which involved sol-gel method followed by an autoclave hydrothermal treatment by Kim and co-workers (Kim et al., 2007). They treated titania sol with 10M NaOH solution followed by a heat treatment in an autoclave at 150^oC for two days. They revealed that calcination temperature and amount of sodium controls the properties like phase, shape, morphology and photo activity.

Hydrothermal mediated synthesis of titanate nanofibers with different sizes was reported by Zhu et al. (2005). They mentioned that these nanofibers were highly reactive

because of their aspect ratio, morphology and large surface to volume ratio. They also reported the low temperature wet-chemical phase transitions of titanate nanostructures to titania polymorphs and the nanofibers change to anatase and rutile polymorphs in aqueous dispersions.

Spherical TiO_2 particles with different particle properties like fraction of crystallization, size, shape etc. were obtained with hydrothermal method by Cho et al. (2003). In another study plate like anatase NPs and $BaTiO_3$ was fabricated by Feng and co-workers (Feng et al., 2001) by using a hydrothermal synthesis methodology. They proposed two mechanisms of $BaTiO_3$ hydrothermal synthesis. First being in situ topotactic transformation reaction and second being dissolution-deposition reaction. A well-defined crystal orientation of plate like $BaTiO_3$ was revealed by these scientists.

Hydrothermally supported 7-25nm TiO_2 NPs were synthesized by Chae et al. (2003). The size was controlled by concentration of alkoxide precursor and solvents. It was mentioned that as prepared TiO_2 NPs were highly stable and showed long term stability and used for the synthesis of transparent TiO_2 films.

The literature reviewed above shows that hydrothermal method of synthesis is well known and documented. This method is frequently used by scientists to synthesize titania nanomaterial with controlled morphological properties. In fact, sol-gel and hydrothermal methodologies can be combined to get more promising results.

2.1.1 Role of Temperature in TiO_2 Synthesis

Different drying methods and calcination temperature of nano-sized TiO_2 have strong effect on crystal structure, energy band structure, optical adsorption property, surface quality and photocatalytic activity (Behnajady et al., 2013). Gervais and co-workers (Gervais et al., 2001) studied that TiO_2 particles heated below 700°C are predominantly anatase and above

700°C it transforms to rutile while Ani and co-workers (Ani et al., 2005) elucidated the influence of temperature, molar ratio of $H_2O/TiCl_4$ and concentration of precursors on particle size and phase composition. They attributed that water vapor has a catalytic role of in the enhancement of amorphous to anatase phase transformation at high molar ratio of $H_2O/TiCl_4$ at low drying temperature. In another study Xu et al. (2013) synthesized sol–gel mediated anatase titania powder by combining sol-gel and thermal techniques. They verified the transformation temperature from anatase to rutile was 510 °C while anatase phase remains predominant at the calcination temperature range of 400–510 °C.

Grzmil et al. (2004) revealed that the ratio of anatase to rutile transformation was higher at elevated temperatures. They noticed that the process temperature affects the conversion ratio considerably more than the calcination time. Calcination temperature controls the fast hole transfer reaction which was more intensive at lower calcination temperature (Salmi et al., 2004). Martyanov and co-workers (Martyanov and Klabunde, 2004) mentioned an annealing temperature of 500^{o}C for the synthesis of the anatase phase in the powder form.

Rod shaped rutile NPs were synthesized by Krivec and co-workers (Krivec et al., 2013) with low-temperature hydrothermal method. They mentioned an amorphous surface layer of 1 nm thickness on rutile NPs which enhanced the photocatalytic properties as compared to NPs synthesized by any other method. The amorphous layer on rutile nanorods enhances the electron transfer with an improvement in photocatalysis of these NPs.

In another study highly active porous biphase TiO_2 anatase nanopowders were fabricated by hydrothermal process followed by a treatment with ammonia (Chen et al., 2003). These NPs exhibited large surface areas and crystallinity which were altered by calcination temperatures up to 900°C. The synthesized NPs showed higher photocatalytic activity as compared to commercial Degussa P25. It was noted that the photocatalysis of TiO_2 increased

with an increase in the calcination temperature which was reduced after 900°C calcination temperature because of a decrease in surface area of NPs (Chen et al., 2003).

Grzmil et al. (2004) synthesized TiO_2 pigment by the sulfate process and hydrated titanium dioxide is calcined. As a result of the polymorphous conversion, rutile was obtained. Roasting additives were introduced into the calciner, in order to achieve required process temperature, crystallite size of individual phases, optical properties, and the pigment photostability. The obtained dependences were described using exponential equations. The ratio of anatase-rutile transformation was higher at elevated temperatures. Grzmil and co-workers (Grzmil et al., 2004) noticed that the process temperature affects the conversion ratio considerably more than the calcination time. During the experiments alkaline metals like potassium, lithium and phosphate were added into the system. They noted that the increase of phosphates content in the calcinated TiO_2 nH_2O (0.1-0.5 mass % P_2O_5 in relation to TiO_2) caused the anatase-rutile transformation ratio to drop 2 to 10 times. Moreover, the phosphates presence restricted an unfavorable anatase and rutile crystallites growth. In fact, their crystallites size was 2-3 times lower, compared to the crystallites size measured when the phosphates were not added. If the potassium content in hydrated TiO_2 was increased (0.05-1.0 mass % K_2O in relation to TiO_2), during calcination the rutile formation passed through a maximum. Similar behaviour was observed when lithium (0.025-0.5 mass % in relation to TiO_2) was introduced instead of potassium. Neither anatase nor rutile average crystallites size was influenced by the potassium or lithium addition.

The literature reviewed in this section advocates the phase control of TiO_2 NPs with temperature. So to engineer titania NPs synthesis and annealing temperature might be a controlling factor and needs further investigation.

2.2.3 Role of pH in TiO_2 Synthesis

Transformation of anatase to rutile depends on several mechanisms including temperature, precursors and pH as elaborated by Zhu et al. (2005) who noticed that the titanate nanofibers transform to anatase and rutile at varying pH and high temperatures. Feng and co-workers (Feng et al., 2001) investigated that pH has detrimental effect when layered titanate $H_{1.07}Ti_{1.73}O_4.H_2O$ were transformed to $BaTiO_3$ or anatase in the presence of $Ba(OH)_2$ solution or DI water during hydrothermal synthesis. They noticed that particle size of anatase TiO_2 was dependent on pH and aging (Sugimoto et al., 2003). They reported that nucleation rate of anatase TiO_2 was reduced with an increase in pH. This happened because of the reduced concentration of precursor in the solution and adsorption of OH^- onto the embryos of TiO_2 (Sugimoto et al., 2003). Triethanolamine acted as a shape controller at high pH value of 11 or more. It enhances the effect of pH on nucleation rate of anatase giving different shapes and sizes (Sugimoto et al., 2003). Velikovska and Mikulasek (Velikovská and Mikulášek, 2007) studied the effects of pH which changes the surface properties of TiO_2 NPs and alumina membrane. Isley and Penn (Isley and Penn, 2006) studied that in sol gel synthesis of TiO_2 at pH3 where HCl addition increased the amorphous TiO_2 during fabrication process as compared to HNO_3. Same results were also reported by Hu and co-workers (Hu et al., 2003) where increased volume fraction of brookite NPs was seen with a decrease in the synthesized pH and amount of brookite phase enhances the anatase-rutile transformation. Also pH affects the anatase-rutile transition temperatures which showed an increase with increasing pH of synthesis (Hu et al., 2003).

Acidic pH showed a higher refractive index, a denser film growth, and a lower surface roughness of TiO_2 multilayer films than those of the films deposited in different conditions (Kim et al., 2006). Luo and his group (Luo et al., 2003) attributed that acidity has detrimental

effect on the crystal structure formation and phase transformation. Chu and co-workers (Chu et al., 2007) revealed that pH is a sensitive parameter to the rate of degradation under UV/TiO_2 and UV/TiO_2/H_2O_2 systems. HO• effects the photoexcitation and ultimately degradation at acidic or basic pH values as the introduction of H_2O_2 an HO• scavenger, slowdown the decay rate at alkaline medium.

Effect of pH on synthesis of highly pure TiO_2 was evaluated by Wang and co-workers (Wang et al., 2007a) who used EDTA (disodium ethylenediamine tetra-acetate) to chelate Fe^{3+} which was used without hydrolysis to Fe(OH) for synthesis of TiO_2. EDTA decreased start of TiO_2^+ hydrolysis hence controlling the desired properties. In this work a more purified TiO_2 product was obtained with chelating property of EDTA. In a generalized reaction EDTA stopped the hydrolysis of Fe^{3+} to $Fe(OH)_3$ precipitate. The formation of TiO_2 NPs increased with increasing EDTA amount which altered the hydrated titanium dioxide. Moreover, EDTA addition at the start of experiment decreased the required amount of washing water, and more TiO_2 grains were harvested which were easily filtrated and washed.

Sol-gel mediated TiO_2 samples were fabricated by Adan and co-workers (Adán et al., 2007) at varying pH and thermal treatments. The synthesized NPs were compared with commercial TiO_2, Degussa P25 and results showed significant differences in the properties of synthesized NPs and most of the properties were dependent on synthesis pH and temperature.

pH effect during synthesis of TiO_2 sols in acidic and basic solutions was evaluated by Cao et al. (2004). They prepared thin TiO_2 films by a spin coating method and checked for photocatalytic activity. They showed that photocatalysis of acidic sol films was much greater than basic sol films. It was identified that active species like hydroxyl group were hindered by the chemisorbed species of CO_2 which form electron traps to lower the photocatalysis.

The review of all the literature above shows that pH is an important factor for synthesis and control of TiO_2 nanomaterials. Although there are many studies on the effect of pH on phase transformation and size control, there is still a need of more comprehensive study to understand its effect on nucleation and agglomeration of TiO_2 nanomaterials.

2.2.4 Role of Precursors in TiO_2 Synthesis

There are only a few studies on the effects of titanium precursors in relation with the resulting titania crystal structure. Wilska reported the effects of sulfate and chloride solutions on synthesis of titania for the first time (Wilska, 1954). According to his findings, the presence of crystalline forms of TiO_2 depended on synthesis method and precursor type. As per his findings sulphate precursors always produced anatase while chloride precursor was responsible for synthesis of rutile. He mentioned that during synthesis process the amorphous phase is always followed by the crystalline phase. He also found that the fraction of rutile phase is attributed to the oxygen precursor while photocatalysis to titanium precursor concentration in the anatase and rutile mixture synthesized by laser pyrolysis of $TiCl_4$ (Alexandrescu et al., 2004, Kozlova and Vorontsov, 2007). In another study Kim and co-workers evaluated that size and number concentration of particles were strongly dependent on the amount and concentration of precursor (Kim et al., 2005a).

Kozlova and Vorontsov (2007) studied the effect of precursors on synthesis of TiO_2 by using tetrabutyl titanate (TBT) and titanyl sulphate (TS) as precursors and cetyl trimethylammonium bromide (CTAB) and dodecylamine (Hearne et al., 2004) as templates. Brookite was main phase of the samples synthesized with TBT. It was evaluated that titania NPs synthesized by PD were more active than by SCR synthesized.

Tang et al. (2005) used low-valent organometallic precursors for the synthesis of titania NPs at low-temperature. They revealed that bis-(cyclooctatetraene) titanium synthesizes TiO_2 after reaction with dimethyl sulfoxide at room temperature. If no supporting ligand is present, amorphous TiO_2 powder is the end result. The ligands like tributylphosphine oxide, trioctylphosphine and tributylphosphine oxide arrest the population during NPs synthesis producing chemically distinct crystalline titania NPs.

None of the known phases of TiO_2 were obtained after the hydrolysis of raw tetraisopropoxytitanium (IV) and tetraisopropoxytitanium. The tetraisopropoxy group was replaced with carboxylic acids like acetic, butanoic and propanoic acids. Venz and co-workers (Venz et al., 2000) synthesized titania hydrolysates from the hydrolysis of unmodified and modified before hydrolysis by replacement of the via a reaction with carboxylic acids, including acetic, propanoic, and butanoic acids to give rise to amorphous phase.

The above mentioned research work highlights a small portion of work done to evaluate the effect of precursor chemicals. It is obvious that precursors can efficiently help in synthesizing desired NPs to engineer the desired properties.

2.2.5 Control of Crystallite Size in TiO_2 Synthesis

Particle size is always an important parameter which emphasize on the detrimental properties of NPs. Shape and size highly influence the physico-chemical properties of metallic NPs (Brown et al., 2001, Müller et al., 2004). At nanometer scale TiO_2 films exhibited size dependent photo degradation of methylene blue (MB) solution (Doong et al., 2007, Chung et al., 2007) and reaction constant is dependent on the diameter of particles as evaluated by Chen et al. (2004). They studied the effect of the particle size on the photocatalysis and seeding of

NPs. Chen and co-workers (Chen and Elimelech, 2007) studied that particle morphology and photocatalytic activity are correlated.

Highly crystalline anatase TiO_2 and Fe-TiO_2 nanocrystals were fabricated by Mi et al. (2013) in a quick reaction and at low temperature. They found that crystallite size could be controlled with isopropanol and water ratio while crystallinity is a function of reaction temperature. Moreover rutile TiO_2 nanowires were prepared in a one-step synthesis process by mixing TiO_2 with an appropriate amount of H_2O_2 and HCl solution under hydrothermal conditions (Liu et al., 2011c). The morphology of nanowires was controlled by temperature and time.

It was studied by Garvie (1978) that phase transformations were dependent on the grain size. He mentioned that the relative stability in a system is also dependent on the grain size.

In a study by Dai and co-workers (Dai et al., 2010), hydrothermally synthesized highly crystalline nanostructures showed hydrochloric acid concentration dependence of the shape, size and crystalline phase. Anatase NPs were thought to be the result of two HCl concentrations 1 and 8 M, while a hybrid of anatase NPs and rutile nanorods and were because of 2 to 7M. They suggested a new possible TiO_2 nanostructures fabrication method to control different shapes and sizes.

2.2.6 Role of alcohol concentration in NPs synthesis

Wang and co-workers (Wang et al., 2002), synthesized a number of different shapes and sizes of nanocrystalline titania with a solvothermal method in the presence of different alcohol solutions. These structures, grain sizes and morphologies were achieved with a simple variation of alcohol concentrations and reaction conditions. Growth of crystal structures was being governed by HCl concentrations. They found that TiO_2 sizes and shapes were guided by

the CH_2 legends in alcohols. They mentioned that this method might be important in fabrication of different metal oxides NPs.

Four different alcohols; ethanol, propanol, butanol, and octanol, were used to fabricate anatase, rutile, and brookite in a solvothermal process without surfactants, using $TiCl_4$ or $TiCl_3$ as precursors (Yoon et al., 2012). The precursor concentration, pH, and alcohol type were considered important in governing the morphology, crystal structure, and crystallite size titania NPs. This study revealed that alcohol type and, pH and concentration and type of precursors can control size and shape of titania NPs.

Anatase crystalline powders were fabricated with the sol-gel and hydrothermal synthesis methods (Castro López et al., 2011). The water, alkoxide and alcohol ratios along with alcohol type have a marked effect on the photoactivity of the powders. The alcohol dilution increased the photo activity which lessened its negative effect towards the hydrolysis of the alkoxide. Also, the use of branched type alcohols, such as, isopropanol increased the activity of the photocatalyst, possibly with an increase in the available area for UV light absorption.

Zinc oxide and ZnO-coated TiO_2 NPs were synthesized with various alcohol solutions by Byun et al. (2008). The optimized synthesis condition using alcohol solutions and zinc acetate dehydrate of 2.75 wt%, NaOH of 1 wt% and titania of 1 wt%, zinc oxide NPs with 7 nm diameter were obtained within 10 min. Also Mi et al. (2013) synthesized anatase TiO_2 and Fe-TiO_2 nanocrystals with use of isopropanol in a quick reaction with a residence time of less than 10 seconds. They found that alcohol and water ratio determine the size of NPs.

Cubic and hexagonal ZnS NPs were fabricated by wet chemical method using polyvinyl alcohol (PVA) (Thottoli and Achuthanunni, 2013). ZnS nanocrystals of less than 2 nm were

fabricated at two different shapes. Concentrations of polyvinyl alcohol controlled the overall particle growth and different sizes can be controlled simply by varying alcohol concentration. Hexagonal ZnS NPs were prepared at low temperature in the presence of sodium citrate and PVA were used to hydrolyse the ZnS precursors.

The literature review above shows that alcohols and their mixtures with water are important reaction constituent in controlling the properties of NPs.

2.2.7 Characterization of Nanomaterials

There are several approaches to characterize NMs as it totally depends upon the material and characteristics to be studied. Many scientists used a combination of two or multiple characterization techniques to study structural and morphological properties. Armelao and co-workers (Armelao et al., 2007) characterized different characteristics of NPs by using the combined approach of glancing incidence x-ray diffraction (GIXRD). While Cheng and co-workers (Cheng et al., 2006) characterized surface modified NMs by a combination of different equipment like fourier-transform infrared spectroscopy (FT-IR), x-ray photoelectron spectroscopy (XPS), transmission electron microscopy (Garzella et al., 2000) and thermogravimetric analysis (TGA). They used auger electron spectroscopy (Fostier et al.) to study about the thickness of the surface layer. Ke et al. (2008) synthesized a novel photocatalyst WO_3/TiO_2 nanocomposite. The synthesized NPs were characterized by different techniques like XRD, FESEM, TEM and diffused reflectance spectroscopy (DRS). Byun and co-workers (Byun et al., 2008) examined zinc oxide and ZnO-coated titania particles by x-ray diffraction, UV-vis spectrophotometer and high resolution TEM while BET, TEM, SEM, X-ray photoelectron spectroscopy (XPS), FT-IR, UV–visible diffuse reflectance spectra (DRS) and XRD were also used to characterize N-doped titania microtubes by Xu and co-workers (Xu et al., 2008). Irradiated thin films were characterized by Van Overschelde et al. (2007) who used

profilometry, SEM and XRD as characterization techniques. Bojinova and co-workers (Bojinova et al., 2007) used only X-ray diffraction to characterize anatase titanium dioxide NPs.

X-ray diffraction (XRD) was also used by Doong and fellow workers (Doong et al., 2007) to examine properties of stabilized titania porous films while XRD, EDX and TEM were the characterization tools used by Rengaraj and co-workers (Rengaraj et al., 2007). Qamar and co-workers (Qamar et al., 2008) evaluated the effect of sodium and calcination temperatures on shape, phase, surface properties and the photocatalytic activity using the world's most modern characterization techniques. Various spectroscopic techniques were used to characterize phenyl porphyrin and its copper(II) complexes by Chen and co-workers (Chen and Elimelech, 2007). Wang and fellow scientists (Wang et al., 2007b) used Raman spectroscopy, TEM and X-ray photoelectron spectroscopy to characterize the carbon incorporated titania thin films. Kim et al. (2005b) utilized the electron spin resonance (Macé et al., 2006) to study the presence of OH and H_2O radicals on TiO_2 surfaces. It was observed with ESR that the OH radicals decomposed the organic pollutants into more environmental friendly products because of their increased oxidizing power.

The short review of literature above on the use of different characterization techniques shows that it is essential to justify and confirm the research results with standard and state of art techniques.

2.2.8 Colloidal stability of TiO_2 in different media

Colloidal stability of NMs in any media is most basic need of nanotechnology. NMs in stable form are a required commodity for applications in physical and biological disciplines (Wang et al., 2009, Barnard et al., 2004).

NPs are sub-fraction of colloidal system so they behave like colloids when dispersed in a suitable medium. The physical properties of colloidal system are dependent on the high interfacial surface area. This subdivision results in a very (Pierotti and Rouquerol, 1985, Hiemenz and Rajagopalan, 1997, Heurtault et al., 2003). Continuous phase in most common colloidal systems is a liquid. Colloidal system always has dispersed phase of the size range of 1-1000 nm. When this size range changes to 1-100nm, the colloidal system switches to a NM dispersion system.

2.2.9 Colloidal and Nanomaterials stability

Brownian movement of colloids or NPs in a dispersion medium cause collisions of particles with each other. Hence stability of colloids or NMs depends on the interaction between the individual NPs during these collisions. These collisions might be due to attractive or repulsive forces. It is well understood that attractions domination will lead to adherence and hence agglomeration and coalescence and repulsion domination will lead to stability of the colloidal or NM dispersion system (Verwey et al., 1999). If the particles are of similar composition, they have van der Waals forces as primary source of attraction. An adequately strong repulsive force is required which can neutralize the van der Waals attractions making the system stable (Schenkel and Kitchener, 1960).

The van der Waals forces are of three types: i) dipole-dipole permanent forces, ii) the dipole-induced dipole forces and iii) dipole-transitory dipole interactions. Dipole-dipole and dipole-induced are short range weak interactive forces while the London forces are longer range strong forces of attractions. For this reason, only van der Waals London forces (VDWL) of attraction are considered important to determine the stability of either colloids or NPs.

2.2.10 Methods for stabilizing Nanomaterials and colloids

Similar colloidal or nano particles always possess strong van der Waals London forces, so to disperse or stabilize them or keep them apart from each other, it is very much necessary to impart strong repulsive interactions. Such repulsive interactions should be at least strong enough to overcome the attractive forces between colloids or NPs. Generally, there are three parameters by which we can impart stabilization for colloidal or nano systems:

1. **Electrostatic or charge stability** (to effect EDL).
2. **Steric stability** (by adsorbed or attached polymer molecules).
3. **Depletion stability** (by free polymer molecules in the dispersion media).

If we combine first two methods of stabilization, it will be called electrosteric stabilization. Second and third methods of stabilization are achieved by the addition of polymers; hence they are called polymeric stabilization.

2.2.10.1 Electrostatic stabilization

Colloidal particles in polar liquids can be stabilized by Columbic repulsion forces to overcome the VDWL attractions. If ionic groups are added in a liquid dispersion media, they stick to the surface colloids or NPs through various arrangements making a charged layer. A charge-neutral double layer will be the result of wrapping of colloids or NPs with an equal number of counter ions having opposite charges. Stability mechanism is simply overcoming these forces which are imparted by surrounding particles to weaken the EDL. Ionic strength of the suspension always determines the thickness of EDL (Pookmanee et al., 2004). The electrostatically stabilized colloids or NPs aggregate or coagulate with an increase of the ionic strength of dispersion medium (French et al., 2009, Napper, 1970). So this is great disadvantage of charge stabilization of colloids or NMs as it is very sensitive to ionic strength of the

dispersion medium. Also it can't work for non-polar liquids those can't dissolve the electrolytes. Main advantages of this technique are low cost, quick results and simplicity which give it an extended use for stabilization of aqueous media dispersions.

2.2.10.2 Polymeric stabilization

The weakening of VDWL attractive forces by polymer chains with high molecular weights, hence imparting stability by generating repulsive forces (Vrij, 1976). So polymers are thought to be best stabilizing agents with more long lasting stabilization. The disadvantages of polymer stabilization include the high cost of polymers and in some cases polymers are either reactant with other constituent of the medium or can serve as food for some microorganisms.

Polymeric stabilization of colloidal suspensions is divided in to two different types: steric and depletion stabilization.

2.2.10.2.1 Steric stabilization

Steric stabilization of colloids or NPs is a process when polymer macromolecules are attached on the surface of colloids or NMs (process also called as grafting or chemisorption). Thus the stabilization because of the adsorbed layers of polymers on the dispersed particles is generally known as steric stabilization.

2.2.10.2.2 Depletion stabilization

Depletion stabilization of colloids or NPs is a process when polymer macromolecules are free in dispersion solution. When we combine both electrostatic and steric methods of stabilization, it is called electrosteric stabilization. Overall net charge on colloidal or nano particle surface and other charges those come through a polyelectrolyte in the solution can impart the electrostatic component in the system. If dispersion medium is dominated with higher concentrations of free polymer, the depletion and steric stabilization combine frequently. Depletion stabilization can combine to any of the steric and/or electrostatic stabilization depending on the availability of free polymer macromocules.

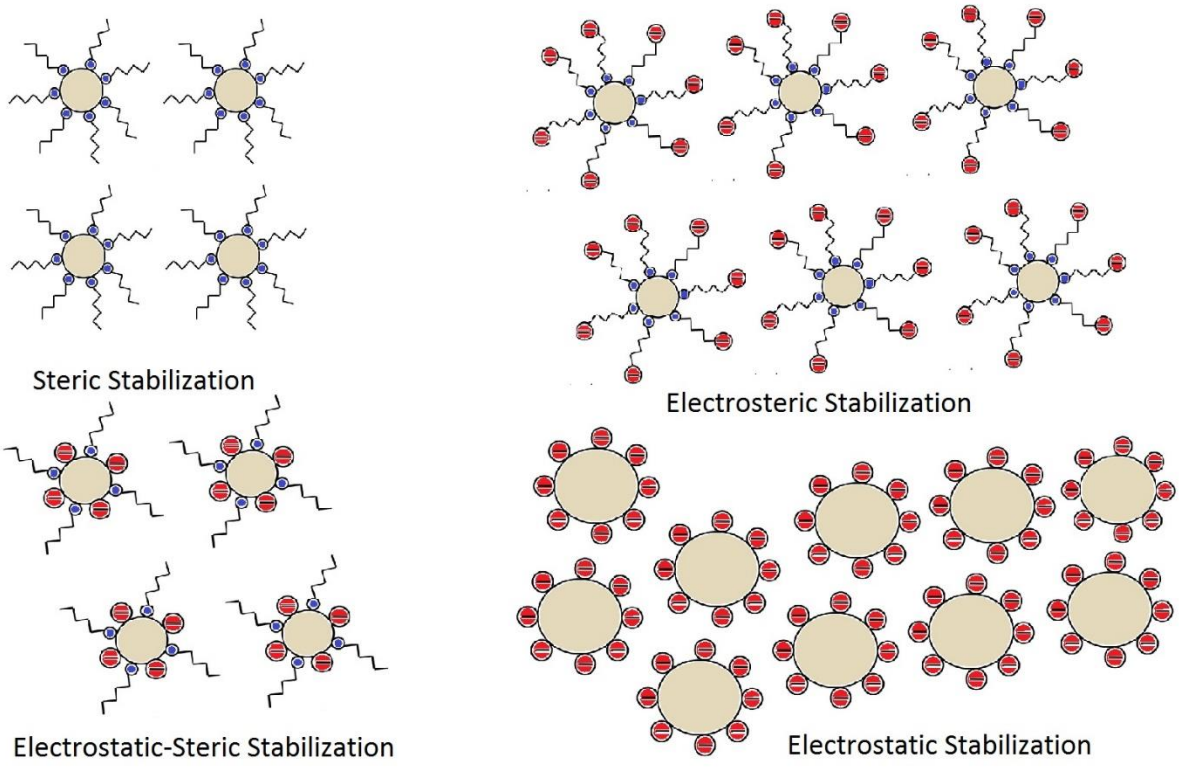

Figure 2.6: Types of colloidal/NPs stabilization

Charge stabilization in a colloidal system is induced by electrostatic repulsion between particles (Zhao et al., 2004). In one study Turkevich elaborated that the surface of citrate-

capped gold NPs (AuNPs) contained a net negative charge which stabilized them against <10 mM Na^+ for a longer duration (Turkevich, 1985). London attractive forces are the main reason of aggregation when particles approach each other (London, 1937, Enustun and Turkevich, 1963). The electrostatic forces can stabilize the particles but this stabilization is not strong enough against salt concentrations. To overcome electrostatic forces barrier, particles surface might be coated with polymers of higher molecular weight preferably greater than London interaction range (PEG, PVP etc.) to achieve steric stabilization (Latham and Williams, 2006). To avoid the blocking of particle surface by polymer layer, electrostatic and steric stabilization could be combined. A hybrid NP-DNA conjugate gave best value by combination of electrostatic, optical and structural properties. This was achieved by Mirkin and fellow scientists (Mirkin et al., 1996) when thiol capped DNA oligo-nucleotides were attached to the surfaces of Au NPs, which bind to Au by combination of electrostatic and steric stabilization process.

2.2.11 Use of surfactants for stabilization of Nanomaterials

Properties like size, porosity and stability of TiO_2 suspensions could be achieved simply by a careful selection of surfactants and salts during the fabrication process (Eiden-Assmann et al., 2003). Surfactants are of scientific interest because they are used in many practical applications ranging from crude oil recovery to drug delivery. Previous researches show that surfactants are being continuously used in the synthesis and stabilization of different NPs (Wu et al., 2011, Morsy, 2014, Yang et al., 2010, Alkilany and Murphy, 2009, Baier et al., 2014). All surfactants molecules consist of two parts; hydrophobic (water insoluble hydrocarbon chain or silicone) and hydrophilic (water soluble ionic group) (Farn, 2008).

It was investigated that adsorption polymers like PVP, PEG, PVA, and poly-ethylene oxide (PEO) modify the surface of NPs and hence improve the stabilization of the dispersion avoiding aggregation and settling (Lakhwani and Rahaman, 1999, Chibowski et al., 2000).

Nonionic polymers adsorb different molecules on their surfaces through hydrogen bonding. The polymers added to a suspension adsorb onto the surface of the metal oxide by different chemical and electrostatic mechanisms, van der Waals forces and hydrogen bonding (Zhang et al., 2003). Hydrogen bonding in this case is by surface absorption and/or reaction with smaller particles, like stearic acid, surfactant $C_{18}H_{37}O$ $(CH_2CH_2O)10H$ etc. (Zhang et al., 2003).

Stability varies from medium to medium and material to material, however in the body of living organisms cell culture media is very important to control stability. TiO_2 dispersion was improved with addition of bovine serum albumin (BSA) in different media. Fetal Bovine Serum (FBS) also proved to be an impressive stabilizing agent for TiO_2 NPs in various media because it contains several protein contents.

2.2.12 Stability of nanomaterials effected with natural organic matter

Natural organic matter (Yamago et al., 1995) is another constituent of the aqueous and subsurface matrices which enhance stability. NOM has been studied by many eminent scientists to affect the stability and transport in porous media for fullerenes, CNTs or quantum dots (Chen and Elimelech, 2007, Navarro et al., 2009, Godinez and Darnault, 2011a). There are several other studies on the interaction of NOM colloids showed that their physico-chemical properties were modified imparting stability (Franchi and O'Melia, 2003, Mylon et al., 2004, Handy et al., 2008a, Pelley and Tufenkji, 2008). Mylon and co-workers (Mylon et al., 2004) studied that the main procedure of stabilization by NOM is electrostatic and steric repulsions

even at higher ionic strengths. In few other studies scientists showed that high concentrations of divalent electrolytes destabilize the suspension because cations make complexes with NOM.

Zhang and co-workers (Zhang et al., 2009) evaluated the stabilization of engineered oxide NPs as a function of NOM and divalent cations. A concentration of 10 mM KCl can impart aggregation of NPs in neutral waters, while only 1 ppm NOM gives the net negative surface charge on NPs reducing their aggregation. A concentration of 4 ppm NOM stabilized almost every NP with pushing zeta potentials to −30 mV or higher. While looking adversely, divalent ions can cancel the effect of NOM on NPs surface, hence destabilizing them. It was noted that 40-60 mM Ca^{2+} could aggregate the NOM stabilized NPs.

The interaction of Suwannee River humic acid (SRHA) with iron oxide nanoparticles was investigated by Baalousha et al. (2008). They revealed that highly acidic pH dissolved about 35% of the total iron, but when pH goes more than 4, hydrolysis makes new particles. Aggregation of NPs started at pH 5-6 with a maximum increase at pH 8.5 in general synthesis conditions. When SRHA added, aggregation occurred at pH values of 4-5 and mainly governed by the SRHA concentration. They studied that approximately 1 nm thick layer on the surface iron oxide nanoparticles was developed by SRHA and this layer increases with an increase in SRHA concentration. From the study it is evident that pH and SRHA concentrations guide the aggregation structure and its mechanism.

In another study Baalousha (2009) evaluated the effect of NOM on the aggregation behaviour of iron oxide NPs. It was revealed that NPs concentration promotes aggregation at a pHzpc. Typically, higher concentration of 100 ppm alters the PZC of NPs giving them extra stability while low concentration of 10 ppm showed no effect on aggregation behaviour. NPs were more stable with start of disaggregation at pH 7 and >50 ppm of SRHA while 10 ppm or less concentration of SRHA showed no effect on disaggregation. The sorption of SRHA

molecules imparted surface charge on NPs which was thought to be the possible effect of disaggregation and stability. They divided disaggregation into two regimes of fragmentation and erosion which were dependent on SRHA concentrations, a fast regime followed by slow regime over a period of 15 days.

The effect of NaCl or $CaCl_2$ electrolytes on the aggregation kinetics of TiO_2 NPs stabilized with SRHA was studied by Thio and co-workers (Thio et al., 2011). They revealed that SRHA significantly increased the stability because of electrostatic and steric repulsions among TiO_2 NPs. Zeta potential was proved to be an important tool in prediction of the interaction forces within particles or with particles and collector surfaces giving an idea of aggregation and deposition behaviour. SRHA layer suggestively stops TiO_2 deposition onto silica surfaces even at very high ionic strength, giving an idea about the transport of these NPs in natural aqueous matrices as all natural waters has substantial concentration of NOM.

2.2.13 Aggregation kinetics of Nanomaterials

PVP and sodium citrate coated silver NPs (AgNPs) were studied for time-resolved aggregation kinetics with use of dynamic light scattering (DLS). It was shown that divalent electrolytes induced more destabilization for the citrate AgNPs, as compared to the PVP AgNPs, because of polymer induced steric repulsion with PVP. More stability was observed with humic acid where macromolecules were adsorbed on surface of AgNPs. Higher concentrations of $CaCl_2$ boosted aggregation in the presence of humic acid because bridging between NPs due to humic acid (Huynh and Chen, 2011).

French et al. (2009) measured aggregation kinetics of nano-TiO_2 with different ionic strengths and electrolytes. An ionic strength of 4.5mM gave stable aggregates of 55±5 nm size at acidic pH. Same pH gave very big aggregates at 16.5 mM NaCl concentration. They

discussed that with basic pH, aggregates are formed quickly as compared to acidic pH values and divalent cations enhance aggregation of TiO_2.

Aggregation kinetics of gold NPs using both experimental and mathematical modelling techniques revealed that replacement of citrate groups with benzyl mercaptan was the main reason of aggregation (Kim et al., 2008). It was found that aggregation of first 11 gold NPs might be giving first colour change of gold NP suspension. Hence the aggregation of Au-NPs can be monitored with the initial change in colour of suspension.

Chemical nature of the electrolyte cations is important in aggregation of titania NPs as studied by Ismagilov et al. (2012). Li^+ was thought to be the least aggregation cation followed by Na^+ and NH_4^+ while the use of phosphate buffers for sol formation gave more stabilized TiO_2.

2.3 TiO_2 mobility in different porous media

In the current scenario of NM's industrial synthesis and use, the knowledge on transport and behaviour of these materials in the complex aqueous matrices is a pre-requisite. While considering the mobility of NMs in real environment, there are many factors which may be responsible for such a transport. Although interaction of NMs with the porous media is an important factor, it is not only limited to this interaction. The interaction between NPs, interaction between NPs and suspended colloids, the interaction between NPs and other organic and inorganic constituents, pH and electrolyte concentration are few of other factors which might be held responsible for the fate and mobility of NMs in real environmental context like soils and aquifers. Realistically, NMs may be deposited with the pore spaces due to their interaction with porous media (aggregations) or they may speed up their travel through pores due to interaction with organic constituents of environment (dis-aggregation). Industrial

processing and use of different NMs and/or their interaction with natural organic matter usually impart new characteristics and stability, hence changing their behaviour and hazard (Labille et al., 2010).

It is typically assumed that there will be very less or low aggregation of TiO_2 NPs in porous media but chemistry of the medium determines the actual fate of NMs. Chemistry of the medium alters the mobility and retention of NMs in different porous media. When chemistry favours more sticking efficiency, more aggregation occurs and transport of these materials through the column is relatively fast. But if sticking efficiency of NPs and collector surface (porous media) is more and favoured by the solution chemistry, NMs retain within the system (Labille et al., 2010).

Chowdhury et al. (2011) conducted a series of experiments to study the effect of chemistry, NPs concentration and hydrodynamic properties in the mobility and retention of TiO_2 NPs through sandy porous media. Results specify that DLVO-type interactions including straining, aggregation, blocking, and ripening are determining factors of such a transport. Factors like pH, ionic strength, NPs concentration and flow velocity are the controlling parameters of retention and removal. Acidic conditions favour more particle removal while on neutral pH and beyond particles tend to aggregate, favouring retention. Same is the behaviour of ionic strength where low ionic strength favours removal and high ionic strength favour retention. Also removal increased with increased flow rate while more retention occurred with a decreased flow rate.

NMs transport and retention experiments by Chen et al. (2011a) showed ionic strength as retention controlling parameter in column because NPs retention profiles displayed an increased NP retention at the end of the column. KCl and $CaCl_2$ solutions increased the deposition of the NP aggregates as per traditional DLVO theory. Overall experimental results

confirmed that NMs mobility and retention is governed by the combination of nanoparticle aggregates depending on pH, ionic strength, moving distance and DLVO interactions.

Fang et al. (2009b) studied the stability and mobility of TiO_2 NPs in saturated homogeneous soil columns experiments. They studied that lower ionic strengths help the TiO_2 to pass through the columns but high salinity and clay contents increased the retention in soil media. The size of the aggregates observed at the far end of column was significantly high as compared to the start of experiment.

Boncagni et al. (2009) studied the transport TiO_2 NMs in laboratory flume, column, and batch experiments. They showed that commercial NPs (P25 TiO_2) are more prone to aggregate as compared with laboratory synthesized NPs. Due to this reason, commercial TiO_2 deposited at a faster rate than the synthesized TiO_2 in the streambed. All NMs which were retained in the streambed were easily released with an increase in stream velocity. The aggregation and deposition were controlled by on pH.

Keller et al. (2010) conducted a number of experiments on mobility, aggregation and sedimentation of three different metal oxide NPs i.e. TiO_2, ZnO and CeO_2 different aqueous media. They showed that natural organic matter (Yamago et al., 1995) adsorption on the surface of these NMs imparted stabilization, significantly reducing their aggregation, under most of the environmental conditions.

2.3.1 Applications of Nanocrystalline TiO_2

When concept of nanotechnology is associated with environmental science and engineering to synthesize nanostructured functional materials which are used for environmental remediation, the technology is known with the term “environmental nanotechnology”. Consequently, controlling materials at the nano-level can accelerate the

development of new types of products with improved properties and functionalities for environmental applications (Liu et al., 2005).

Almost all environmental pollutants can be degraded by TiO_2 photocatalytic systems as mentioned by Matos et al. (2001) who applied titania for photocatalytic degradation different pollutants including phenol, 4-chlorophenol and herbicide 2,4-dichlorophenoxy-acetic acid in the presence of two different commercial activated carbons. Also Wu et al. (2004) photocatalytically degraded 1,2,3,6,7,8-hexachlorodibenzo-*p*-dioxin and octachlorodibenzo-*p*-dioxin with immobilized titania, zinc oxide and SnO_2 films under UV light of 300 and 450 nm wavelength. Robert et al. (2004) used TiO_2 for the photodegradation of 4-hydroxybenzoic acid and benzamide under solar irradiation. Chiang et al. (2004) used different TiO_2 photocatalysts at pHs 3 and 10 for degradation of Bisphenol A. They found that pH and different oxidation govern the mineralization of BPA at pHs 3 and 10. Figgemeier and co-scientists (Figgemeier et al., 2007) evaluated TiO_2 films for their photocatalytic activity to degrade of 4-chlorophenol in the presence of UV illumination. (Yu et al., 2002) used transparent anatase titania films on soda-lime glass and fused quartz for photocatalytic oxidation of acetone in an air environment. Lin et al. (2004) studied the photocatalytic degradation of ethylene over titania-based photocatalysts under a non-circulating system using visible or near-UV light. Alvaro et al. (2004) compared self-synthesized TiO_2-NPs and P-25 titania standard for degradation of phenol and aniline in water with strong efficiency of self-synthesized titania over P-25. Blount et al. (2001) studied degradation of acetic acid, acetaldehyde and toluene by TiO_2 photocatalyst.

Chung et al. (2007) tested photocatalytic performance of the titania films for photocatalytic degradation and antimicrobial efficacy for medical grade AISI 304 and JIS Z2801:2000 industrial standard respectively. Zlamal and co-workers (Zlamal et al., 2007)

photocatalytically degraded acid orange 7 with nanotube layers/Ti structures as photo-anodes in the presence of UV light.

Acher et al. (1997) used sunlight or artificial UV radiation for photochemical disinfection of water while Arana and his group (Arana et al., 2002) applied solar TiO_2-photocatalysis to waters from a natural wastewater treatment plant in the Universidad de Las Palmas de Gran Canaria.

Titanium dioxide photocatalysis is much important for solar degradation as concluded by Ljubas (Ljubas, 2005) that solar radiation alone does not have enough energy for sufficient degradation of Natural Organic Matter (Yamago et al., 1995) in drinking water, but in combination with heterogeneous photocatalyst-titanium dioxide, with or without other chemicals, the degradation potential could increase.

The literature reviewed above shows different uses of TiO_2 in different fields specially photodegradation which shows increased demand of such materials (other than that of industrial purposes) in current and future scenario.

2.3.2 Hypothesis

The research work during this study was mainly technology driven rather than hypothesis based. Few studies planned were hypothesized e.g. the first hypothesis which governs this study was "Size, phase and aging of TiO_2 NMs play an important role in their behaviour in natural water systems". Many experiments were conducted and reported in this thesis. Size and phase was controlled by pH, temperature, precursors and alcohol water ratios. Different shapes and sizes of TiO_2 nanomaterials were fabricated and studied for their stability in different media. Lastly, two different shapes were studies for their transport through different type of porous media to prove the concept.

Secondly “Properties of engineered NMs get affected with strong interactions with natural colloids and humic substances”. To test this hypothesis, different types of TiO_2 nanomaterials were stabilized with five different types of stabilizing agents including humic substance SRFA. The aggregation kinetics of such stabilized nanomaterials were then studied with different type of salts. In end stabilized nanomaterials with humic substances were found to be more actively transported in different types of porous media proving that behaviour of nanomaterials gets affected by the constituents of natural environments.

2.3.3 Conclusion

From the reviewed literature it is obvious that there was much done on TiO_2 NMs but still there are gaps to understand the total chemistry of synthesis and interaction of TiO_2 NPs with environmental constituents. To understand the environmental behaviour of TiO_2 NMs, a comprehensive study on synthesis with a synthesis control on the properties of the resulting material, its complete aggregation kinetics and transport behaviour in a porous media under different media, is much needed.

The current research was initiated with the idea that manufactured NPs can be traced in an environmental system if we can control their chemistry. Understanding of complete chemistry will certainly help to engineer NMs as per environmental monitoring requirements. For this purpose, a detailed synthesis behaviour of titania NMs at different synthesis conditions was studied along with its aggregation kinetics and mobility in a simple and complex porous media. This thesis addresses all of the above mentioned issues.

Chapter 3

MATERIALS AND METHODS

3.1 Introduction

The thesis research work was divided into three phases. The first phase is the synthesis of TiO_2 NMs using sol-gel and hydrothermal methods. The focus of the synthesis part of research work was the determination of each variable's effect on the structure and morphology of synthesized NMs. The independent variables included pH, gel drying/calcination temperature, different stabilizing agents and precursors. With use of three precursors (titanium isopropoxide, $TiCl_3$ and $TiCl_4$), different shapes and sizes of TiO_2 NMs were prepared by varying alcohol water ratios and mixing different concentrations of alcohol solutions.

The second phase focuses on the stabilization of TiO_2 NPs using different coatings (PEG, PVP, Sodium citrate, SDS, SRFA) and the aggregation kinetics of TiO_2 NPs in mono and divalent electrolytes ($NaNO_3$, NaCl, CaN_2O_6, $CaCl_2$). The aggregation kinetics was performed on the sodium citrate and SRFA-coated TiO_2 NMs. Two different types of morphologies of TiO_2 NMs were used during these studies i.e. round anatase NPs and rutile ellipses.

In the third phase the stabilized nanomaterials were checked for their mobility through different natural and synthetic porous media (sandstone and glass bead columns). The mobility studies were firstly modelled on the basis of DLVO theory and then evaluated experimentally. This chapter demonstrates; the experimental methods, the analytical techniques and the theoretical background, used during this research work.

3.2 Materials

Titanium isopropoxide, titanium trichloride and titanium tetrachloride were of analytical grade and were purchased from Sigma Aldrich. All other chemicals used throughout this research work were of analytical grade or higher and were used as purchased from different commercial vendors (Fisherscientific, Aldrich, Sigma) without any further purification. Suwannee River fulvic acid (SRFA) was purchased from the International Humic Substances Society (IHSS). Ultra-high purity water (18.2 $M\Omega cm^{-1}$) was used throughout the experiments. 300 mesh size Cu grids coated with holey carbon were used for TEM analysis.

3.3 Synthesis of titanium dioxide

TiO_2 NMs were synthesized using three precursors: titanium isopropoxide (TTIP) for TiO_2 nanopowder, $TiCl_3$ and $TiCl_4$, for stabilized TiO_2 suspensions. The detailed methodology for each precursor is discussed as follows under three different headings.

3.3.1 Synthesis of TiO_2 nanopowder

In an optimized synthesis procedure for TiO_2 nanopowder, 25 ml volume of titanium isopropoxide was vigorously mixed with 25 ml absolute ethanol. Resultant solution was ultrasonically mixed for 10 minutes to form a mixture. The ultrasonic bath used during the synthesis process was Grant XUBA5 with 150W heating power. The obtained mixture was then magnetically stirred for 3 hours after drop wise addition of 10ml of de-ionized water. It is much better to use a spray gun that can make a fine mist by optimizing its flow for volume in one press (Puetz et al., 2003). As per methodology of synthesis given by Yang et al. (2005), pH was maintained at 4 by using HCl and NaOH. The resulting "sol" was kept for 72 hours aging period followed by drying at 100^oC for 24 hours. The test conditions like pH, quantity

of precursor and drying temperature were chosen and modified on the basis of optimization work done by Yang et al. (2005). The obtained sol was turned to viscous gel with hydrolytic polycondensation. The gel was calcined at 700°C for couple of hours to produce the TiO_2 NPs. A schematic diagram of the process for producing TiO_2 sol is shown below in Figure 3.1.

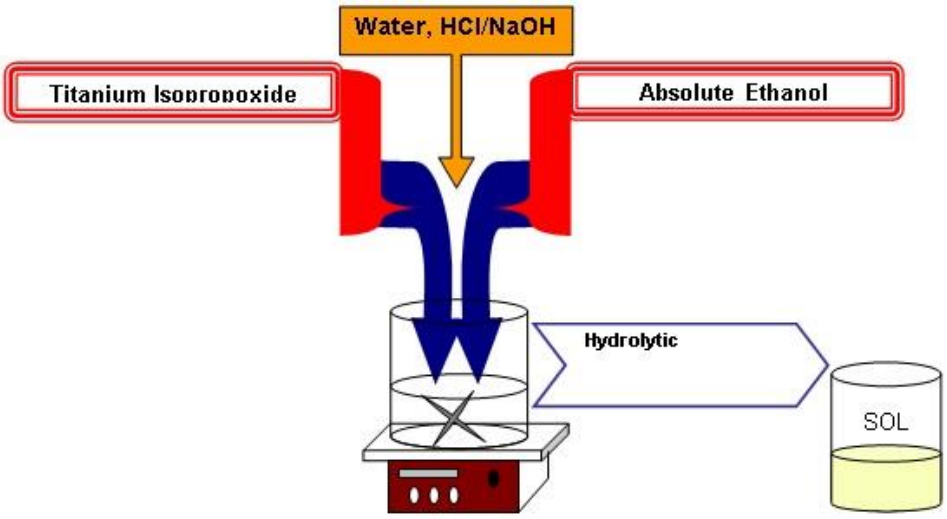

Figure 3.1: A schematic diagram for producing titania sol

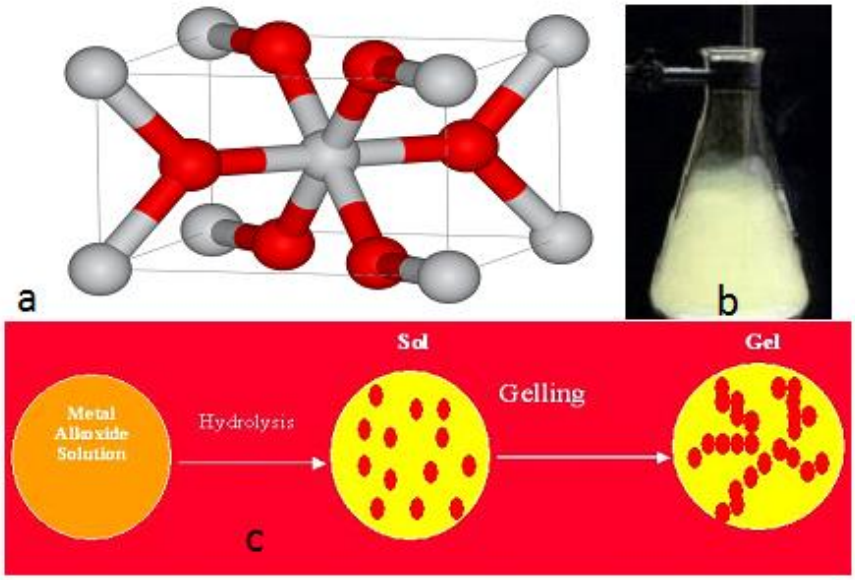

Figure 3.2: a) Structure of Titanium Isopropoxide b) Titania Sol c) Sol and Gel formation from metal

During the whole process of sol-gel synthesis of TiO_2 NPs following reactions take place.

$$Ti(OR)_4 + 2H_2O \longrightarrow TiO_2 + 4\ R\text{-}OH \quad \text{(Hydrolysis)}$$

$$Ti[OCH(CH_3)_2]_4 + 2H_2O \longrightarrow TiO_2 + 4\ (CH_3)_2CHOH$$

3.3.1.1 pH studies for TiO_2 synthesis

During the whole research work, pH was adjusted with HCl and NaOH and measured using Hanna 8521 pH and conductivity meter. Different types of samples were prepared at pH values from 1-11. The influence of pH values on the particles agglomeration, size, phase transformation and surface structure has been investigated at four gel-drying temperatures as described below. pH was adjusted during the hydrolysis step. The synthesis methodology was modified only for the pH value which was optimized at 4 in previous research work (Kumar and Raza, 2009).

3.3.1.2 Temperature studies for TiO_2 synthesis

To study the effect of temperature, the above methodology was tried for four different temperature values. For all pH samples four gel-drying temperatures i.e. room temperature, 100^{o}C, 400^{o}C and 700^{o}C to clarify the effect of gel drying temperature on TiO_2 phase transformation.

3.3.2 Synthesis of TiO_2 suspension

For synthesis of TiO_2 suspensions, $TiCl_3$ and $TiCl_4$ precursors were used because TTIP is usually used for quick hydrolytic polycondensation and requires calcinations of gel for final product. While both titanium trichloride and tetrachloride give direct ripening of nanoparticles at room or near room temperature. So control of shape and size is relatively easy for both precursors.

In a typical synthesis, 4.17ml of 1.5 molar $TiCl_3$ was added to 250ml of agitated distilled water. Soon after adding $TiCl_3$, the colour of water turned violet. The pH of the system was measured as highly acidic (1-2.8) and adjusted to 3.8 for rutile and 4.0 for anatase (room temperature and microwave treatment), using of NaOH and HCl. After adjustment of pH to desired level, the colour of suspension became bluish black which turned to white colour after overnight stirring at room temperature for rutile synthesis. While for anatase synthesis, the as prepared black suspension was shifted to Teflon lined tubes and refluxed in a microwave oven at 110^{o}C for an hour duration. The power of microwave was adjusted at 1200W and temperature was ramped 3^{o}C per minute, while pressure was set at 350PSI.

Nanocrystalline TiO_2 suspensions were fabricated by hydrolysis of $TiCl_4$. In the first step $TiCl_4$ was diluted with 5% solution of HCl (36%). In a typical step 1:19 acid water ratio was set to give solution 1. $TiCl_4$ was diluted to 1mol/L in solution 1 in an ice bath. Solution 2 was prepared as ratios of different alcohols and water (1:2 Eth:Water, 1:2Meth:Water and 1:2Ace:Water). Both solutions 1 and 2 were mixed to get 0.1mol/L final concentration of $TiCl_4$. Ice cooled temperature was maintained throughout the preparation process. Final solution was stirred at different temperatures including room, 45^{o}C, boiling point and 110^{o}C (microwave for 40 minutes in Teflon lined vessels). In last NPs three repetitive washings were given to NPs by ultrafiltration and/or centrifugation.

3.4 Nanoparticles clean-up

After synthesis process, cleaning of NPs is important to remove the unreacted chemicals. There are several methods to clean NPs after reaction. In this research work two different NP's cleaning processes were used. Ultrafiltration was used to remove all unwanted chemicals from NPs suspensions while ultracentrifugation was used where desired end product was in powder form. Both cleaning methods are briefly discussed here under.

3.4.1 Nanoparticles washing by ultrafiltration

It is a separation process in which high pressure is used to pass liquid and dissolved reagents through a porous membrane. In the whole process NPs are too big to pass through membrane pores.

Millipore stirred ultrafiltration cell model 8400, with filters of cellulose membrane of 1 kDa pore size and diameter of 47 mm, was used (Figure 3.3). The filters were pre-soaked in 2% HNO_3 and were thoroughly rinsed with milli-Q water before use. At least 100ml of milli-Q water was filtered before the final filtration in order to eliminate any impurities. This was repeated at least two times.

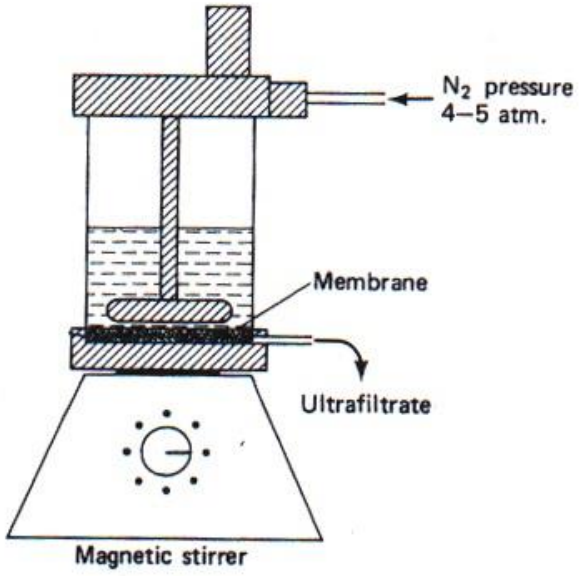

Figure 3.3: A schematic diagram of the ultrafiltration process

3.4.2 NPs washing by ultracentrifugation

Ultracentrifugation is a technique in which sample is rotated at very high speed (up to 40000 rpm in some cases) so that the NPs settle down in a sampling tube while unused reactants remain in supernatant. Supernatant was discarded and the process was repeated with an alcohol

or water or mixture of both. In some cases, alternate alcohol water washings were given to clean the excessive reactants after a reaction. The ultracentrifugation equipment used in this research work is the temperature controlled Beckman XL-I analytical ultracentrifuge.

3.5 Stabilization of titanium dioxide suspensions

If NPs in suspension experience no change in their agglomeration and/or aggregation state over period of time, the suspension is called stable suspension. Stability of NPs is desired for most applications especially for getting reliable results for NPs toxicology studies. Factors which influence the interactions between particles (like surface properties, ionic strength, ionic composition, pH, concentration of NPs, sticking coefficient) and forces on these particles are important in controlling the stability of NPs. A suspension of NPs with low surface charge that does not experience a change in surface charge is likely to be unstable. So, it is level of surface charge which makes a suspension stable. As a rule of thumb, if the particles have a zeta potential >±30 mV, they are considered stable. Addition of salts in an aqueous medium increases the ionic strength and hence their sticking efficiency increases when opposite surface charges attract each other. Addition of salts can alter zeta potential when salt ions will influence the electrostatic double layer (Handy et al., 2008a) by decreasing its thickness. This decrease in thickness of electrostatic double layer, allows two nano-TiO_2 particles to come more close to each other by attractive force giving rise to aggregates (Jiang et al., 2009a). The collision rate between NPs and the sticking efficiency after these crashes define the stability of NPs. So sticking efficiency could be used to predict the ability of NPs to aggregate. The collisions between NPs result from Brownian movement and local mechanical stirring (Hogg et al., 1966). But due to minute size of the NPs, the local mechanical stirring has no weighty effect and the only driving force for aggregation is the Brownian motion.

Another factor affecting the stability of NPs in water is the pH value of the medium. Surface ionization is the process which controls the surface charge of metal oxides dispersed in water, including TiO_2 (Morrison and Ross, 2002). Morrison and Ross elaborated that the isoelectric point is the neutral point where there is no net charge on NPs (5.8 for TiO_2). The value to zeta potential is more (either +ive or –ive) when pH value is far from the isoelectric point increasing repulsion between particles. Limiting aggregation by increasing repulsion between particles is called electrostatic repulsion.

3.5.1 Mechanisms of Nanoparticles stability

In literature two types of stability mechanisms are reported: electrostatic stabilization and steric stabilization. Figure 3.4 shows the basic concept of both types of stabilization processes. Both mechanisms have its merits and demerits according to particulate systems (D. H. Napper, 1986).

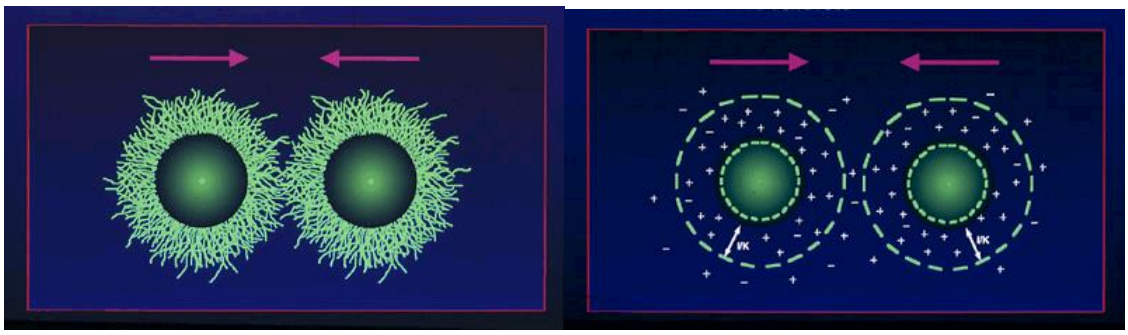

Steric Stabilization Electrostatic Stabilization

Figure 3.4: Types of colloidal stabilization mechanisms (PAAL, 2014)

3.5.1.1 Electrostatic Stabilization

In electrostatic interaction the surface charge affects the scattering of nearby ions in the polar medium. Surface charge plays an important role in electrostatic stabilization of NPs. The surface charge is a result of interaction between solids and liquids interfaces in the polar

medium of colloidal suspensions. The electrostatic stability is a result of balance between attractive and repulsive forces of particle interaction. Theoretically, one can imagine that it is an easy process but practically the configuration of NPs in a suspension is not that simple. NPs arrange themselves in layers having different chemical configuration. The interaction between NPs and ions give rise to electrical double layer (Figure 3.5). The suspension consists of positive ions called counter ions (+ive charge) and negative ions called co-ions (-ive charge). The counter ions can be either positive or negative, depending on the surface charge of the particles. For negatively charged NPs, the counter ions are those that have a positive charge; whereas for positively charged NPs, the counter ions are those that are negatively charges. Electroneutrality principle tells that counter-ions should be attracted towards the NP surface. Few counter-ions make a Stern layer on NP surface which is a firm layer and adhere very strongly on surface of NPs. The potential developed due to Stern layer is called stern potential. The remaining counter-ions make Gouy-Chapman layer due to Brownian movements. Counter-ions have the highest concentration close to surface NPs as compared to lowest concentration for co-ions. The phenomenon of electrophoresis develops when ions stick to the NPs on an area of shear plane between Stern layer and Gouy-Chapman layer. These ions move along the NPs surface when and external electrical field is applied. The electric double layer gives the electrostatic stability to NPs.

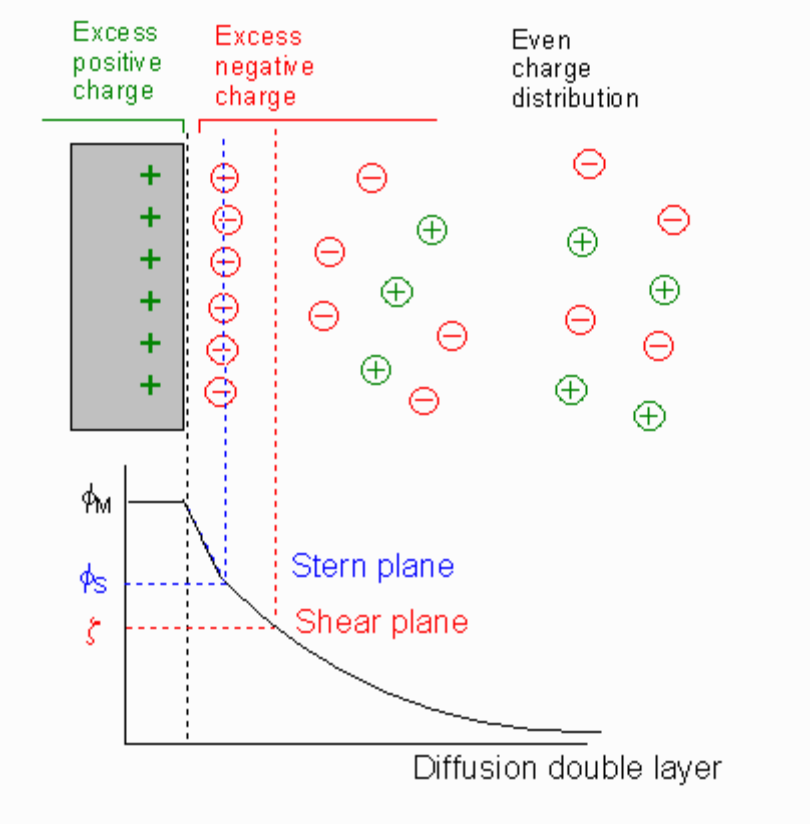

Figure 3.5: The electrical double layer (NMSU, 2014)

3.5.1.2 Steric Stabilization

Steric stabilization of NPs is a process in which a suitable polymer is added to stabilize a suspension. The polymers adsorb on the NP surface causing repulsion. These polymer molecules in solution make a surface coating on the NPs. There are two types of polymers called homopolymer and copolymer. The surface polymer layer gives the attractive force between NP surface and polymer and also provides a repulsive force among individual particles. Such stabilization is also called “Polymer-induced stability”. Steric stabilization of the colloidal dispersion is attributed to the long chain molecules of colloidal particles. On approaching close to each other, particles get repelled by stabilizing polymer action. The phenomenon can be well understood when compared with electrostatic stabilization method discussed in next section.

3.5.2 Stabilization with addition of different surfactants

Several surfactants including PEG, PVP, SDS, sodium citrate and SRFA were used to stabilize TiO_2 NPs. Different concentrations of surfactants (0.3% for PEG, PVP, SDS and sodium citrate while SRFA concentrations were optimized separately for 10, 25, 50, 75 and 100ppm) were mixed and the resultant suspension was sonicated for different periods of time (from 10 minutes to 12 hours) and tested for their stability immediately after mixing and then for over a period of two weeks.

NOM is an important stabilizing agent and it can also affect the aggregation behaviour of NPs. Steric stabilization was the proposed mechanism by Domgos et al. 2009 for different NPs including TiO_2. In steric stabilization the NOM gets adsorbed onto the NPs, physically prevent two particles from approaching each other (Chen and Elimelech, 2007). Zhang and co-workers (Zhang et al., 2009) gave another proposed mechanism of NOM stabilization, in which they were of the thought of surface charge or electrostatic stabilization was the main cause of NOM stabilization. This is because of presence of negative charge on NOM which alters the surface charge on NPs, measured in terms of zeta potential of NPs. In a nutshell, the two mechanisms (charge and steric stabilization) work together to stabilize the NPs i.e. NOM induces electrosteric stabilization effect. The presence of salts in media alters the effect of NOM on the aggregation of NPs by breaking the intermolecular bridging of aggregates and nanoparticles thus decreasing aggregation. The concentration of NOM is also important in defining the aggregation state of NPs as a low concentration of 10ppm SRHA didn't affect the aggregation kinetics of NPs while a concentration of 100ppm demonstrated a pronounced affect (Baalousha, 2009). The presence of mono- and di-valent cations affect the aggregation of NOM coated NPs. The aggregates in a suspension form bridges between NPs clusters in the

presence of background mono- or di-valent electrolyte solution (Chen et al., 2006). Thus mono- or di-valent electrolyte solution encourages enhanced aggregation of the NPs.

3.6 Characterisation techniques

NP characterization is always needed to evaluate the desired characteristics of NPs. Multiple techniques were usually used to avoid any sort of error in the process. In NPs characterization, the most important parameters are their size, shape and phase in case of TiO_2 NPs. In current study, the particle size was measured using DLS and TEM and zeta potential was measured using laser doppler electrophoresis. TEM was used to study the topography, morphology, and crystallographic properties of the NPs.

NP crystalline phase was determined by powder X-Ray diffraction (D-8 Advance with PANalytical X'pert Pro). Powdered samples were collected by drying NPs at room temperature in air environment. Concentration of Ti in synthesized samples was analyzed by ICP-MS. Suspensions of NPs were studied by stability of hydrodynamic diameter over time.

3.6.1 Transmission electron microscopy (TEM)

Transmission Electron Microscopy (Garzella et al., 2000) is a method to produce micrographs by sample illumination with electronic radiation in vacuum environment. The electrons emitted through samples are then detected and imaged. This technique is similar to optical microscopic techniques with a difference of use of electrons instead of photons. Main advantage of this technique is high resolution imaging as electrons exhibit much smaller wavelength as compared to photons.

TEM gives in situ high resolution imaging of atomic level dynamic behaviour of chemical reactions as affected by different temperatures and gas pressures. A TEM can analyse

morphological, structural and compositional behaviour of different materials up to as low as atomic level. In TEM techniques, the Point of resolution is up to ≥0.12 nm, and particle size is down to 5 nm.

All advanced analysis and HRTEM was done using a Phillips Tecnai F20 (Figure 3.6) with EDX and Gatan Digital Micrograph software. TEM data was analysed using Gatan Digital Micrograph for size distribution and Image J for circularity. EDX data was analysed with INCAEnergy software by Oxford Instruments.

Figure 3.6: Phillips Tecnai F20

Standard morphological investigations were done using a JEOL 1200ex machine (Figure 3.7), having a tungsten filament and operating voltage of 40-120kV. High resolution micrographs and characterisation of all the samples have been performed (operating at 200kV) in centre for electron microscopy, University of Birmingham. This JEOL 1200 can operate at a voltage of 80-200kV.

Figure 3.7: JEOL 1200ex TEM

3.6.1.1 TEM sample preparation techniques

As TEM measures the transmitted electrons through the sample to study, therefore, only very thin samples can be looked at. So TEM requires preparation techniques to make a thin sample transparent enough to pass the electrons. Hence sample thinning is crucial in getting good TEM images. The powder samples were mixed with high purity acetone (99.9%) and if needed, were ground in mortar and pestle which was previously washed to avoid any

contamination. Then the paste was diluted with acetone water mixture and sonicated for 15-20 minutes. The NP suspensions were diluted or used as such according to the method of grid preparation described below. Holey carbon coated grids were used throughout the research work. Four different methods of carbon grid preparation were tried during this work. In first method, the carbon grids were dipped into the NPs solution (for a time up to 30 seconds), partially dried in air, rinsed, dried again and preserved carefully. In the second method, grids are mounted on acrylic stubs which can fix on bottom of a test tube and a 10 ml of diluted sample was centrifuged to get uniform distribution of samples over grid. The resultant grid was then dried and preserved carefully. In third method, a drop of sample was placed on grid, partially dried, washed and re-dried before storage for analysis (Baalousha et al., 2008). In fourth method, a new approach was tried; the carbon grids were pre-soaked with milli-Q water by putting a 50µl drop, and then this drop was inoculated by a very tiny droplet of the NPs suspension (typically less than 5µl). Another 50µl was then added on top of everything to finalize the process. This method was given name of sandwich method due to nature of preparation technique. The grids were covered and put in a clean place for drying. When partially dried these were rinsed with few drops of deionized water. Samples were dried completely and stored for further analysis.

3.6.2 Dynamic light scattering

Dynamic light scattering (DLS) is a recognised technique for size and zeta potential measurement along with all size related parameters of colloids and NPs. In DLS NPs are quantified when they move with Brownian motion on the way of a laser beam. This technique is also called as Photon Correlation Spectroscopy (PCS) or Quasi-Elastic Light Scattering (QELS). In detail, the dynamic light scattering theory uses the knowledge of Brownian motion mediated random pattern movement of small particles in a suspension. At same temperature,

due to Brownian motion, small particles move at a fast speed than large particles. DLS instrument uses this important feature of Brownian motion to quantify the size of the NPs and other related parameters (Malvern, 2014). This concept is achieved with illumination of the NPs with laser beam and analysis of the fluctuations in intensity of the scattered light.

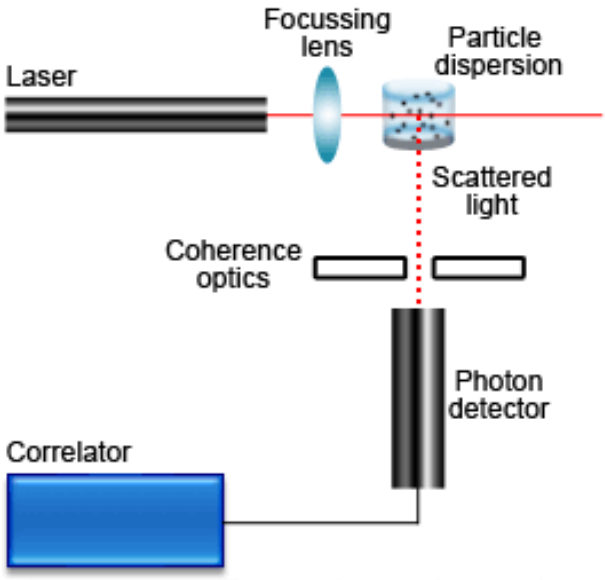

Figure 3.8: Principle of Dynamic Light Scattering (Malvern, 2014)

3.6.2.1 Hydrodynamic diameter by DLS

DLS is based on Stokes-Einstein equation which shows the relationship between the size of a nanoparticle and its diffusion because of Brownian motion. According to Einstein's equation, molecules having smaller size have different velocity in a suspension. It is assumed that the diameter given by DLS is of round particle having uniform translational diffusion coefficient at the time of measurement. According to Stokes-Einstein**,** hydrodynamic diameter can be calculated by this equation (Edward, 1970).

$$d_H = \frac{K_B T}{6\pi\eta D}$$

Where;

d_H = Hydrodynamic diameter

K_B = Boltzmann constant

H = Solvent viscosity

T = Absolute temperature

D = Diffusion coefficient

Doppler effect to the beam wavelength is caused by the movement of the particles which influence the intensity of scattered light. This change in the intensity of scattered light is directly linked with the size of the particles and is measured by a photon correlator which monitors the fluctuations in situ. Time dependent intensity correlation function can be measured by using this data (Berne and Pecora, 2000).

There can be error data during DLS measurements as reported by Römer et al. (2011). According to them, the average diameters measured by DLS are weighted towards larger agglomerates neglecting smaller particles, because larger NPs and agglomerates scatter more light than smaller or hiding particles. This gives the overestimate in average hydrodynamic diameter.

Measurements were conducted with a Malvern Zetasizer NanoZS90 5001. For all the measurements disposable cuvettes were used to take at least five concordant measurements for mean hydrodynamic diameter at 20^{o}C.

3.6.2.2 Zeta potential measurements by DLS

Zeta potential is defined as “the electrical potential at the shear plane with respect to the bulk liquid” (Hehlen et al., 2014)(page 186). It is usually denoted by using the Greek letter zeta ζ, hence also known as ζ-potential. Zeta potential value determines the overall stability of the colloidal dispersion. The value of zeta potential determines the level of repulsion between alike charged particles in a suspension. It is understood that mostly particles in an aqueous medium acquire a surface charge, mainly either by ionization, or adsorption of charged species on the surface of particles. The surface charge on the particles alters the availability of the surrounding ions which results in a layer around the particle giving it a different potential than the bulk solution. Every particle in a solution acquires such a layer of charge. Zeta potential is an indicator of this charge. The effective charge on the particle surface is related to electrostatic repulsion and is measured as zeta potential (Borm et al. 2006).

Zeta potential is associated with the surface charge which is a property of all nanomaterials dispersed in a fluid. Zeta potential value controls the process, quality and stability of nanomaterials. Simply it helps to maintain nanomaterials stability but speaking precisely, zeta potential control can clearly improve the characteristic of nanomaterials.

For example, when a single nanoparticle is considered, its surface has a charge, called “surface charge”. Let’s assume that the nanoparticle surface is positively charged, then zeta potential will be having a positive value. As this nanoparticle is present in solution which contains ions, these positive surface charges attract negative charges in the solution forming a strong inner layer called "stern layer" and a weak outer layer, both these layers collectively are called electrical double layer. On the diffused double layer there is a potential difference that exists at the boundary of nanoparticle surface. In other words, there is a potential difference

between the surface charges and outer media. This potential difference is called "Zeta potential".

Several factors can influence the zeta potential of the particles including particle surface chemistry, dispersant, pH of solution, ionic strength and capping agents (like surfactants). Point of zero charge is the pH where the value of zeta potential is zero. Higher values of zeta potential give more stability to the system because of the repulsion between charged particles.

The zeta potential in this research work was measured with the Malvern Zetasizer NanoZS90 5001. Disposable capillary cells (DTS1070) purchased from Malvern instruments were used for this purpose and at least 5 readings were taken to minimize error.

3.6.3 X-Ray diffraction

XRD is a powerful technique for determining the structure of materials with long-range order (Cullity and Stock, 2001). However, for disordered and amorphous materials this technique finds only limited applications. The XRD pattern of each pure substance is unique, so for different substances there are no identical patterns. The availability of numerous standard patterns in data libraries allows identifying pure substance or crystalline phases in this substance by using simple search and matching procedures (Demydov, 2006). When an X-ray beam heats the atoms in the solid sample the electrons of these atoms start to oscillate and form constructive interference, which is characteristic of the arrangement of atoms in the crystal (Demydov, 2006). The diffracted beam consists of in phase X-rays which mutually reinforce one another.

X-ray diffraction (XRD) has been widely used to characterize sol-gel nanoporous materials. X-rays radiations are electromagnetic having short wavelength, high energy

radiation. After they are generated from a source and focused into a fine beam, the X-ray can be shined on a solid sample. Structural information can therefore be deduced from the knowledge of scattering intensity and angle (Huber et al., 1978).

The XRD patterns were collected on a Bruker D800 Advance Diffractometer which uses a Cu*K*α (λ =1.5418 angstroms) radiation source having a nickel filter and a 2θ range of 5-90^{o}C. A step size of 0.1 with data collection time of 4 seconds was adjusted for all measurements. This diffractometer can be used for routine measurement when sample are available in large quantity. An automatic sample loader is available for this purpose (Figure 3.9).

Figure 3.9: Bruker D8 Advance Diffractrometer.

Polycrystalline phases of materials are ideally characterized and ultimately identified with powder diffraction technique. A diffraction pattern is a result of interaction of X-rays with a crystalline material. Diffraction pattern is achieved for all crystalline materials while amorphous materials can't be identified with x-ray technique. Goniometer is the mechanical unit of XRD machine which consists of three parts; a sample holder, a detector arm and an

associated gearing (Figure 3.10) (Stanjek and Häusler, 2004). XRD works on the principle of Bragg's law, a schematic diagram of which has been shown in Figure 3.11.

Bragg's law equation is given as follows (Washington, 2014),

$n \lambda = 2d \sin \theta$

Where, θ = angle of incidence of X-ray beam, degrees

d = the distance between atomic layers in a crystal, Å

λ = the wavelength of the incident X-ray beam, Å

n = an integer

X-rays have wavelengths on the order of a few angstroms, a typical distance between atoms in all crystalline materials. X-ray diffraction pattern is achieved when X-rays interact with a regular structure with similar distance to the wavelength. As all crystalline materials have repeated atomic structures, so the diffracted X-rays give fingerprint patterns of the material.

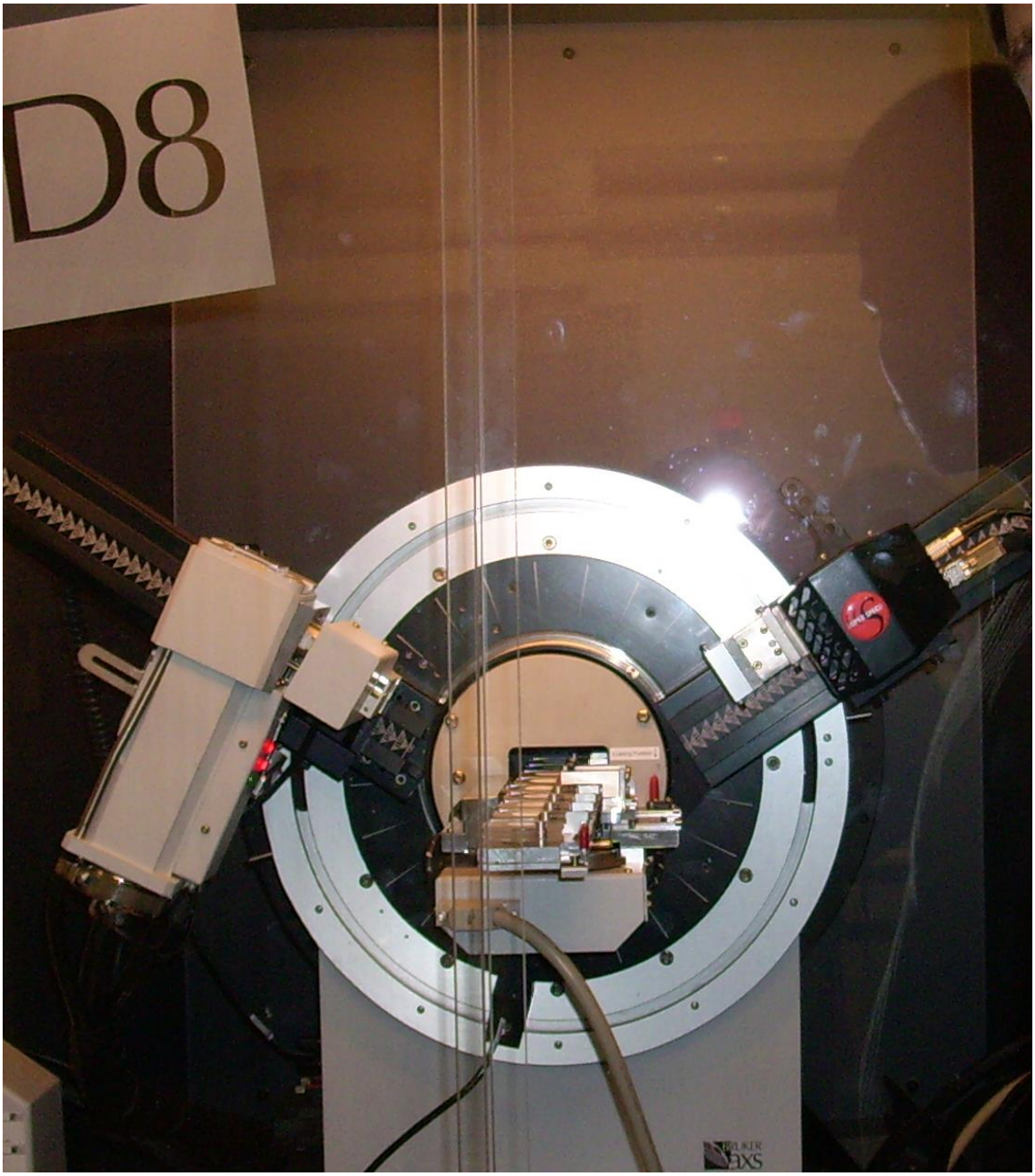

Figure 3.10: Goniometer for Bruker D8 Advance Diffractrometer

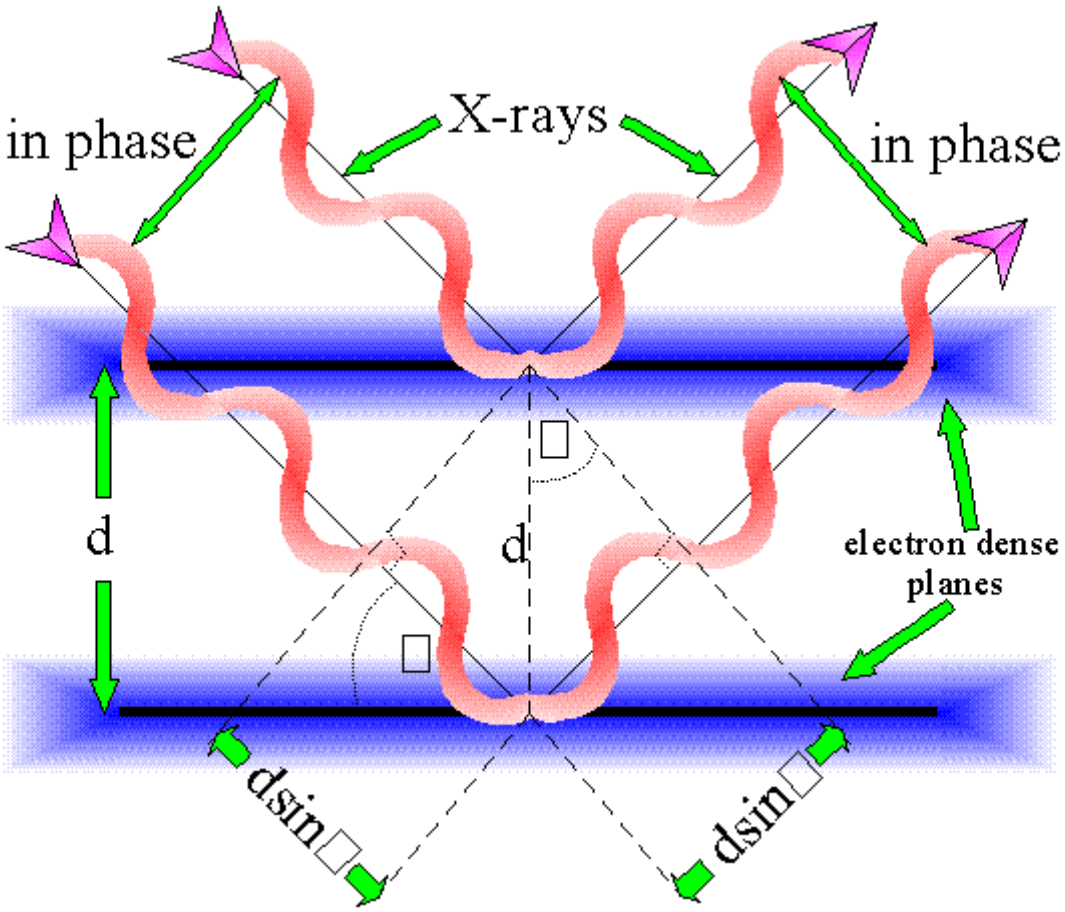

Figure 3.11: Bragg's Law (Taverner, 2014)

In current research work the (101) peak (2 θ =25.28°) is used for anatase and the (110) peak (θ =27.42°) for rutile as given by the reference peaks. Scherrer equation was used to calculate the grain size with peak broadening analysis (Li et al., 2003).

$$D = k\lambda/\beta\cos(\theta)$$

In which D is diameter of nanocrystals, β is the full width at half maximum length of the diffraction peak on a 2θ scale, λ is the radiation wave-length (1.5418°A or 15.418 nm) and k is a constant value (k=0.9). The value of k is based on assumptions made in the theory (e.g. the peak shape and crystallite habit, spherical crystallites being the easiest case to interpret).

The value of D was computed from the (101) diffraction peak, which was the best resolved in the diffractograms.

3.6.4 Inductively coupled plasma mass spectrometry (ICP-MS)

Inductively coupled plasma mass spectrometry (ICP-MS) is a characterization method which can measure traces of most of the elements in the periodic table. It is quite new method as first ICP-MS publication was in 1980 (Houk et al., 1980) and first commercial ICP_MS was introduced by Perkin Elmer in 1983 (Rakhi et al., 2008). It is a very powerful analysis tool for metallic (Hirner, 2006) and non-metallic (Wuilloud and Altamirano, 2006) elemental quantifications in a system (Mitrano et al., 2012). ICP-MS is most suitable analytical technique in almost all fields (Ammann, 2007) due to its ability to measure very low concentrations up to ppt (Ray et al., 2004, Moldovan et al., 2004, Poda et al., 2011) in a short time (Montaser, 1998). It is considered superior analytical technique to others like atomic absorption spectrometer (Talapin et al., 2001) and inductively coupled plasma optical emission spectrometer (ICP_OES). ICP-MS can use any type of samples including solid and gas. So total elemental quantifications of the colloidal solutions could be perfectly done with this technique (Scheffer et al., 2008).

Figure 3.12 Agilent 7500 ICP-MS

In current work Agilent 7500 ICP-MS instrument was used to quantify the concentration of titanium in the final suspension of the synthesised TiO_2 NPs. All analysis was done by Dr. Steve Baker, University of Birmingham, UK.

3.7 Stability Studies

The effect of varying pH values, different surfactants and ionic strengths on the aggregation of titania NPs was studied in detail for a period of 2 weeks. The pH was systematically changed in the presence of PEG, PVP, SDS, sodium citrate and SRFA. Hydrodynamic diameter was measured immediately after adjusting the pH and every week up to 2 weeks. pH was changed by addition of few drops of dilute NaOH and HCl as per requirement.

3.7.1 Aggregation kinetics studies

Aggregation kinetics of anatase round NPs and rutile ellipses, as a function of time at different ionic strengths of $Ca(NO_3)_2$, $NaNO_3$, $CaCl_2$ and NaCl was examined. The aggregation of TiO_2 NPs was monitored with time-resolved DLS analysis with Malvern zeta-sizer. For size instrumental temperature was set at 20^0C while for zeta potential it was adjusted at 25^oC. The scattering angle was adjusted at 90^o for 10 second interval measurements. 1ml NPs suspension was simultaneously mixed in a mixing vial with required amount of stock solution to get desired ionic strength. The vial was gently shaken and quickly moved to the holder of pre-programmed DLS instrument to take immediate readings without any delay. A total of 500 readings were taken with every 10 second measurements. Rate of change of hydrodynamic diameter was used for final calculations. Attachment efficiency α for TiO_2 NPs was calculated with the following equation.

$$\alpha = k_{slow}/k_{fast}$$

where, k_{slow} is the overall aggregation rate and k_{fast} is the average of fastest aggregation rate at a specific ionic strength. All aggregation rates and attachment efficiencies were adjusted to $\alpha \sim 1$. The critical coagulation concentration (CCC) was the value when there was a crossover between k_{slow} and $k_{fast.}$

In current study the aggregation kinetics of titanium dioxide NPs in the presence of mono and divalent salts was measured.

3.7.1.1 Aggregation kinetics by DLS

The time-resolved DLS readings were taken with a Malvern Zetasizer NanoZS90 5001.This instrument utilizes a laser gun which operates at a wavelength of 630 nm. For the

aggregation measurements in the presence of $Ca(NO_3)_2$, $NaNO_3$, $CaCl_2$ and NaCl electrolytes, 500ml of titania NPs stock suspension was prepared with a final concentration of 2mg/L stabilized with SRFA100 and sodium citrate. For every aggregation measurement, a new disposable vial was used to hold approximately 2 mL of the TiO_2 NP suspension. Ultimate care was taken to work in dust free environment.

3.7.1.2 Observation of Aggregate Structures.

Bare and stabilized titania as affected by different electrolytes were observed by TEM. A holey carbon-coated grid (300 mesh) was prepared as per method described above. Aggregate images were then digitally recorded and analysed with fractal dimension calculations. Fractal dimension were calculated by online software JavaAplet and Fractop. A comparison of 6 different methods of fractal dimension values was evaluated.

3.8 Porous media transport studies

3.8.1 Column studies apparatus.

The apparatus used during the column studies was developed by Richard Greswell. A schematic diagram of the apparatus is shown in Figure 3.13. A peristaltic pump is used to pump the stock sols at a constant speed through the column. After the column, a set of measuring devices, provide online measurement of the effluent turbidity, temperature, pH and differential pressure across the column. Output data is in the form of a series of voltages representing the measurement from each device. The output voltages are recorded by MS-DOS software developed previously by Richard Greswell (Greswell et al., 2010). This data is also readable by data logger software in windows environment.

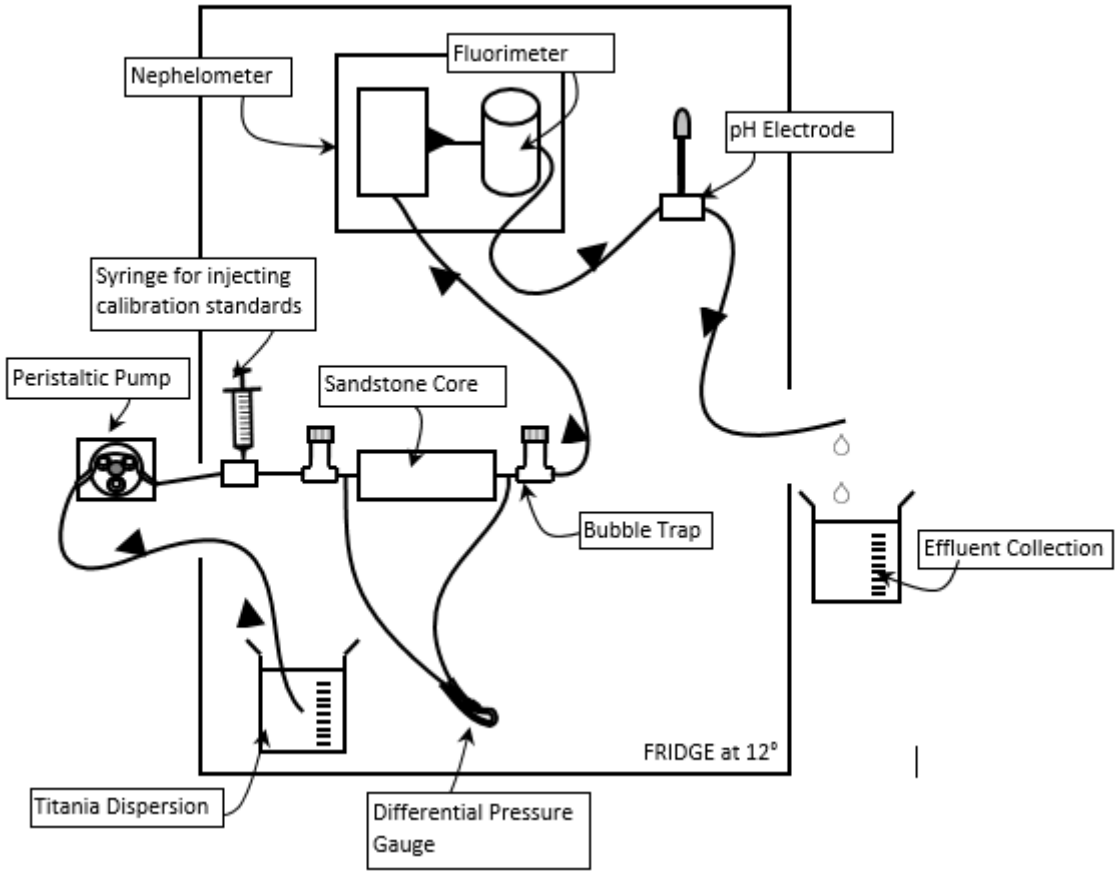

Figure 3.13 A schematic of column experiment laboratory kit

The measuring devices are sensitive to temperature, pressure and light so these are set up in a fridge. To reduce the overall effect of temperature and light, it was assured that the fridge door was kept shut unless adjustments to the equipment were necessary. Figure 3.14 shows the photos of the inside of the fridge for sandstone and glass beads column.

Figure 3.14: Photos of column apparatus with sandstone and glass beads column

The tubing of the apparatus is adjusted in such a way that air bubbles can be trapped on both sides of column. This helps to avoid any error in the data due to air bubbles which can

clog the column. In order to convert the voltages to real values of each parameter, the software provides the facility to calibrate each instrument against standards of known value. A linear calibration relationship is assumed for all standardized measurements.

3.8.2 Turbidity calibrations

The concentration of TiO_2 NPs was measured by nephelometer (Greswell et al., 2010). Nephelometer gives turbidity measurements in the form of electrical signals on the datalogger. In nephelometer, a small, lower power laser is aligned to pass through a small volume flow through cell containing the colloidal dispersion. The light undergoes a complex scattering process as it passes through the sol with the scattering intensity depending on both the particle size and concentration. The scattering is measured by a photodiode at 90° to the incident light of the laser beam. Greswell and co-workers (Greswell et al., 2010) found the correlation between voltage output and nanoparticle concentration showed excellent linearity for a range of manufactured nanoparticles. As the authors noted, clearly the slope is dependent on the physical and optical properties of each suspension. Quantitative analysis against calibrations of known standards can give the values of unknown concentrations.

For nephelometer calibration purposes eight known standards: 0, 0.5, 1, 2, 3, 4, 5 and 10ppm titania NPs; were used. Each standard solution was run for at least half an hour to get the stabilized. A graph of voltage output versus standard concentration was plotted to assess the linear correlation of the data. Actual standardization graph is shown in Figure 3.15.

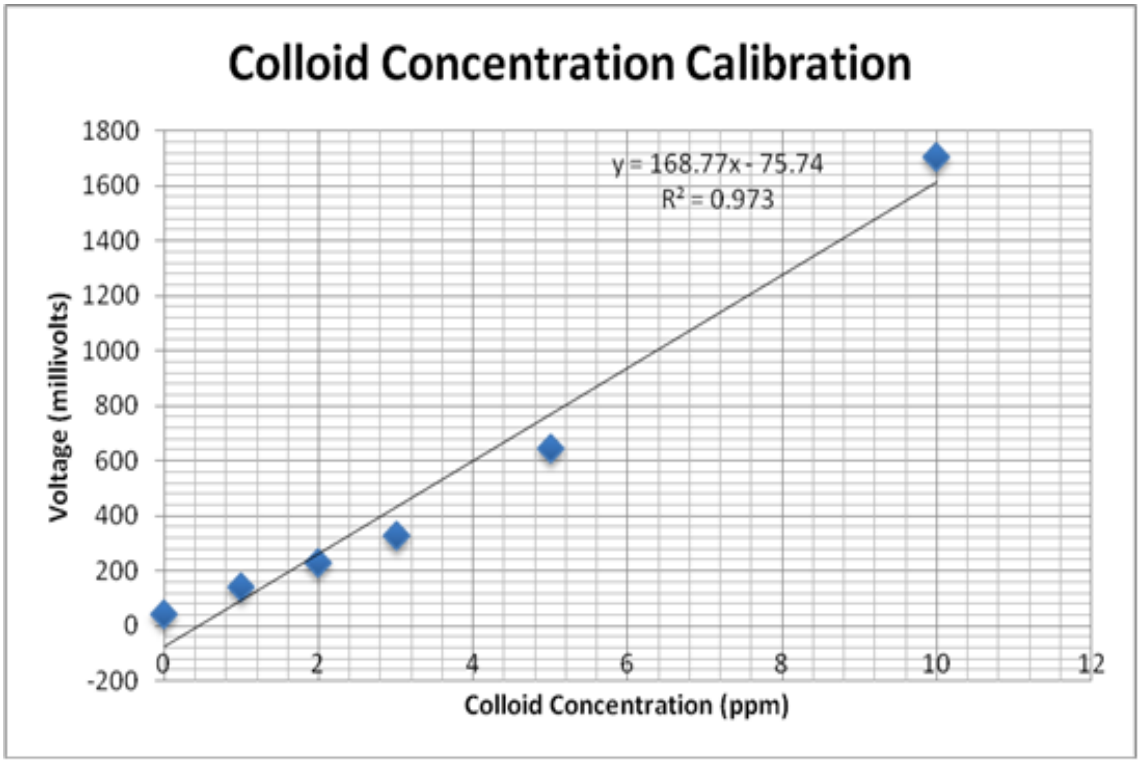

Figure 3.15: Nephelometer calibration curve

3.8.3 pH calibrations

The pH electrode was calibrated using stock solutions of pH 4, 7 and 10.2. These solutions were prepared by dissolving buffer tablets from Fischer Scientific in deionized water. The pH electrode was left in each solution for a time until the reading is stabilized. A graph showing the linear relationship is given Figure 3.16 below.

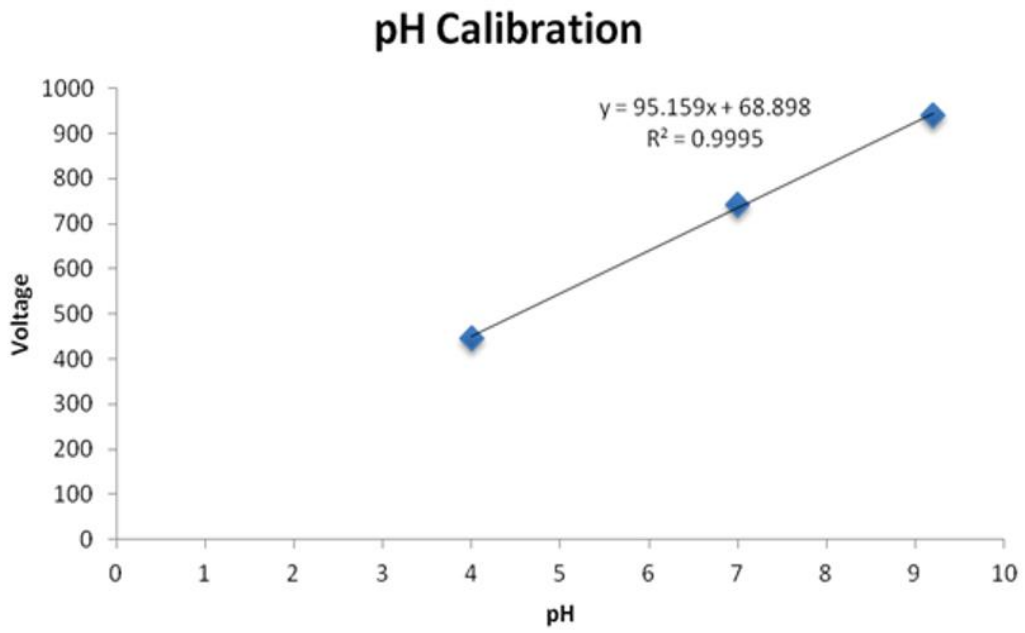

Figure 3.16: Graph showing linear relationship of pH calibration

3.8.4 Temperature calibrations

The temperature calibration was done only at two points; one inside fridge and other outside. Although there was a need of third point calibration at relatively high temperature but it was not done because of health and safety measures. The temperature readings were taken from an average of all readings taken for about 30 minutes inside and outside fridge. The temperature calibration graph showing a linear relationship is shown in Figure 3.17 below.

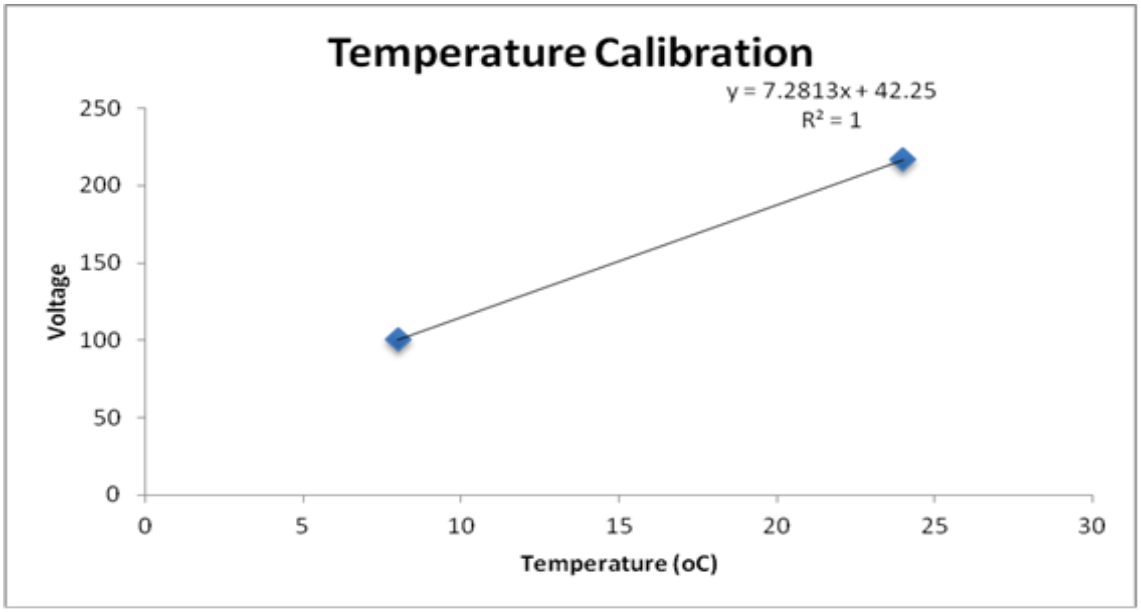

Figure 3.17: Temperature calibration graph showing linear relationship

3.8.5 Differential pressure calibrations

The differential pressure across the column gives some insight into pore clogging. The apparatus comprises a differential pressure sensor and a voltage regulator soldered to a circuit board Figure 3.18. Flexible tubing connects the instrument to each side of the column.

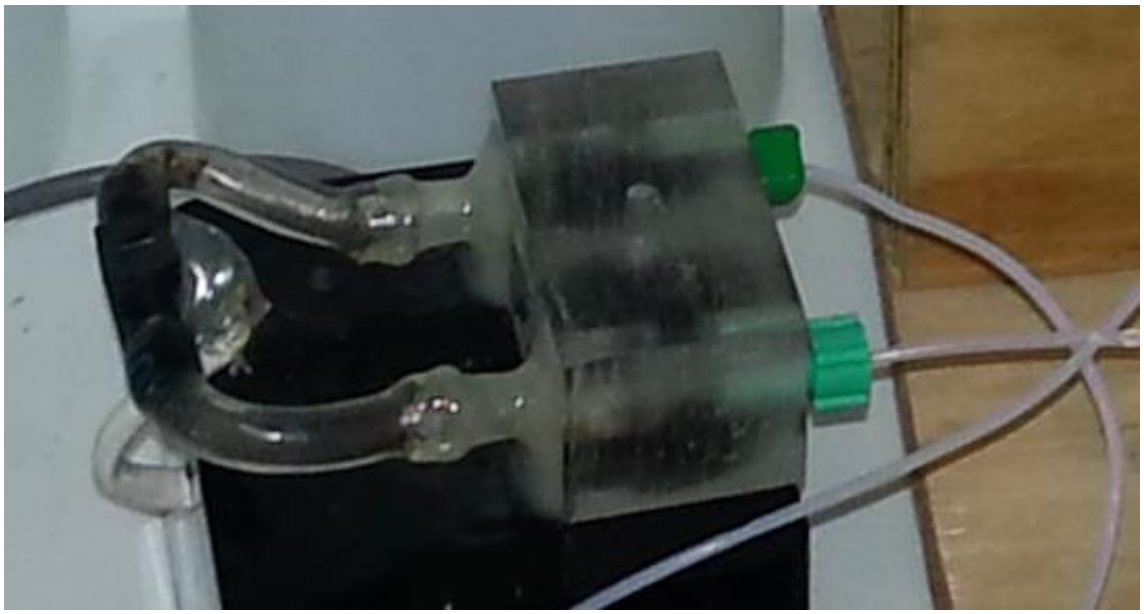

Figure 3.18: Differential Pressure Meter

The pressure transducer was calibrated using a single standpipe connected to the upstream tube of the transducer. The downstream tube was left open to the atmosphere. A three-way valve allowed water to be injected into the standpipe and the head of water measured. These known heads of water were then used to calibrate the device. It is not possible to remove all air between the column of water and the transducer however the density of air compared with water is such that a small head of air in the column is negligible. A graph of calibration curve is given in Figure 3.19.

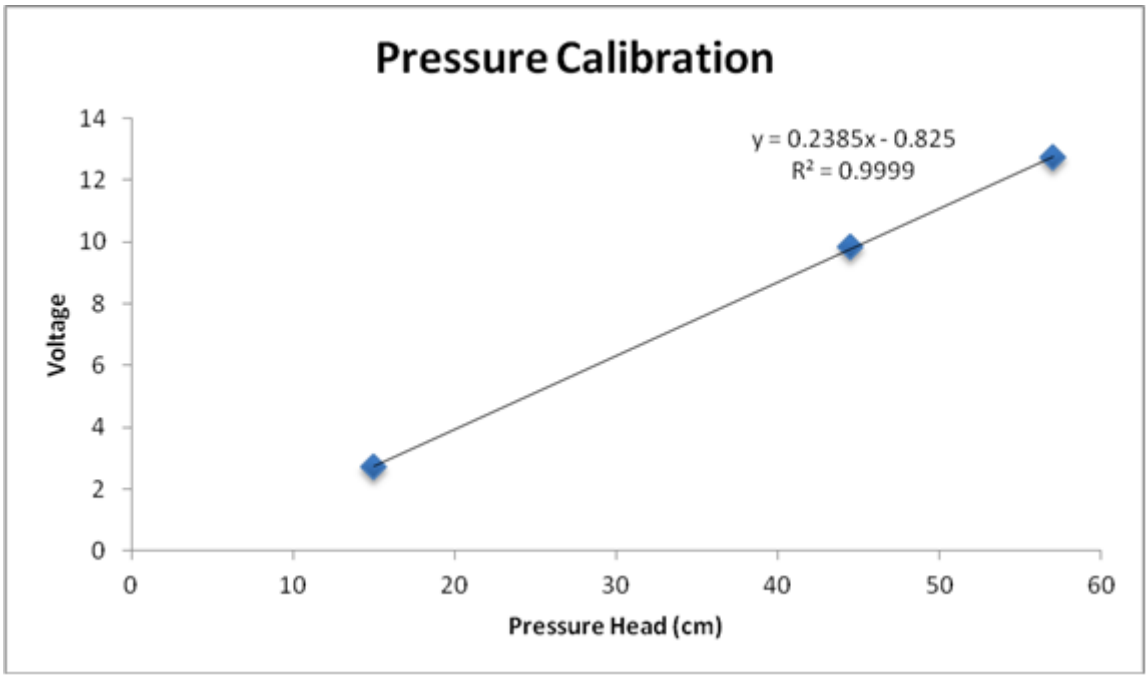

Figure 3.19: Differential Pressure Meter Calibration Curve

3.8.6 Peristaltic pump calibrations

Solutions were pumped through the column using a peristaltic pump. In order to calibrate the pump, five different dial settings: 1, 2, 3, 4 & 5 were measured again the total volume of the effluent in 5 minutes. Each measurement was repeated three times and the average volume is calculated against each dial setting. A measured calibration curve is shown in Figure 3.20.

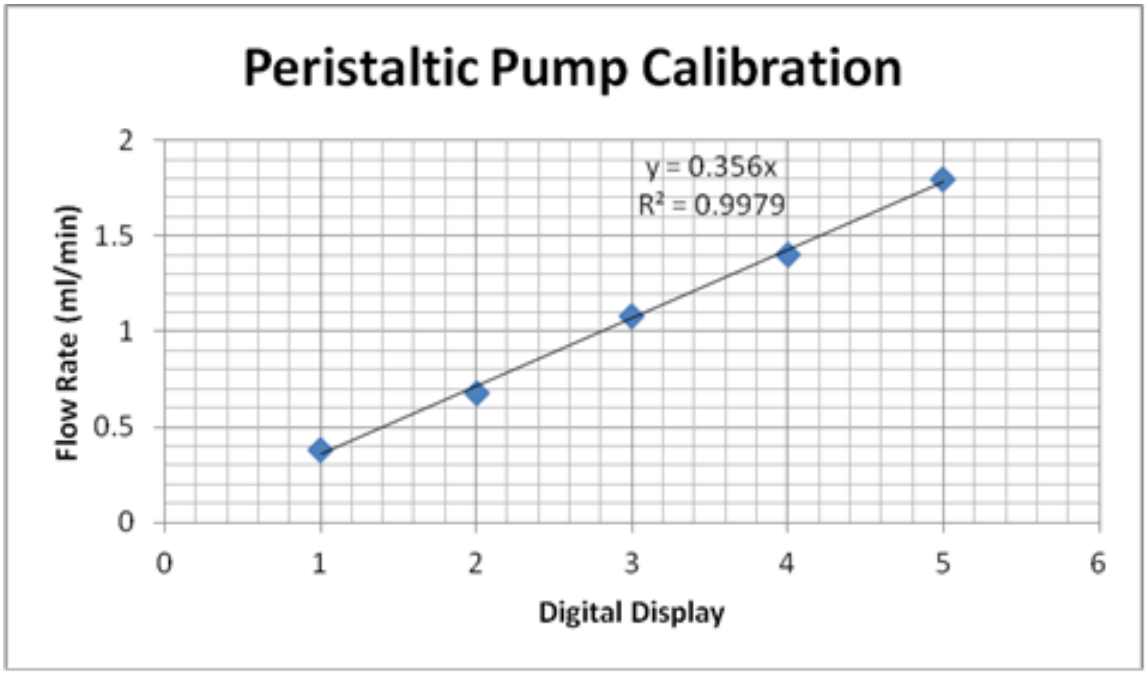

Figure 3.20: Peristaltic Pump Calibration Curve

The pump speed was regularly monitored during the experiments by measuring the volume of effluent output over a period of time. Commonly the pump remained constant over a relatively long period of time. In the long run the tygon pump tubing starts to elongate and collapse decreasing the pump speed. The tubing was replaced in such a case and the pump recalibrated with the new tubing.

3.8.7 Materials and Sample Preparation

Glass beads of 0.1 mm size were purchased from Stratech UK Ltd. Glass columns were manufactured by glass solutions. Tubing for peristaltic pump was purchased from Cole Palmer UK along with other fittings needed.

3.8.8 Suspensions and solutions

Care was taken to use same solutions and suspensions which were synthesized and stabilized during this research work. Firstly, 10ppm TiO_2 was tried but due to variable readings and noise in data, all further runs were with 5ppm TiO_2 solution.

3.8.8.1 Water used

Deionized water was used throughout the experimentation either for blank runs or for solutions or suspension preparations.

3.8.8.2 Sodium citrate solution

0.3% sodium citrate solution was used throughout experimentation. Utmost care was taken to make new solutions for each experimental setup. The solution was kept in fridge for at least an hour prior to its use for any run.

3.8.8.3 SRFA solution

Freshly made 100 ppm SRFA solution in deionized water was used for the experiments which were designed to study a SRFA effect. All solutions were brought to the equivalent temperature of fridge by keeping them stable for at least an hour prior to use.

3.8.8.4 Titania suspensions

The experimentation was started with 10ppm freshly made titania suspensions but further on concentration was decreased to 5ppm due to a visual drift in colloidal data obtained for 10ppm. The data obtained for 5ppm suspensions was relatively consistent without any noise and/or drift in the data obtained.

All TiO_2 suspensions were made either with round anatase NPs or rutile ellipses in the presence of 0.3% sodium citrate or SRFA100. Simple serial dilution procedure was used to make all suspension from 100 and 500ppm stock solutions. Titania suspensions were left to equilibrate in the fridge at least one hour before use.

3.8.8.5 Fluorescein standard runs

Freshly prepared 0.5ppm fluorescein solution was used as a standard run for colloidal solution. Fluorescein is subject to photo-degradation so to minimise this process, the solutions were wrapped in tinfoil and stored in the fridge for at least one hour prior to its use.

3.8.9 Sandstone Cores

The sandstone samples used in the column experiments was taken from Ban To (a PhD student from the University of Birmingham, UK), who drilled these in 2012. The sandstone samples were taken from variable depths. The borehole core analysis logs indicate different textures and properties which are mentioned in Table 3-1.

3.8.10 Measured Rock Properties

Three horizontal cores were used in the experiments. A summary of their previously measured properties is given in Table 3-1. The porosities were calculated using the saturation method.

Table 3-1: Sandstone Core Properties (data taken from Ban To)

Core ID	Location	Depth (m)	Age	Sedimentology	Dry mass (g)	Wet mass (g)	Length (cm)	Width (cm)	Vol (Kaegi et al.)	Bulk density (g/ml)	Porosity (%)
7664	Preston Laundry borehole	76.64	Triassic	Medium-grained, lamination steeper downwards and less obvious	102.387	112.781	6.35	3.15	49.49	2.07	21
8620	Preston Laundry borehole	86.20	Triassic	Medium-grained, cross-bedding sandstone	111.304	121.571	6.7	3.15	52.22	2.13	19.7
PL18 H	Preston Laundry borehole	56.15	Triassic	Medium- to coarse-grained, lamination steeper downward, lots of mudclasts	111.97	118.668	6.15	3.1	46.42	2.41	0.144
6305	Preston Laundry borehole	63.05	Triassic	Medium- to coarse-grained, flat to low-angle cross laminated sandstone	117.229	125.449	6.75	3.15	52.61	2.23	0.156
7100	Preston Laundry borehole	71.00	Triassic	Medium-grained, lamination steeper downwards and less obvious	110.878	120.785	6.75	3.15	52.61	2.11	0.188
9706	Preston Laundry borehole	97.06	Triassic	Medium- to coarse-grained, flat to low-angle cross laminated sandstone	101.47	110.037	6	3.15	46.76	2.17	0.183

Additionally, initial permeability for each core was estimated by measuring the initial differential pressure across each core for a known discharge. The permeability can be calculated by rearranging Darcy's law:

$$K = -\frac{Qdx}{Adh}$$

Here

$$A = \pi \times core\ radius^2$$

Where

Q = flow rate in cm^3/s

K = Permeability in Darcy

A = Area $in\ cm$

$dx = Core\ Length$ in cm

$dh = Differential\ Pressure\ across\ the\ core\ in\ atm$

3.8.11 Theoretical aspects of transportation studies

All research work conducted was directly or indirectly related with Colloid Filtration Theory (CFT). The transport of nanoparticles through saturated homogeneous porous media depends on nanoparticles advection, hydrodynamic dispersions and deposition. If low particle concentrations at lowest ionic strength are used, blocking and ripening effects could be minimized. In such a condition, the concentrations of suspended NPs C(x,t) and deposited NPs S(x,t) at a column depth x and time t can be simulated by one dimensional advection dispersion equation with a term for first-order particle deposition kinetics.

$$\frac{\partial C}{\partial t} + \frac{\rho b}{\varepsilon}\frac{\partial S}{\partial t} = D\frac{\partial^2 C}{\partial x^2} - v\frac{\partial C}{\partial x} \qquad 6.1$$

$$\frac{\rho b}{\varepsilon}\frac{\partial S}{\partial t} = kC \qquad 6.2$$

Where, v is the interstitial particle velocity, D is the hydrodynamic dispersion coefficient, ε is the porous medium bulk density and k is particle deposition rate coefficient and it is related to single collector efficiency η

$$k = \frac{3(1-\varepsilon)v}{2d_c}\eta \qquad 6.3$$

Where, d_c is the diameter of collector grains and η is actually multiplication of η_o and α i.e.

$$\eta = \eta_o \alpha \qquad 6.4$$

Where, α is the sticking (collision or attachment) efficiency calculated in aggregation kinetics chapter. Here η is calculated by following formula

$$\eta \approx \gamma^2\left[4A_s^{1/3}N_{PE}^{-2/3} + A_s N_{LO}^{1/8} N_R^{15/8} + 0.00338 A_s N_G^{1.2} N_R^{-0.4}\right] \qquad 6.5$$

Here γ^2 represents particle flux into the Happel sphere, γ is (1- ε)1/3, ε is porosity, As is a function of porosity accounting the impact of nearby particles in the flow field. Its value is given by

$$A_s = \frac{2(1-\gamma^5)}{2-3\gamma+3\gamma^5-2\gamma^6} \qquad 6.6$$

ϒ is defined above. In equation 6.5 N_{PE} is called Peclet number which is a dimensionless number characterizing the effect of Brownian diffusion. Its value is calculated by the following formula

$$N_{PE} = u\frac{dc}{Dp} \qquad 6.7$$

Where u is interstitial fluid velocity, d_c is diameter of spherical collector grains and Dp is particle diffusion coefficient. In equation 6.5 N_{LO} is a dimensionless number characterizing the van der Waals force and its value can be calculated by

N_{LO} = 4H/(9πdp^2U)

$$N_{LO} = \frac{4H}{9\pi d_p^2 U} \qquad 6.8$$

Where H is Hamaker constant, dp is particle diameter and U is superficial velocity. In equation 6.5 N_G is a dimensionless number characterizing the effect of gravitational sedimentation and it is calculated by dividing particle settling velocity Up by u which is interstitial fluid velocity (N_G=Up/u). The value of Up can be calculated by

$$U_p = \frac{g(\rho p - \rho f)d_p^2}{18u} \qquad 6.9$$

Where g is gravitational constant, ρp is particle density and ρf is fluid density. In equation 6.5 N_R is a dimensionless number characterizing the effect of relative particle and collector sizes. It is a simple ratio of particle diameter and collector grain diameter (N_R=dp/dc).

In this transport modelling, it is assumed that the rate of NPs deposition is both spatially and temporally invariant which means a single value of k is specified. For steady state filtration equation 6.1 can be reduced to

$$v\frac{dC}{dx} + kC = 0 \qquad 6.10$$

If we apply boundary conditions $C=C_0$ at x=0, equation 6.10 can be solved as (continuous particle injection at C_0 concentration and t_0 time)

$$C(x) = C_0 \exp\left[-\frac{k}{v}x\right] \qquad 6.11$$

$$S(x) = \frac{t_0 \epsilon k}{\rho_b} C(x) = \frac{t_0 \epsilon k C_0}{\rho_b} \exp\left[-\frac{k}{v} x\right] \quad 6.12$$

k/v in this equation is equivalent to λ which is filter coefficient and was first introduced by Iwasaki (Iwasaki et al., 1937).

A second boundary condition of length at column outlet where x=L is introduced.

$$\left.\frac{dC}{dx}\right|_{x=L} = 0 \quad 6.13$$

The solutions for equations 6.1, 6.2 and 6.13 for the spatial distribution of suspended and retained NPs are respectively

$$C(x) = C_0 \times \left\{ \frac{\exp\left[\frac{vx}{2D}(1-\omega)\right] + \frac{(1-\omega)}{(1+\omega)} \exp\left[\frac{vx}{2D}(1+\omega) - \frac{vL\omega}{D}\right]}{1 + \frac{(1-\omega)}{(1+\omega)} \exp\left[-\frac{vL\omega}{D}\right]} \right\} \quad 6.14$$

$$S(x) = \frac{t_0 \epsilon k}{\rho_b} C(x) \quad 6.15$$

Where

$$\omega = \sqrt{1 + \frac{4kD}{v^2}} \quad 6.16$$

3.8.12 Laboratory experimentation

The column experiments were conducted using acrylic columns. Column length and width along with the flow rate is given in Table 3-2.

Table 3-2: Calculated parameters for column width and length with expected breakthrough curves

Flow Rate (ml/min)	Velocity (m/sec)	Residence Time (min)	Column Length (cm)	Column Width (cm)	Calculated Breakthrough
0.3673	0.0000499	13.6	10	2.5	45%
0.3673	0.0000963	13.6	10	1.8	60%
0.3673	0.000078	13.6	10	2.0	56%
0.5696	0.0000774	8.8	10	2.5	54%
0.5696	0.000189	8.8	10	1.6	70%
0.5696	0.0001493	8.8	10	1.8	68%
0.5696	0.0001209	8.8	10	2.0	64%
0.7789	0.0001058	6.4	10	2.5	61%
0.7789	0.0105832	6.4	10	0.3	60%
0.7789	0.0001654	6.4	10	2.0	70%
0.9906	0.0001346	5	10	2.5	68%

A column with 10 cm length and 5 cm width was manufactured by glass solutions Cambridge. All experiments were conducted with same column size but different flow rates. The column was fitted with plastic tubing to reduce sorption of the TiO_2 nanoparticles to the system. The tubing was selected as per requirement of the pressure of peristaltic pump. These columns were packed with the 0.1mm glass beads and saturated with de-aired, double-distilled

water. Then the system was flushed with 0.3% sodium citrate solution or SRFA to condition the beads with the stabilizers. Glass beads were selected for these studies to minimize complexity SRFA is surface active and alters zeta potential of any surfaces by sorption.

A peristaltic pump was used to inject nanoparticles solutions into the vertically-positioned columns from the top. Breakthrough concentrations were recorded as it provides information on attachment and staining along with presence of ripening and blocking.

3.8.13 Washing of glass beads

0.1mm uniform size glass beads were used as the granular porous medium. The glass beads were thoroughly washed prior to use. The glass beads were ultra-sonicated for 30 min in deionized water, followed by 2 h dithionite solution (0.1M$Na_2S_2O_4$) treatment for removal of metal impurities on the surface of beads such as iron and manganese oxides (Elimelech et al., 2000). The glass beads were then overnight treated with a mixture of chromic and sulfuric acids, followed by ultra-sonication for 1h. These glass beads were immersed in hydrogen peroxide (5% H_2O_2) for 3h to remove organic impurities, followed by a washing with deionized water. The sulfuric/chromic acid treatment was repeated again followed by ultra-sonication for 1h. Overnight hydrochloric acid (12 N HCl) was given in the last followed by washing with deionized water and sonication. The deionized washing procedure was continued until the conductivity of the supernatant in the deionized washing was dropped below 2µS/cm.

3.8.14 Operation of column experiments

Below was the standard operating procedure (SOP) for the column experiments.

1. Concentrations were measured by nephelometer (colloid meter) and all measurements were calibrated.

2. Column was flushed with deionized water until electrical conductivity is below 2µS/cm.
3. Next the column was flushed with 0.3% sodium citrate (or SRFA100 as per run of the experiment) to condition the media with the stabilizing agents
4. The stabilized nanomaterials suspension (either spherical or rod shaped NPs) was injected into the column.
5. Some samples taken at different points were also be analysed for size and zeta potential.
6. System was flushed with deionized water until stable concentration.
7. Calibrations were done again at the end of experiment to compare calibrations at start of experiment.

3.8.15 Variables

3.8.15.1 Blank column run

At the start of experimental procedure, the column was flushed with DI water, sodium citrate, sodium citrate stabilized NPs, sodium citrate and DI water to flush the column. This was done after calibration of the standardized sodium citrate stabilized TiO_2 NPs suspension. The purpose of this study was to evaluate the full transport of suspended material through the porous membrane of column.

3.8.15.2 Sodium citrate stabilized rutile ellipsoids

The system was bypassed with DI water until the stabilized voltage reading. Then standard 5ppm solution of rutile ellipsoids stabilized with sodium citrate was run until the stabilized voltage was achieved. Then the pump and data-logger was halted to attach the column in the system. The column was flushed with DI water followed by 0.3% sodium citrate. Sodium citrate stabilized ellipsoids standard suspension (5ppm concentration) was injected and breakthrough curve was recorded with colloid meter. pH, temperature and differential pressure (at both ends of column) of the solution was monitored continuously throughout the

experiment. Effluent was calculated and labelled to be disposed of properly. The data was recorded until a stabilized voltage reading point was achieved. The column was flushed with 0.3% sodium citrate until a stabilized voltage value followed by DI water flushing towards a point where stabilized voltage values were achieved for DI water (compared to start of experiment).

3.8.15.3 SRFA100 stabilized rutile ellipsoids

The system was bypassed with DI water until the stabilized voltage reading. Then standard 5ppm solution of rutile ellipsoids stabilized with SRFA was run until the stabilized voltage was achieved. Then the pump and data-logger was halted to attach the column in the system. The column was flushed with DI water followed by SRFA. SRFA stabilized ellipsoids standard suspension (5ppm concentration) was injected and breakthrough curve was recorded with colloid meter. pH, temperature and differential pressure (at both ends of column) of the solution was monitored continuously throughout the experiment. Effluent was collected and labelled to be disposed of properly. The data was recorded until a stabilized voltage reading point was achieved. The column was flushed with SRFA until a stabilized voltage value; followed by DI water flushing towards a point where stabilized voltage values were achieved for DI water.

3.8.15.4 Sodium citrate stabilized spherical anatase NPs

After getting the bypass readings of DI water and sodium citrate stabilized NPs suspension; the column was attached by halting the pump and data-logger. The column was flushed with DI water followed by 0.3% sodium citrate. The sodium citrate stabilized ellipsoids standard suspension (5ppm concentration) was injected and breakthrough curve was recorded with colloid meter. pH, temperature and differential pressure was monitored continuously

throughout the experiment. Eluent was collected and labelled to be disposed of properly. The data was recorded until a stabilized voltage reading point was achieved. The column was flushed with sodium citrate until a stabilized voltage value; followed by DI water flushing towards a point where stabilized voltage values were achieved for DI water.

3.8.15.5 SRFA100 stabilized spherical anatase NPs

All procedure for this run was same as described above for three different runs except SRFA was the stabilizing agent and was injected before and after the run. The data for the breakthrough curve was recorded and eluent was collected and discarded properly.

3.8.15.6 Bare NPs run without any stabilization

Following the above procedure, bare NPs suspension without any stabilization was passed through the column after calibrations. The experimental procedure for this run was DI water bypass, bare NPs bypass, DI water through core, bare NPs through core, flushing of column with DI water, DI water bypass, bare NPs bypass and DI water flushing bypass.

3.8.16 Sandstone column experiments

The experimental procedure for the sandstone columns details of which is given above is same for all the runs. Variable flow rates were checked for the sandstone columns. The texture of sandstone was evaluated against different flow rates and total pore volumes.

3.8.17 Size and Zeta Potential Analysis

Few random samples of TiO_2 suspensions concentrations in the effluent were measured with UV-vis spectrophotometry and DLS. Zeta potential of few selected samples was also measured.

3.8.18 Particle Analysis

The morphology of the TiO_2 nanoparticles in the influent and effluent solutions was investigated by Transmission Electron Microscopy (Garzella et al., 2000) (Jeol 1200).

Samples taken from the TiO_2 nanoparticle suspension and the effluent; were analysed for particle size, zeta potential and hydrodynamic diameter by DLS and TEM. The influent was sampled at different times over the entire column studies to have a look at the changes in the stock solution. The effluent was sampled in similar fashion to examine potential changes in particle size or surface charge after transport through the glass bead medium and sandstone columns.

3.9 Washing of glassware and storage of nanomaterials

Glassware that has been in contact with titania was etched clean for 24 hours by filling them with a solution of KOH (2 litres of isopropanol + a handful of KOH pellets). To neutralize the base, fill the glassware was dipped in a 2 M HNO_3 solution and left at least for 12 hours and then rinsed with milli-Q water. Glassware that has only come in contact with ethanol solution was cleaned with soapy water and rinsed with deionized water. All glassware was put in an oven to dry completely. The cleaning solutions were periodically remade.

The synthesized NPs were stored in labelled containers and surfactant treated samples were always kept in fridge all the time. Powder samples containers were sealed tightly and were kept on a cool and dry place.

Chapter 4

Synthesis of TiO_2 Nanomaterials

4.1 Overview

Nanocrystalline titanium dioxide has received a lot of interest by scientists and industry. This interest is due to the unique nanoscale properties which find use in numerous hi-tech applications such as catalysis, sensors, solar cells, memory devices, along with daily use products like cosmetics, sun screens, paints, self-cleaning glass etc.

Titanium dioxide nanomaterials in the form of nanopowders and stabilized suspensions were synthesized using a method described in chapter 3. The effect of pH, precursors, temperature and zeta potential on nanoparticles nucleation, agglomeration, shape, size, and phase transformation were investigated. In the first part of the study, the variation of pH from 1 to 11 was systematically examined at different calcination temperatures i.e. room temperature (RT), 100^oC (100T), 400^oC (400T) and 700^oC (700T). The prepared nanocrystalline materials were characterized by XRD for their phase and TEM for their phase, size and shape. Four gel-drying temperatures as mentioned above were also used to look into the effect of gel drying temperature on TiO_2 phase transformation. The pH was maintained by HCl and NaOH throughout the synthesis process. The results showed that pH and temperature had pronounced effect on the size, shape and phase control. A temperature of 400^oC was considered best for crystalline growth while a pH value of 4 gave the best morphology for TiO_2 nanopowders. XRD results showed that with variation in pH, TiO_2 nanopowders can be controlled for either anatase/rutile or a mixture of two phases. Room temperature at all pH values gave amorphous material which was not easy to characterize by TEM. From the data

generated it is obvious that with an increase in pH there is a decrease in agglomeration and increase in dispersion and vice versa.

In the second phase of synthesis study, effect of different precursors and alcohol water concentration was studied with special emphasis on stable titania-water suspensions with a controlled morphology. Effect of three different titania precursors was also evaluated for their final product morphology. During this study most of the suspensions were studied with dynamic light scattering (DLS) for their size, agglomeration, stability behaviour and with TEM for their shape and size. The results suggested that shape and size of titania nanomaterials could be efficiently controlled by controlling the synthesis solution chemistry. Different alcohols and alcohol water ratios proved to be the best method of controlling the NPs morphology at room or very low temperatures. $TiCl_4$ was evaluated as best precursor in controlling shape and size at low temperature synthesis processes. High temperature treatment was essential for NP grain growth for the materials synthesized with titanium isopropoxide (TTIP).

4.2 Background

Nanocrystalline TiO_2 is an important material in all disciplines of science including material engineering and biomaterials (Yang et al., 2005). The ultrafine crystals have rare characteristics due to quantum confinement effects and higher surface area/volume, the properties which are needed for the chemical during different processes. Anatase and rutile are the most important and commonly used polymorphs of TiO_2. Commercially available titania powders are usually composed of a mixture of the two polymorphs but it is not difficult to get phase pure TiO_2.

Physico-chemical properties of metallic nanoparticles are highly influenced by their shape, size, specific surface area, adsorption ability, crystal composition and structural phase

etc. (Brown et al., 2001, D. H. Napper, 1986, Horie et al., 2012). The unique properties of various engineered nanomaterials make them novel, having enhanced electrical, catalytic, magnetic, mechanical, thermal, or imaging properties.

Synthesizing nanoparticles is a complex task. Nanoparticles could be obtained from colloidal suspensions using several different techniques such as sol-gel, hydrothermal and solvothermal (Hu et al., 2003, Chae et al., 2003, Lue, 2007, Othman et al., 2012). In laboratory one of the efficient technique is sol-gel synthesis (Hu et al., 2003), which involves two stages. 1) Precursors initially form high molecular weight but still soluble oligomeric intermediates, called a "sol". 2) The intermediates further link together to form a three-dimensional cross linked network, called a "gel". The precursors for a sol-gel reaction could be either inorganic salts or organic mixtures, such as metal alkoxides (Römer et al., 2011). Sol-gel method and hydrothermal synthesis showed better means of controlling powder characteristics (Cullity and Stock, 2001). Conventional sol-gel synthesis produces strong agglomerates after calcination to obtain a crystalline phase which alters the properties of the final products (Huber et al., 1978). The nucleation of TiO_2 nanocrystals is dependent on pH value and sintering temperature as claimed by Hu et al. (2003). In this chapter, results obtained from the synthesis of titania NPs, using multiple approaches like sol-gel, hydrothermal and solvo-thermal synthesis, are discussed. The variation of pH from 1 to 11 at different temperatures (room temperature, 100^{o}C, 400^{o}C and 700^{o}C), effect of precursors (TTIP, $TiCl_3$ and $TiCl_4$) and different alcohol:water ratios (1:2 ethanol:water, 1:2 methanol:water, 1:2 2-propanol:water, 1:2 acetone:water and 1:1:1:2 ethanol:methanol:acetone:water) were systematically examined and results are discussed.

Since there are a lot of synthesis variables that could be studied, the focus had to be narrowed. Due to relative simplicity a solution chemical synthesis method was chosen. The

effects of pH, type of precursors, temperature and alcohol:water ratios were investigated. The objective of this study was to synthesize titania nanopowders with controlled grain size, shape, phase content and environmentally relevant stabilized suspensions.

4.3 Results

4.3.1 Synthesis of TiO_2 Nanopowders

Nanocrystalline titanium dioxide powders were successfully synthesized by sol-gel process as described in chapter 3. To evaluate effect of pH and temperature, a total of 11 pH values and 4 temperatures as described above, were selected. The images shown below (Figure 4.1 & Figure 4.2) are for one selected sample synthesized at pH4 and calcined at 400^{o}C. The X-ray diffraction data in Figure 4.1 indicates the formation of mainly anatase phase with some rutile. From TEM results, it was calculated that the particles were of 16±3nm diameter and have spherical shape (Figure 4.2). More TEM results have been discussed in the coming sections of this chapter.

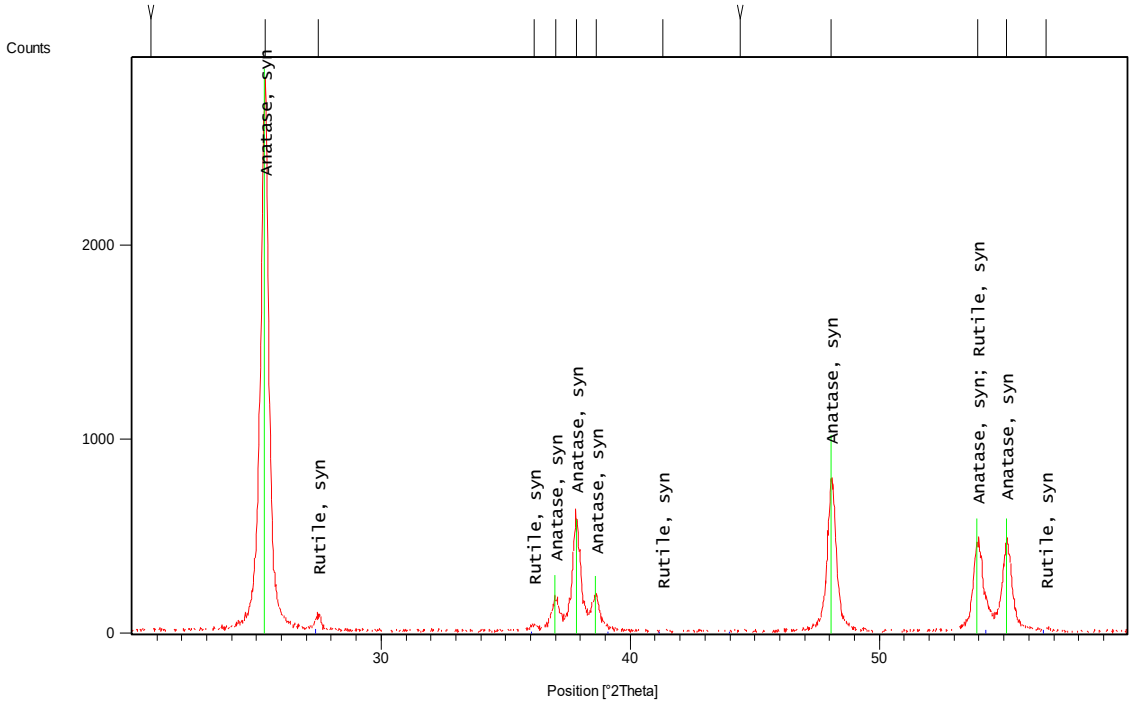

Figure 4.1: XRD Diffraction patterns showing anatase phase as major composition of TiO_2 nanopowder synthesized at pH4 after heat treatment of 400°C for two hours

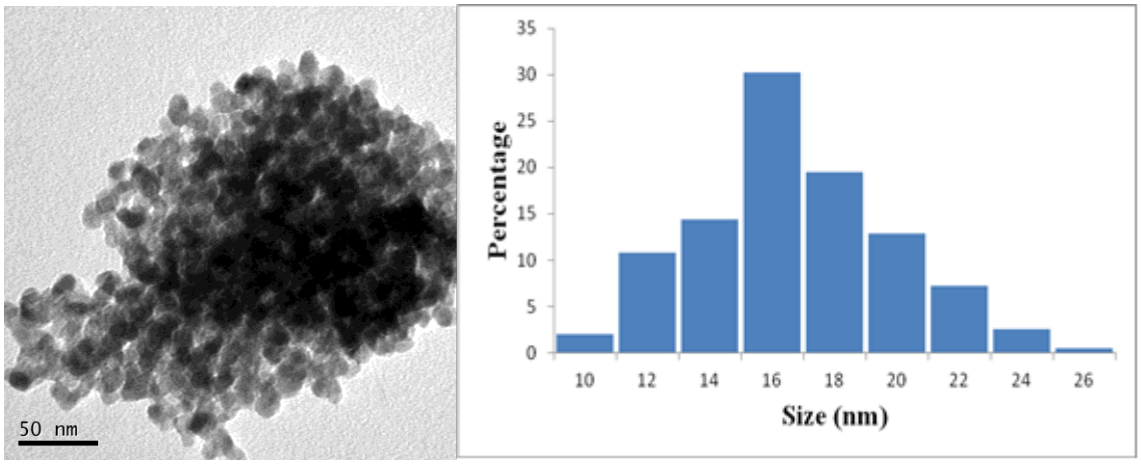

Figure 4.2: a) TEM Images (taken at 200kV extraction voltage) for TiO_2 nanopowder synthesized at pH4 after heat treatment of 400°C for two hours b) Size histogram of randomly selected 195 NPs from 5 different micrographs

4.3.2 Effect of pH on TiO_2 Nanoparticles

Different types of samples were synthesized from pH 1-11. One set of as prepared samples was dried at room temperature, while 3 other similar sets were dried at 100°C (24 hours), 400°C (2 hours) and 700°C (2 hours).

4.3.3 Effect on nanoparticles agglomeration

At an acidic pH, the synthesized TiO_2 consisted of relatively large particles with dimensions of the order of 50 nm with strong agglomeration. Regardless of the drying temperature, nanoparticles at an acidic pH are tightly packed with each other; while on the other hand, at basic pH, particles are well dispersed and are of narrower size range i.e. 10-20 nm (Table 4-1). These nanoparticles after high temperature treatment (especially 700^{o}C) turned into larger aggregates called sinters, i.e. fused particle aggregates, which in most of the cases are out of nanomaterials size range. From the data generated it appears that with an increase in pH there is a decrease in agglomeration and increase in dispersion and vice versa. Variation of pH resulted in significant change of particle surface charge and the hydrodynamic size.

Table 4-1: Summary showing the effect of pH and temperature on size and shape of TiO_2 nanopowders

pH value	Gel Drying Temperature	Estimated Primary Size	Morphology	Corresponding Image/Figure
1	Room	Aggregates of 5-10nm	Irregular	3a
1	100^{o}C	Undefined	Undefined	3b
1	400^{o}C	10-15nm	~Spherical	3c
1	700^{o}C	60-130nm	Irregular	3d
2	Room	Undefined	Undefined	4a
2	100^{o}C	Undefined	Undefined	4b
2	400^{o}C	10-15nm	Irregular	4c
2	700^{o}C	50-120nm	Irregular	4d
3	Room	5-7nm	Spherical	5a
3	100^{o}C	Aggregates of 150-200nm	Irregular	5b
3	400^{o}C	15-20nm	Spherical	5c
3	700^{o}C	200nm	Irregular	5d
4	Room	Aggregates of 80-120nm	Undefined	6a
4	100^{o}C	5-7nm	Spherical	6b
4	400^{o}C	10-20nm	Spherical	6c

4	700ºC	Aggregates of >500nm	Irregular	6d
5	Room	Aggregates of >200nm	Undefined	7a
5	100ºC	20-25nm	Spherical	7b
5	400ºC	12-15nm	Spherical	7c
5	700ºC	30-200nm	Irregular	7d
6	Room	Aggregates of >300nm	Irregular	8a
6	100ºC	Aggregates of 100-200nm	Irregular	8b
6	400ºC	<10nm	Spherical	8c
6	700ºC	100-150nm	Spherical	8d
7	Room	30-40nm	Irregular	9a
7	100ºC	Aggregates of 150-200nm	Irregular	9b
7	400ºC	10-12nm	Spherical	9c
7	700ºC	25-30nm	Spherical	9d
8	Room	Aggregates 0f >500nm	Undefined	10a
8	100ºC	10-13nm	Spherical	10b
8	400ºC	Bunch of nanowires	nanowires	10c
8	700ºC	20-80nm	Elongated	10d
9	Room	>5nm	Spherical	11a
9	100ºC	Aggregates 0f <100nm	Undefined	11b
9	400ºC	Bundle of nanowires	nanowires	11c
9	700ºC	Capsules	Elongated	11d
10	Room	Nanoneedles 5x300nm	Needles	12a
10	100ºC	Aggregates of <500nm	Undefined	12b
10	400ºC	Nanorods 5x100nm	Nanorods	12c
10	700ºC	Nanorods 40x200nm	Nanorods	12d
11	Room	Needles 10x200nm	Needles	13a
11	100ºC	Bunches 80x300nm	Capsules	13b
11	400ºC	Nanorods 5x150nm	Nanorods	13c
11	700ºC	Nanorods 20x250nm	Nanorods	13d

4.3.3.1 pH1

When the conditions are highly acidic, very fine amorphous material (verified through XRD analysis) was observed at room temperature which started aggregation at 100^{o}C (Figure 4.3). It converted to reasonably fine small nanoparticles of 10-15nm at 400^{o}C which converted to incredibly fine crystals of 60-130nm size at a calcination temperature of 700^{o}C (Figure 4.3).

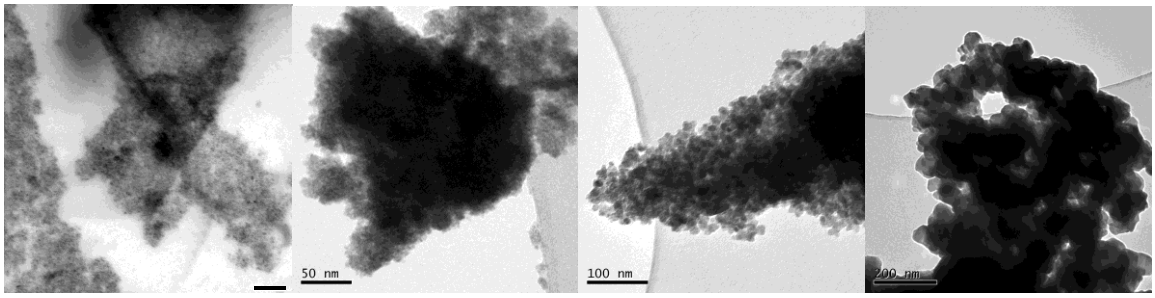

Figure 4.3: TEM images (taken at 200kV extraction voltage) for TiO_2 nanopowder synthesized at pH1 a) Room Temperature b) 100^{o}C c) 400^{o}C d) 700^{o}C

4.3.3.2 pH2

There is not much difference between pH1 and pH2 except shape of particles sintered at 400 and 700^{o}C (Figure 4.4). Particles shifted from roundness to edged shape and have few corners.

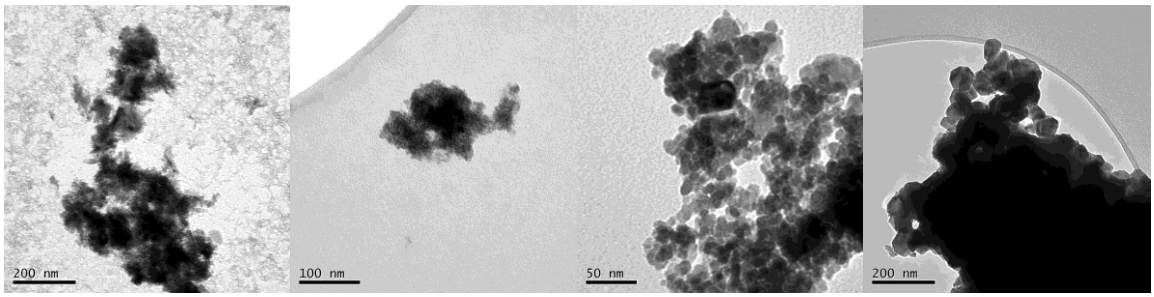

Figure 4.4:TEM images (taken at 200kV extraction voltage) for TiO_2 nanopowder synthesized at pH2 a) Room Temperature b) 100^{o}C c) 400^{o}C d) 700^{o}C

4.3.3.3 pH3

At pH3, considerable fine amorphous material was observed at room temperature which started aggregation at 100^{o}C (Figure 4.5). It converted to spherical shaped small particles of

15-20nm at 400ºC which sintered to irregular shaped particles of around 200nm size at a calcination temperature of 700ºC as visible in Figure 4.5.

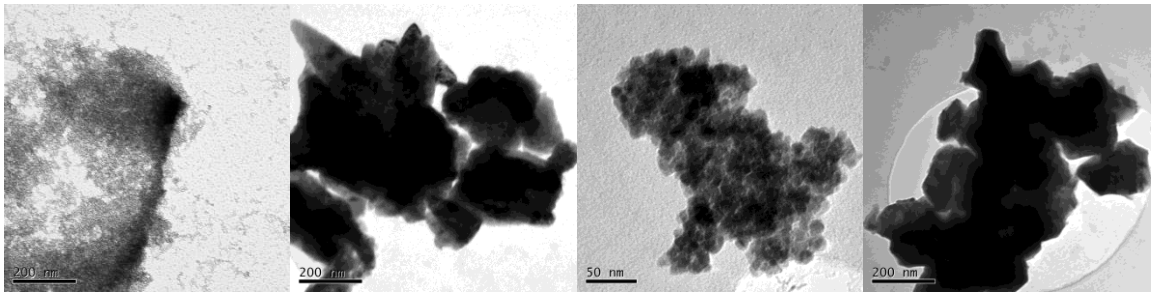

Figure 4.5: TEM images (taken at 200kV extraction voltage) for TiO_2 nanopowder synthesized at pH3 a) Room Temperature b) 100ºC c) 400ºC d) 700ºC

4.3.3.4 pH4

At pH4 amorphous material at room temperature transformed into reasonably small nanoparticles of 5-7nm at 100ºC (Figure 4.6b). These nanoparticles ripened to fine nanoparticles of 10-12nm at 400ºC. 700ºC temperature sintered these fine nanoparticles to larger structures which showed aggregated nanoparticles with no proper dimensions (Figure 4.6d).

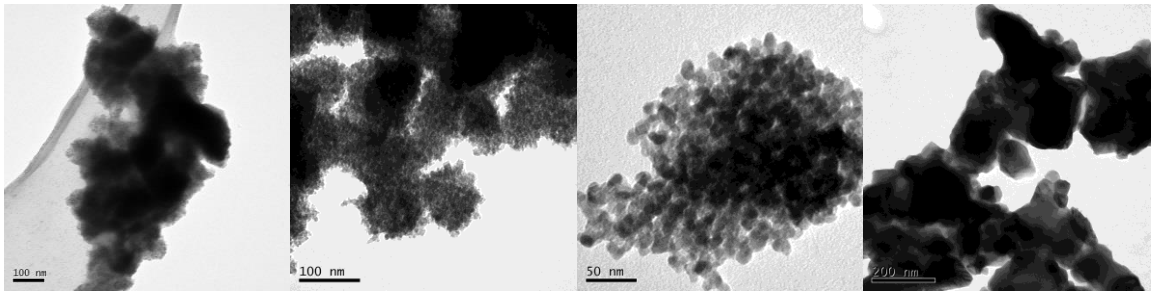

Figure 4.6: TEM images (taken at 200kV extraction voltage) for TiO_2 nanopowder synthesized at pH4 a) Room Temperature b) 100ºC c) 400ºC d) 700ºC

4.3.3.5 pH5

Reasonably fine agglomerates of amorphous material can be seen from TEM images at room temperature which transformed to round nanoparticles of 20-25nm size at 100ºC (Figure

4.7b). Spherical shaped small nanoparticles of 12-15nm can be identified at 400°C which converted to irregular capsulated form of 30-200nm size at a calcination temperature of 700°C (see Figure 4.7).

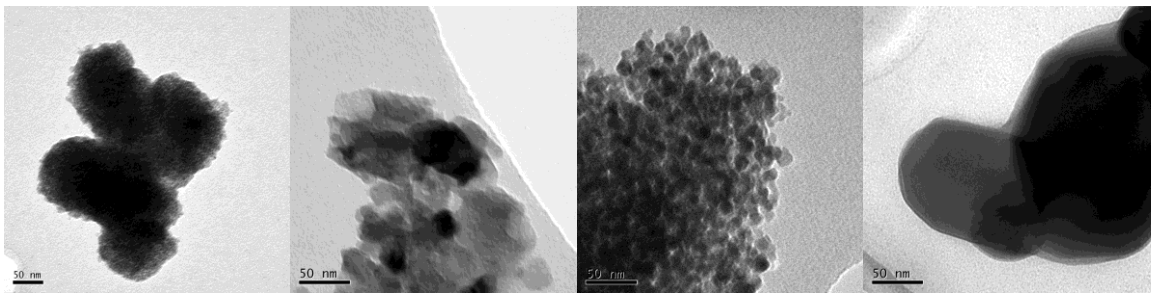

Figure 4.7: TEM images (taken at 200kV extraction voltage) for TiO_2 nanopowder synthesized at pH5 a) Room Temperature b) 100°C c) 400°C d) 700°C

4.3.3.6 pH6

Aggregates of ~200nm amorphous nanoparticles were seen at room temperature which aggregated at 100°C (Figure 4.8b). Considerably fine particles of ~10nm are the result of 400°C temperature treatment which converted to incredibly fine crystals of 100-150nm size at a calcination temperature of 700°C (see Figure 4.8).

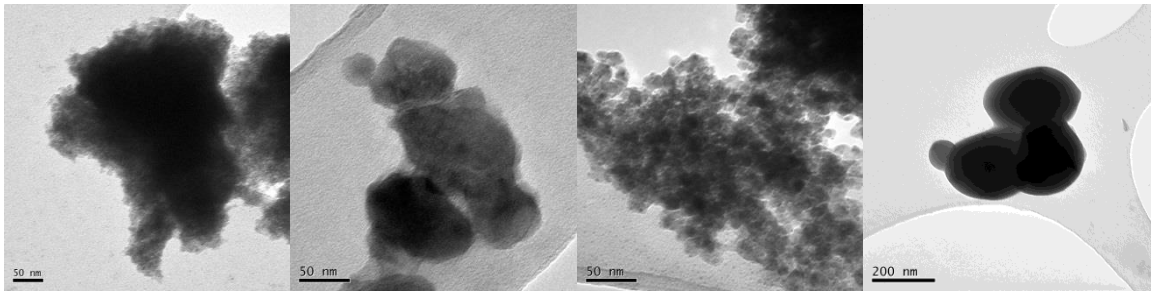

Figure 4.8: TEM images (taken at 200kV extraction voltage) for TiO_2 nanopowder synthesized at pH6 a) Room Temperature b) 100°C c) 400°C d) 700°C

4.3.3.7 pH7

At pH7 nanoparticles of 30-40nm were seen at room temperature which agglomerated at 100°C (Figure 4.9b). The 400°C heat treatment fabricated spherical shaped small crystals of

10-12nm. For the first time reasonably fine and small nanoparticles (~30nm) were the product of 700^{o}C temperature treatment (Figure 4.9d).

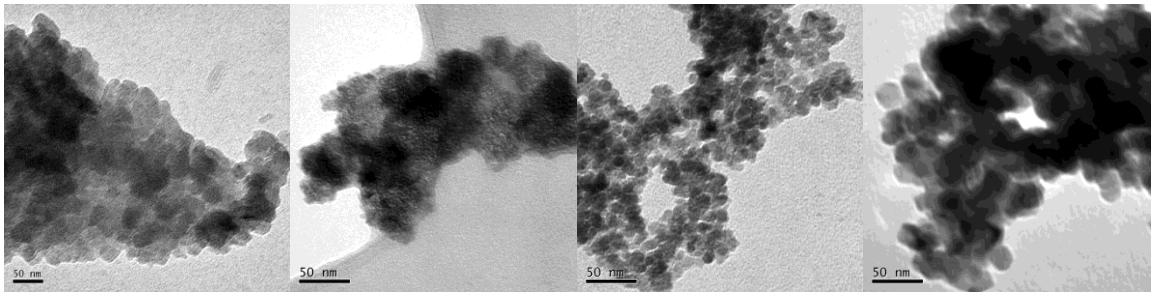

Figure 4.9: TEM images (taken at 200kV extraction voltage) for TiO_2 nanopowder synthesized at pH7 a) Room Temperature b) 100^{o}C c) 400^{o}C d) 700^{o}C

4.3.3.8 pH8

Room temperature gave rise to fine particles of ~5nm which matured to 10-13nm size at 100^{o}C (Figure 4.10b). The 400^{o}C temperature treatment gave an assemblage of nanowires have 5x100nm size. These nanowires transformed to capsule like nanostructures 20x80nm at calcination temperature of 700^{o}C (Figure 4.10).

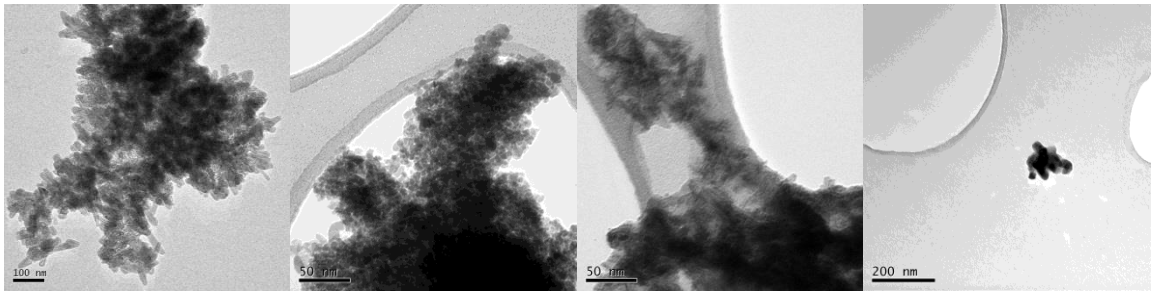

Figure 4.10: TEM images (taken at 200kV extraction voltage) for TiO_2 nanopowder synthesized at pH8 a) Room Temperature b) 100^{o}C c) 400^{o}C d) 700^{o}C

4.3.3.9 pH9

At pH9 treatment, 100-200nm aggregates of amorphous particles were observed at room temperature. These nanoparticles agglomerated to big aggregates of >100nm needle like

structures at 100°C (Figure 4.11b). Nanorods of 5x120nm were synthesized at 400°C which transformed to elongated NPs of 50-100nm at calcination temperature of 700°C (Figure 4.11d).

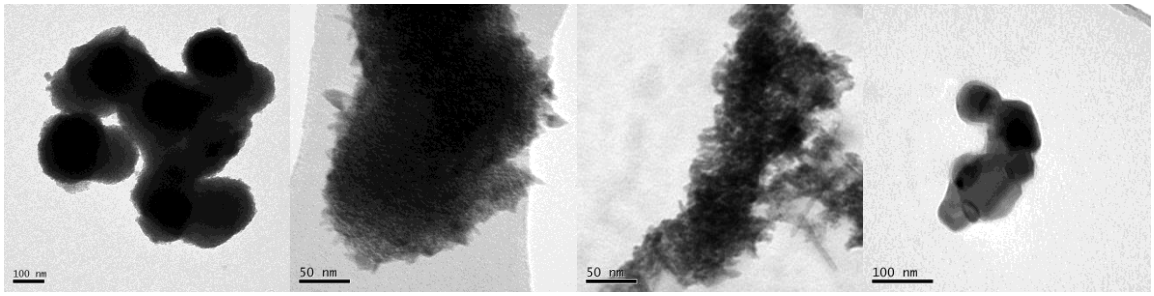

Figure 4.11: TEM images (taken at 200kV extraction voltage) for TiO_2 nanopowder synthesized at pH9 a) Room Temperature b) 100°C c) 400°C d) 700°C

4.3.3.10 pH10

In figure 12a nanoneedles are visible product of room temperature treatment which coalesced into an undefined aggregate at 100°C (see Figure 4.12b). This coalesced bunch transformed to fine nanorods of 5-100nm at 400°C. Mixture of fine edged nanorods of 40x100nm and other shaped NP with different sizes were the product of 700°C calcination temperature (Figure 4.12d).

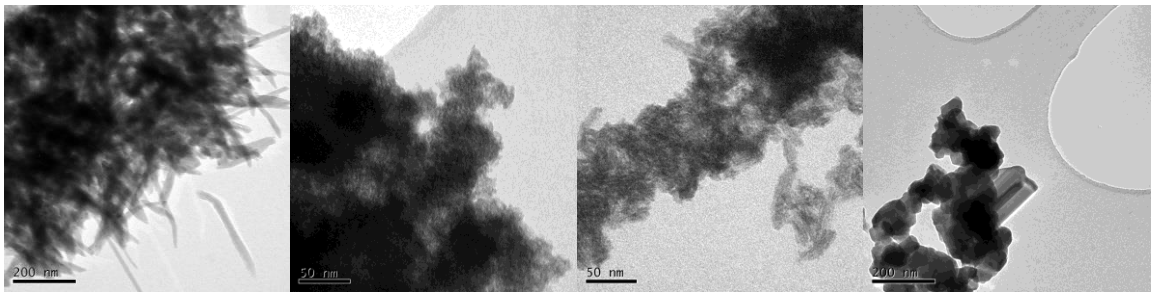

Figure 4.12: TEM images (taken at 200kV extraction voltage) for TiO_2 nanopowder synthesized at pH10 a) Room Temperature b) 100°C c) 400°C d) 700°C

4.3.3.11 pH11

Needle like structures are visible at room temperature treatment which consolidated in to rod like bigger aggregates at 100^{o}C (Figure 4.13b). These consolidated aggregates metamorphosed at 400^{o}C, to fine nanorods of 5x100nm. Distinct nanorods of 25-30nm diameter and several hundred nm length with broken edges were the result of 700^{o}C treatment (see Figure 4.13d).

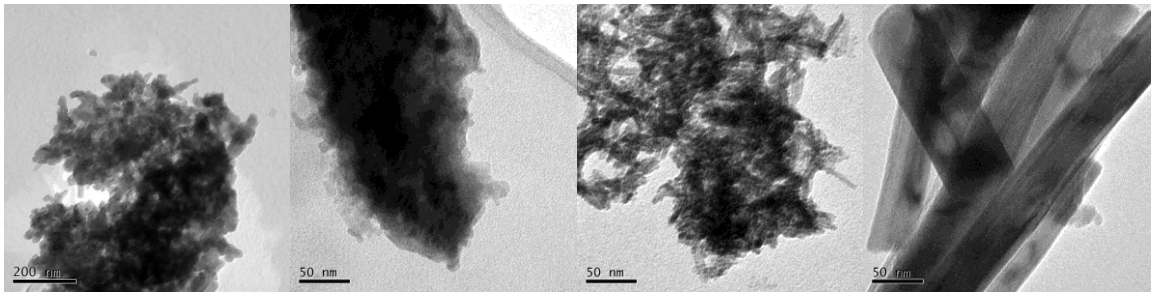

Figure 4.13: TEM images (taken at 200kV extraction voltage) for TiO_2 nanopowder synthesized at pH11 a) Room Temperature b) 100^{o}C c) 400^{o}C d) 700^{o}C

4.3.4 Effect on Nanoparticles size

Transmission electron micrographs (Figure 4.3-Figure 4.13) of TiO_2 nanopowders revealed that the morphology depends on the pH during synthesis. Nanoparticle size could be changed and controlled with change in pH value. Nanoparticles with the best size range were synthesised at pH4 with a good uniform size distribution. In general nanoparticles tend to be large with irregular size range at acidic pH values as compared with basic pH values which gave relatively uniform size.

4.3.5 Effect on nanoparticles shape

The results mentioned above prove that shape could be controlled simply by changing the pH during synthesis process. Although shape factor at highly acidic pH was more than 0.8

but size was not uniform. Shape factor is most regular at pH4 where it is more near to 1 but as pH goes towards basic range, shape factor tends to decrease and nanoparticles changes different shapes (Figure 4.3-Figure 4.13). Perfect nanorods were obtained with a shape factor of 0.3 or less at pH 10 and 11.

4.3.6 Effect on nanoparticles phase and phase transformation

In this experiment few selected samples are evaluated by XRD. Figure 4.14 shows the XRD patterns for three selected samples prepared at pH values 3, 6 and 8. Only room temperature and 700°C treatments were analyzed. It can be seen that the XRD data for these samples show some variation of different phases of TiO_2.

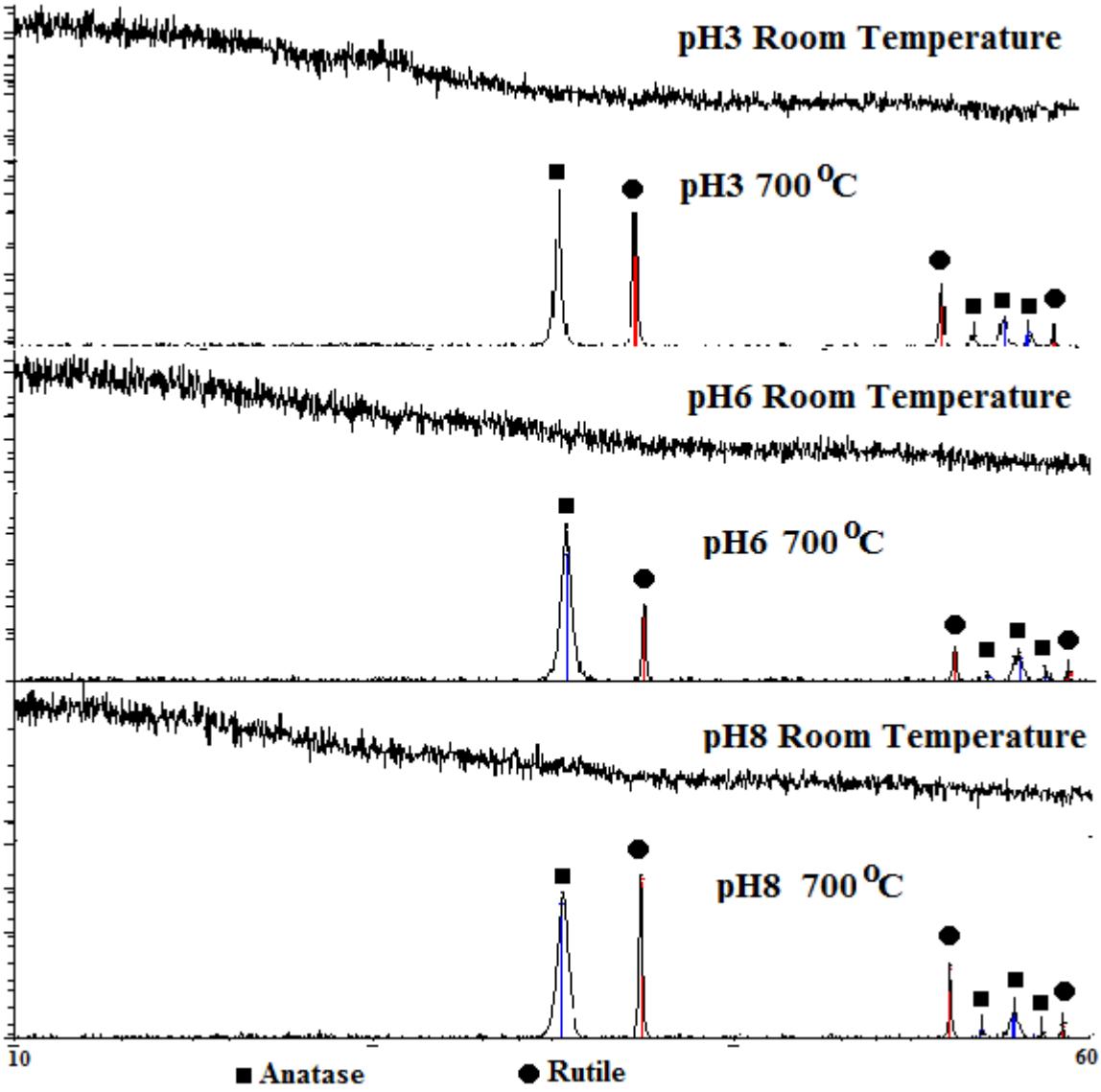

Figure 4.14: Effect of pH on XRD patterns: TiO_2 gel synthesized with pH3, pH6 and pH8 and calcined at 700°C

Room temperature gave all amorphous material and no peak was observed for gel dried at room temperature for pH 3, 6 or 8. An insignificant effect on phase transformation at selected pH values with a temperature treatment of 700°C was observed in XRD analysis (Figure 4.14).

From the TEM micrographs presented above (Figure 4.3-Figure 4.13), it is evident that with titanium isopropoxide precursor, crystalline form is only possible with heating treatment. Without calcination, nanoparticles remain in amorphous form. After calcination at 400°C for 2 hours, the observed primary TiO_2 particles were significantly small with mostly irregular shape.

It is also observed that the structure and size of the TiO_2 crystals are affected by the calcination temperature and pH.

4.4 Synthesis of Stabilized Suspensions

To synthesize stable titania suspensions, two hydrothermal synthesis methods were also investigated. Detailed methodology of both methods has been discussed in chapter 3. Effect of different alcohols (ethanol, methanol, 2-propanol) and mixture of alcohols at different ratios (mostly 1:2 alcohol:water and few 2:1 and 3:1 ratios) with water were studied.

Ethanol is usually used during sol gel process for fabricating titania nanoparticles and provides for excellent chemical homogeneity but usual precipitates of sol gel reaction are amorphous at room and low temperature. As described in previous section, calcination at high temperature is required for proper shape and phase control. As compared to sol gel process, hydrothermal synthesis process in which chemical reactions can occur in aqueous or organic media under the self-produced pressure at low temperature is more reliable technique which produces unique metastable structures at low reaction temperature. For all alcohol studies only $TiCl_4$ precursor is used as described in previous chapter.

4.4.1 Effect of precursors

The term "precursor" is applied to an inactive substance converted to an active one (such as an enzyme, vitamin, or hormone). This term also applies to any chemical that is transformed into another. Usually precursors are alkoxide with chemical formula M(OR)z, where z is an integer equal to the valence of the metal M, and R is an alkyl chain. They can be considered as derivatives of either an alcohol, ROH, in which the hydrogen is replaced by the metal M, or of a metal hydroxide, M(OH)z, in which the hydrogen is replaced by an alkyl group. Vorkapic and Matsoukas (2000) studied effect of alkoxide and their relative

performances in much detail. In this study three different types of titanium metal precursors were used. Titanium isopropoxide is the main precursor which was used for sol-gel and pH studies. Titanium trichloride and titanium tetrachloride are two other precursors which were used for room temperature or near room temperature synthesis. Generally alkoxides do not have a significant impact on synthesis but titanium isopropoxide (TTIP) is preferred over others because of its high reactivity, low electronegative value of titanium, ease of use and low toxicity (Wang et al., 2012). Metal alkoxides need to be dissolved in organic solvents before hydrolysis is performed. Purity and crystal structure was examined by XRD as shown in Figure 4.1 and Figure 4.14. All the three precursors have same prominent crystallographic planes of the TiO_2. There was no difference in the intensities and positions of the peaks. However, it is noted that there was a significant difference between the shapes and dispersion of nanomaterials synthesized by these precursors. $TiCl_3$ was the best precursor for the synthesis of smaller size of nanoparticles at room temperature while $TiCl_4$ required mild heat treatment for growth of nanoparticles. Moreover, handling of $TiCl_4$ is more difficult than $TiCl_3$ or TTIP. Figure 4.15 shows the rutile nanorods synthesized by $TiCl_3$ while anatase NPs are presented in Figure 4.16. It is obvious that NPs fabricated by this method are smaller in size but these are densely populated and are in aggregated form. Keeping in view the purpose of synthesis, this method was tried to get a good dispersion of NPs without any success. So $TiCl_4$ was selected to proceed further and investigate the effect of alcohols and microwave heat treatment.

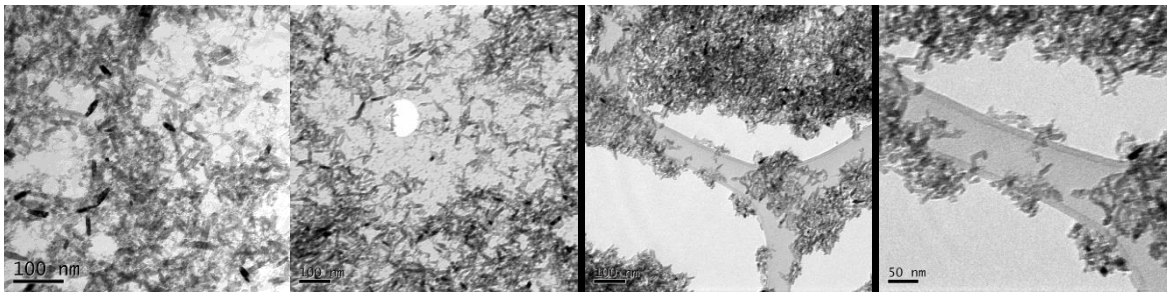

Figure 4.15: TEM images (taken at 200kV extraction voltage) for rutile NPs synthesized with $TiCl_3$ precursor

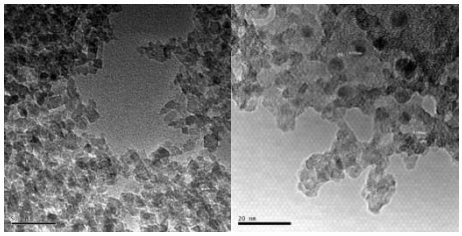

Figure 4.16: TEM images (taken at 200kV extraction voltage) for anatase NPs synthesized with $TiCl_3$ precursor

4.4.2 Effect of alcohols

This study has been done with the use of $TiCl_4$ as a precursor using the methodology described in previous chapter. The effect of the alcohol to water ratio on size and shape of titanium dioxide nanoparticles was investigated and the results are shown in Table 4-2. DLS and TEM results in support of Table 4-1 are also shown in next section.

Table 4-2: Effect of alcohol and water ratios on morphology of TiO_2

Ratio	**Amount of $TiCl_4$**	**Temperature**	**Shape**	**Size**	**Corresponding Figure**
1:2 Ethanol:Water	10ml	80°C	Bunches	~200nm	Figure 4.17
1:2 Methanol:Water	10ml	80°C	mixture	5-100nm	Figure 4.18
1:2 Acetone:Water	10ml	80°C	Nanorods	10-120nm	Figure 4.19
1:2 2-Propanol:Water	10ml	80°C	Capsules	10-20nm	Figure 4.20
1:1:1:2 Mixed EMA*	25ml	80°C	Rods	30-100nm	Figure 4.21
11112 Mixed EMAP**	25ml	80°C	Round	<40nm	Figure 4.22
11112 Mixed EMAP**	25ml	Boiled 100°C	Round	20-80nm	Figure 4.23
1:2 Ethanol:Water	10ml	Microwave 130°C 45min	Mixture	30-50nm	Figure 4.24
1:2 Methanol:Water	10ml	Microwave 130°C 45min	Square	35-40nm	Figure 4.25
1:2 Acetone:Water	10ml	Microwave 130°C 45min	Round Irregular	10-40nm	Figure 4.26
1:2 2-Propanol:Water	10ml	Microwave 130°C 45min	Bunches	100-200nm	Figure 4.27

1:1:1:2 Mixed EMA*	10ml	Microwave 130°C 45min	Round	40-90nm	Figure 4.28
11112 Mixed EMAP**	10ml	Microwave 130°C 45min	Round	30-80nm	Figure 4.29

*Mixture of Ethyl, Methyl and Acetone ** Mixture of Ethyl, Methyl, Acetone and 2-Propanol

It is obvious from the above table that alcohols have a well-defined effect on the size and shape of TiO_2 nanomaterials. An increase in the alcohol to titanium tetrachloride ratio also affected the size probably due to formation of more HCl in the reaction system. The difference of TiO_2 phase and morphology is attributed to the contribution of the equilibrium concentration of H^+, Cl^- (Buzea et al., 2007a). A shape factor of >0.9 (40% nanoparticles) was given by microwave treatment of mixed alcohol sample. This sample was further used in stability and column studies. The detailed shape information of the figures below (Figure 4.17-Figure 4.29) is given in table 2 above. It is obvious that with changing alcohol to water concentration and type of alcohol, the shape characteristics of TiO_2 nanoparticles can be controlled.

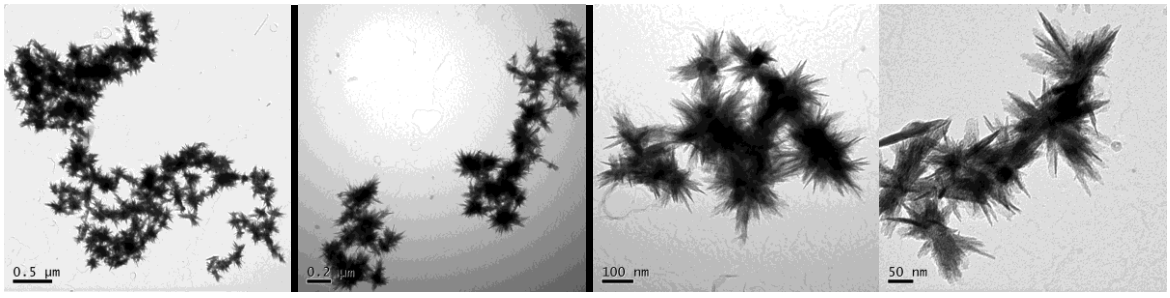

Figure 4.17: TEM images (taken at 200kV extraction voltage) showing the effect of ethanol and water ratio of 1:2 on morphology of TiO_2

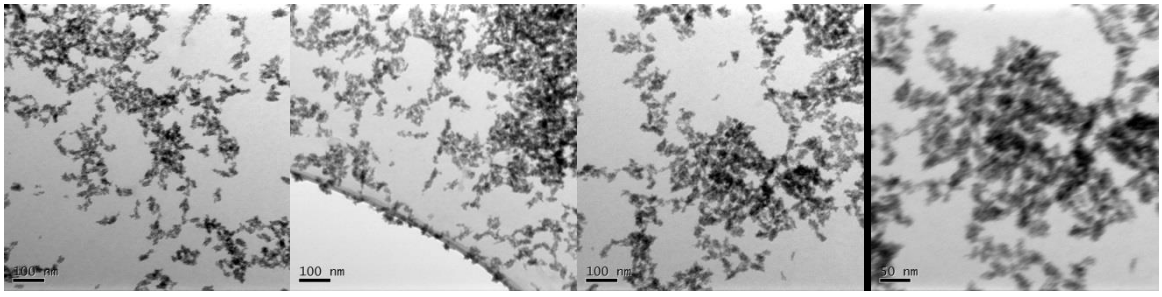

Figure 4.18: TEM images (taken at 200kV extraction voltage) showing the effect of methanol and water ratio of 1:2 on morphology of TiO_2

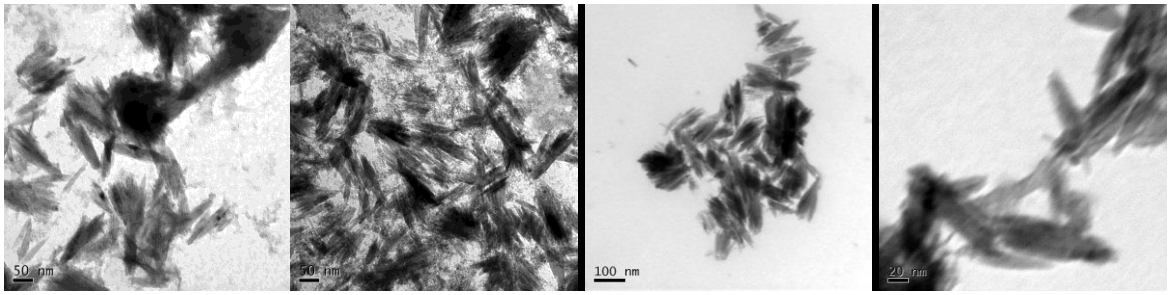

Figure 4.19: TEM images (taken at 200kV extraction voltage) showing the effect of acetone and water ratio of 1:2 on morphology of TiO_2

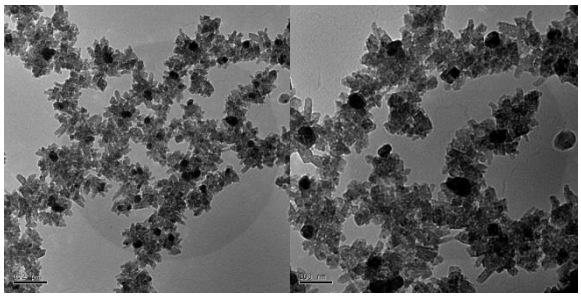

Figure 4.20: TEM images (taken at 200kV extraction voltage) showing the effect of 2-propanol and water ratio of 1:2 on morphology of TiO_2

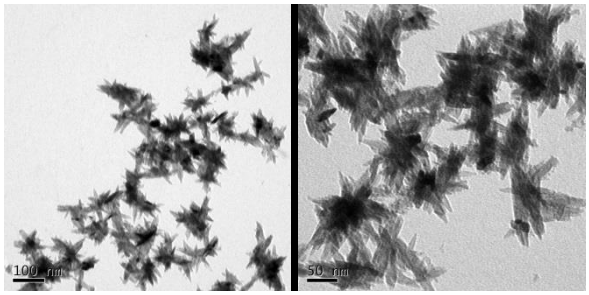

Figure 4.21: TEM images (taken at 200kV extraction voltage) showing the effect of mixture of ethanol, methanol, acetone and water at ratio of 1:1:1:2 on morphology of TiO_2

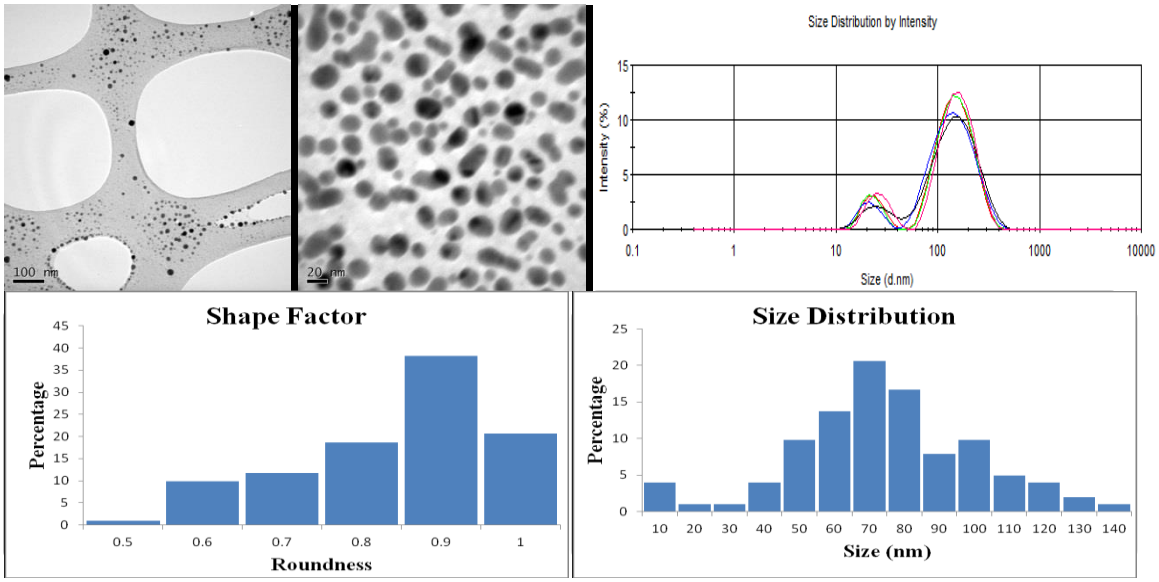

Figure 4.22: TEM images (taken at 200kV extraction voltage) showing the effect ethanol, methanol, acetone, 2-propanol and water at ratio of 1:1:1:2 on morphology of TiO_2

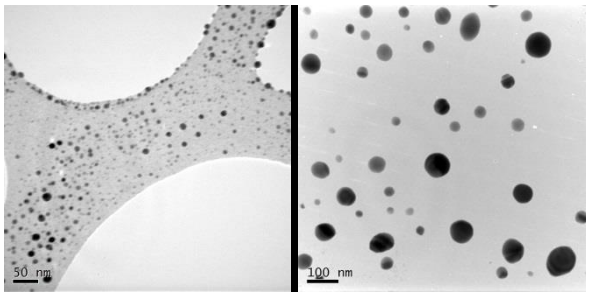

Figure 4.23: TEM images (taken at 200kV extraction voltage) showing the effect of ethanol, methanol, acetone, 2-propanol and water (ratio 1:1:1:2) on morphology of TiO_2 (Boiled)

4.4.3 Effect of Microwave Heat Treatment

It is quite clear from the Table 4-2 that microwave heat treatment of the samples gave a change in size and shape. The methanol and water ratio of 1:2 gave optimum particle shapes (Figure 4.18), while capsule like shapes were obtained from 2-propanol and water ratio of 1:2 (Figure 4.20). Well oriented round particles with a shape factor of >0.9 were obtained with microwave heat treatment of mixed alcohol sample (Figure 4.22 and Figure 4.23).

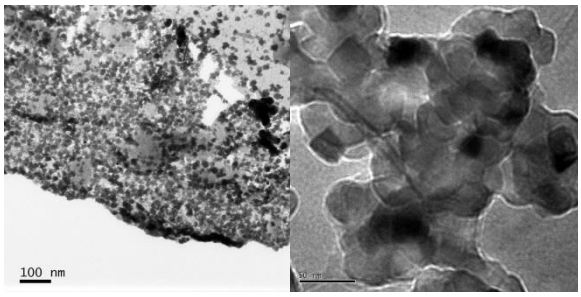

Figure 4.24: TEM images (taken at 200kV extraction voltage) showing the effect of microwave treatment with ethanol and water ratio of 1:2 on morphology of TiO_2

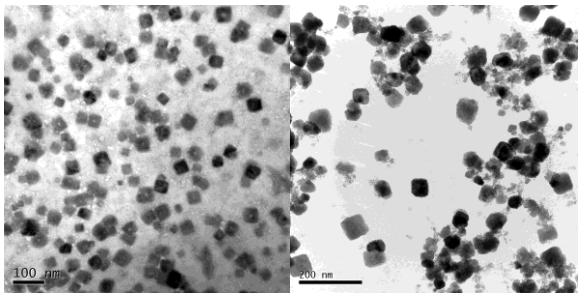

Figure 4.25: TEM images (taken at 200kV extraction voltage) showing the effect of microwave treatment with methanol and water ratio of 1:2 on morphology of TiO_2

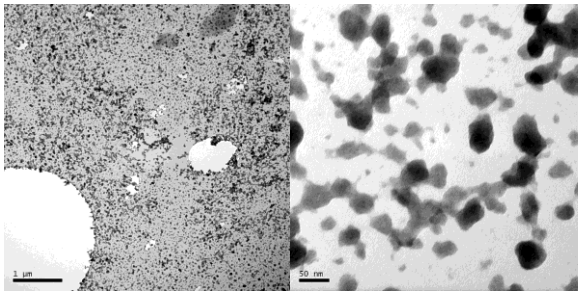

Figure 4.26: TEM images (taken at 200kV extraction voltage) showing the effect of microwave treatment with acetone and water ratio of 1:2 on morphology of TiO_2

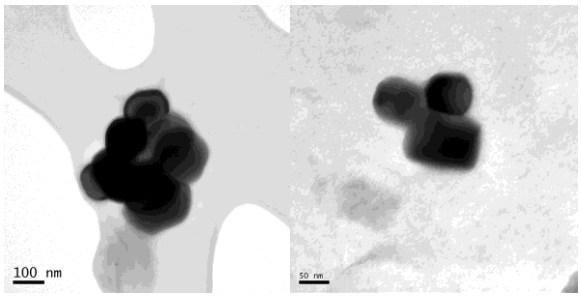

Figure 4.27: TEM images (taken at 200kV extraction voltage) showing the effect of microwave treatment with ethanol, methanol, acetone and water (1:1:1:2) on morphology of TiO_2

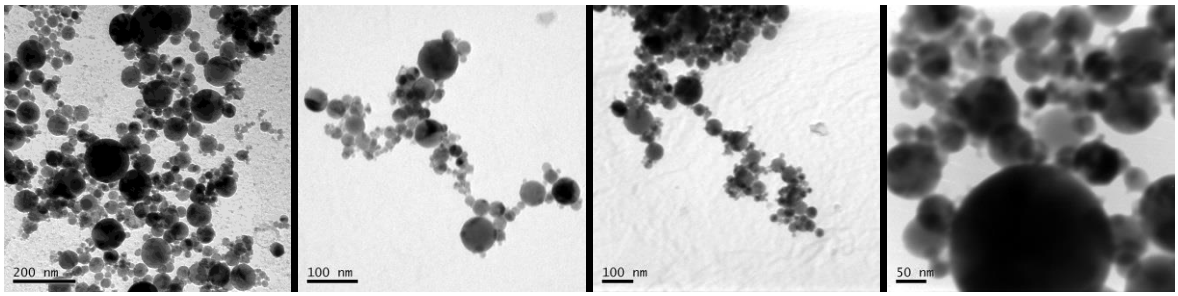

Figure 4.28: TEM images (taken at 200kV extraction voltage) showing the effect of microwave treatment with ethanol, methanol, acetone, 2-propanol and water (1:1:1:1:2) on morphology of TiO_2

Irregular edged cubes were the result after microwave treatment to the sample with 1:2 ratios of ethanol and water (Figure 4.24). Methanol water treatment of 1:2 ratios gave cube shapes which were readily stabilized in the suspension (Figure 4.25). Morphology of NPs for acetone and water at ratios of 1:2 can't be judged properly but clearly those show less or no edges (Figure 4.26). A treatment of ethanol, methanol, acetone and water at ratios of 1:1:1:2 gave morphology of irregularly round NPs (Figure 4.27). These irregularly round NPs turned in to perfectly round NPs with a shape factor of 0.9 or more with a treatment of ethanol, methanol, acetone, 2-propanol and water at ratios of 1:1:1:1:2 (Figure 4.28).

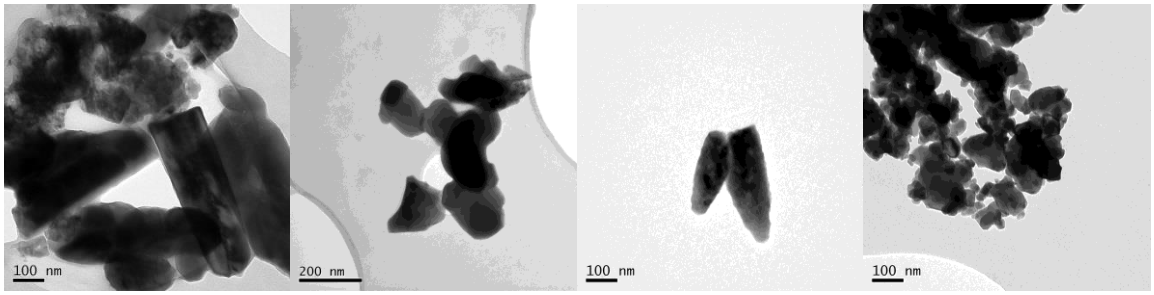

Figure 4.29: TEM images (taken at 200kV extraction voltage) showing the effect of post synthesis treatment of 700°C on morphology of TiO_2

4.5 Stable titania suspensions

As explained previously, the objectives of this synthesis study was to produce highly dispersed and stable suspensions of nanoparticles and nanorods. Detail of stability processes and aggregation kinetics will be discussed in chapter 5. The results obtained from such mono-dispersed suspensions are presented and discussed here. Figure 4.30 shows nanoparticles synthesized by mixed alcohol method with use of $TiCl_4$ precursor. From TEM micrograph and shape factor analysis, it appears that synthesized nanoparticles are mainly 30-40nm in diameter, with more than 65% of NPs showing perfect spherical shape, and a shape factor of 0.9 or more (Figure 4.30 and Figure 4.31). These nanoparticles are initially well dispersed but after washing they tend to agglomerate. So they were again stabilized by sodium citrate and Suwannee River fulvic acid (SRFA100). Detailed stabilization process is discussed in chapter 5. While Figure 4.33 shows the mixed alcohol particles stabilized by sodium citrate. All particles selected for shape factor have perfect round shape with a shape factor of 0.9 or more (Figure 4.34). Size graph shows that most of the particles are in the size range of 40-60nm (Figure 4.35). Figure 4.35 below shows TEM images of nanorods with almost uniform diameter of about 30 nm and length of up to 250 nm. Shape factor for these nanorods is ~0.2.

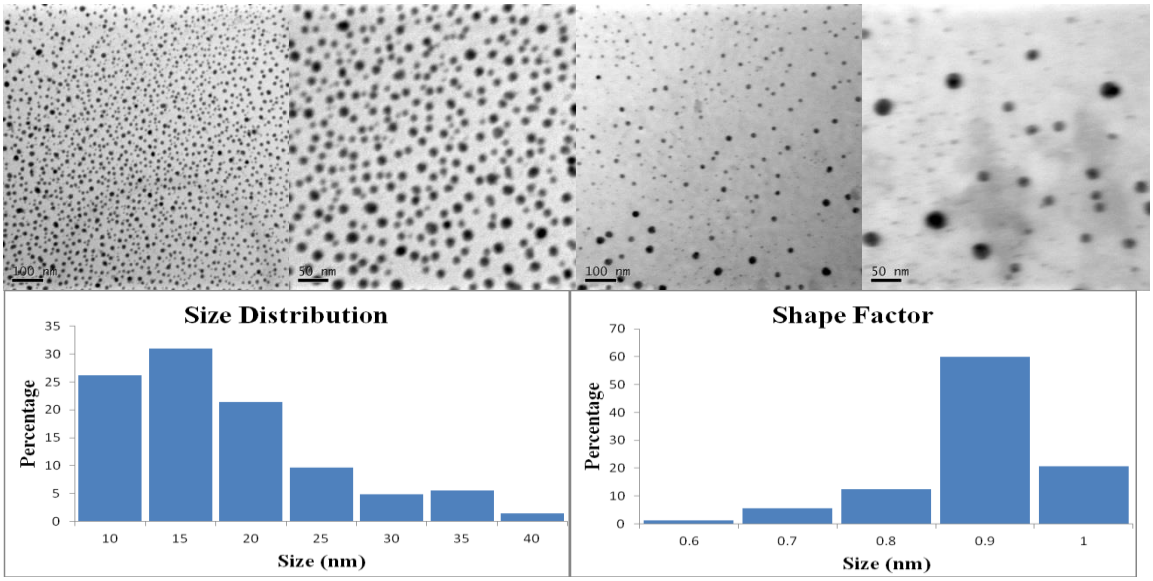

Figure 4.30: TEM images (taken at 200kV extraction voltage) showing significantly mono-dispersed Anatase NPs with shape factor ~1

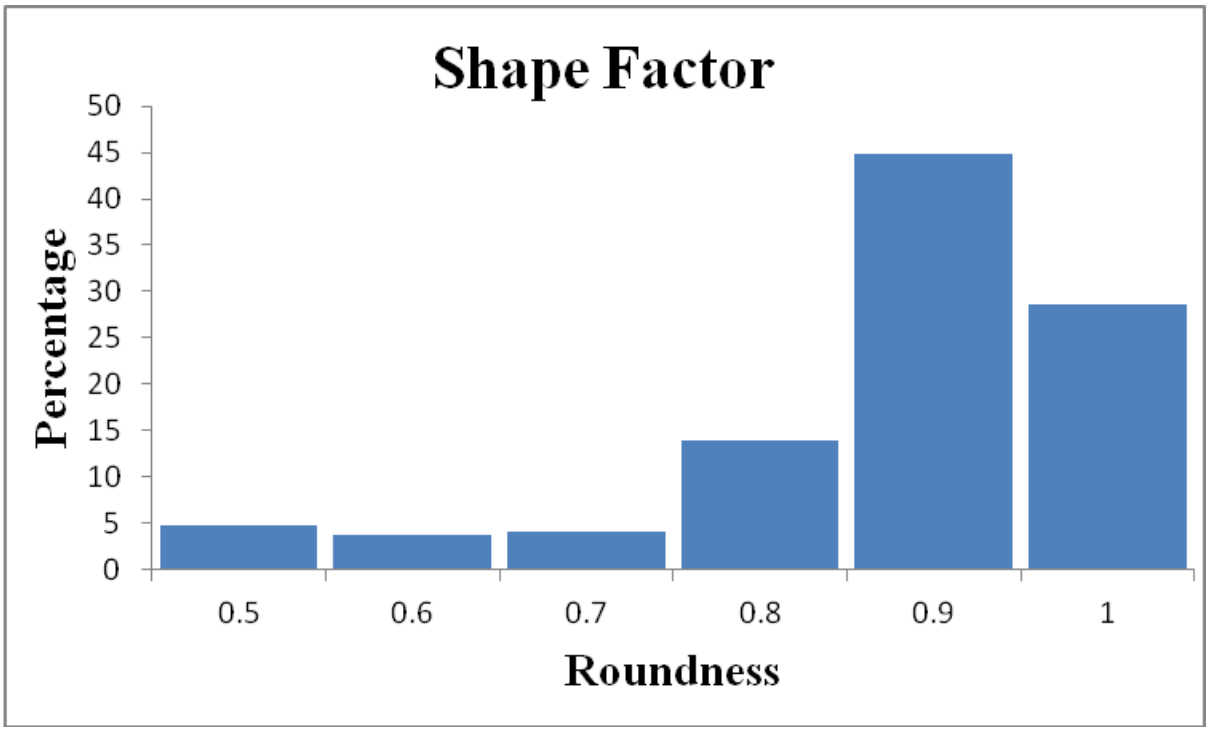

Figure 4.31: Percentage shape factor of mono-dispersed anatase NPs.

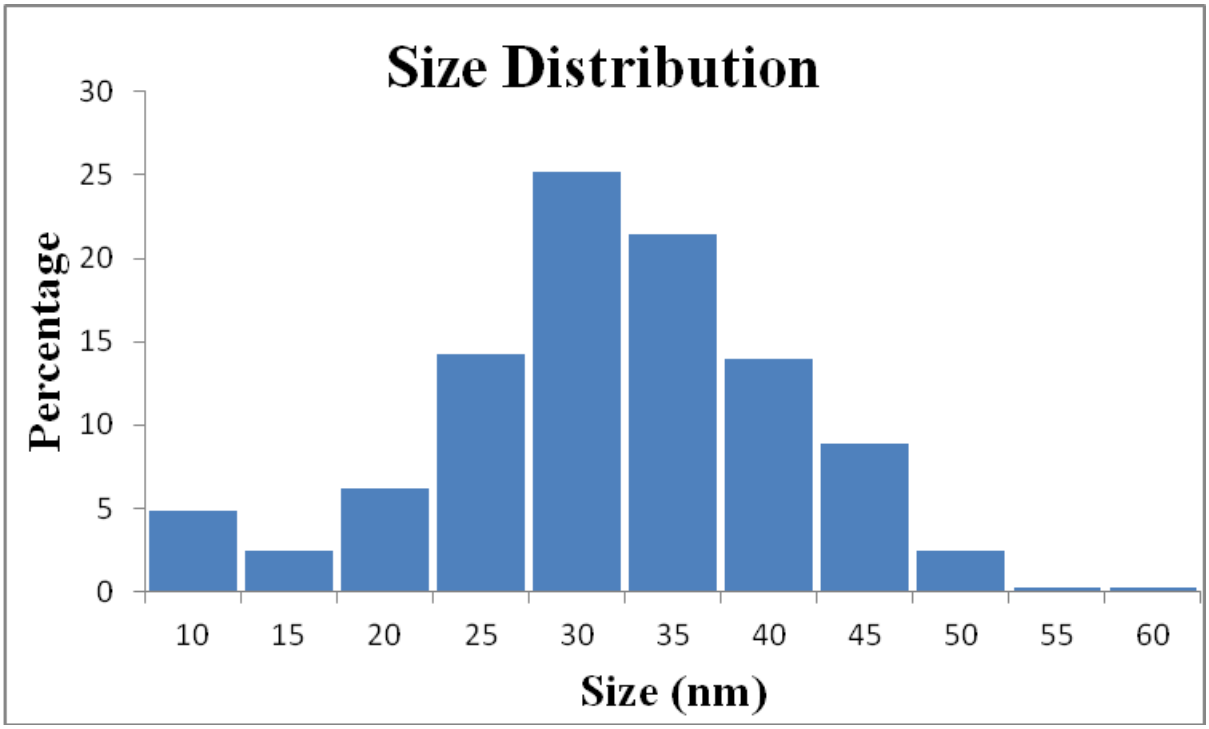

Figure 4.32: Percentage diameter (nm) of mono-dispersed anatase NPs

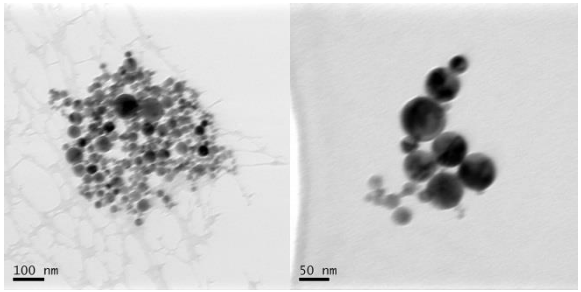

Figure 4.33: TEM images (taken at 200kV extraction voltage) showing anatase nanoparticles stabilized by sodium citrate

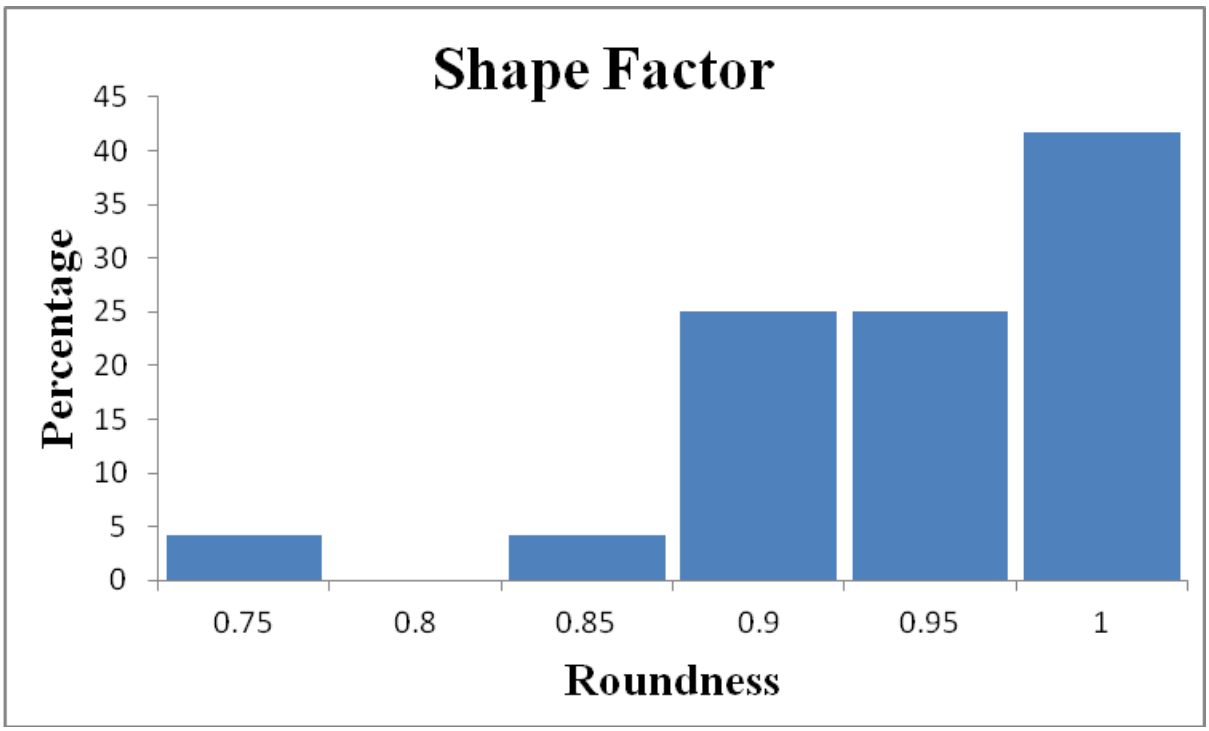

Figure 4.34: Percentage shape factor of sodium citrate stabilized anatase NPs.

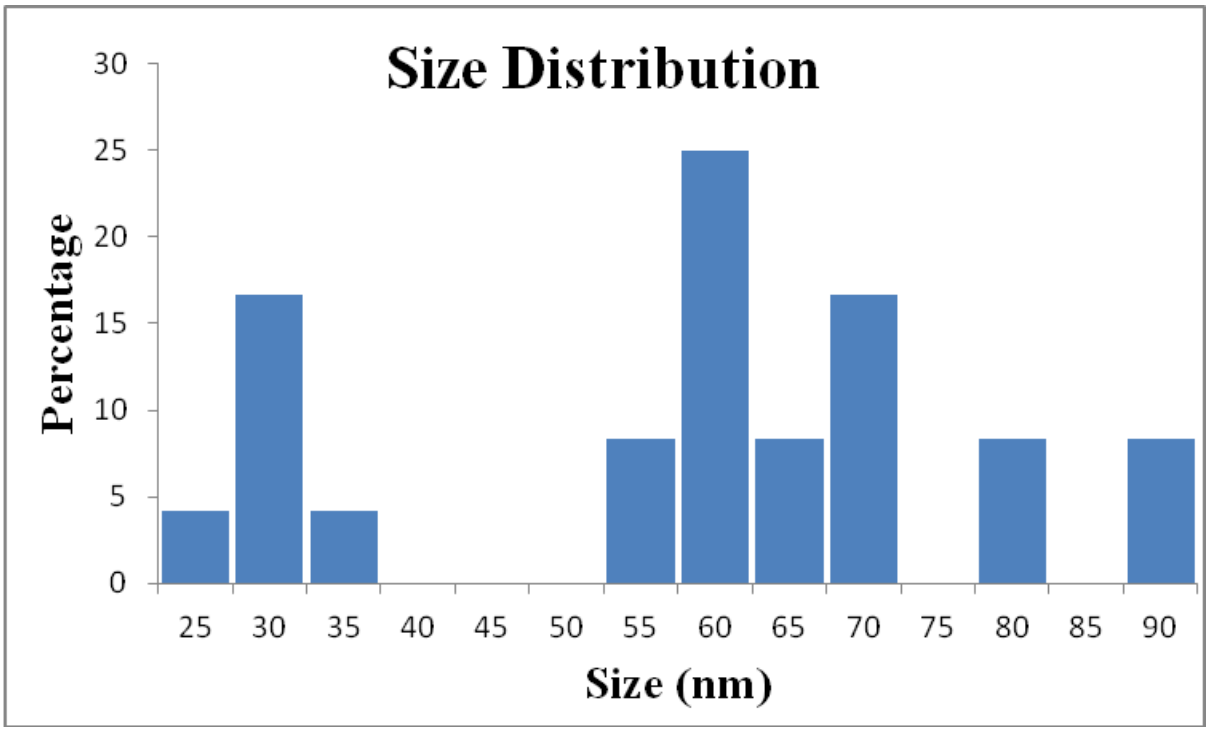

Figure 4.35: Percentage diameter (nm) of sodium citrate stabilized anatase NPs.

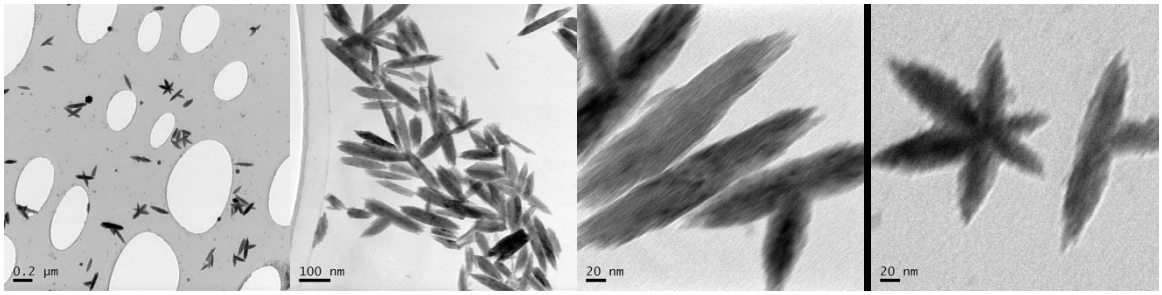

Figure 4.36: TEM images (taken at 200kV extraction voltage) showing sodium citrate stabilized nanorods (shape factor 0.2).

4.6 Detailed TEM Analysis

High resolution TEM was carried out on selected samples. The achieved results were compared with the XRD of same material. Figure 4.37 shows the XRD patterns of the as-synthesized samples prepared with $TiCl_4$ and after microwave treatment. It was indexed on the basis of tetragonal anatase TiO_2 (JCPD 21-1272) without any impurity phases. The mean crystallite size calculated based on the (101) reflection using Scherrer's equation is 14 nm for as prepared anatase and 34nm for microwave treated.

The selected individual single particle in Figure 4.38 shows a rough surface, perhaps due to a large number of mesopores on the round surface. HRTEM micrograph of the anatase TiO_2 shows lattice fringes with a d-spacing value of 0.189 nm, which corresponds to the (200) plane of anatase TiO_2. Figure 4.39 shows some more HRTEM micrographs along with the SAED pattern confirming (101), (004), and (200) planes of the anatase phase, in line with the XRD data.

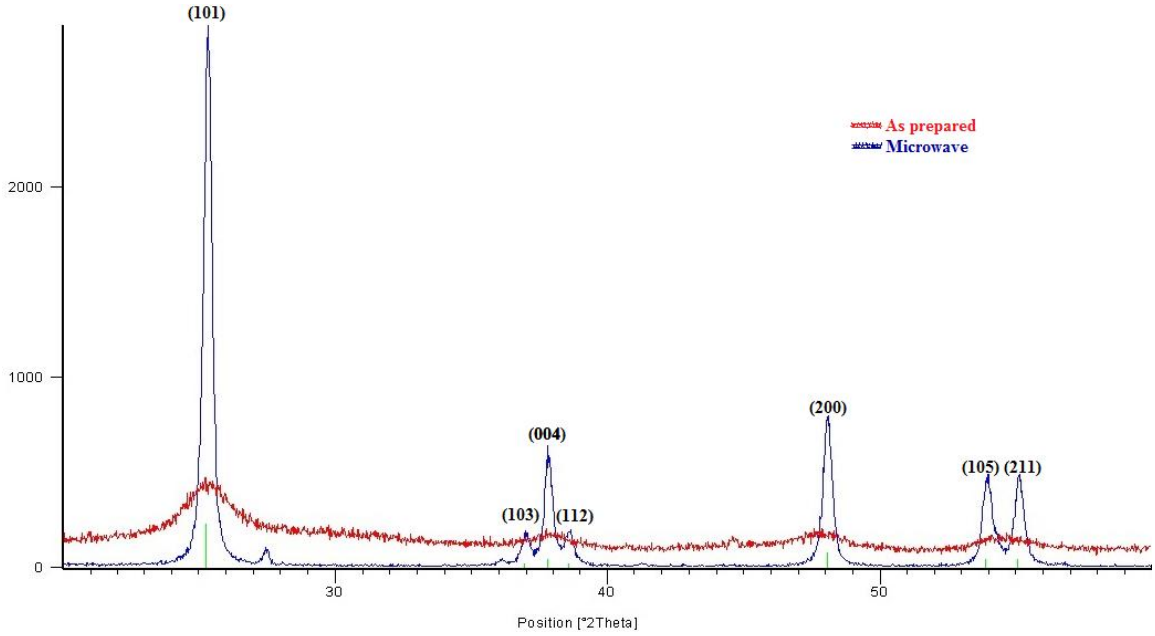

Figure 4.37: XRD comparison of as prepared and microwave treated anatase NPs.

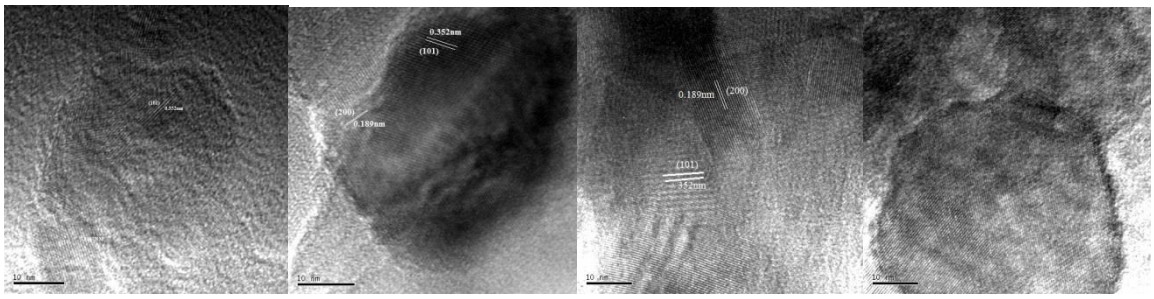

Figure 4.38: HRTEM images (taken at 200kV extraction voltage) of anatase NPs showing lattice fringes of (101) and (200) corresponding Figure 4.28

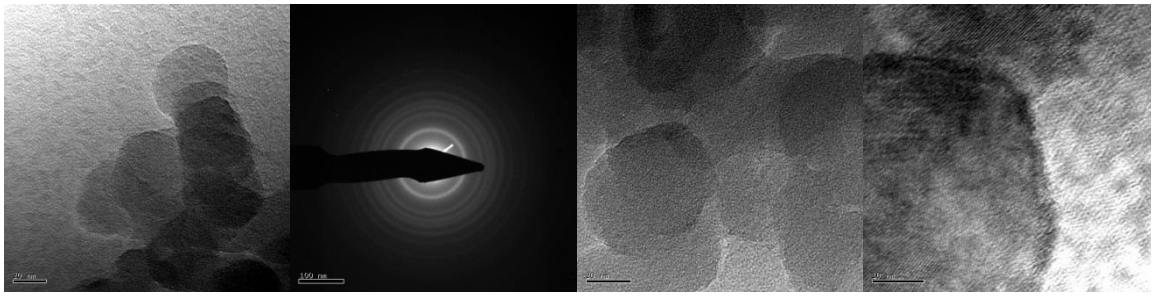

Figure 4.39: HRTEM images (taken at 200kV extraction voltage) of anatase NPs showing lattice fringes and SAED pattern corresponding Figure 4.28

The HRTEM images in Figure 40 indicate lattice fringes of mixed anatase and rutile sample. Lattice fringe with a d-spacing value of 0.189 nm, corresponds to the (200) plane of anatase TiO_2 while d-spacing of 0.352nm is for (101) plane of anatase. Lattice fringe with a d-spacing of 0.290nm reflects (121) plane of rutile phase.

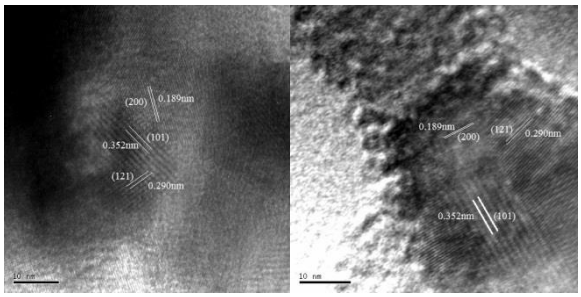

Figure 4.40: HRTEM images (taken at 200kV extraction voltage) of mixed anatase and rutile NPs showing lattice fringes (101), (121) and (200) corresponding Figure 4.5

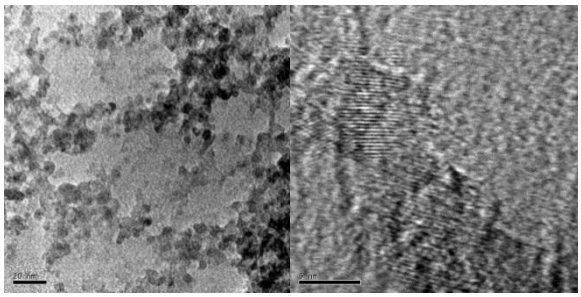

Figure 4.41: HRTEM images (taken at 200kV extraction voltage) of anatase NPs showing lattice fringes (101) corresponding Figure 4.16

The HRTEM images in Figure 4.41 indicate lattice fringes with a d-spacing value of 0.352nm is for (101) plane of anatase phase. The image on left hand side shows anatase nanoparticles of 5-6nm size.

Figure 4.42 presents the TEM images of a single nanorod surface, showing the lattice fringes with a d-spacing values of 0.248 nm and 0.324nm, which correspond to the (101) and (110) planes of rutile phase respectively. The SAED image in Figure 4.42 intimate a set of sharp rings corresponding to the (110) and (101) planes of the rutile phase.

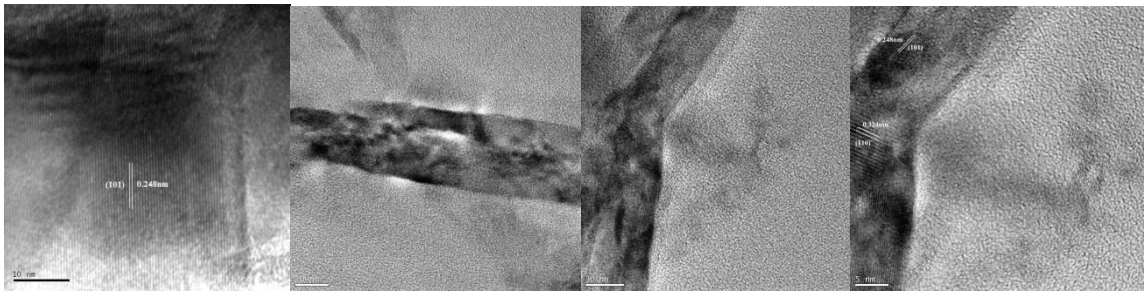

Figure 4.42: HRTEM images (taken at 200kV extraction voltage) of rutile nanorods showing lattice fringes (101) and (110)

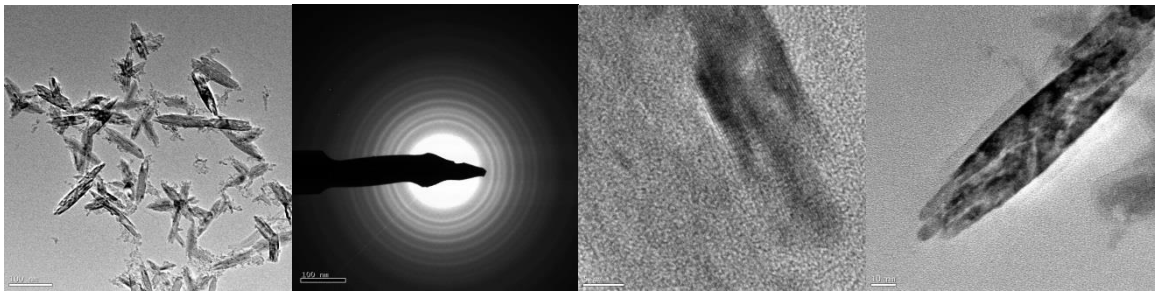

Figure 4.43: HRTEM images (taken at 200kV extraction voltage) of rutile nanorods showing lattice fringes and SAED pattern corresponding figure 4.19

All the suspensions were studied for hydrodynamic diameter right after synthesis and for stability over time. Few selected DLS graphs are presented here which clearly show the size and monodispersity of the materials synthesized. The samples were tested for their stability over time. The figures below (Figure 4.44 a-g), proved the success of synthesis process of mono-dispersed titania suspensions. Each figure confirms the TEM results presented above.

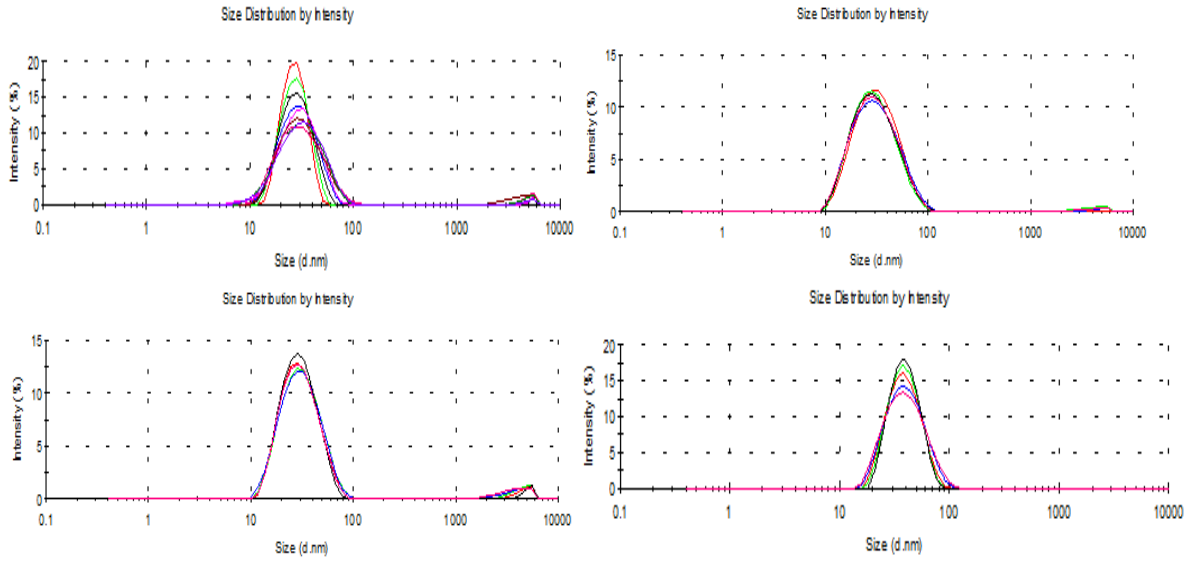

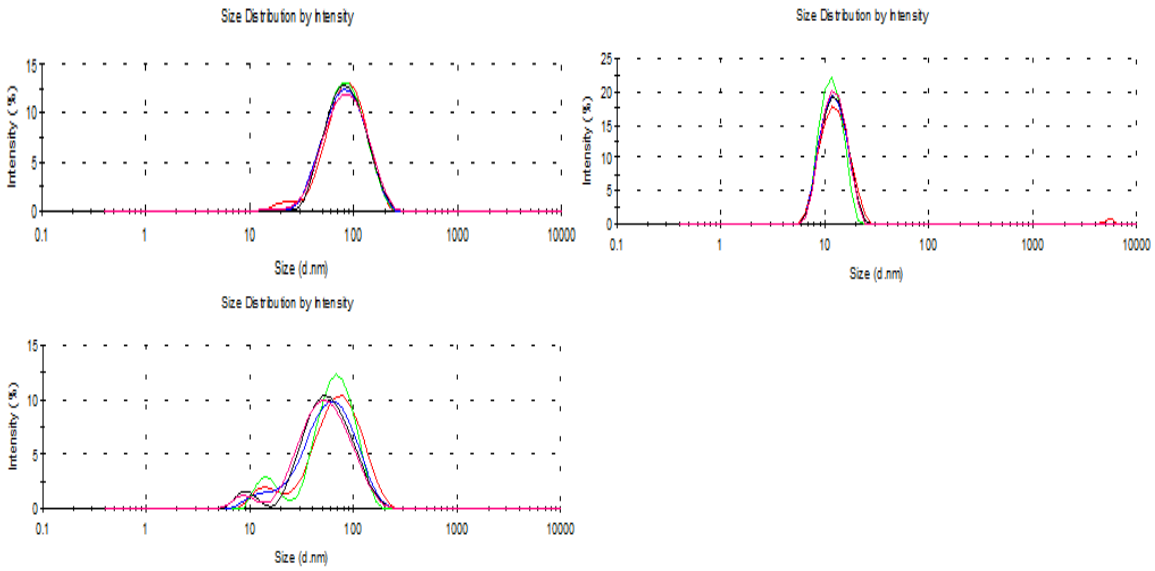

Figure 4.44: Mixed alcohol synthesis ethanol, methanol, Acetone (1:1:1:2 ratio) b) Mixed alcohol synthesis ethanol, methanol, Acetone (1:1:1:2 ratio) after 1 month c) Effect of sonication on mixed alcohol synthesis ethanol, methanol, Acetone (1:1:1:2 ratio) d) Mixed alcohol synthesis ethanol, methanol, propanol (1:1:1:2 ratio) e) Effect of microwave treatment on mixed alcohol synthesis ethanol, methanol, Acetone (1:1:1:2 ratio) f) Effect of boiling on mixed alcohol synthesis ethanol, methanol, Acetone (1:1:1:2 ratio) g) Mixed alcohol synthesis ethanol, methanol, Acetone, 2-propanol (3:3:3:1 ratio)

4.7 Discussions

As shown above, nanopowders and mono-dispersed suspensions were synthesized and characterized with different techniques. The effect of pH on nucleation and structural properties of TiO_2 NPs was investigated. It was found that pH has an influential effect on the morphology of the NPs. NPs synthesized at pH4 were having well controlled morphology, with anatase phase. It is observed that strong agglomerates were formed in the sol-gel or precipitate-derived nano-powders after calcination to get a crystalline phase, which deteriorated the properties of the end products. From the results presented above it can be observed that higher calcination temperature of 700^{o}C deteriorated NPs morphology in most of the cases. The results presented above are quite in line with the findings of Hu et al. (2003). They proved that nucleation of TiO_2 nanocrystals is dependent on pH value and sintering temperature. Moreover, Sugimoto and Zhou (2002) reported that for the exact control on the morphology of oxide particles, pH is main key factor, as shape and size along with phase are strongly guided by pH.

In alcohol water ratio study, the alcohol media, type of precursor, pH of the solution, and effect of temperature are considered to influence synthesis of the TiO_2 nanomaterials. The reactivity, solubility, and diffusion of the reactants are being influenced by the physical and chemical properties of solvents. Different alcohols gave different morphologies of nanomaterials and results are in line with the previous studies (Morrison and Ross, 2002, Chen and Elimelech, 2007, Mitrano et al., 2012). The polarity and harmonizing capability of the solvent can influence the morphology and the crystallization behaviour of the end products (Lue, 2007). Alcohols at different concentrations cause the polarity of the solvent and change zeta potential value of the reacting materials. In one study, short and wide flake like structures were obtained without the use of ethanol which converted to nanowires with ethanol and chloroform (Alagarasi, 2011).

HCl is the important constituent in hydrolysis of $TiCl_4$ which is produced during hydrolytic process. It controls the etherification process thus affecting the growth of crystallite size. HCl in its differentiating concentration promotes hydrolysis process acting as a catalyst. On the other hand HCl while acting as an electrolyte prevents particle nucleation or agglomeration. So mainly strong acid delays the quick gelation process as compared to TTIP hydrolysis (Spurr and Myers, 1957). Idea behind the alcohol and water ratios is to make this acid assisted hydrolysis easier and to bring it to lower nucleation temperature. In this hydrothermal synthesis process, many other factors like; peptization temperature (Balikdjian et al., 2000) and pH (Stanjek and Häusler, 2004), might be the factor to change the morphology and/or phase of TiO_2 nanomaterials. It was observed that addition of $TiCl_4$ to the alcohol media quickly reduces the pH near or below a value of 1 (highly acidic). Low pH values show that HCl is a reaction product in the system. The produced HCl in the reaction system involves in the etherification of alcohols. Although water was already present in the system, more water

would be produced as a by-product of etherification. This water dissolves more HCl produced from the reaction between $TiCl_4$ and alcohols.

Heating temperature is another important parameter which affected the growth of NPs. In the $TiCl_4$ system, no nucleation of particles was observed at room temperature. A temperature of 80^oC gave significant NPs growth results while microwave treatments gave precise crystal structure as mentioned in Table 4-1.

In conclusion, titania nanomaterials could be successfully synthesized in alcohols under hydrothermal conditions. The amount and type of alcohols along with the reaction temperature defines the crystal structures, grain sizes and morphologies of the end products. HCl produced during the reaction process promotes etherification and stops agglomeration. The mixture of different alcohols gave promising results but the reason behind this controlled nucleation of nanomaterials is still questionable. One possible reason may be the miscibility and etherification of mixed alcohols to a point where the reaction system becomes neutral with no external forces gave round shape factor to the nanoparticles. From the results obtained, it is obvious that needle like structures are firstly produced (even in case of TTIP and pH studies) in the reaction system which turns to needle bundles (Figure 4.45). These bundles can either combine to form capsule or rod like structures or turns to individual needles. The separated needles get twisted and form round particles (Figure 4.46), and on the other hand nanorods and capsules join to form nanosquares or heat treatment under certain pressurized conditions, gave rise to round, non-uniform sized nanoparticles. This nucleation process is described in Figure 4.46 below.

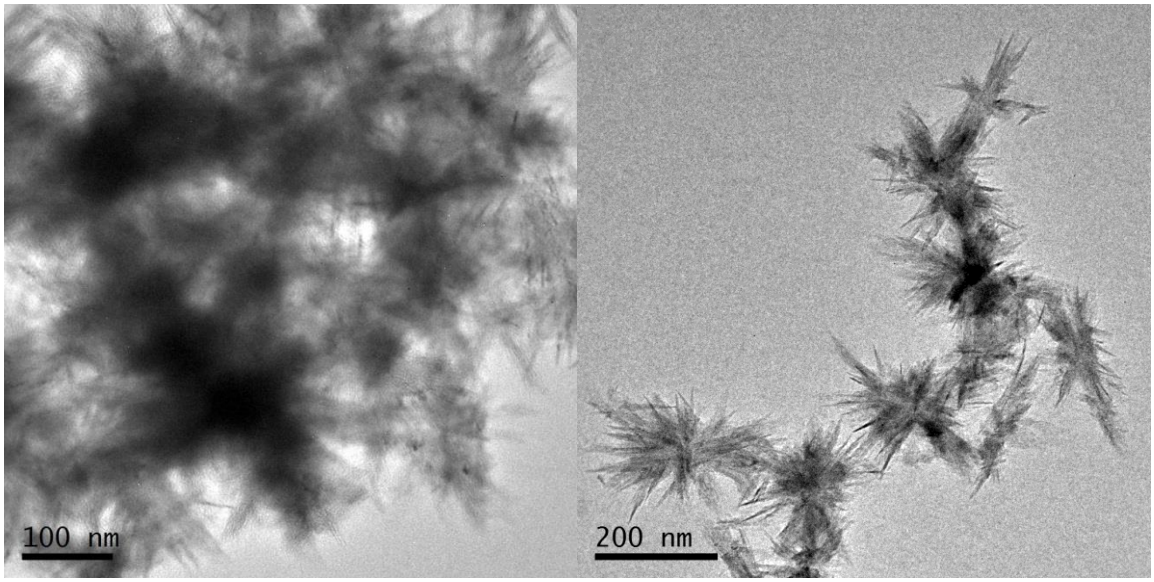

Figure 4.45: TEM images (taken at 200kV extraction voltage) showing needle like rutile structures during synthesis process

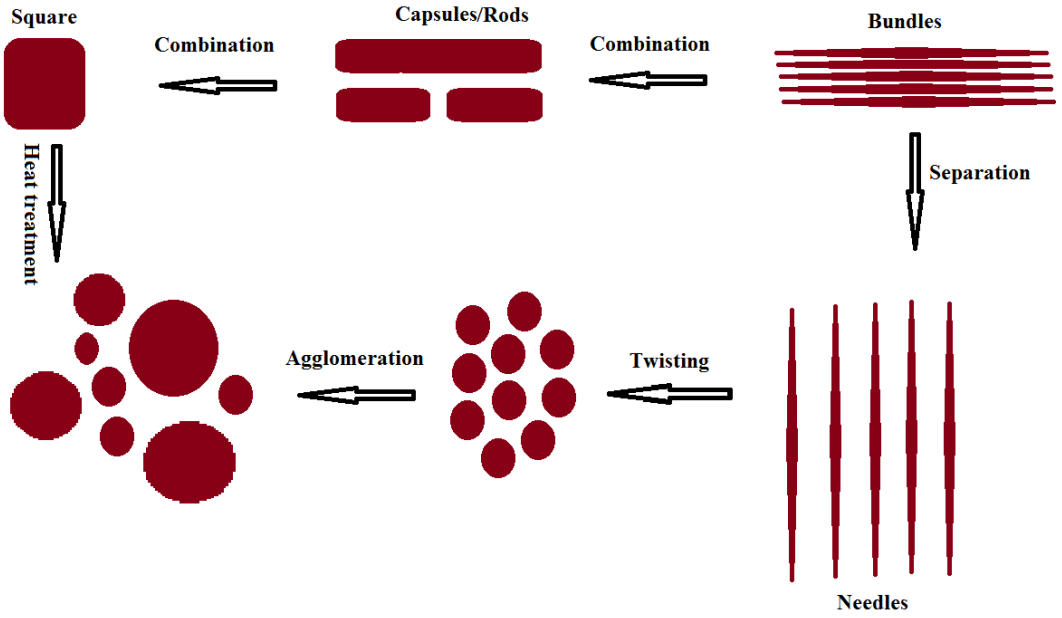

Figure 4.46: A schematic of the nanomaterials fabrication process

It was observed that nanoparticles at highly acidic condition were very stable but as soon as alcohol and organics were removed through washing or pH was maintained at or near neutral point, the suspension resulted in aggregation. Previous research work shows that stability of nanoparticles is mainly dependent on synthesis temperature (Kanel and Choi, 2007).

Dielectric constant of suspension decreases with an increase in temperature (Chen and Elimelech, 2008). This decreases the electrostatic influence against aggregation by decreasing the solvent viscosity. Larger particles are the result of an increase in the rate of aggregation. According to the continued observation and different sets of experiments, the optimum temperature for a better range of titanium dioxide nanoparticles is found to be 400°C. 700°C temperature gave larger aggregates which are generally out of nanoparticles range while room temperature gave amorphous material which again is not a desired product. pH is another variable which really influence the shape, size and dispersion of titania nanoparticles. Generally the addition of the acid gave smaller sized particles during the hydrolysis and this is quite in line with the findings of Vorkapic and Matsoukas (1998). When there are more H^+ ions present, there is more dispersity and less size. Low temperatures although give peptization to the sol but after XRD analysis it is clear that there was no crystal growth below 100^{o}C. Insufficient acid ratios, there is no peptization of TiO_2 aggregates remain unpeptized, but higher acid or H^+ ions, nanoparticles are very stable. This was the reason that most of suspensions made from $TiCl_4$ were stable until they were washed. Washing removes excess alcohol which promotes aggregation. The smallest particles are produced highly acidic pH values but as acidity decreased with addition of more water to the system, particles and agglomerate size increases and system moves towards instability. At high pH values the suspension consists of only few primary particles with bulk of organic material as shown by micrographs of high pH samples at room temperature. Even after peptization the addition of the acid governs the long-term stability of the sol. After several months of experiments, the sols with high pH are found to be stable. This clearly shows that titanium nanoparticles can be stabilized by using acids or bases (electrostatic stabilization).

4.8 Chapter Summary

The results presented above show that highly crystalline, stable TiO_2 nanoparticles and nanorods suspensions have been synthesized by controlled hydrothermal reactions. It has been proved that a selection of crystal shapes, grain sizes and morphologies could be achieved by a simple variation of the alcohol ratios and mixtures. Varying temperature and pH gave different and prominent results to control sized and shape of particles. Previously it was studied that HCl is a defining factor for titania nanomaterials size and shape. Results of current study suggest that concentration of alcohol and precursors have a profound effect in controlling size and shape of titania nanomaterials. It was noted that mostly in alcohol systems, nanoparticles remained in suspension form with little or no agglomeration but as soon as such nanoparticles were washed, they started to make bigger agglomerates. Stabilized suspensions synthesized during the processes mentioned above were used for post stabilization aggregation kinetics and glass bead column transport studies.

Chapter 5

Colloidal Stability of Titania Nanoparticles

5.1 Overview

Uncoated TiO_2 NMs tend to have a point of zero charge in the range of pH 5.5-6.0 (Suttiponparnit et al., 2010), and therefore charge stabilized NPs are largely unstable at environmentally relevant pH values (i.e. pH 5-8). This chapter investigates the post-synthesis stabilization of TiO_2 NMs after mixing the NMs with two steric i.e. PEG, PVP, and three electrostatic i.e. SDS, sodium citrate and SRFA stabilizing agents. SRFA was applied at two concentrations i.e. 10 ppm called SRFA10 and 100 ppm called SRFA100. Sodium citrate and SRFA100 were found to produce stable suspensions of TiO_2 NPs at pH 7.0±0.2 over a period of 2 weeks. Whereas PEG, PVP, SDS and SRFA10 did not improve the stability of TiO_2 NMs at all. The aggregation of the stabilized TiO_2 NPs (citrate and SRFA stabilized NPs) in the presence of both monovalent and divalent electrolytes (e.g. NaCl, $NaNO_3$, $CaCl_2$ and $Ca(NO_3)_2$) was also investigated. It has been observed in this study that SRFA stabilized NMs proved to be slightly less stable in either mono or divalent cations as compared to sodium citrate stabilized NMs of same kind. The critical coagulation concentrations (CCCs) of the SRFA-stabilized NMs were 3.8 and 3.2 mM $CaCl_2$, 5.5 and 5.5 mM $Ca(NO_3)_2$, 103 and 1025 mM NaCl, 72 and 115 mM $NaNO_3$, for rutile ellipses and anatase spherical NPs, respectively. In comparison CCC's observed for sodium citrate stabilized NMs were significantly higher than SRFA stabilized NMs, showing that sodium citrate is a better stabilizing agent than SRFA. The CCCs observed for sodium citrate stabilized NMs were; 10.7 and 9.4 mM $CaCl_2$, 16 and 9.7 mM $Ca(NO_3)_2$, 1.7 and 0.9 M NaCl, 238 and 90 mM $NaNO_3$ for rutile ellipses and anatase spherical NPs, respectively.

5.2 Background

Uncoated TiO_2 NPs have tendency to aggregate very easily forming larger particles. Such aggregation behaviour is undesirable for most applications due to difficulty in separation and recovery of TiO_2 particles in their primary size form (Wang et al., 2000). The colloidal stability of NPs is determined by pH, salinity, size, surface chemistry, NP concentration and other factors (Mylon et al., 2004, Dunnivant et al., 1992). For charge stabilized-NPs, the aggregation behaviour of NPs depends on the net electrostatic surface interactions of the colloids, as described by the classic Dejaguin–Landau–Verwey–Overbeek (DLVO) theory (Verwey, 1947). DLVO theory highlights the stability of colloids in different solution and electrolyte conditions, which is mainly governed by the surface charge (French et al., 2009).

The physico-chemical properties of NPs also determine their stability by affecting their behaviour in suspension and reactions on particle surfaces (Tourinho et al., 2012) concluded from their critical review of metal-based NPs in soil, that the characteristics of NPs (for instance size, shape, zeta potential) and soil (e.g., pH, ionic strength, organic matter, and clay content) affect physical and chemical processes, which result in NP dissolution, agglomeration, and aggregation. Studies are largely conducted on surface zeta potential, ionic strength and pH because these are the primary stability determining factors of colloidal stability for different NPs (Mandzy et al., 2005, Kretzschmar and Schäfer, 2005, Kataoka et al., 2004, Klaine et al., 2008b, Chen et al., 2011b, Edgington et al., 2010). Furthermore, stability of TiO_2 NPs over a range of pH values could be correlated with the zeta potential. The possible mechanism of this correlation might be the alteration of the reaction kinetics at different extreme environments (Dysart and Hines, 1969, Carole and et al., 2009).

From all of these studies, it is evident that for electrostatically stabilized NPs, increasing ionic strength or bringing the pH close to the NP isoelectric point (Cao et al., 2011); increase the agglomeration called reduction of material or shielding of charge around individual NPs. This concept does not support the sterically stabilized NPs. All physical and chemical factors enhance agglomeration results for larger hydrodynamic sizes (Jiang et al., 2009b). Therefore, to enhance colloidal stability, different surfactants are used to stabilize NPs in the pre- or post-synthesis processes (Chen and Elimelech, 2008), but the relation of adsorbed ions on NPs surface with respect to stability is still not yet fully understood (Fatisson et al., 2012).

Most research on TiO_2 nanotoxicity does not consider NP agglomeration or aggregation state (Chowdhury et al., 2011, Jin et al., 2011, Findlay et al., 1996, Hall-Stoodley et al., 2004). In real environmental conditions, the aggregation behaviour of TiO_2 might differ from the lab scale studies. This may result in bias data collection giving inaccurate result of different lab studies due to use of aggregated NPs considering manufacturer's label information only. Thus, researchers conducting toxicological studies might have overlooked the actual behaviour of NPs in the test media.

The aggregation kinetics and stability of titania NPs is a rather complex process that depends on the pH, zeta potential, solute concentration and solvent type of the NP suspension. Moreover, humic substances may also have steric stabilization, so it gives either extra stability and/or aggregation because of two mechanisms; OM-NPs bridging and steric interactions.

Zeta potential is defined as the electrical potential at the shear plane with respect to the bulk liquid (Greenwood, 2003). It is an important parameter which is related to the capacity of electrostatic repulsive or attractive force between NPs which in turn defines their stability in an aqueous medium (Wamkam et al., 2011). This is true for electro-statically stabilised NPs but not for sterically stabilized NPs. In sterically stabilized NPs, the amount of polymers and

their arrangement on NPs surface account in overall stability. Zeta potential is an essential factor which determines the stability of TiO_2 NPs in aqueous media and depends on the sticking ability of TiO_2 NP surfaces (Fatisson et al., 2012, Sperling and Parak, 2010, Mylon et al., 2009). Studies have shown that the zeta potential of particles depends on several factors such as the chemical composition of the NP surfaces, the nature of the solvent, the pH of media, ionic composition of media and reaction with other media constituents (Mandzy et al., 2005, Kim and Walker, 2001, Walker and Bob, 2001, González-Mozuelos and de la Cruz, 2009, Kung et al., 2010). Zeta potential of TiO_2 NPs also depends on their shape and size (Mandzy et al., 2005). Mandzy and co-workers also determined that different shapes and sizes of TiO_2 NPs significantly control zeta potential by controlling isoelectric point (Mandzy et al., 2005) of NPs in the presence of different surfactants. They showed that SDS coated TiO_2 NPs had two IEP values, most likely due to complex chemistry and chemical impurities of the reaction system. The addition of SDS into the TiO_2 NP suspension caused a shift of IEPs to lower pH values; thus the surfactants controls the IEPs and zeta potential, hence the size and shape of TiO_2 NPs during the synthesis process.

DLVO interactions discussed with detail in chapter 3 are the governing factor of stability and instability of nanoparticles. Negative surface charge on NPs increases the hydrodynamic layer thickness and adsorption density with decreasing pH and increasing ionic strength, thus giving them stability in aqueous media (Au et al., 1999, Mohammed, 2009, Mandzy et al., 2005). Au et al. (1999) concluded from modelled simulations and experimental research work that adsorption density and adsorbed hydrodynamic layer thickness of hematite, decreased with increasing pH and with decreasing ionic strength, while the adsorption density decreased with the increasing pH and negative surface charge. Also the adsorbed hydrodynamic layer thickness increased with increasing pH of the suspension. This explains the importance of negative surface charge in the stability of NPs.

The surface charge density on a nanoparticle surface is defined as the total amount of charge q per unit area a. $\sigma = q/a$. The overall stability of nanoparticles depends on the repulsive forces caused by surface charge in the dispersion. If somehow these repulsive forces get changed either by addition of a stabilising agent like a surfactant or polymer or by a destabilising agent like a salt, it will effect overall stability of the suspension. The zeta potential of a nanoparticle suspension is due to its surface charge density, i.e. the number of charge ligands on nanoparticles surface per unit area. The higher the magnitude of surface charged ligands, the greater will be the zeta potential. It is important to consider that the zeta potential and surface charge density are both intensive properties of nanoparticles which are least affected by the size of nanoparticles but more surface area definitely gives more space for charged ligands to be attached to surface of nanoparticles.

The post synthesis stabilization of TiO_2 NPs and its evaluation in terms of aggregation kinetics will help to understand the ultimate fate and behaviour in real environments.

According to the DLVO theory (Verwey, 1947) the aggregation in a medium is determined by the thickness of EDL and charges on the particle surfaces. The sum of van der Waals attraction and EDL repulsion forces defines the DLVO total interaction energy (Dunphy Guzman et al., 2006, Elimelech, 1995). When NPs approach each other, certain forces like London–van der Waals, solvation, electrical double layer, steric and hydrophobic forces impart aggregation (Sayes et al., 2006). NPs physicochemical properties (Lin et al., 2010) and chemical interactions of exposed surfaces like sorption (Fukushi and Sato, 2005, Kobayashi et al., 2005). Very small entities or particles have negligible settling velocity (Yamago et al., 1995, Gamer et al., 2006) so destabilization of NPs could result in the formation of larger aggregates at the expense of smaller NPs which might lose their NPs characteristics (Kalsin et al., 2006, Domingos et al., 2009). This process may lead to an increased settling rate making

NPs unavailable for any toxicology studies at lab scale (Ottofülling, 2010) but in real environmental conditions, they may become more available to benthic organisms (Eckelman et al., 2012). Also the reactions of NPs with other water constituents could end up with products which might be harmful to ecosystem.

In one lab study by Linse et al. (2007), protein fibril nucleation increased as a result of interaction of soluble protein and hydrophobic NPs like CeO, MWCNTs and quantum dots. According to them the actual mechanism of this protein fibril nucleation was not known but speculations of interaction with the NPs still exist. NPs could increase the probability of homogeneous nucleation of different proteins and other constituents of environment. Table 5-1 shows a summary of selected findings of aggregation studies conducted for different NPs.

The purpose of this study is (i) to investigate the impact of different stabilizing agents (e.g. citrate, SRFA, PVP, etc.) on the stability of the synthesized TiO_2 NPs and (ii) to evaluate the behaviour of the stabilized TiO_2 NPs under a range of environmentally relevant conditions (pH, phase, shape, monovalent and divalent cation concentration and HA presence and absence). The stability of TiO_2 was assessed by measuring the aggregation kinetics and fractal dimensions of TEM images.

Table 5-1: Review of few selected papers on aggregation behaviour of different NPs

Title	**NPs Type**	**NPs Shape**	**NPs Size**	**Key Observations**	**Reference**
Aggregation and disaggregation of iron oxide nanoparticles: Influence of particle concentration, pH and natural organic matter.	FeO	Round	20nm	• Interactions between NPs and natural organic matter are important for NP fate and behaviour in environment. • NP aggregates at a range of environmental relevant conditions, including variable pH, ionic strength and different components and concentrations of NOM. • Disaggregation is as important as aggregation process.	(Mohammed, 2009)
Stability of titania nanoparticles in soil suspensions and transport in saturated homogeneous soil columns.	TiO_2	Spherical	35nm	• TiO_2 nanoparticles were stable in soil suspensions. • Suspended TiO_2 relative concentrations were positively correlated with DOC and clay contents, and negatively correlated with ionic strength, zeta potential and pH. • The higher stability of TiO_2 suspensions resulted in a higher mobility of TiO_2 through soil layers.	(Fang et al., 2009b)
Influence of Surface Potential on Aggregation and Transport of Titania Nanoparticles	TiO_2	-	5-12nm	• 80% of suspended particles and aggregates have no mobility issue except for pH values, close to the point of zero charge (pH_{zpc}) • pH_{zpc} of TiO_2 NPs changes with size, with the smaller particle sizes exhibiting the lowest pH_{zpc} (pH_{zpc} of 3.6 nm particles = 4.8) and larger size by coarsening of small particles exhibiting higher pH_{zpc} (pH_{zpc} of 8.1 nm particles = 6.2) •	(Dunphy Guzman et al., 2006)
Nanoparticle characteristics affecting environmental fate and transport through soil	Al	Round	50, 80, 120nm	• Surface functionalization had a marked effect on charge, stability and agglomeration state of nanoparticles • Transport of NPs is dependent on the size of the nanoparticles • Solutions having moderate ionic strength rapidly agglomerated to form micron sized agglomerates restricting transport of NPs through soil columns	(Darlington et al., 2009)

Using a Surface complexation model to predict the nature and stability of nanoparticles	Hydrous Ferric Oxide (HFO)	-	-	• Surface complexation occurs at the bulk of the nanoparticles, as in a solution. • Particles (either colloids or nanoparticles) come close to each other certain forces act on them which tend either to disperse them or aggregate them	(Fukushi and Sato, 2005)
Aggregation and Charging of Colloidal Silica Particles: Effect of Particle Size	Silica	Spherical	30, 50, 80nm	• NPs were neutral at low pH and their zeta potential decreased with increasing pH and increasing ionic strength • Aggregation was a result of growth of clusters and was governed by media conditions and chemical interactions of exposed surfaces • Only the aggregation of the largest particles exhibited features similar to predictions of the DLVO theory. The smaller particles, on the other hand, aggregated much more slowly at higher pH and were completely stable at low pH	(Kobayashi et al., 2005)
Effects of Natural Organic Matter and Solution Chemistry on the Deposition and Re-entrainment of Colloids in Porous Media	Sulfate latex	Spherical	98nm	• No effect on the overall behaviour of nanoparticles in natural waters • They associated with organic macromolecules, regardless of size, that subsequently alter the particle's interfacial and physical characteristics like charge, reactivity, size etc. • Adsorption of humic acid on latex colloids and silica collectors reduced the deposition of suspended particles and enhanced the re-entrainment of deposited particles in porous media	(Franchi and O'Melia, 2003)

5.3 Results and discussion

Two types of NMs were used for the stability studies, rutile ellipses and anatase spherical NPs (Figure 5.1, Figure 5.2, Table 5-2). Both types of NPs were stabilized separately with optimised concentrations of 0.3% sodium citrate and 100 ppm SRFA. The average length of rutile ellipses measured with TEM was 100 ± 20nm (n = 214) with average width of 20 ± 5 nm (an aspect ratio of 4.5 ± 0.3 and hydrodynamic diameter of 55 ± 5 nm measured by DLS). Ellipses used for stability experiments were dispersed for a period over 6 months after use of stabilizing agents (Figure 5.1) with no observed aggregation or agglomeration.

Table 5-2: Size distribution of NMs measured with TEM and DLS

Type of NMs	**Size with TEM (nm)**	**Size with DLS (nm)**
Anatase Spherical NPs	60 ± 35	100 ± 10
Rutile Ellipses	100 ± 20 (length) 20 ± 5 (diameter)	55 ± 5

The spherical NPs had a core size range between 60±35nm (measured by TEM) and hydrodynamic diameter of 100±10nm, for both citrate and FA stabilised (Table 5-2). Figure 5.1a shows TEM micrograph of TiO_2 ellipses dispersed with SRFA100 while 5.1b shows magnified image of same ellipses. Both figures explain the dispersity of SRFA stabilized ellipses showing that individual particles are separated from each other maintaining a separation distance. Figure 5.1c is a micrograph of ellipses stabilized with sodium citrate while 5.1d shows the same picture at higher magnification. Both figures show the behaviour of sodium citrate for the stability of TiO_2 ellipses. Although they are stabilized and TEM figures show that they are keeping themselves separate from each other with weak inter-particle forces. Figure 5.2a below shows spherical anatase NPs stabilized with SRFA100 while Figure 5.2

shows sodium citrate stabilized anatase NPs. Both figures show the effect of SRFA and sodium citrate where SRFA is behaving as a better stabilizing agent than that of sodium citrate; maybe due to inter-molecular bridging of fulvic acid molecules.

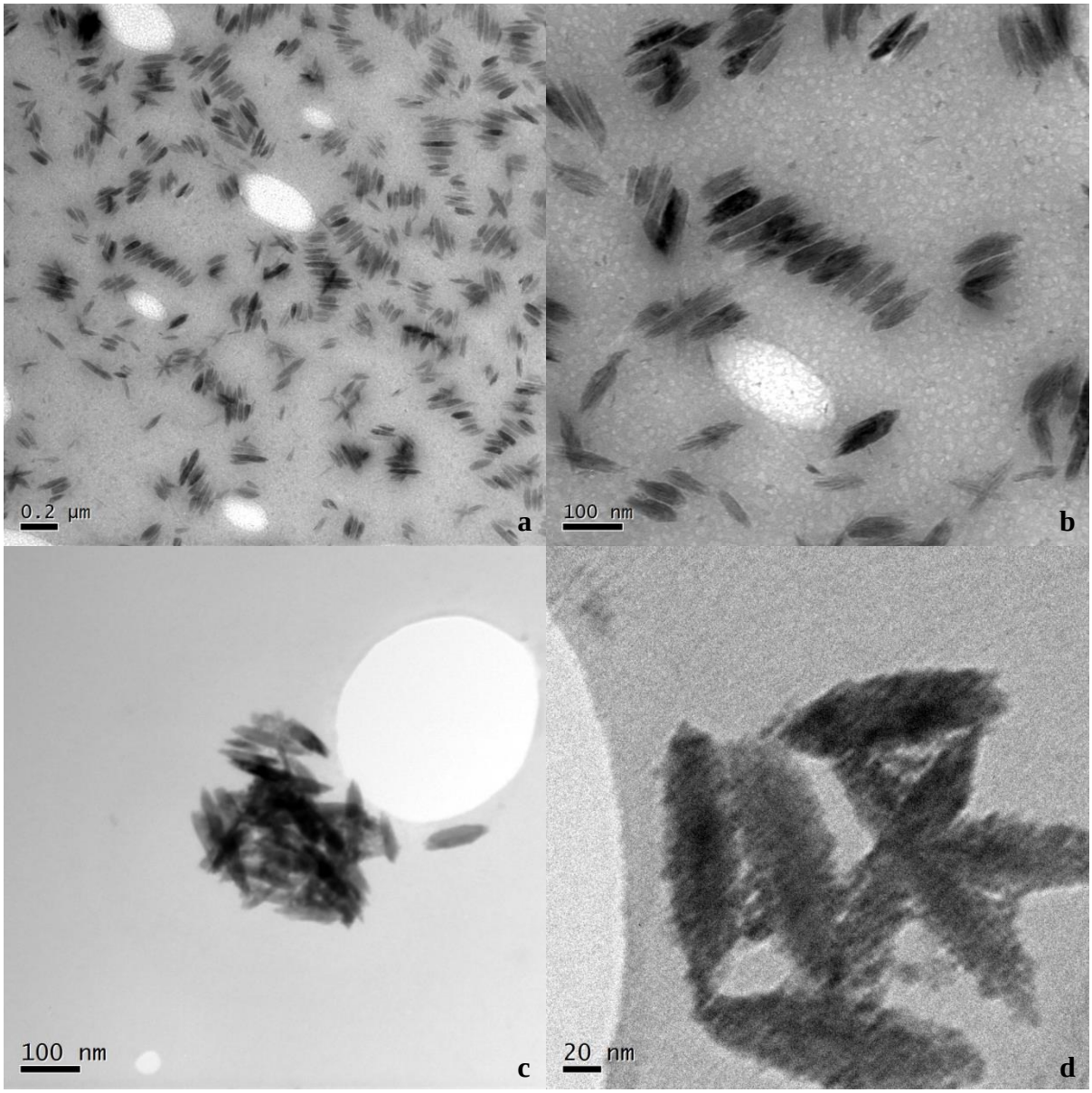

Figure 5.1: a) TEM micrograph of TiO_2 ellipses dispersed with SRFA100 b) Stability with SRFA100 at higher magnification C) Sodium citrate stabilized ellipses D) Image taken at 500K magnification (HRTEM and other details has been reported in chapter 4

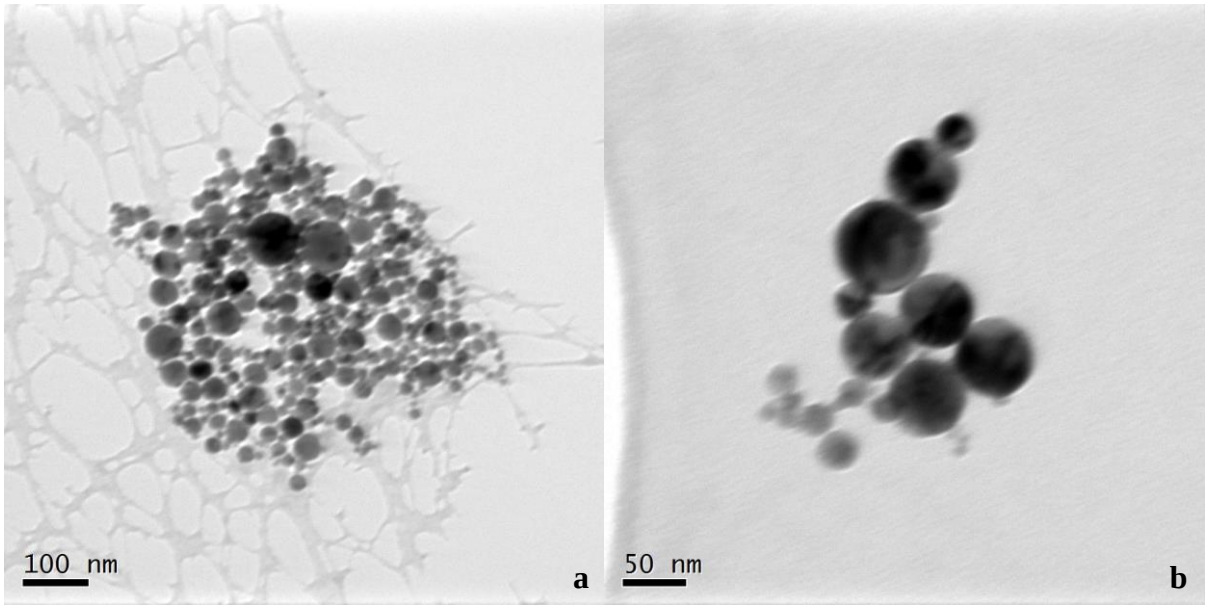

Figure 5.2: Spherical anatase NPs a) SRFA100 stabilized b) Sodium Citrate stabilized (Detailed analysis of these NPs has been discussed in chapter 4

5.3.1 Effect of surface functionalization on the stability of TiO_2 NPs

The effect of PEG, PVP, SDS, sodium citrate, SRFA10 and SRFA100 on the stability of TiO_2 NMs was investigated by measuring the zeta potential and hydrodynamic diameter of TiO_2 NPs following mixing TiO_2 NPs (at pH 7) with the above mentioned stabilizing agents. Effect of pH, surfactants and zeta potential on the aggregation was also studied in detail for a period of 2 weeks.

Different surfactants i.e. 0.3%PEG, 0.3%SDS, 0.3%PVP, 0.3% sodium citrate, 10ppm SRFA and 100ppm SRFA were used to stabilize the ellipses at pH values of 1-10. Change in size and zeta potential were observed over a period of 2 weeks with Malvern nanosizer DLS by monitoring changes in Z_{Avg}. The pH was adjusted with NaOH and HCl and solutions were left for at least 24 hours to reach the steady state aggregation and therefore, no change in aggregation was assumed to occur during the actual measurements. The pH was checked again before studying the zeta potential and size by DLS. Therefore, aggregation and zeta potential

were solely attributed to the measured pH value. Suspension was gently shaken before measurements.

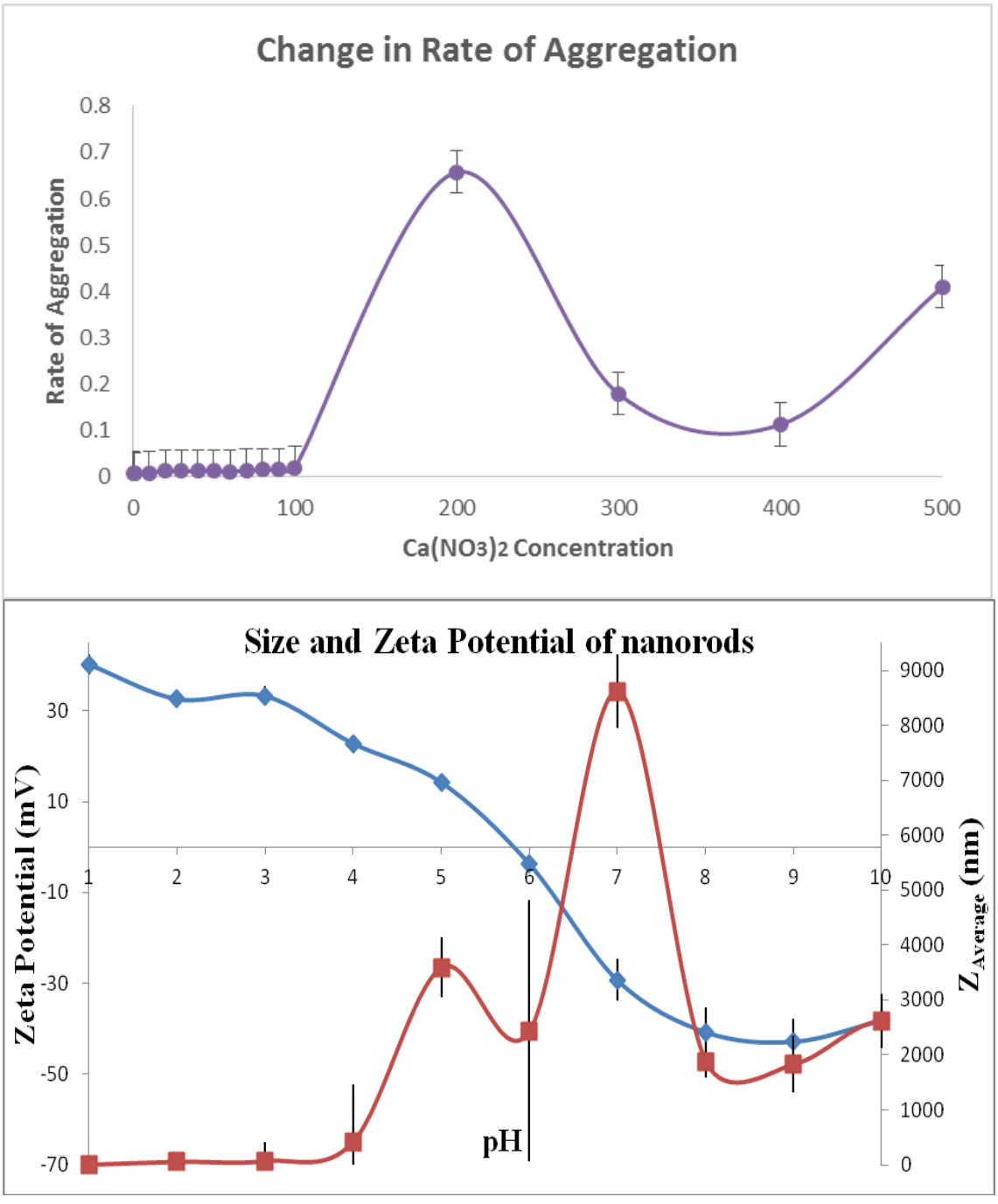

Figure 5.3 a) Change in rate of aggregation (m^3s^{-1}) of 20 ppm TiO_2 with time in the presence of $Ca(NO_3)_2$ at 2.8 pH b) Size and zeta potential of ellipses as a function of pH

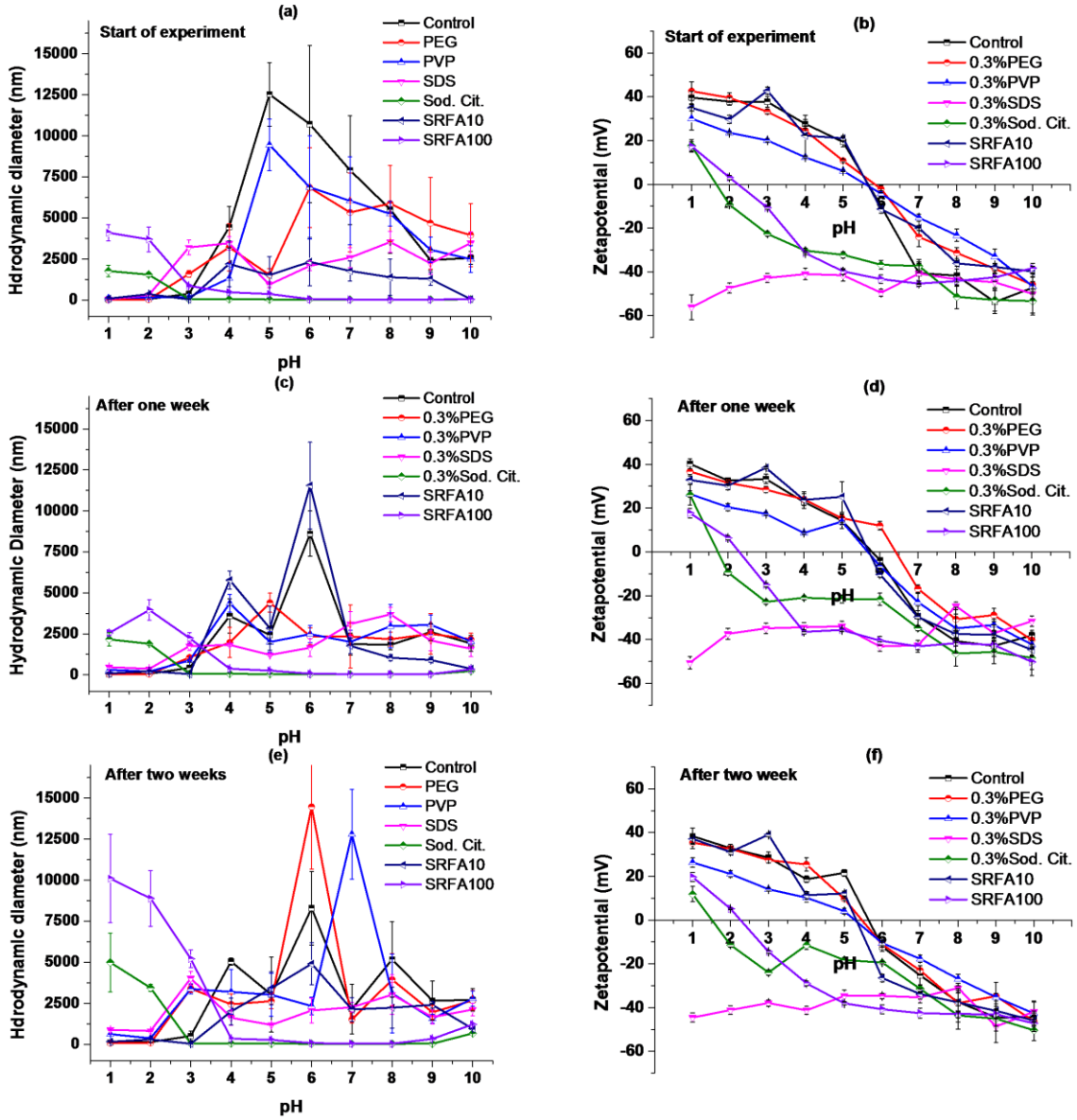

Figure 5.4 Effect of surfactants and pH on hydrodynamic diameter and zeta potential of TiO_2 NPs a) Size at start of experiment i.e. zero minutes b) Zeta potential at start of experiment c) Size after one-week d) Zeta potential after one-week e) Size after two weeks f) Zeta potential after two weeks

Figure 5.4a shows the result for the change in hydrodynamic diameter at different pH values for different surfactants at start of experiment. This change in size shows that the raw suspension of TiO_2 NPs was unstable at all pH values except the highly acidic range (pH 1-4). Figure 5.3 shows that larger agglomerates were observed at pH 5 which is a value near to point of zero charge (pH_{zpc}).

All other surfactants showed similar behaviour except SRFA100 and sodium citrate. Sodium citrate showed greatest stabilization for almost all pH values except the highly acidic range (pH 1-3) because pH_{zpc} was shifted to these values. The behaviour of these NPs showed that pH_{zpc} plays an important role in stability of NPs. Figure 5.4c and Figure 5.4e shows the change in hydrodynamic diameter one and two weeks after adding the stabilizing agents. No significant change was observed in change of hydrodynamic size over the period of two weeks. Visual settling of larger aggregates was observed for PEG, PVP and SRFA10 samples for the pH values near to the pHzpc (Figure 5.4e). Standard deviations of change in hydrodynamic diameter for three replicates show that there are non-significant changes in NPs size confirming the stability at a range of pH values (3-9). Control, PEG and PVP agree with high aggregation rate at a pH value near to point of zero charge (pH_{zpc}) as larger aggregates were observed near pH where net charge on NPs was nearly zero or negligible.

Figure 5.4 (b, d and f) shows that pH_{zpc} for sodium citrate and SRFA100 treatments were at pH values of ~ 1.6 and ~2.2, respectively. That is why aggregation can be seen for these samples at pH 1.6 and 2.2 (Figure 5.4a, c and e). The SRFA10 treatment showed similar aggregation behaviour as PEG, SDS and PVP, on stabilization as pH_{zpc} was at a pH value of ~5.6. Similar aggregation trend as shown by SRFA10, PEG, PVP and SDS, was also observed for the particles without any surfactant (Control) which showed maximum hydrodynamic size at pH_{zpc}. All stability experiment results were correlated with corresponding zeta potential values (Figure 5.6) which confirms the effect of pH on the aggregation of TiO_2 NPs.

Figure 5.4 (b, d and f) shows that sodium citrate and SRFA100 changed zeta potential from positive to negative. The point of zero charge for sodium citrate and SRFA was pH1.6 and pH2.3 respectively. Zeta potential for 0.3% SDS remained on negative side all the time starting from pH1 up to pH10. Point of zero charge remained between pH5.5 and pH6 for all

other surfactants including control. Size change was fairly consistent with the positive and negative charge of the particles for all the surfactants over a period of two weeks. Maximum aggregation was observed with control at start of experiment having no surfactant which correlated with the corresponding zeta potential value (Figure 5.3a). Generally, the presence of negative charge on particles is prone to stability of NPs but this is not true with 0.3% SDS which gave inconsistent aggregation values. This may be attributed to the amount of surfactant present in the suspension or excessive bubbling behaviour of SDS. Optimization of SDS concentration might help to understand about the exact value of pH_{zpc} and zeta potential but it was beyond scope of current research work.

Figure 5.4a shows effect on stability of TiO_2 NPs over a period of one week. The SRFA10 treatment illustrated more aggregation than all other surfactants which stabilized the suspensions as compared to the start of experiment. This aggregation by SRFA10 may be attributed to the presence of less negative charges in the medium than actually required to occupy the NPs surface, hence destabilizing the suspension. All other surfactants gave better stability than at the start of the experiment after one week because polymer molecules occupied all the attachment positions with time. All these size values are reasonably consistent with corresponding zeta potential values after one week (Figure 5.4).

There was no significant change observed in zeta potential values over time except change of point of zero charge with 0.3%PEG which increased from pH5.7 to pH6.4 (Figure 5.4b, d and f).

Figure 5.4e shows the effect of surfactants after 2 weeks of stabilization. SRFA100 and sodium citrate showed no change in size over time. PEG and PVP showed an increase in aggregate size at neutral or near neutral pH or close to their point of zero charge.

Zeta potential after 2 weeks (Figure 5.4f) showed no change for all surfactants at all pH values except sodium citrate which showed a slight increase in value at pH 4-7. No change in zeta potential after 2 weeks shows that all sites on the particle surfaces are occupied by relevant charge to stabilize the size as well as zeta potential values. This is also true for SRFA10 which was not visibly able to provide enough negative charges to cover all particles and their surfaces. In comparison, SRFA100 provided enough concentration of charges to stabilize the suspension.

The results above show that sodium citrate and SRFA100 improved the stability (reduced the aggregated size) among all those investigated in this research work. All further stabilizations were made with SRFA100 and sodium citrate throughout the research work. Figure 5.4 suggests that SRFA10 did not improve the stability of TiO_2 NPs. PEG, PVP and SDS also showed visible aggregation behaviour throughout the experimental time. This behaviour of all surfactants used might be due to inappropriate binding forces for titania NPs which made their clusters giving higher hydrodynamic diameter. SRFA100 proved to be significantly better stabilizer than SRFA10 because later concentration did not occupy all the binding sites with FA molecules, due to which there was destabilization in the NP suspension. At higher concentrations of SRFA100 all the binding sites were completely occupied by the FA molecules as another experiment was done to have optimum SRFA concentrations (Figure 5.5). Moreover, SRFA might involve in intermolecular bridging with NPs, hence giving destabilization to the system. This is specifically true for the lower concentrations of SRFA. In case of sodium citrate all the binding sites were occupied by negative charges hence giving stability to the suspension.

5.3.2 Impact of pH on as synthesized TiO_2 Nanomaterials

The detailed impact of pH on the stabilization of TiO_2 NMs was studied and results are presented here.

5.3.2.1 Aggregation kinetics of as synthesized NMs (pH 2.8)

The results showed no significant change on Z_{Avg} and it was noted that as prepared suspension remained stable (pH 2.8) even in the presence of 100 mM $Ca(NO_3)_2$ (Figure 5.3). To evaluate the effects of concentration, the Zavg of above mentioned titania NPs between 200 and 500 mM of $Ca(NO_3)_2$ were also measured by DLS. Concentrations of 200 and 500 mM $Ca(NO_3)_2$ showed an increase in aggregation without any obvious trend. This deviation of data from the obvious trend might be due to the inability of DLS to measure larger agglomerate size in a consistent manner. This needs a further investigation by getting more data points between 200 and 500 mM $Ca(NO_3)_2$ concentration. This was not needed for current research work as it was realised that pH plays a role in such a stability behaviour at higher salt concentrations. Aggregation rate (calculated the rate of change in hydrodynamic data) increased to a value of 0.38 m^3s^{-1} at 200 mM concentration of $Ca(NO_3)_2$ which decreased to 0.1 m^3s^{-1} for both 300 and 400 mM concentrations (Figure 5.3a). The aggregation rate increased up to 0.5 m^3s^{-1} for 500 mM concentration of $Ca(NO_3)_2$.

5.3.2.2 Effect of pH on stability of nanomaterials

As synthesized rutile ellipses at pH 2.8 showed no significant aggregation at different concentrations of NaCl. When the pH was adjusted to 7, settling of the NP aggregates was observed by eye. The hydrodynamic diameter measurements showed inconsistent data of several thousand nanometer size for three replications. For all replicates there was a continuous

fluctuation in hydrodynamic diameter which indicated the overall decrease in stability of NPs with pH adjustment. The zeta potential for the suspension with pH adjustment was not changed and it remained on -32±0.02 mV. Following this trend of change of aggregation behvaior, a comprehensive study was conducted to evaluate the effect of pH on hydrodynamic diameter and zeta potential (Figure 5.3b).

As mentioned above, the as prepared ellipses had a pH value of 2.8 which was re-adjusted incrementally up to pH 10 with dilute NaOH. pH adjustment along with the measurement of hydrodynamic diameter and zeta potential is shown in Figure 5.3b. It can be seen that aggregation started at pH 4 which gradually increased up to pH 7. The pH_{zpc} of 5.9 was observed where maximum fluctuation occurred in hydrodynamic diameter. Maximum aggregate size was observed at pH 7, while dispersion remained stable with non-accountable changes in hydrodynamic diameter at pH 1-3. This increase in aggregation was lowered at higher pH values. Although aggregation was observed, its intensity was not as high as pH values near to pHzpc. The aggregation is due to the reduction in electrostatic repulsion of the NPs near to point of zero charge (pHzpc).

Keeping in view the above scenario, the NP suspensions stabilized at an environmental relevant pH range (6-8) with addition of different ionic and non-ionic surfactants. Figure 5.3a shows the stability of as prepared ellipses against different concentrations of $Ca(NO_3)_2$. There was no variation in the rate of change of the hydrodynamic diameter for $Ca(NO_3)_2$ salt concentrations up to 100 mM. Only the effect of $Ca(NO_3)_2$ was evaluated because Ca^{+2} salts tend to aggregate colloids very quickly even at lower concentrations (French et al., 2009). But for the NPs suspension with an acidic pH, had a net positive charge in the solution phase. When $Ca(NO_3)_2$ was introduced into the system, NO_3^- reacted with H^+ charge giving HNO_3 giving more stability to the system rather than showing the destabilizing effects of Ca^{+2}. So it was the

effect of NO_3^- for the stabilization of these NPs by giving a highly acidic environment to the reaction system. The protonated dispersant counter ions present in the aqueous phase, stabilized the ellipses suspensions (at pH 2.8), due to the evident buffering effect of acid present in the system.

Figure 5.3b shows the zeta potential values of the suspension when attempted to change the pH values from pH 1-10.

5.3.3 SRFA optimal concentration

The SRFA at 10 and 100 ppm showed significant difference in the stability of NPs. This experiment was performed to optimize the amount of SRFA needed for stability over a longer time period. Optimal concentration is the point at which the condition, degree, or amount of something (chemical, surfactant, solvent etc.) is the most favourable (Yang et al., 2002). During the stabilization experiments, it was noticed that SRFA10 and SRFA100 aided stability of NPs in some differential ways. Almost no effect was observed for SRFA10 while SRFA100 gave ultimate stability to NPs over a period of two weeks. While considering the above scenario, SRFA optimum concentration was calculated with 10, 25, 50, 75 and 100ppm of SRFA (Figure 5.5) at pH 7 and 8. Figure 5.8 reveals a change of sticking efficiency at these concentrations over one-week period. SRFA 25 at pH7 gave increased aggregation at the start of experiment which may be due to the presence of unsettled positive and negative charges in suspension. However, this charge settlement behaviour was not observed for the samples with SRFA25 at pH8. At pH8 more negative charges were present in particle dispersion to give it more consistency at start of experiment and even after one week. This is confirmed by SRFA10 at start of the experiment but after 1 week SRFA25 suspension showed consistent readings while SRFA10 suspension remained in the same aggregation state. The balance of the overall charges present on NPs surface changed after one week for SRFA50 giving a shift to overall

a

aggregate size in suspension. SRFA100 proved to be the best in NP suspension stability as it gave consistent size reading even after two weeks.

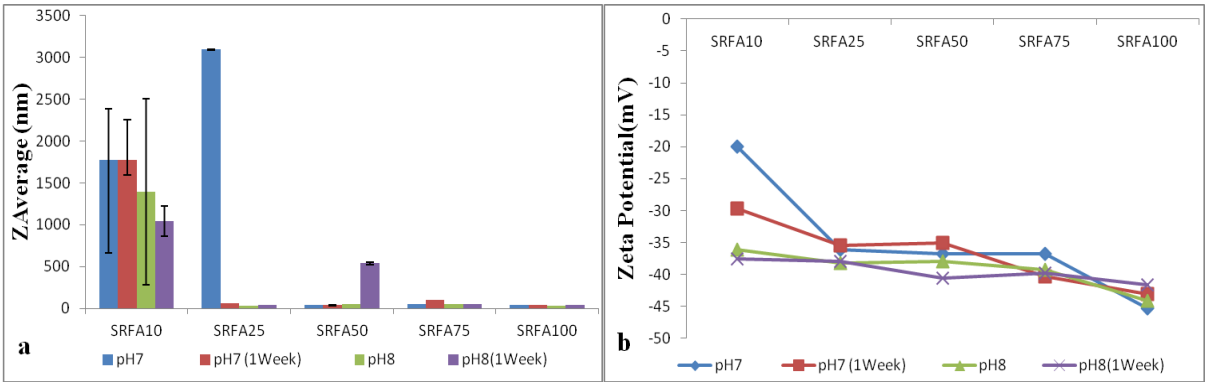

Figure 5.5: a) Comparison SRFA concentration on size of TiO_2 NPs over time b) Comparison SRFA concentration on zeta potential of TiO_2 NPs over time (pH7 and pH8 at start and after 1 week).

It is clear from Figure 5.5a that SRFA100 have significantly changed the stability for both pH values over a period of one week. SRFA10 illustrated least stability with no change in Z_{Avg} over a period of one week at pH 7 while pH8 treatment showed stable behaviour after one-week time. Figure 5.5b confirms the effect of SRFA concentration on zeta potential over a week time. More negative charge was observed after one week for SRFA10 after one week which potentially should show less size after one-week time. This change in negative charge is covered by the standard deviation of the size changes for pH7 at start of experiment which proves irregularity in readings and same is true with S_{Dev} of SRFA10 at pH8. All other zeta potential values remained more or less same after one week of time showing consistency in the aggregation and stability process as a function of SRFA concentrations.

5.3.4 Impact of ionic strength on the aggregation of SRFA and citrate coated-TiO_2 Nanoparticles at pH 7

5.3.4.1 Impact on rutile ellipses

Two types of sodium citrate and SRFA stabilized NPs were studied for their aggregation kinetics as per method described in methodology section. Four salts NaCl, $NaNO_3$, $Ca(NO_3)_2$ and $CaCl_2$ at different concentrations were used for both stabilized batches of NPs. The final results for the studies with three replications were as follows.

Figure 5.6a shows effect of NaCl salt concentrations on sticking efficiency and change in zeta potential. Sodium citrate stabilized ellipses showed more stability with a critical coagulation concentration of 1.68 ± 0.095 (n=3) M NaCl (Figure 5.7a). It was observed that with an increase in salt concentration, there was a decrease in stability and an increase in zeta potential value (from negative to positive value). The zeta potential values significantly increased from a value of -47mV (no salt) to -17mV at NaCl concentration of 8M.

Figure 5.6b shows effect of NaCl salt concentrations on sticking efficiency and change in zeta potential on SRFA100 stabilized titania ellipses. As compared to sodium citrate, SRFA100 critical coagulation concentration decreased from 1.68M to 1.025M NaCl (Figure 5.7b). These are results of three replicates which confirms that SRFA100 stabilized ellipses were less stable than sodium citrate stabilized. Decrease in zeta potential (Lin et al.) value was observed at critical coagulation concentration(s) otherwise ZP went up as the salt concentration increased.

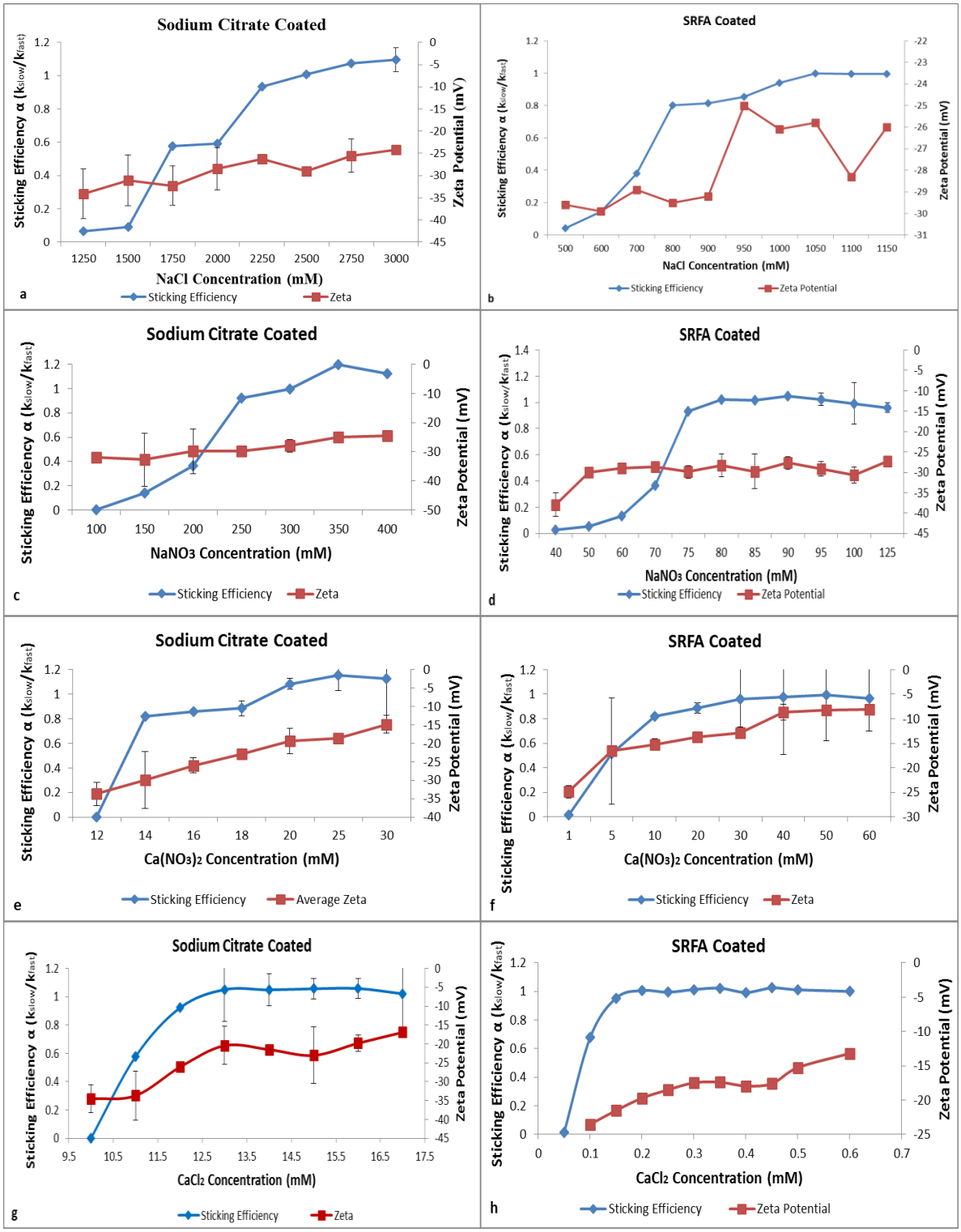

Figure 5.6: Effect of salt concentrations on titania ellipses a) NaCl on sodium citrate coated b) NaCl on SRFA100 coated c) $NaNO_3$ on sodium citrate coated d) $NaNO_3$ on SRFA100 coated e) $Ca(NO_3)_2$ on sodium citrate coated f) $Ca(NO_3)_2$ on SRFA100 coated g) $CaCl_2$ on sodium citrate coated h) $CaCl_2$ on SRFA100 coated (experiments were done at pH 7 ± 0.2 and sticking efficiencies were calculated by detailed method given in section 3.3.4)

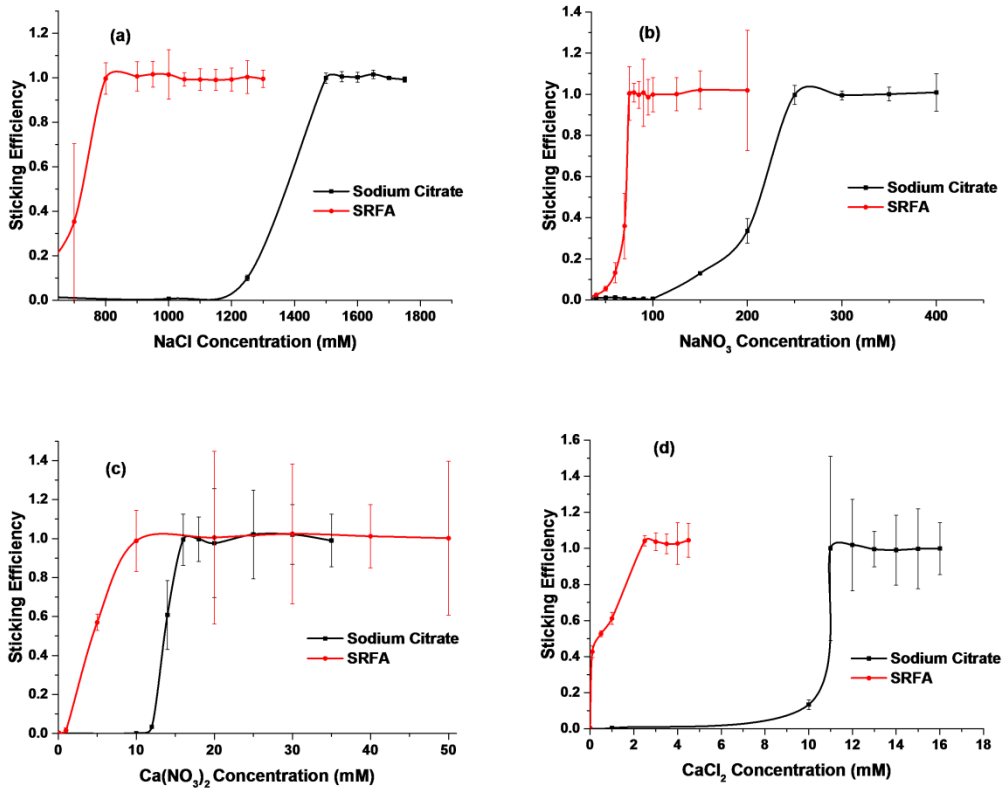

Figure 5.7: Sticking efficiency of sodium citrate and SRFA100 stabilized titania against a) NaCl b) $NaNO_3$ c) $Ca(NO_3)_2$ d) $CaCl_2$ (Briefly sticking efficiency was calculated by dividing all values of slope [change of hydrodynamic diameter] with average of few consistant values of fast aggregation. Detailed procedure of sticking efficiency calculations is discussed in chapter 3 along with theory. All experiments were done at pH 7 ± 0.2)

Figure 5.6c above shows effect of $NaNO_3$ salt concentrations on sticking efficiency and change in zeta potential for sodium citrate stabilized NPs. These showed critical coagulation concentration of 238mM $NaNO_3$ (Figure 5.7b). As these results are from three replicates, it is confirmed that sodium citrate stabilized NPs are more stable than SRFA100 NPs as is the case with NaCl. The zeta potential values significantly increased from a value of -53mV (no salt) to -14mV at $NaNO_3$ concentration of 1000mM.

Figure 5.6d above shows effect of $NaNO_3$ salt concentrations on sticking efficiency and change in zeta potential on SRFA100 stabilized titania NPs. As compared to SRFA100, critical coagulation concentration decreased from 238mM to 72mM $NaNO_3$ which means these are less stable than sodium citrate stabilized NPs. These results are comparable with

NaCl concentration and are based on three replicates. Decrease in zeta potential (Lin et al.) value was observed at CCC concentration(s) which was again as per NaCl concentration results. Generally, ZP increased with increasing salt concentration.

Figure 5.6e shows effect of $Ca(NO_3)_2$ salt concentrations on sticking efficiency and change in zeta potential for sodium citrate stabilized NPs. The results showed critical coagulation concentration of 16mM $Ca(NO_3)_2$ (Figure 5.7c). Generally, values of zeta potential moved from negative to positive values as the salt concentration increased except minor fluctuations at very low $Ca(NO_3)_2$ concentrations. It was observed that there was a significant change of zeta potential that increased from a value of -50 mV (no salt concentration) to -5mV at 100mM $Ca(NO_3)_2$ concentration.

Figure 5.6f shows effect of $Ca(NO_3)_2$ salt concentrations on sticking efficiency and change in zeta potential on SRFA100 stabilized titania NPs. As compared to sodium citrate stabilized NPs, critical coagulation concentration (Figure 5.6c) decreased from 16mM to 5.5mM $Ca(NO_3)_2$ which means these are less stable than sodium citrate stabilized NPs. These results are quite comparable with NaCl and $NaNO_3$ concentration studies. Generally, ZP increased with increasing salt concentration except few minor fluctuations at very low salt concentrations.

Figure 5.6g shows effect of $CaCl_2$ salt concentrations on sticking efficiency and change in zeta potential for sodium citrate stabilized NPs. These showed critical coagulation concentration of 10.7mM $CaCl_2$ (Figure 5.7 d). It was observed that the zeta potential values significantly increased from a value of -57mV (no salt) to +1mV at $CaCl_2$ concentration of 8000mM.

Figure 5.6h above shows effect of $CaCl_2$ salt concentrations on sticking efficiency and change in zeta potential on SRFA100 stabilized titania NPs. As compared to sodium citrate stabilized NPs, critical coagulation concentration decreased from 10.7mM to 3.8mM $CaCl_2$ (Figure 5.7d) which means these are less stable than sodium citrate stabilized NPs. These results are quite comparable with NaCl, $NaNO_3$ and $Ca(NO_3)_2$ concentration studies. In all studies ZP increased with increasing salt concentration except few minor fluctuations at very low salt concentrations.

5.3.4.2 Impact on anatase spherical Nanoparticles

Due to many fluctuations in aggregation behaviour of rutile ellipses as described above, round anatase NPs with a shape factor of 0.9 or above were selected. These NPs were stabilized in similar manner with sodium citrate and SRFA100 and used during further studies.

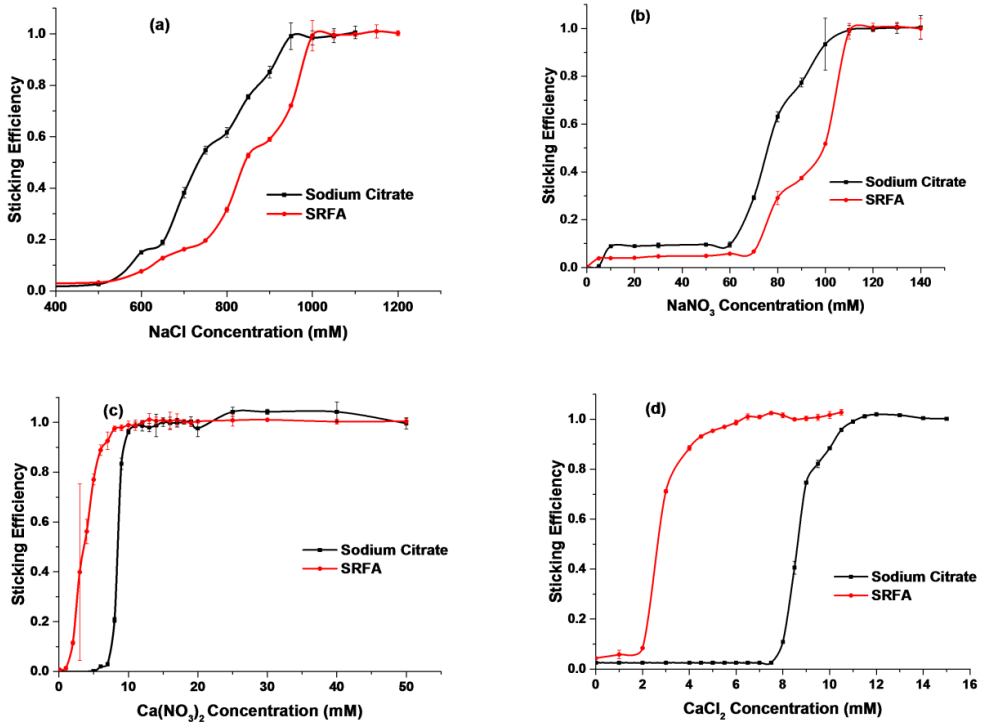

Figure 5.8: Sticking efficiency of sodium citrate and SRFA100 stabilized round anatase NPs against a) NaCl b) $NaNO_3$ c) $Ca(NO_3)_2$ d) $CaCl_2$. (All experiments were done at pH 7 ± 0.2 and sticking efficiencies were calculated by detailed method given in section 3.3.4)

TEM micrographs of both stabilized types have been presented in Figure 5.2 above. Detailed synthesis and characterization has been discussed in chapter 4. Aggregation behaviour of round particles proved to be entirely different from ellipses.

Figure 5.8a above shows effect of NaCl salt concentrations on sticking efficiency of sodium citrate and SRFA100 stabilized titania NPs. CCC decreased from 1025mM to 900mM NaCl for sodium citrate stabilized NPs. These results are quite opposite with NaCl concentration studies for ellipses which showed that sodium citrate stabilized ellipses were more stable than SRFA100 stabilized (Figure 5.7).

Figure 5.8b above shows effect of $NaNO_3$ salt concentrations on sticking efficiency of sodium citrate and SRFA100 stabilized titania NPs. CCC decreased from 115mM to 90mM $NaNO_3$ for sodium citrate stabilized NPs. These results are quite opposite with $NaNO_3$ concentration studies for ellipses which showed that sodium citrate stabilized ellipses were more stable than SRFA100 stabilized ellipses (Figure 5.7b).

Figure 5.8c above shows effect of $Ca(NO_3)_2$ salt concentrations on sticking efficiency of sodium citrate and SRFA100 stabilized titania NPs. CCC decreased from 9.7mM to 5.5mM $Ca(NO_3)_2$ for SRFA100 stabilized NPs. These results are quite comparable with $Ca(NO_3)_2$ concentration studies for ellipses except that sodium citrate stabilized ellipses can tolerate more $Ca(NO_3)_2$ (Figure 5.7c).

Figure 5.8d above shows effect of $CaCl_2$ salt concentrations on sticking efficiency of sodium citrate and SRFA100 stabilized titania NPs. CCC decreased from 9.4mM to 3.2mM $CaCl_2$ for SRFA100 stabilized NPs. These results are quite in line with $CaCl_2$ concentration studies for ellipses which showed that sodium citrate stabilized ellipses were more stable than SRFA100 stabilized ellipses (Figure 5.7d).

If we compare effect of Na^{+} and Ca^{+2} on stability of SRFA and sodium citrate stabilized NPs then it gave more stability to SRFA stabilized NPs with higher CCC values (Figure 5.8a&b, Table 5-3) than that of Ca^{+2} where sodium citrate stabilized NPs are more stable with higher CCC values (Figure 5.8b&c, Table 5-3).

Table 5-3: Comparison of effect of Na^{+} and Ca^{+2} ions on stability of SRFA and sodium citrate stabilized round NPs

Salt	CCC for SRFA stabilized NPs	CCC for sodium citrate stabilized NPs
NaCl	1160	850
$NaNO_3$	135	110
$CaCl_2$	5.2	9.2
$CaNO_3$	3.8	11.5

Table 5-4: Comparison of TiO_2 ellipses and spherical TiO_2 NPs CCC values (All experiments were done at pH 7 ± 0.2)

Salt	Stabilizing agent	CCC (mM) ellipses	CCC (mM) spherical NPs
NaCl	SRFA100	1025	1025
NaCl	Sodium citrate	1680	900
$NaNO_3$	SRFA100	72	115
$NaNO_3$	Sodium citrate	238	90
$CaCl_2$	SRFA100	3.8	3.2
$CaCl_2$	Sodium citrate	10.7	9.4
$Ca(NO_3)_2$	SRFA100	5.5	5.5
$Ca(NO_3)_2$	Sodium citrate	16	9.7

Table 5-4 shows comparison of CCC values of titanium ellipses and spherical particles for two types of stabilizing agents. It is obvious from the data presented above that SRFA100 stabilized NMs showed inconsequential change in CCC values. However, sodium citrate stabilized NPs were less stable than that of ellipses stabilized with same stabilizing agent.

The aggregation kinetics of TiO_2 NMs in NaCl varied with the type of stabilizing agent. Results for sodium citrate stabilized titania ellipses reproduced in Figure 5.7a were in accordance with DLVO theory and gave an estimated CCC of 1680 mM NaCl. This result was high as compared with previous research work (Liu et al., 2011b, Li et al., 2010) but sodium citrate stabilized NP also resulted in a CCC value of 900mM (Figure 5.8a & Table 5-4). However, there was no difference in the CCC values of both SRFA100 stabilized ellipses and NPs, which remained constant at a value of 1025 (Figure 5.7a, Figure 5.8a & Table 5-4). This result also shows high stability of both suspensions under extreme environmental conditions. However, hydrodynamic diameter decreased giving negative rate of change followed by the aggregation for NaCl concentrations lower than 500mM this is in accordance with the findings of Li et al. (Li et al., 2010) who found similar behaviour in their experiments on Ag aggregation kinetics. This decline in hydrodynamic diameter, which was dependent on NaCl concentration, reveals a disturbance in the equilibrium of the NMs surface layer followed by erosion of the primary metallic particle and/or settling of larger aggregates (Li et al., 2010). Differences in sticking efficiency and the initial particle size of SRFA100 and sodium citrate coated NMs with changing NaCl concentration showed no obvious differences with change of shape and phase (Figure 5.7a, Figure 5.8a & Table 5-4), similar trends in initial particle size with changing NaCl concentration were observed for citrate-coated Ag NPs by Huynh and Chen (2011). It was observed that sodium citrate stabilized ellipses showed more stability against NaCl as compared to SRFA100 stabilized ellipses, while sodium citrate stabilized NPs showed lower CCC values compared to SRFA100. This behaviour of ellipses is due to steric interactions for the particles having larger aspect ratio. In one study on colloidal haematite, Lenhart and Honeyman (1999) investigated that dicarboxylic organic acids provided steric forces of interaction which resulted in the aggregation of haematite particles.

Ellipses stabilized with SRFA100 exhibited aggregation behaviour quite similar to that for SRFA100 stabilized spherical NPs (Figure 5.7a, Figure 5.8 & Table 5-4). There was no obvious increase in the CCC both for ellipses and spherical NPs stabilized with SRFA100. SRFA may enhance particle stability by promoting electrosteric repulsion.

5.3.5 TEM analysis of aggregation behaviour

The aggregates structure of TiO_2 NPs was investigated by TEM at two electrolyte concentrations; one in the slow aggregation regime and the other in the fast aggregation regime. All four salts which were used for aggregation kinetics i.e. $Ca(NO_3)_2$, $CaCl_2$, $NaNO_3$ and NaCl, were studied in this experiment. The TEM micrographs obtained were analysed for the fractal dimensions to know the aggregation behaviour. All aggregation experiments were carried out at a pH value of 7 ± 0.2.

5.3.5.1 Aggregation of TiO_2 Nanomaterials in the Presence of Sodium Chloride

The aggregates structure of stabilized ellipses and spherical TiO_2 NPs were investigated by TEM at two concentrations of NaCl; one in the slow aggregation regime and the other in the fast aggregation regime. Most of the images shown below are for the ellipses and NPs stabilized with sodium citrate. Only a few SRFA100 TEM images were collected due to salt crystal development during sample preparation. The grids were prepared with different sample preparation techniques as described in chapter 3 followed by washing a couple of times. In some TEM grids such high NaCl concentrations have totally hidden the NPs especially ellipses. Images of sodium citrate aggregates illustrated aggregates connecting different particles to one another (Figure 5.9 to Figure 5.12). There is a general trend that NPs tended to develop an outer layer of salt to make different sized aggregates. From these TEM results it is concluded that

the ionic strengths below 5 mM NaCl at pH 7 ± 0.2 do not affect the stability of nano-TiO_2 dispersion because of its inability to overcome the electrostatic repulsive forces.

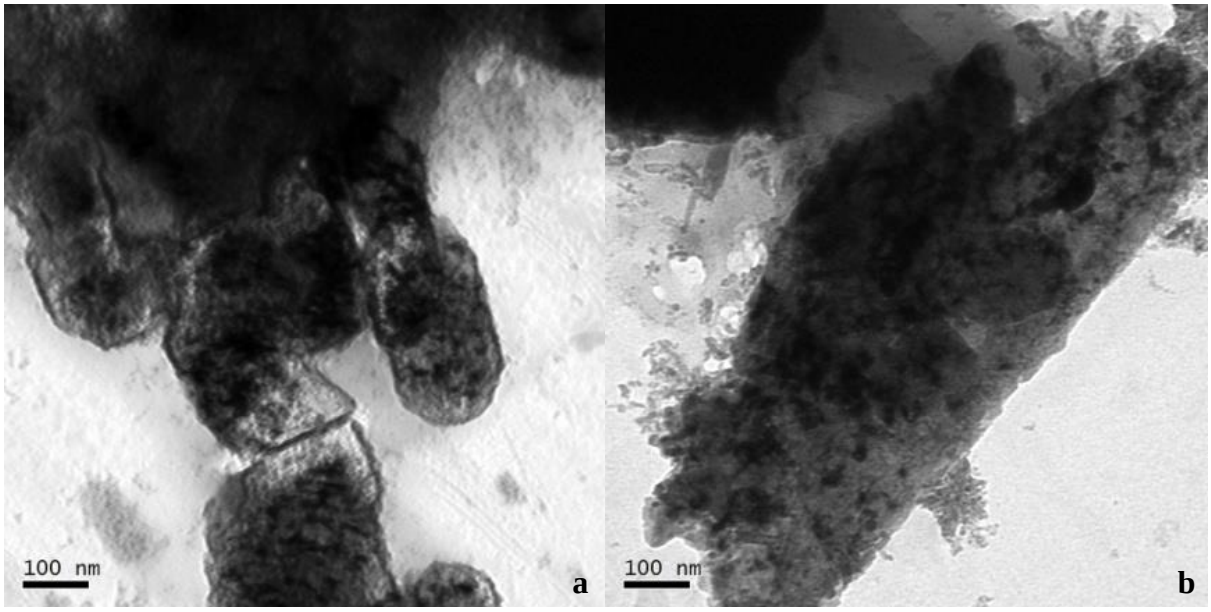

Figure 5.9: a) TEM micrograph (taken at 200kV extraction voltage) on effect of 1250 mM NaCl on Sodium Citrate stabilized TiO_2 ellipses b) TEM micrographon effect of 2000 mM NaCl on Sodium Citrate stabilized TiO_2 ellipses

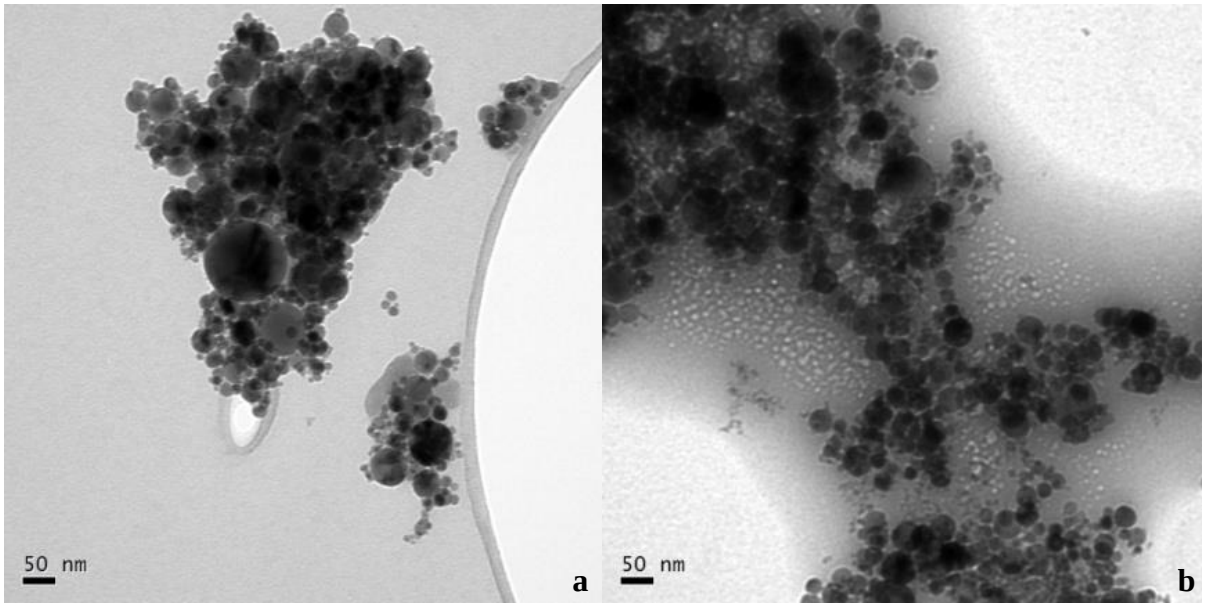

Figure 5.10: a) TEM micrograph (taken at 200kV extraction voltage) on effect of 700 mM NaCl on Sodium Citrate stabilized TiO_2 NPs b) TEM micrograph on effect of 1100 mM NaCl on Sodium Citrate stabilized TiO_2 NPs

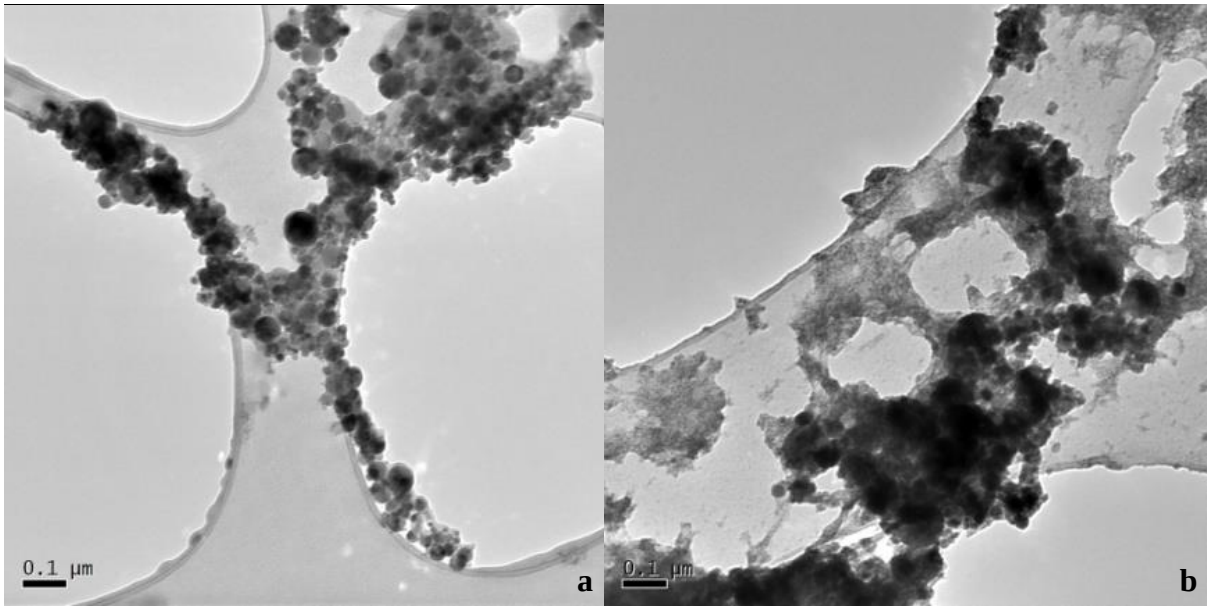

Figure 5.11: a) TEM micrograph (taken at 200kV extraction voltage) on effect of 1300 mM NaCl on SRFA stabilized TiO_2 NPs b) TEM micrograph on effect of 800 mM NaCl on SRFA stabilized TiO_2 NPs

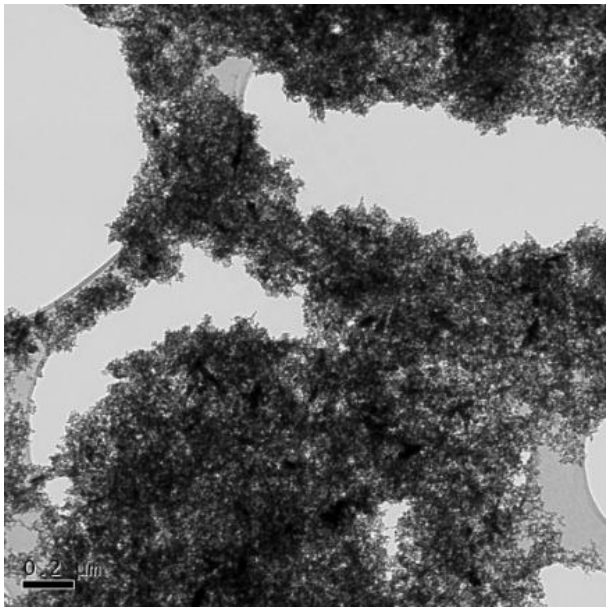

Figure 5.12: TEM micrograph (taken at 200kV extraction voltage) on effect of 900 mM NaCl on SRFA stabilized TiO_2 ellipses

The initial particle size of NPs did not increase until the concentration of NaCl reached 500 mM for SRFA100 and 1025mM for sodium citrate stabilized ellipses. In comparison, this growth started from 500 and 560 mM of NaCl for sodium citrate and SRFA100 stabilized spherical NPs. Thereby suggesting the influence of aspect ratio which enhanced stability under

similar solution conditions. This enhanced stability for NaCl might be due to the ability of synthetic stabilizing agents or natural organic matter like SRFA to restrain electron transfer reactions by reducing accessibility of reactants to the particle surfaces (EU, 2011, NNI, 2013, Aitken et al., 2004). The structure of the sodium citrate coating was not visible under TEM cross-examination but from Figure 5.12 it was obvious that behaviour of SRFA100 as compared to sodium citrate was different as sodium citrate induced salt bridging between individual particles (Figure 5.9 and Figure 5.10 above) which cannot be seen in case of SRFA. TEM images of the sodium citrate and SRFA stabilized NMs did not provide evidence of any obvious changes in the shape, morphology, or size of the particles (Figure 5.1 & Figure 5.2). SRFA100 TEM images were also collected in different concentrations of NaCl, corresponding to the slow and fast aggregation regimes, but salt crystals developed during sample preparation and also such high NaCl concentrations totally hidden the NMs especially ellipses. Images of sodium citrate aggregates illustrated a deposit connecting different particles to one another (Figure 5.9 to Figure 5.12). These results showed images quite similar to that for the uncoated silver particles observed by Li et al. (2010) with the presence of similar features in images of citrate coated Ag NP aggregates.

5.3.5.2 Aggregation of TiO_2 Nanomaterials in the Presence of Sodium Nitrate

TEM images were also collected at slow and fast aggregation regimes of $NaNO_3$ concentrations. It is obvious that $NaNO_3$ gave different orientation of NPs aggregates as compared to NaCl (Figure 5.14 a-d). SRFA100 and sodium citrate stabilized NPs give different shapes to the aggregates. These shapes were more compact at fast aggregation regime (Figure 5.14 a and c) than slow aggregation (Figure 5.14 b and d).

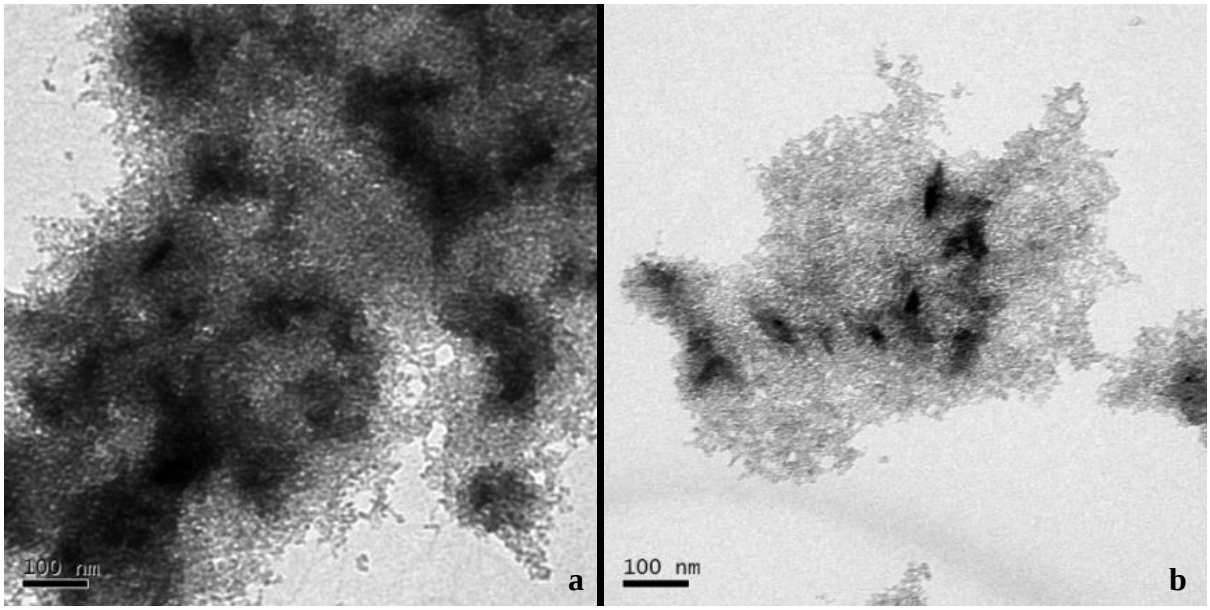

Figure 5.13: a) TEM micrograph (taken at 200kV extraction voltage) on effect of 200 mM $NaNO_3$ on Sodium Citrate stabilized TiO_2 ellipses b) TEM micrograph on effect of 300 mM $NaNO_3$ on Sodium Citrate stabilized TiO_2 ellipses

Table 5-5: Effect of NaCl concentrations on aggregation of NPs and ellipses coated with SRFA and sodium citrate. Comparison of fractal dimensions calculated by 7 different methods described in section 3.7.1.2

*A 2D fractal dimension cannot be over two. A value of 2 is the maximum possible value but these two methods gave values above 2 which show their reliability in calculating fractal dimensions.

Fractal Dimension Method Used	**SRFA Ellipses**		**SRFA NPs**		**Sodium Citrate Ellipses**		**Sodium Citrate NPs**	
	0.9M	**1.2M**	**0.8M**	**1.3M**	**1.25M**	**2M**	**0.7M**	**1.1M**
Cumulative Intersections	1.726±0.009 n=3	N/A	1.595±0.0 n=1	1.8075±0.502 n=8	1.366±0.171 n=5	1.4224±0.198 n=10	1.4613±0.291 n=9	1.6344±0.271 n=9
Mass Radius	1.67±0.006 n=3	N/A	1.465±0.0 n=1	1.6964±0.447 n=8	1.3302±0.183 n=5	1.3809±0.214 n=10	1.3458±0.258 n=9	1.5669±0.25 n=9
Vectorized Intersections	1.795±0.094 n=3	N/A	1.552±0.0 n=1	1.9436±0.711 n=8	1.4304±0.188 n=5	1.541±0.22 n=10	1.4906±0.306 n=9	1.5211±0.159 n=9
Convex Hull Intersections	2.098±0.378* n=3	N/A	2.026±0.0* n=1	2.1281±0.663* n=8	2.0568±0.3* n=5	2.21±0.3* n=10	1.9788±0.554 n=9	1.934±0.193 n=9
Convex Hull Mass Radius	1.834±0.059 n=3	N/A	2.051±0.0* n=1	2.2035±0.732* n=8	1.8704±0.216 n=5	1.6792±0.263 n=10	1.8741±0.473 n=9	1.8971±0.221 n=9
Box Counting by Fractop	1.809±0.085 n=3	N/A	1.453±0.0 n=1	1.5106±0.108 n=8	1.6114±0.11 n=5	1.564±0.244 n=10	1.5317±0.109 n=9	1.6038±0.13 n=9
Box Counting by Java Applet	1.653±0.146 n=3	N/A	1.68±0.0 n=1	1.665±0.138 n=8	1.526±0.242 n=5	1.658±0.08 n=10	1.6744±0.091 n=9	1.7622±0.092 n=9

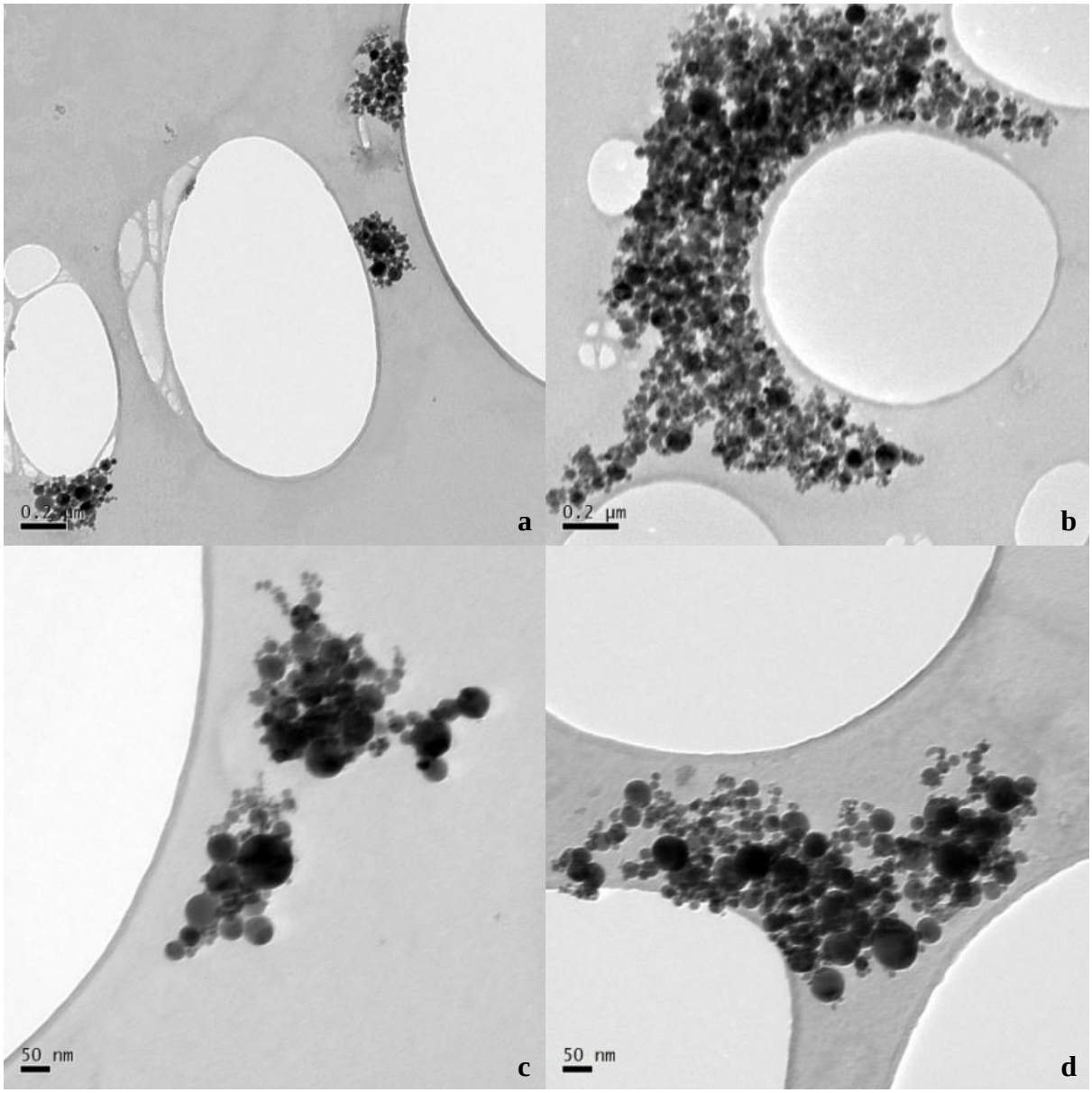

Figure 5.14: TEM micrograph (taken at 200kV extraction voltage) on; a) effect of 70 mM $NaNO_3$ on Sodium Citrate stabilized TiO_2 NPs b) effect of 120 mM $NaNO_3$ on Sodium Citrate stabilized TiO_2 NPs c) effect of 90 mM $NaNO_3$ on SRFA stabilized TiO_2 NPs d) effect of 130 mM $NaNO_3$ on SRFA stabilized TiO_2 NPs

Table 5-6: Effect of $NaNO_3$ concentrations on aggregation of NPs and ellipses coated with SRFA and sodium citrate. Comparison of fractal dimensions calculated by 7 different methods described in section 3.7.1.2

Fractal Dimension Method Used	**SRFA Ellipses**		**SRFA NPs**		**Sodium Citrate Ellipses**		**Sodium Citrate NPs**	
	0.9M	**1.2M**	**90mM**	**130mM**	**200mM**	**300mM**	**70mM**	**120mM**
Cumulative Intersections	N/A	N/A	1.4556±0.177 n=5	1.9258±0.904 n=15	1.7173±0.344 n=8	2.1774±1.157 n=8	1.8237±0.508 n=15	1.5671±0.733 n=12
Mass Radius	N/A	N/A	1.3956±0.172 n=5	1.8261±0.857 n=15	1.6784±0.474 n=8	2.0244±1.057 n=8	1.6924±0.399 n=15	1.4728±0.740 n=12
Vectorized Intersections	N/A	N/A	1.4892±0.185 n=5	1.9715±0.973 n=15	1.6731±0.230 n=8	1.9436±0.876 n=8	1.7799±0.439 n=15	1.5509±0.659 n=12
Convex Hull Intersections	N/A	N/A	1.9370±0.477 n=5	2.6172±1.490 n=15	2.1181±0.151 n=8	2.2871±0.985 n=8	2.2859±0.599 n=15	1.9193±0.869 n=12
Convex Hull Mass Radius	N/A	N/A	1. 6502±0.116 n=5	2.4061±1.233 n=15	2.1858±0.719 n=8	1.4538±1.207 n=8	2.0986±0.599 n=15	1.8330±0.846 n=12
Box Counting by Fractop	N/A	N/A	1.6120±0.149 n=5	1.5277±0.126 n=15	1.6655±0.076 n=8	1.3846±0.171 n=8	1.4789±0.262 n=15	1.3669±0.182 n=12
Box Counting by Java Applet	N/A	N/A	1.7640±0.067 n=5	1.64±0.091 n=15	1.67±0.056 n=8	1.6375±0.090 n=8	1.6146±0.268 n=15	1.5692±0.263 n=12

It was observed that the only difference in the aggregation behaviour of NaCl and $NaNO_3$ was the formation of different shape structures in case of $NaNO_3$. The CCC for citrate-coated NPs in $NaNO_3$ was 72 mM (Figure 5.7b & Table 5-4) for SRFA100 stabilized ellipses which increased to 115 mM for spherical NPs (Figure 5.8b & Table 5-4). There was a drop in CCC, from a value of 238 mM for titania ellipses (Figure 5.7b & Table 5-4) to 90 mM $NaNO_3$ (Figure 5.8b & Table 5-4) which was similar to the value measured in case of NaCl. These CCC values are far less than NaCl CCC values although both salts are monovalent. In case of NaCl aggregation, sodium citrate stabilized NPs provided a degree of stability to the ellipses. The starting aggregate size of the sodium citrate stabilized NPs in $NaNO_3$, just like in NaCl, followed a decrease in size with increasing electrolyte concentration (Figure 5.7b & Figure 5.8b). It was noted that the aggregate sizes were higher in high concentrations of $NaNO_3$ (Figure 5.13) than in similar concentrations of NaCl (Figure 5.9), suggesting the effect of stabilizing agents was enhanced in NaCl than in $NaNO_3$. It is attributed to chaotropic anionic effect of Cl^- ions which impart additional stability in NPs as compared to kosmotropic anions (Fang et al., 2009b). Effect of NO_3^- is still inconsistent as it caused destabilization for gold (Gu et al., 1994) and stabilization for silver (Kim et al., 2009).

It was observed that CCC was different for differently stabilized NPs and for NaCl or $NaNO_3$, which obviously suggest that the electrolyte anion have very important role. Previous research studies on different salinities revealed that CCC is anion specific, as chaotropic anions (Cl^-,Br^-, I^-) only induce stability, whereas kosmotropic anions (F^-,SO_4^{-2}) did not show any stabilizing effect (Fang et al., 2009b). NO_3^- can induce either stability (Kim et al., 2009) or instability (Gu et al., 1994). The role of anion was further confirmed by differences in the aggregation of sodium citrate stabilized NPs in NaCl and $NaNO_3$. The difference in the CCC and aggregation behaviour was not dependent on ion size, because the hydrated radius of Cl^- at 3.32 Å and NO_3^- at 3.35 Å (Richards et al., 2011) are quite close and might not be able to

give much difference in behaviour. It might be NO_3^- which made complexes with SRFA100 and sodium citrate.

5.3.5.3 Aggregation of TiO_2 Nanomaterials in the Presence of Calcium Nitrate

$Ca(NO_3)_2$ affected TEM images were also collected at slow (Figure 5.15a and Figure 5.16) and fast (Figure 5.15b) aggregation regimes. The NPs in the presence of $Ca(NO_3)_2$ made an outer layer around themselves and made chained aggregates (Figure 5.15 to Figure 5.16). The SRFA100 and sodium citrate stabilized NPs gave no difference in aggregate structures except the size of aggregates at fast aggregation regime than slow aggregation.

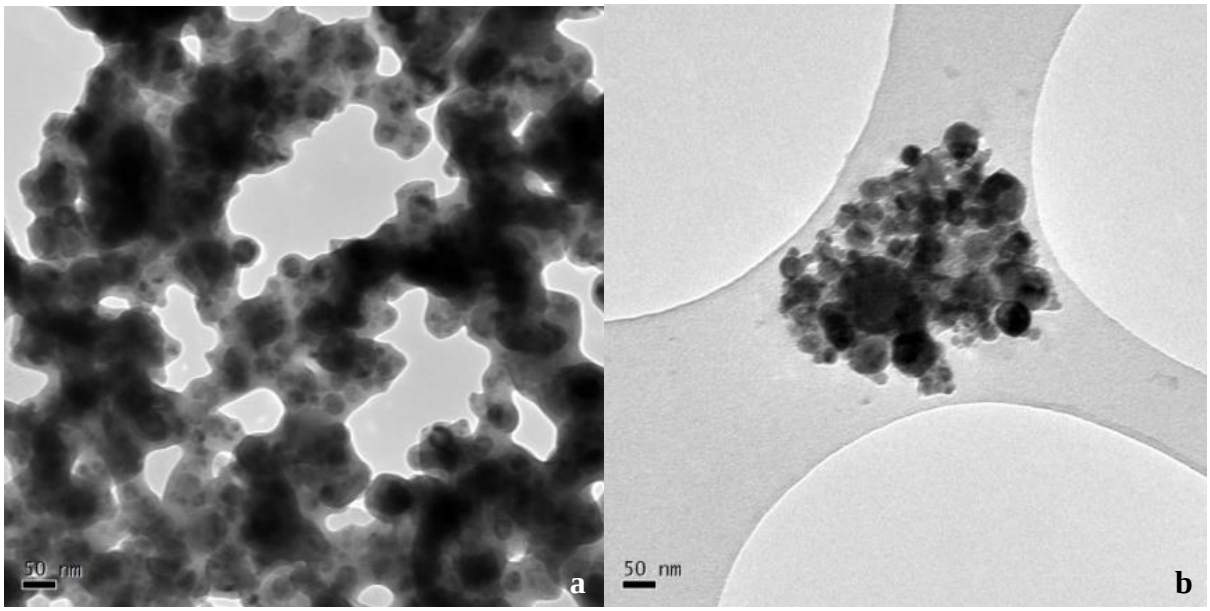

Figure 5.15: a)TEM micrograph (taken at 200kV extraction voltage) on effect of 12mM $Ca(NO_3)_2$ on Sodium Citrate stabilized TiO_2 NPs b)TEM micrograph on effect of 9.5 mM $Ca(NO_3)_2$ on Sodium Citrate stabilized TiO_2 NPs

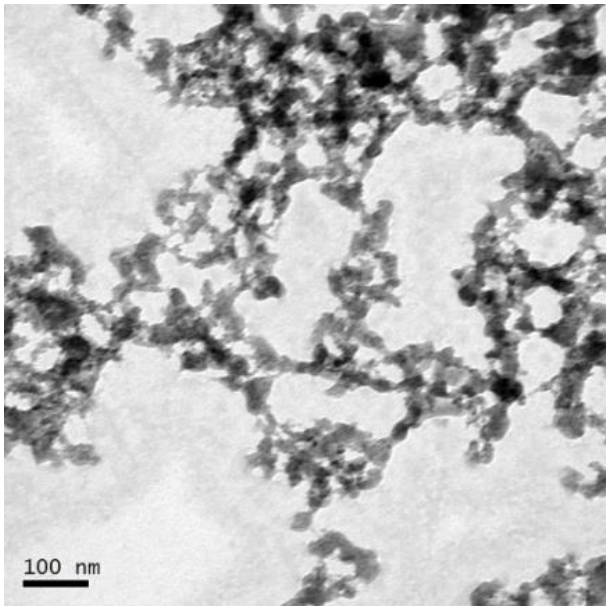

Figure 5.16: TEM micrograph (taken at 200kV extraction voltage) on effect of 16 mM $Ca(NO_3)_2$ on Sodium Citrate stabilized TiO_2 ellipses

$Ca(NO_3)_2$ showed aggregation behaviour which was quite in line with $NaNO_3$. The CCC for citrate-coated NPs in $Ca(NO_3)_2$ was 16 mM (Figure 5.7c & Table 5-4) for SRFA100 stabilized ellipses which decreased to 9.7 mM for spherical NPs (Table 5-4). There was no change observed between CCC values of SRFA stabilized ellipses and spherical NPs. These CCC values are far less than $NaNO_3$ CCC value, which was attributed to Ca^{+2} because of its quick screen of surface charge by divalent ions. As compared to SRFA, sodium citrate provided a degree of steric stability to the ellipses. Similar to the NaCl and $NaNO_3$, SRFA stabilized ellipses were difficult to be imaged but spherical NPs chain like structures in which NMs can be seen (Figure 5.15). These chain structures were more compact for all cases of rapid aggregation regime both for SRFA100 and sodium citrate stabilized NPs.

5.3.5.4 Aggregation of TiO_2 Nanomaterials in the Presence of Calcium Chloride

Interestingly $CaCl_2$ showed characteristics of both $NaNO_3$ aggregation behaviour both like NaCl and $Ca(NO_3)_2$ (Figure 5.17 and Figure 5.18). As discussed above, Cl^- and NO_3^- ions

play an important role in determining the aggregation behaviour. SRFA100 stabilized NPs showed a different behaviour (Figure 5.19) by making branched structures.

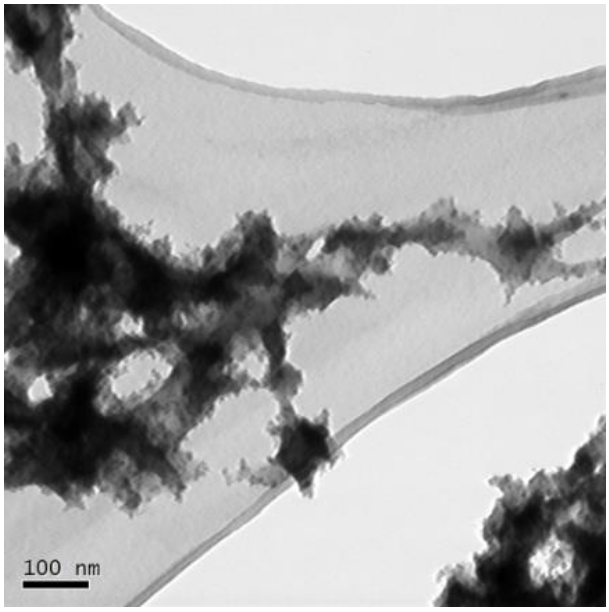

Figure 5.17: TEM micrograph (taken at 200kV extraction voltage) on effect of 10.1 mM $CaCl_2$ on Sodium Citrate stabilized TiO_2 ellipses

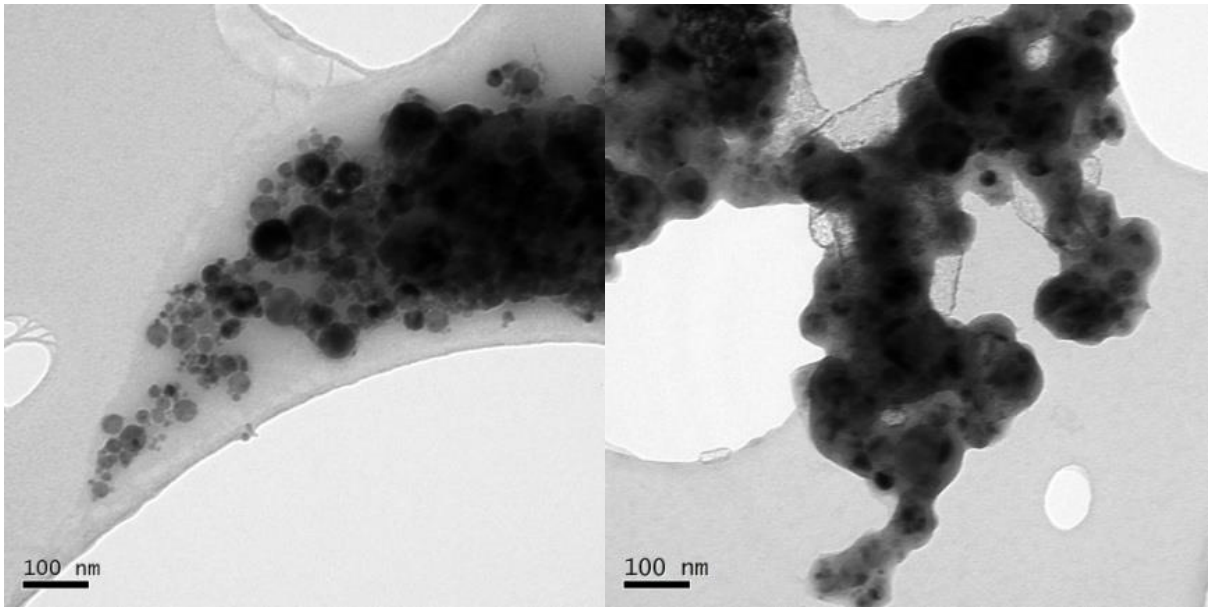

Figure 5.18: a) TEM micrograph (taken at 200kV extraction voltage) on effect of 8 mM $CaCl_2$ on Sodium Citrate stabilized TiO_2 NPs b) TEM micrograph on effect of 11 mM $CaCl_2$ on Sodium Citrate stabilized TiO_2 NPs

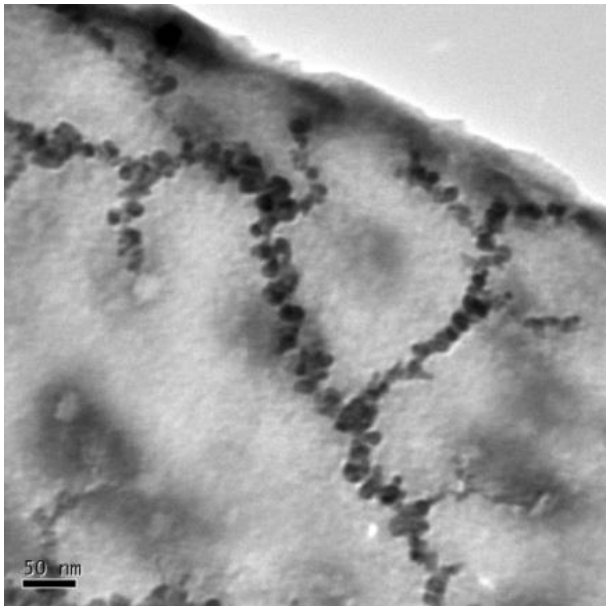

Figure 5.19: TEM micrograph (taken at 200kV extraction voltage) on effect of 3 mM $CaCl_2$ on SRFA stabilized TiO_2 NP

The aggregation behaviour observed in $CaCl_2$ was similar to that observed in NaCl. The CCC shifted to lower concentrations as the divalent calcium ion was more effective in screening surface charge (Figure 5.7c), but trends observed with the sodium citrate and SRFA100 stabilized NMs were similar to those for the same NMs in NaCl. The stability of the SRFA100 stabilized NMs in $CaCl_2$ was obviously different from that in NaCl, as divalent cation quickly changed the aggregation stage. For $CaCl_2$, the CCC for SRFA100 stabilized NMs decreased from 3.8 mM to 3.2 mM $CaCl_2$, for ellipses and spherical NPs, respectively. While the maximum CCC, 10.7mM $CaCl_2$ was given by sodium citrate stabilized ellipses which decreased to 9.4mM $CaCl_2$ for spherical NPs. The high charge screening efficiency of Ca^{+2} ions for the NMs could be the possible aggregation mechanisms along with the specific interaction of NMs, Ca^{+2} ions and stabilizing agents (Konradi and Rühe, 2005). In TEM images, formation of chain like structure were observed (Figure 5.19), while gel like structures like in $NaNO_3$ and $Ca(NO_3)_2$ were observed which were more intense at fast aggregation regime (Figure 5.18). Interestingly $CaCl_2$ showed characteristics of both $NaNO_3$ aggregation behaviour by making gel like structures and $Ca(NO_3)_2$ like behaviour making the outer crust

(Figure 5.16 to Figure 5.18). It is presumed that Cl^- and NO_3^- ions might play an important role in determining the aggregation behaviour. This obviously needs to be investigated further.

5.4 Conclusions and Implications

It is concluded that pH is the key factor in determining the stability of NPs suspension as pH 2.8 suspension was stable against 400mM NaCl. This pH mediated stabilization made NPs suspension more available to react with other constituents of the system. Sodium citrate and SRFA proved to be the best stabilizers of the TiO_2 NPs as compared to PEG, PVP and SDS. The stability with SRFA helped in understanding the retention and transport of TiO_2 NPs in real environment with aid of humic and fulvic acid.

Time-resolved DLS aggregation kinetics studies showed that along with the presence of different mono or divalent cations, the role of anions and stabilizing agents is equally important to determine aggregation kinetics. The aggregation kinetics of TiO_2 NPs in different salt concentrations increased with the type and increasing concentration of salts. Results for SRFA100 stabilized round NPs reproduced in above experiments were consistent with Derjaguin-Landau-Verwey-Overbeek (DLVO) sort of behaviour and resulted in estimated CCC values of 5.5, 115, 1015 and 3.2 mM for $Ca(NO_3)_2$, $NaNO_3$, NaCl and $CaCl_2$ respectively. Differences in CCC values for sodium citrate stabilized NPs showed no obvious differences with SRFA100 stabilized, with CCC values of 9.7, 90, 900 and 9.4 mM $Ca(NO_3)_2$, $NaNO_3$, NaCl and $CaCl_2$ respectively. Anatase spherical NPs gave aggregation kinetics following DLVO but rutile ellipsoids did not follow the assumptions given in the theory. Rutile NPs proved to have greater stabilization than anatase spherical NPs and SRFA was revealed to have better stabilizing potential than sodium citrate. Moreover, ellipsoid shape proved to be the best stabilized NPs as compared to anatase round NPs.

Current research has an impact in understanding the effect of different TiO_2 morphologies, phase and stabilizing agents in different environments. Aggregation kinetics of stabilized NPs gave an understanding of NPs behaviour in extreme environments. Stability at varying levels of salt concentrations in the presence of stabilizing agents can help in evaluation of NPs fate and behaviour in natural environments especially in the presence of natural organic matter.

Chapter 6

Fate and transport of manufactured nanoparticles in artificial and natural porous media

6.1 Overview

As TiO_2 NMs are extensively used in different commercial products, they become a part of natural environments. Due to the excessive use in consumer products, these NMs are prone to cause a potential threat to natural ecosystems in the near and/or far future. This study is designed to determine the behaviour of these NMs in artificial and natural media to evaluate the risk involved with release to subsurface waters. Stability of NMs may increase their mobility and the associated risk in groundwater.

The ultimate goal of this research work was to begin to understand the behaviour of different forms of synthetic TiO_2 NMs which were stabilized by two different stabilizing agents in glass bead and sandstone columns. Two different polymorphs with two different morphologies were selected for their transport in artificial and natural porous media because each of these properties may affect mobility. To accomplish the above mentioned goal, the column experiments were carried out on Triassic sandstone columns and 0.1mm glass bead filled columns. An instrument previously designed by Greswell et al. (2010) is used during the experimental work, details of which are given in section 3.12.

The results indicated that the stabilization agents have a pronounced effect on the TiO_2 breakthrough. The mobility of the spherical anatase NPs is less than the rutile rods. Bare anatase NPs gave no breakthrough and the NPs clogged both the sandstone and glass bead columns. The behaviour of transport for sandstones and glass beads was broadly similar, except retention of NPs is more in sandstone columns than in glass bead columns.

Glass beads were selected because colloid filtration theory, often used in NP mobility studies, is developed using a conceptualisation that is much more likely to be appropriate for uniform glass bead media. As compared to natural soil or sandstone materials, glass beads are a simple, homogeneous medium. It has yet to be demonstrated that glass bead media are an adequate conceptualisation for transport of nanomaterials in natural granular (e.g. sandstone) media. The results indicated that behaviour of the systems used was similar in the glass bead and sandstone columns. Breakthrough curves (BTCs) for rutile ellipsoids were at higher concentrations as compared to the curves for anatase. Also BTCs of glass beads for both anatase and rutile were at higher concentrations than for the sandstone cores. However bare anatase NPs showed almost complete retention for both glass bead and sandstone cores. Breakthrough curves were usually tailed. NPs were released with flushing for all the experiments and more release was observed with deionized water flush. Rutile ellipsoids proved best mobility in all cases as compared to anatase spherical NPs. Among stabilizing agents, SRFA proved best followed by sodium citrate and bare NPs except bare rutile. In a nutshell, glass bead behaved similar order of mobility in different stabilizers as compared to sandstone cores, but with differences in degree.

It is concluded that in two NPs shape and phase scenario, rutile ellipsoids showed greater mobility for both bare and stabilized forms. SRFA has an edge on sodium citrate stabilizer for both anatase and rutile NPs. SRFA gave increased release of NPs when the columns were flushed after NPs run as compared to sodium citrate. Bare anatase NPs showed no or very less movement in both sandstone and glass bead media. Transport of NPs was similar in both glass bead and sandstone columns except order of breakthrough magnitude and retention of NPs. Glass bead columns demonstrated greater breakthrough curves and less retention as compared to lower breakthrough curves and greater retention in sandstone

columns. In a nutshell, glass bead columns proved to be better analogous to the natural porous media.

6.2 General background of research work

Self-manufactured and stabilized TiO_2 NPs were selected for transport studies due to the wide use of titania in number of consumer products. With the intense use of these NMs, they are likely to be released in to the natural environment. The other reason for selecting these materials is their low solubility in different media (Seo et al., 2007). So use of TiO_2 NMs in research studies minimize the loss of mass through dissolution process as compared to many other NMs (Ivanova et al., 2013, Mukherjee et al., 2005).

Basic understanding of the processes involved in transport of engineered NMs in saturated porous media is critically important for all subsurface environmental systems. Previous research on the mobility of colloids and nanoparticles articulate that these particles can also facilitate the movement of pollutants sorbed onto their surfaces in groundwater systems (Macé et al., 2006, Zhang, 2003, Elimelech and O'Melia, 1990). They also hold promise for use in groundwater remediation especially with use of iron zero (Mosley et al., 2003, Godinez and Darnault, 2011b). With an interpretation of these important processes for mobility of NMs in the subsurface water zone, research workers can model more inclusive processes, thus facilitating risk assessment and policy making.

To delineate the transport behaviour of engineered NMs, scientists are making continuous efforts by conducting different transport studies. They have utilized NPs and aggregates of submicron size range. There are several factors which affect the deposition of NMs, including: ionic strength, pH, flow velocity, change in ionic composition, the presence of NOM including polymers and surfactants (Wang et al., 2012, Chen and Elimelech, 2008).

Fang et al. (2009b) studied the mobility of TiO_2 NPs in saturated homogeneous soil columns. It was found that deposition was enhanced with more clay content and more highly saline environments.

NOM is an important parameter which imparts stability of NMs in aquatic and subsurface environments. (Chen and Elimelech, 2007) suggested that NOM has detrimental effects on the stability and transport of CNT's in porous media. NOM may modify the physico-chemical properties of the underlying solid and impact the stability and behaviour of colloids (Gu et al., 1994, Kim et al., 2009, Mosley et al., 2003, Godinez and Darnault, 2011b). It is well understood that electrostatic and steric repulsions are the main reason of NOM stabilization of colloids (Tiller and O'Melia, 1993, Amirbahman and Olson, 1993, Stankus et al., 2010) in the presence of monovalent ions. However, divalent ions at relatively high dose do not impart colloidal stability because cations make a complex with NOM (Li and Elimelech, 2006).

The sticking and deposition of colloidal materials is often described by the classic colloidal filtration theory but few scientists since last decade are continuously working on inadequacy of this filtration theory. Tufenkji and Elimelech (2004) evaluated such deviation from CFT because of the simultaneous existence of both favourable and unfavourable colloidal interactions in the presence of repulsive Derjaguin−Landau−Verwey−Overbeek (DLVO) interactions. Christenson and Verwey (Christenson, 1984, Verwey, 1947) gave the concept of repulsive Derjaguin–Landau–Verwey–Overbeek (DLVO) interactions which may give favourable (in the absence of repulsive colloidal interaction energies) and unfavourable (in the presence of repulsive colloidal interaction energies) deposition (Ogwu et al., 2005). Some researchers have verified that deposition in the secondary energy minimum can be reversed with the elimination of the energy well by decrease in the ionic strength of the electrolyte solution (Franchi and O'Melia, 2003, Baalousha, 2009, Hahn and O'Melia, 2003).

Titanium dioxide has different industrial uses including paints, plastics, paper, inks, fibres, foods, pharmaceuticals, self-cleaning glass and cosmetics industries. Another important aspect of TiO_2 applications is the photocatalytic use where it is used in self-cleaning glass (Zhao et al., 2008) or in the degradation of pollutants (Zhang et al., 2010, Zhao et al., 2004). TiO_2 nanoparticles have also been used for heavy metal remediation from wastewater(Wu et al., 2011). Just because of intensive use of titania nanomaterials, it might be a potential risk to human health and the environment. They are toxic to the human body (Singh and Nalwa, 2007) and to the aquatic organisms like rainbow trout (Federici et al., 2007).

Transport of titania has been previously studied considering different parameters but there is a lack of data on the evaluation of post stabilized NP's transport. Also there is no significant amount of data available for the transport of different shapes of TiO_2 NPs. So this study was conducted with following aims and objectives:

1. To compare the transport of TiO_2 NPs in artificial glass bead and natural sandstone media.
2. To understand the behaviour of different morphologies of self-fabricated TiO_2 NPs.
3. To know the effect of injection velocities, stabilizing agents and different phases of TiO_2 NPs on their mobility.

6.3 Results

6.3.1 Introduction

Detailed methodology for this research work is discussed in chapter 3 of this thesis (section 3.8). In short, two different types of porous media were used during this study; sandstone porous medium as representative of natural porous media and 0.1mm glass beads medium as a representative of artificial porous media. For all studies two types of surfactants i.e. sodium citrate and SRFA, were used to stabilize NPs and the columns were conditioned

using these solutions before passing the actual NPs solutions through these media. Experiments were also run using unstabilized NPs (Bare NPs). The general injection procedure was:

1. Standard DI water bypassing
2. NPs (C_o) bypassing column to establish calibration
3. DI bypassing
4. DI water through column
5. Stabilising agent bare (if used to stabilize NPs) through column
6. NPs (C_o) through column
7. Stabilizing agent flushing (if used to stabilize NPs)
8. DI water flushing
9. DI water bypassing
10. NPs standard (C_o) bypassing to establish post run calibration
11. DI water bypassing.

All experiments were conducted at the original pH of the glass bead or sandstone columns. The pH values noted during the injection phase are listed in Table 6-1.

Table 6-1: pH, pressure, temperature and velocity data during injection phase for all experiments conducted

Column	Stabilizer	Linear Velocity cm/min	Run	Av. pH	Av. temp (°C)
Bare	SC	0.002	A	7.7	4.8
GB	None	0.01	Fl	7	5
Sst PL18HV	None	0.05	Fl	9.2	6.5
GB	Bare	0.007	A	6.6	4.4
GB	SC	0.007	A	7.4	5.3
GB H	SC	0.007	A	7.7	4.2
GB	SC	0.03	A	7.8	5.8
GB	SRFA	0.02	A	8.8	6.5
Sst 6305	Bare	0.04	A	9.08	5.8
Sst 7664H	SC	0.09	A	10.2	6
Sst 8620H	SC	0.03	A	10.4	4.7
Sst 8620V	SC	0.03	A	10.6	4.8
Sst PL18HV	SC	0.01	A	8.7	4.4
Sst 7100V	SRFA	0.06	A	6.3	5.8
GB	Bare	0.01	R	8.7	4.1
GB	SC	0.01	R	10.3	5.4
GB	SRFA	0.01	R	9.2	5.6
Sst PL18HV	Bare	0.05	R	6.7	3.4
Sst 6305V	SC	0.04	R	8.1	5.8
Sst 9706V	SRFA	0.04	R	6.2	4.9

A = Anatase R = Rutile SC= Sodium Citrate, SRFA = Swannee River Fulvic Acid, GB = Glass Bead Column, Sst = Sandstone Column, Fl = Fluorescein, V = Vertical, H = Horizontal

Not much difference of pH values was observed. Two types of NP shapes and phases were used during this study i.e. anatase spherical NPs and rutile ellipsoids/nanorods. Different bare runs were also conducted to compare the results with stabilized and non-stabilized media. A standard run of fluorescein was also performed to determine solute dispersivity and kinematic porosity / average linear velocity: in effect the fluorescein, which is unreactive, provides a base against which the reacting NM breakthrough can be compared. Following table

shows the number of experiments conducted along with pH, pressure, temperature and flow velocity data. Table 6-1 shows that pH values of sandstone columns are all high because of dissolution of carbonate minerals (calcite and dolomite) in the rock using CO_2 dissolved from the atmosphere before injection. This table shows that the sandstone experiments were undertaken generally though not entirely at higher pH values than the GB experiments. On the basis of above table of all experiments conducted, following table can explain the basic possible comparisons which can be made to accomplish the aims and objectives. Comparison of stabilizer effects is made in Sections 6.3.3 and 6.3.4 for GB and sandstone respectively; comparison of GB and sandstone column behaviour is made in Section 6.3.5; and comparison of anatase and rutile behaviour is made in Section 6.3.6. Section 6.3.7 then explores the results and implications of the differences observed.

Table 6-2: A tabular expression of all possible comparisons of the conducted studies. For fluorescein runs 0.01 and 0.05 cm/min were linear velocities for both glass bead and sandstone columns respectively (Unrecorded cell entries indicate same entry as cell above). pH variation is ignored at this stage.

R	None	GB	0.01V		R	None	Sst	0.046V***
	Na Cit		0.01V			Na Cit		0.039V**
	SRFA		0.01V			SRFA		0.036V
A	None	GB	0.007V		A	None	Sst	0.039**
	Na Cit		0.007H			Na Cit		0.011V**
			0.03V					0.03H,V*
	SRFA		0.021V					0.09V
						SRFA		0.064V

A v R

GB v Sst

Stabilizers

Velocity & H/V

R=rutile; A = anatase; GB=glass beads; sst=sandstone;V=vertical orientation; numbers = linear velocity cm/min

**run on same core – H was the first*
***run on same core – H was the first*
****Same core and H was the first to run*

6.3.2 Effect of velocity on nanoparticles transport

6.3.2.1 Velocity through sandstone cores

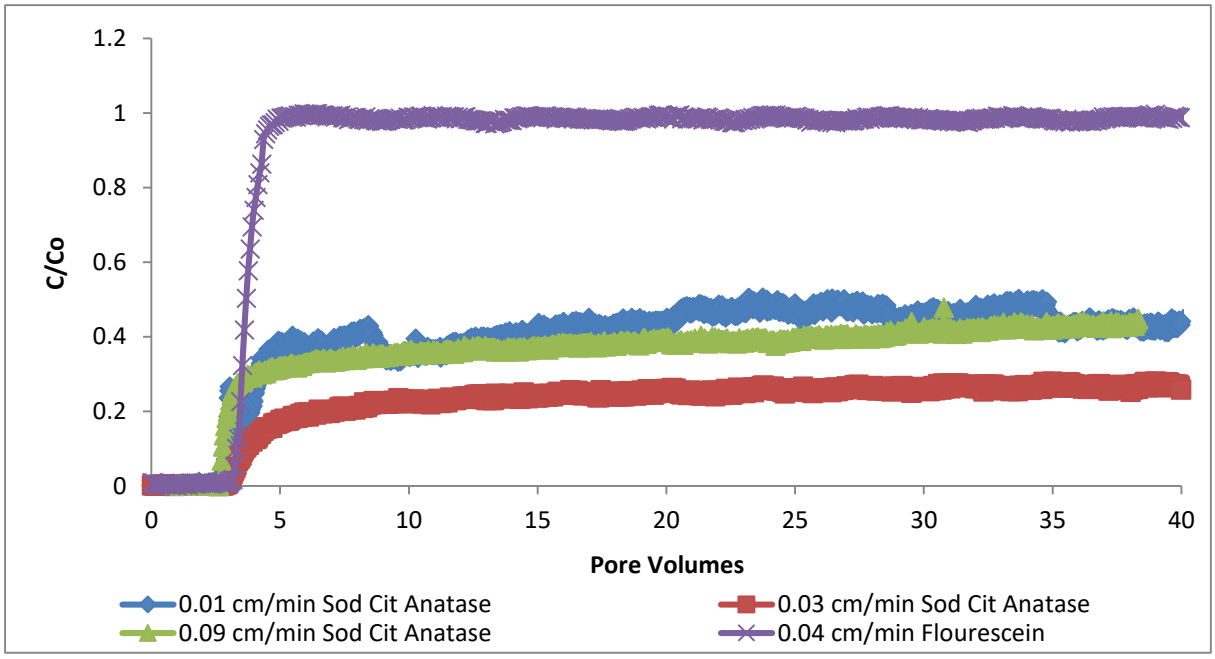

Figure 6.1: Comparison of sodium citrate stabilized anatase through sandstone columns at different velocities (all vertically oriented experiments)

It is important to consider velocity first as, if it affects the breakthrough curves significantly, it will have to be taken into account in the interpretation of all the other experiments. It is important to consider the sandstone case as this should have most uncertainty, as each column is unavoidably different in terms of porosity, internal architecture, and mineral composition, and so any effect of velocity would have to be bigger that effects caused by differences in these parameters. Most data on the effects of velocity are available for the sandstone cores (Table 6-2).

Transport of sodium citrate stabilized anatase NPs through different sandstone cores was evaluated with varied velocities (cm/min), including a slow rate of 0.01 and a high flow rate of 0.09 cm/mins. The C'/C_o was plotted against the number of pore volumes (PV) of the

solution introduced, are presented in Figure 6.1. For comparison purposes, a standard 100% C'/C_o obtained from passing fluorescein through one of sandstone cores is also plotted.

In sandstone cores, TiO_2 nanoparticles concentrations broke through at about the same time as the fluorescein (at greater than one PV because of the volumes present in the tubing and manifolds).

Figure 6.1 demonstrates a 40% breakthrough (i.e. C'/C_o) for slowest velocity of 0.01 cm per second through sandstone cores which is similar to that for the highest velocity of 0.09 cm/min. A velocity of 0.03 cm/min gave a breakthrough which is 20% less than other two velocities for NPs flow, which means the equilibrium C'/C_o values at breakthrough (C'/C_o) are only dependent to a limited extent on the velocity.

6.3.2.2 Velocity through glass bead columns

Transport of sodium citrate stabilized anatase NPs through glass bead columns was evaluated with two different velocities, including a very slow rate of 0.007 and a high flow rate of 0.03 cm/mins. Fluorescein as a standard non-reactive material was also run through glass bead column at a velocity of 0.01 cm/min. The C'/C_o was plotted against the number of pore volumes (PV) of the solution introduced (Figure 6.2).

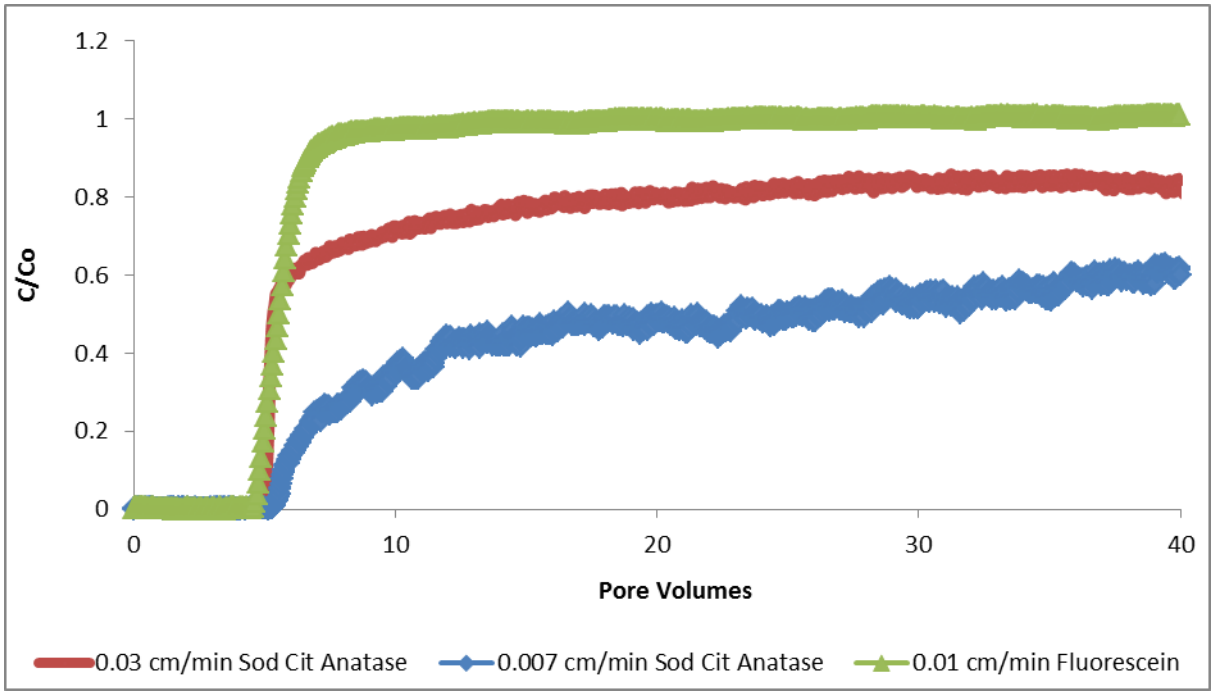

Figure 6.2: Comparison of sodium citrate stabilized anatase through glass bead columns at different velocities

Figure 6.2 demonstrates a 60% breakthrough for slowest velocity of 0.007 cm/min at the point when the experiment was stopped, though it is clear that the concentrations were still rising, i.e. that the breakthrough shows extensive 'tailing'. For the higher velocity of 0.03 cm/min, much less tailing was displayed and the final, stable C'/C_o (a true C'/C_o) was 78.4%. The slower flow experiment was undertaken when the column was horizontal, the faster velocity experiment when the column was vertically mounted.

6.3.2.3 Discussion

The results from the sandstone experiments, where velocity varied over a range of nearly an order of magnitude, indicate that if velocity is important it has an effect that is difficult to determine above the differences due to different columns.

For the glass bead experiments, there was a clearer difference between the experiments carried out over a range of about half an order of magnitude. However, this difference was in

both concentration and degree of tailing and the slower velocity experiment did not reach a stable C'/C_o concentration before the end of the experiment. As the slower experiment was undertaken with the column mounted horizontally whereas the faster experiment was undertaken under the usual vertically mounted conditions, little can be deduced.

It seems likely that velocity does affect the breakthrough curves in the case of the sandstone experiments within the uncertainty caused by the necessity of having to use different columns for each experiment. In the case of the glass bead medium an effect is likely to be seen so the most confident comparisons in the following sections will be between experiments undertaken at similar velocities.

6.3.3 Bare vs stabilized nanoparticles through glass bead columns

Figure 6.3 shows the glass bead breakthrough plots for anatase in the different stabilizing media and also fluorescein. Unstabilized, 'bare' anatase is completely retained in the column, and SRFA stabilized anatase is more mobile than sodium citrate stabilized anatase, despite the greater velocity in the SRFA experiment. The 0.007 cm/min (horizontally mounted) sodium citrate experiment Figure 6.2 has a significant breakthrough, so the complete attenuation of the bare anatase at 0.007 cm/min is not just due to the slower velocity. The SRFA concentrations follow the fluorescein very closely before tailing starts. The sodium citrate breakthrough is apparently delayed, initially more sharply defined, but also tailed.

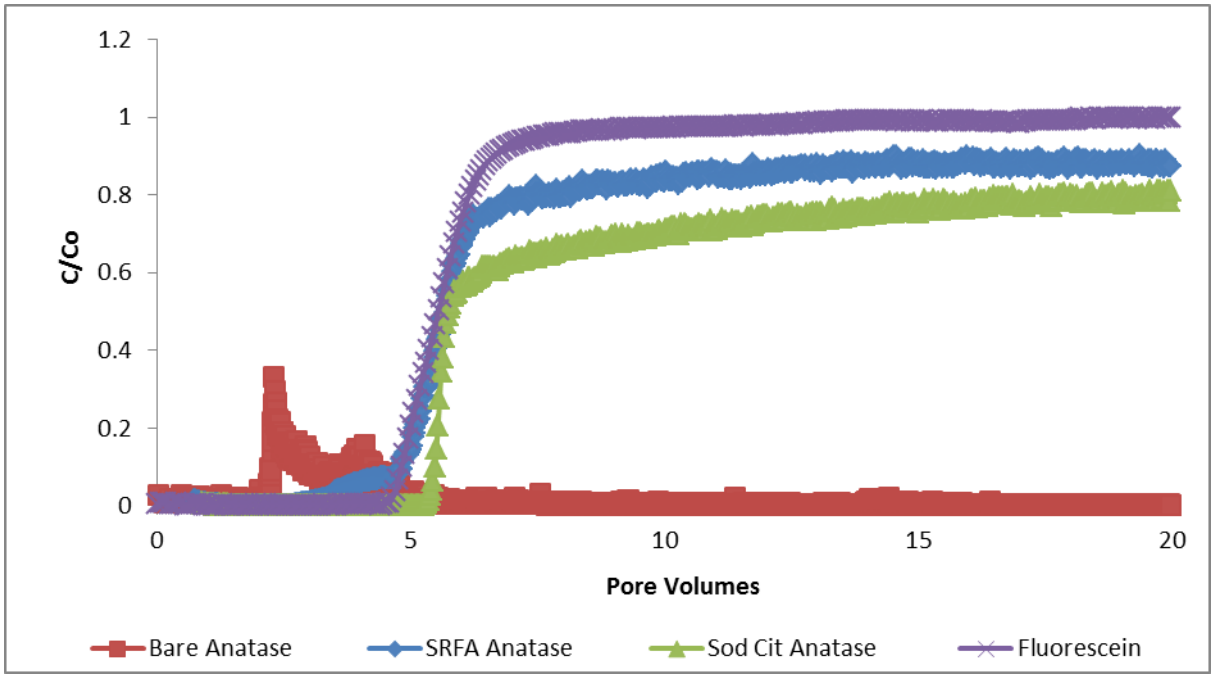

Figure 6.3: Anatase bare (0.007 cm/min) compared with sodium citrate (0.03 cm/min) and SRFA (0.02 cm/min) stabilized anatase through glass bead columns.

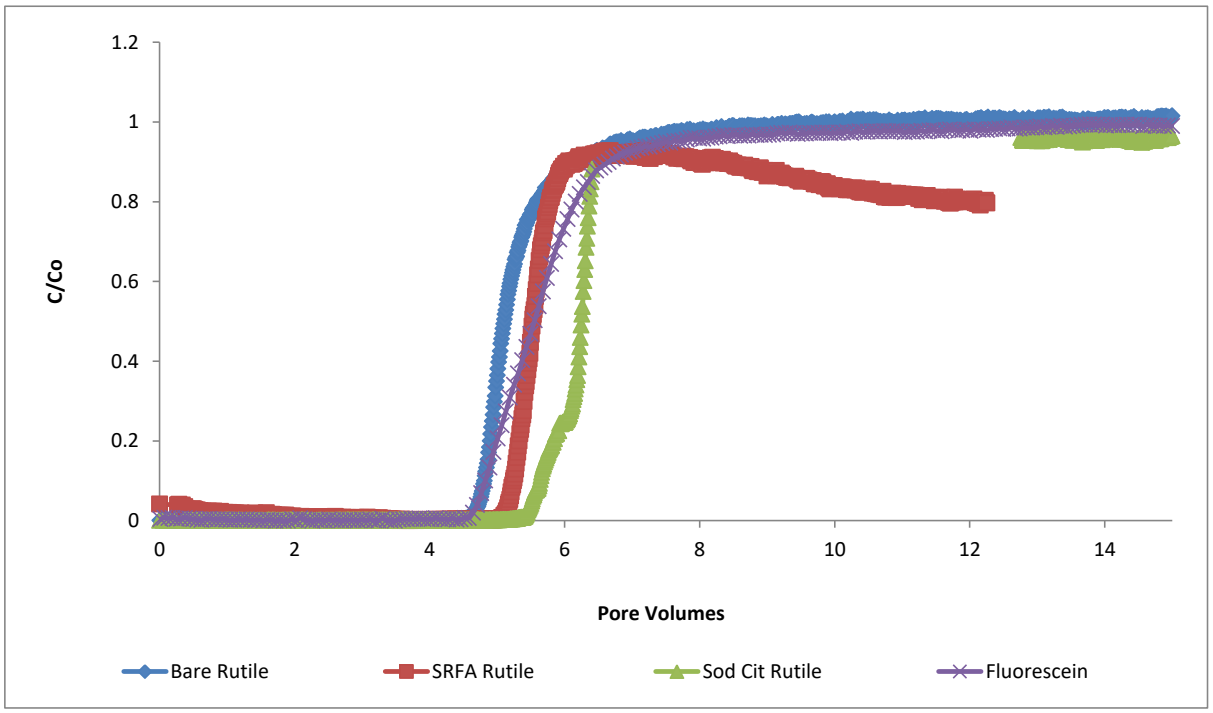

Figure 6.4: Rutile ellipsoids bare compared with sodium citrate and SRFA stabilized rutile through glass bead columns. All experiments were completed at the same velocity (0.01 cm/min).

Figure 6.4 demonstrates a 100% breakthrough for bare rutile at a velocity of 0.01cm/min which is equal to fluorescein although broke apparently a little early. The curve

has similar shape to fluorescein i.e. unattenuated and a little less dispersed. The behaviour of SRFA and sodium citrate is very similar, showing 92 and 88% breakthrough respectively, at a linear velocity of 0.01 cm/min. In both cases of SRFA and sodium citrate, the breakthrough is followed by a little ripening effect which is not continuous, as is much more usual, but a stabilized C'/C_o becomes more established.

Table 6-3: Total release of NPs after flushing with relevant surfactant solution followed by DI water through glass bead columns

NPs	C'/C_o	pH	Retained as % total injected	Released by stabilizer flush as % injected	Released by DI water flush as % injected	Total released as % total injected	Total released as % retained
Bare anatase	0	6.6	100	-	-	-	0
Sod cit anatase	0.74	7.4	26	6.64	14.39	21.03	80.9
SRFA anatase	0.76	8.8	24	13.58	9.35	22.93	95.5
Bare rutile	0.98	8.7	2	0	2.07	2.07	103
Sod cit rutile	0.88	10.3	12	5.61	5.84	11.45	95.4
SRFA rutile	0.95	9.2	5	3.4	1.4	4.8	96

Table 6-3 summarizes the flushing behaviour during the GB experiments. It is noticeable that in all cases except for the bare anatase experiments, there is significant release of NPs in the flushing phase with the stabilizer in solution and that the deionized water flushes out most of the rest of the retained particles. For bare anatase the particles seem to be irreversibly retained.

In summary, these experiments have shown the following features:

1. C'/C_o of zero for anatase bare (Figure 6.3)
2. Early breakthrough and then clogging of column with bare anatase
3. 100 % C'/C_o for rutile bare (Figure 6.4)
4. A finite ripening behaviour for rutile ellipsoids for both sodium citrate and SRFA (Figure 6.4)
5. $0< C'/C_o<1$ for all the cases (Figure 6.4) except bare rutile

6. Breakthrough curves for anatase are tailed, those for rutile are not
7. Mass balances show >90% release from glass bead columns except 0% bare anatase NPs and 80.9% sodium citrate anatase (Table 6-3)
8. SRFA is not equal to Sodium Citrate nor equal to bare NPs
9. Sodium citrate and SRFA are not equal in behaviour

It is found with these experiments that SRFA and sodium citrate behaved very differently during transport of NPs in glass bead columns. Mass balances showed that SRFA released more NPs with flushing as compared to sodium citrate followed by less release with DI water for SRFA and more release for sodium citrate flushed columns (Table 6-3).

6.3.4 Bare vs stabilized nanoparticles through sandstone columns

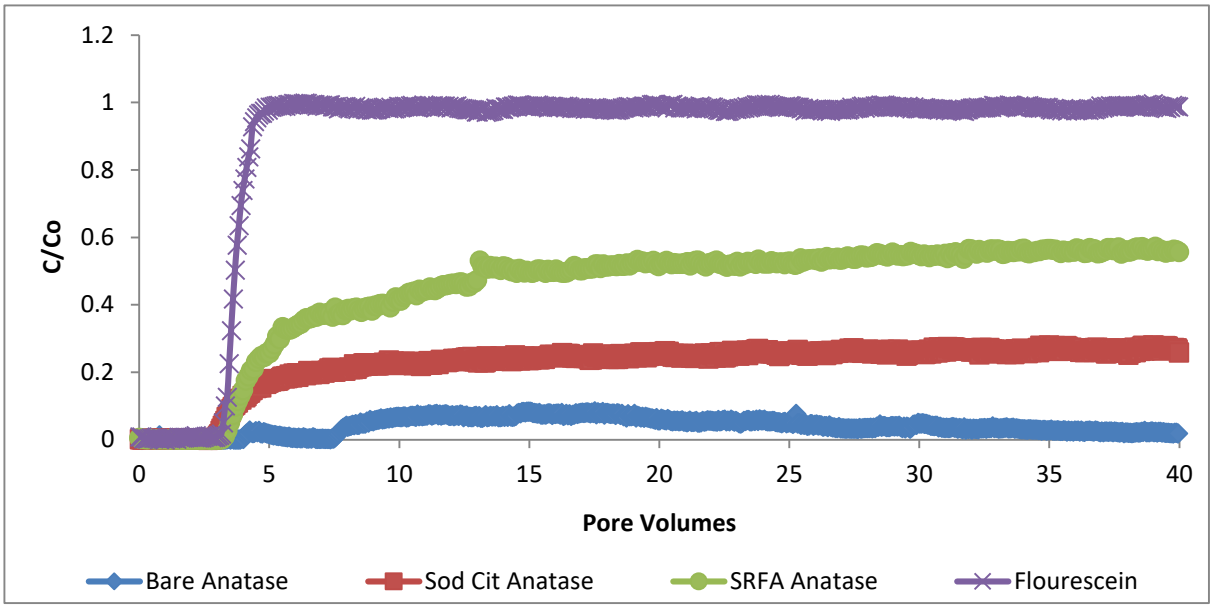

Figure 6.5: Comparison of bare anatase (0.039 cm/min) with SRFA (0.064 cm/min) and sodium citrate (0.03 cm/min, vertically oriented) stabilized anatase through sandstone columns

Table 6-4: Total release of NPs after flushing with relevant surfactant solution followed by DI water through sandstone cores

NPs	C'/C_o	pH	Retained as % total injected	Released by stabilizer flush as % injected	Released by DI water flush as % injected	Total released as % total injected	Total released as % retained
Bare anatase	0	9.08	100	-	-	-	0
Sod cit anatase	0.31	10.4	69	3.24	11.77	15.01	22.6
SRFA anatase	0.59	6.3	41	13.27	4.01	17.28	42.1
Bare rutile	0.97	6.7	3	-	2.12	2.12	70.7
Sod cit rutile	0.82	8.1	18	2.02	5.97	7.99	44.4
SRFA rutile	0.74	6.2	26	14.12	5.14	19.26	74.1

Figure 6.5 shows that when passing through sandstone columns anatase NPs are most mobile when stabilized in SRFA and are largely retained when bare. However, Figure 6.1

indicates that the C'/C_o for sodium citrate was closer to that for SRFA for velocities above and below that. The experiments shown in Figure 6.5 are on different sandstone samples, so the difference between sodium citrate and SRFA may not be as great as Figure 6.5 appears to suggest. The breakthrough curves are tailed. No delay in breakthrough is seen compared with fluorescein. In terms of NPs released during flushing with stabilizing solution and deionized water as a % of NPs retained, the order was: 99.8% fluorescein; 42.1% SRFA anatase; 22.6% sodium citrate anatase; 0% bare anatase (Table 6-4). It showed that rutile was more loosely attached to the sandstone column as compared to anatase, and attached NPs in SRFA systems are more easily released.

In summary, these experiments have shown the following features for sandstone breakthrough curves:

1. C'/C_o <0.5 bare for anatase (Figure 6.5)
2. $0< C'/C_o<1$ for all the cases (Figure 6.5)
3. Possible blocking in the case of bare anatase
4. Low retardation
5. Breakthrough curves are usually tailed
6. Mass balances for stabilizers show >40% release from sandstone cores
7. SRFA ≠ Sodium Citrate ≠ Bare (Figure 6.5)

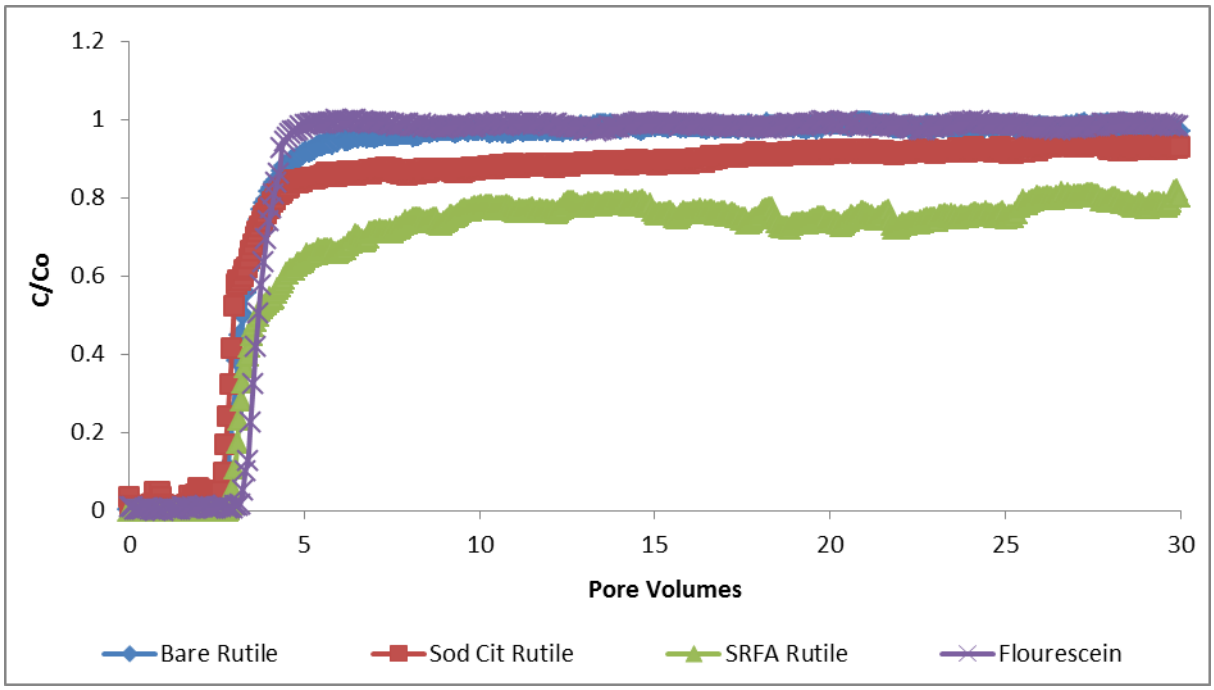

Figure 6.6: Comparison of bare rutile (0.046 cm/min) with SRFA (0.036 cm/min) and sodium citrate (0.039 cm/min) stabilized rutile through sandstone columns

Figure 6.6: compares the breakthrough curves for rutile stabilized in the different ways in the sandstone columns at similar velocities. The order of increasing attenuation is bare, sodium citrate and SRFA (Figure 6.6), the opposite of what was found for anatase (Figure 6.5); though because the results are similar with those presented in section 6.3.2.1 for sodium citrate stabilized anatase. Only the SRFA appears tailed significantly. In terms of releasing behaviour during stabilizing solution and deionized water flushes, the total NPs released as a % of that retained during injection was: 100% fluorescein; 74.1% SRFA rutile; 70.7% bare rutile; 44.4% sodium citrate rutile.

In summary, these experiments have shown the following features for sandstone breakthrough curves:

1. $0< C'/C_o<1$ for all the cases of stabilizers (Figure 6.6)
2. Low retardation
3. Breakthrough curves are usually tailed

4. Mass balances for stabilizers show >40% release from sandstone cores
5. SRFA ≠ Sodium Citrate ≠ Bare (Table 6-4)

It is found with these experiments that SRFA and sodium citrate behaved very differently during transport of NPs in sandstone columns. Mass balances showed that SRFA released more NPs with flushing as compared to sodium citrate followed by less release with DI water for SRFA and more release for sodium citrate flushed columns (Table 6-4).

6.3.5 Glass beads vs sandstone columns

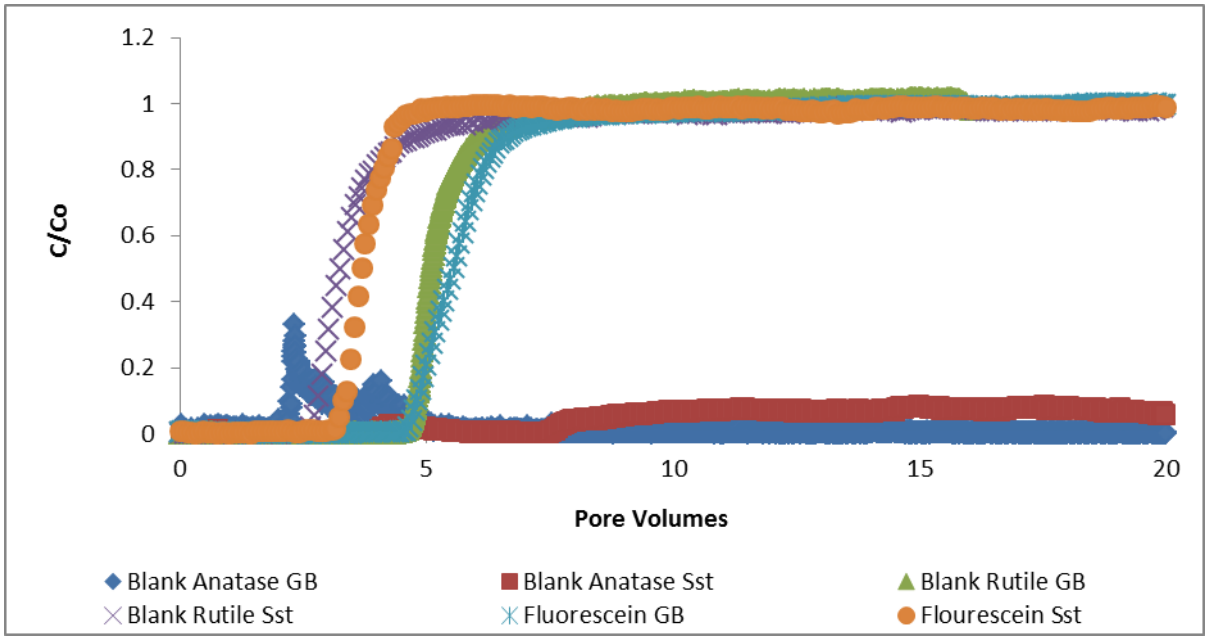

Figure 6.7: Comparison of glass bead (GB) and sandstone (Sst) for anatase and rutile bare run and fluorescein (Bare Anatase GB = 0.007 cm/min, Bare Anatase Sst = 0.04cm/min, Bare Rutile GB = 0.01 cm/min, Bare Rutile Sst = 0.05 cm/min, Fluorescein GB = 0.01 cm/min, Fluorescein Sst = 0.05 cm/min)

Figure 6.7 indicates that generally the sandstone and glass bead columns show similar results for the case of bare anatase and rutile suspensions. Bare anatase is largely retained in both media and bare rutile is largely unattenuated in both media. It should be noted that in general the pHs of the sandstone experiments are larger than those of the glass bead experiments and the velocities were higher. In both cases the rutile appears to have a sharper

breakthrough than the fluorescein, providing confirmation that this is a real phenomenon. The anatase in the sandstone case may show some indication of blocking, with a slow rise of concentration.

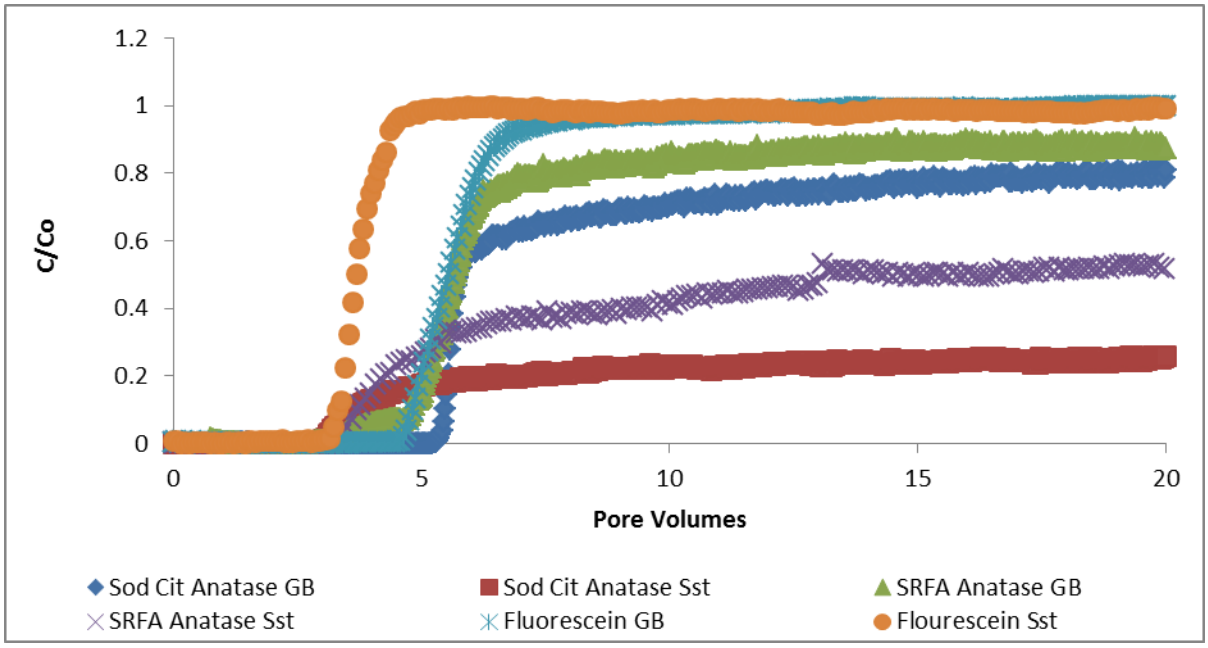

Figure 6.8: Comparison of glass bead (GB) and sandstone (Sst) for anatase stabilized with sodium citrate and SRFA (Sod Cit Anatase GB = 0.03 cm/min, Sod Cit Anatase Sst = 0.03cm/min, SRFA Anatase GB = 0.02 cm/min, SRFA Anatase Sst = 0.06 cm/min, Fluorescein GB = 0.01 cm/min, Fluorescein Sst = 0.05 cm/min)

Figure 6.8 compares the breakthrough curves for anatase with the SRFA and sodium citrate stabilizers in the two porous media types. The order of C'/C_o is the same for the two media, but the values are lower for the sandstone. In terms of releasing behaviour during stabilizing solution and deionized water flushes, the total NPs released as a % of that retained during injection was: 100% Fluorescein GB; 99.8% Fluorescein Sst; 95.5% SRFA Anatase GB; 80.9 % Sod Cit Anatase GB; 42.1% SRFA Anatase Sst; 22.6 % Sod Cit Anatase Sst.

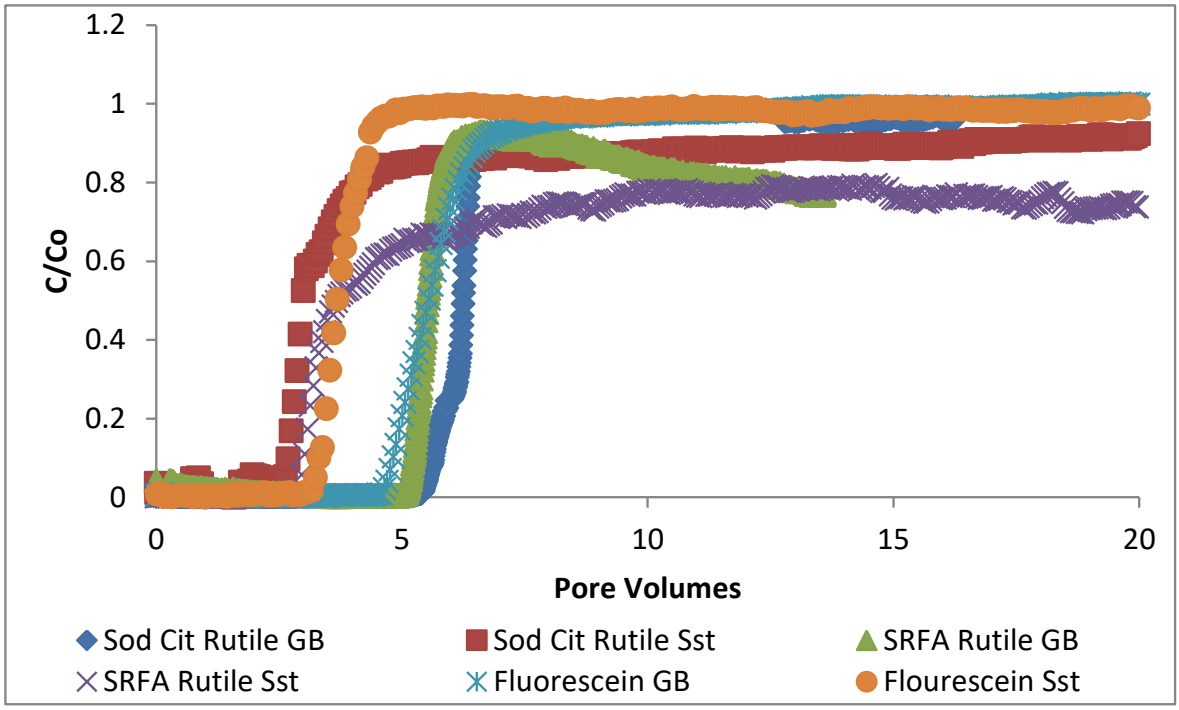

Figure 6.9: Comparison of glass bead (GB) and sandstone (Sst) for rutile stabilized with sodium citrate and SRFA (Sod Cit Rutile GB = 0.01 cm/min, Sod Cit Rutile Sst = 0.04cm/min, SRFA Rutile GB = 0.01 cm/min, SRFA Rutile Sst = 0.036 cm/min, Fluorescein GB = 0.01 cm/min, Fluorescein Sst = 0.05 cm/min)

Figure 6.9 compares the breakthrough curves for the stabilized rutile for the two media. It shows that sodium citrate has greater breakthrough for sandstone columns than SRFA but both sodium citrate and SRFA are similar for glass bead columns. Glass bead columns for both sodium citrate and SRFA showed a finite ripening behaviour which is unusual and not seen in sandstone. Initial breakthrough is earlier for NPs which sometimes can be compared with fluorescein, but this could be due to difference in cell size between the nephelometer and the fluorimeter. In a nutshell, both sandstone and glass bead columns have similar behaviour in comparison for both sodium citrate and SRFA stabilized rutile NPs. The order of the total released as a % of retained NPs through the glass bead and sandstone columns is as follows: 95.4% Sod Cit rutile GB; 92.9% SRFA rutile GB; 74.1% SRFA rutile Sst; 44.4% Sod Cit rutile Sst.

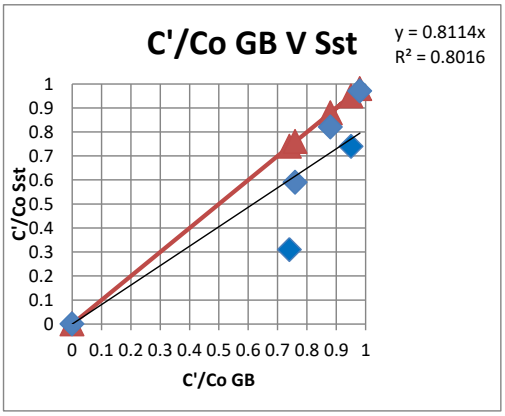

Figure 6.10: Comparison of the C'/Co for the glass bead (GB) and sandstone columns (sst)

Figure 6.10 gives a comparison of the entire C'/Co values for the glass bead and sandstone columns. The concentrations of glass bead are on same 1:1 plan and give nice linear relationship while sandstone are scattered and well below the equilibrium line.

In summary, these experiments have shown the following features:

1. GB and sandstone columns are equal in anatase breakthrough without any C'/C_o (Figure 6.14)
2. ~100 % C'/C_o of rutile bare for glass bead and sandstone (Figure 6.14)
3. Low retardation for both glass bead and sandstone
4. Ripening behaviour, though over a finite number of pore volumes, for rutile ellipsoids in glass bead and sandstone
5. $0< C'/C_o<1$ for all the cases in both glass bead and sandstone (Figure 6.11)
6. Breakthrough curves are usually tailed for both glass bead and sandstone
7. Mass balances show >40% release both from glass bead and sandstone
8. Anatase is not equal to rutile for breakthrough in glass bead and sandstone (Figure 6.8 and Figure 6.9)
9. Bare rutile > SRFA ≥ Sodium Citrate for both glass bead and sandstone
10. Bare anatase is not equal to bare rutile for both glass bead and sandstone

6.3.6 Anatase vs Rutile

6.3.6.1 Anatase vs rutile through glass bead columns

Figure 6.11 compares the breakthrough curves for sodium citrate and SRFA stabilized anatase and rutile through glass bead columns. It shows that rutile ellipsoids have greater breakthrough curves than anatase regardless of the surfactant use. However, glass bead columns for both sodium citrate and SRFA stabilized rutile ellipsoids showed a finite ripening behaviour which is not seen in anatase. Initial breakthrough for rutile ellipsoids once approached near 100% and can be compared with fluorescein, but these were ripened up to the levels of anatase breakthroughs after 10 pore volumes. In a nutshell, both anatase and rutile NPs through glass bead columns gave similar behaviour in long run irrespective of the stabilizing agent used. The order of the total released as a % of retained NPs through the glass bead columns is as follows: 95.5% SRFA Anatase; 95.4% Sod Cit rutile; 92.9% SRFA Rutile; 80.9% Sod Cit Anatase (Table 6-3).

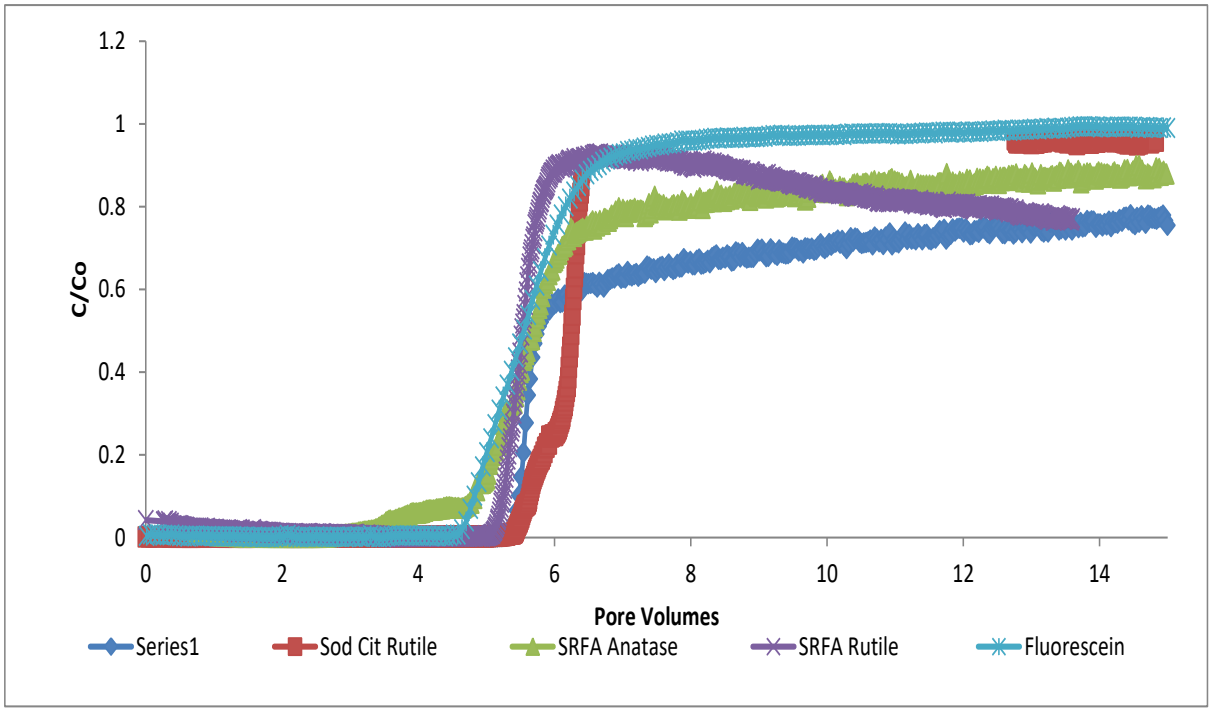

Figure 6.11: Sodium citrate and SRFA stabilized anatase and rutile ellipsoids through glass bead columns (Sod Cit Anatase = 0.03 cm/min, Sod Cit Rutile = 0.01cm/min, SRFA Anatase = 0.02 cm/min, SRFA Rutile = 0.01 cm/min, Fluorescein = 0.01 cm/min)

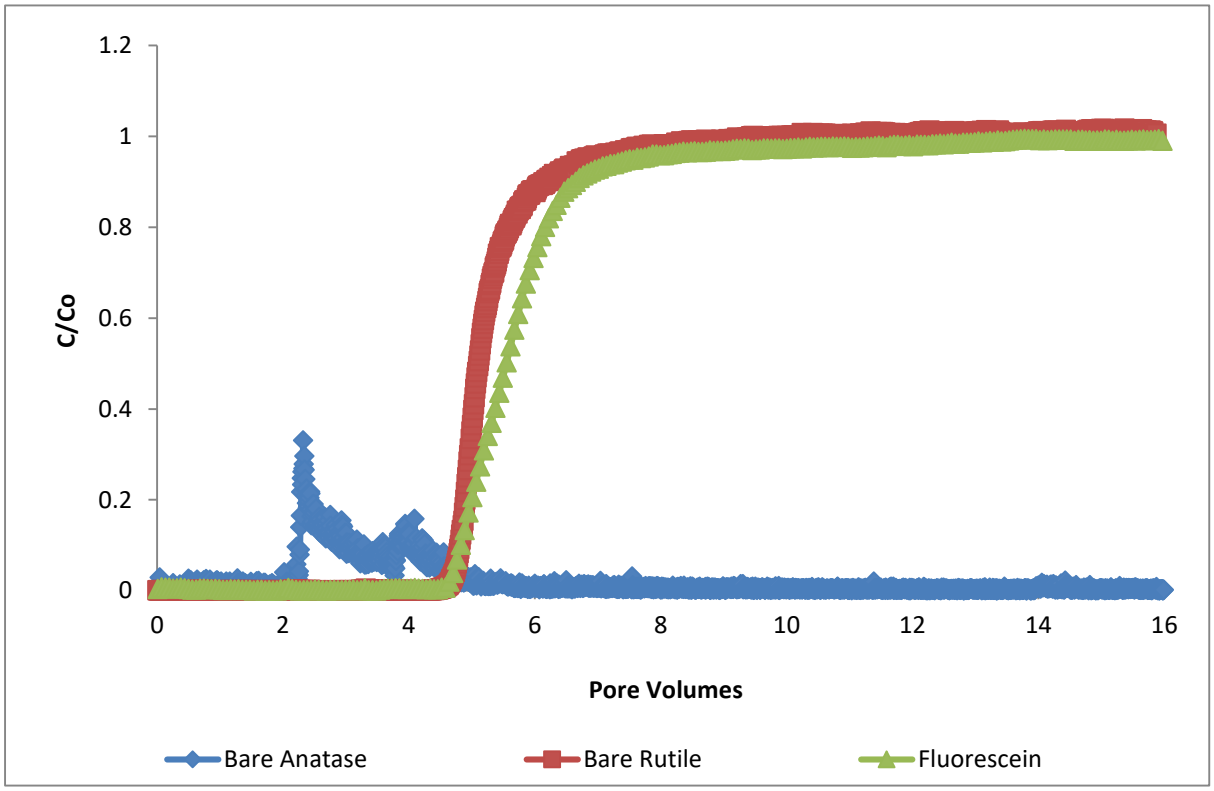

Figure 6.12: Comparison of bare anatase (0.007 cm/min) and rutile (0.01 cm/min) along with fluorescein (0.05 cm/min) through glass bead columns

Figure 6.12 compares the breakthrough curves of bare anatase and rutile through glass bead columns. Bare anatase showed no breakthrough curve while bare rutile showed ~100% breakthrough. This clearly shows that anatase without surfactants behaved in an entirely different way than rutile ellipsoids without surfactants. The glass bead column in case of bare anatase was clogged but in case of rutile ellipsoids 100% NPs were recovered (Table 6-3).

In summary, these experiments have shown the following features:

1. C'/C_o of zero for bare anatase (Figure 6.12)
2. 100 % C'/C_o for bare rutile (Figure 6.11)
3. A finite ripening behaviour for rutile ellipsoids (Figure 6.11)
4. $0< C'/C_o<1$ for all the cases (Figure 6.11) except bare anatase
5. Breakthrough curves for anatase are tailed, those for rutile are not
6. Mass balances show >80% release from glass bead columns except 0% bare anatase NPs (Table 6-3)
7. Stabilized anatase = stabilized rutile regardless of surfactant
8. Bare anatase is not equal to bare rutile

6.3.6.2 Anatase vs rutile through sandstone columns

Figure 6.13 shows a comparison between sodium citrate and SRFA stabilized anatase and rutile NPs through sandstone columns. It shows that rutile ellipsoids have greater breakthrough curves than anatase regardless of the surfactant use. This is quite similar behaviour to the one we have seen in case of glass bead columns. However, the differences from glass bead columns are order of magnitude of breakthrough and lack of ripening behaviour. In the entire cases breakthrough curves are tailed. The order of the total released as a % of retained NPs through the sandstone columns is as follows: 74.1% SRFA Rutile; 44.4 % Sod Cit rutile; 42.1 % SRFA Anatase; 22.6% Sod Cit Anatase (Table 6-4).

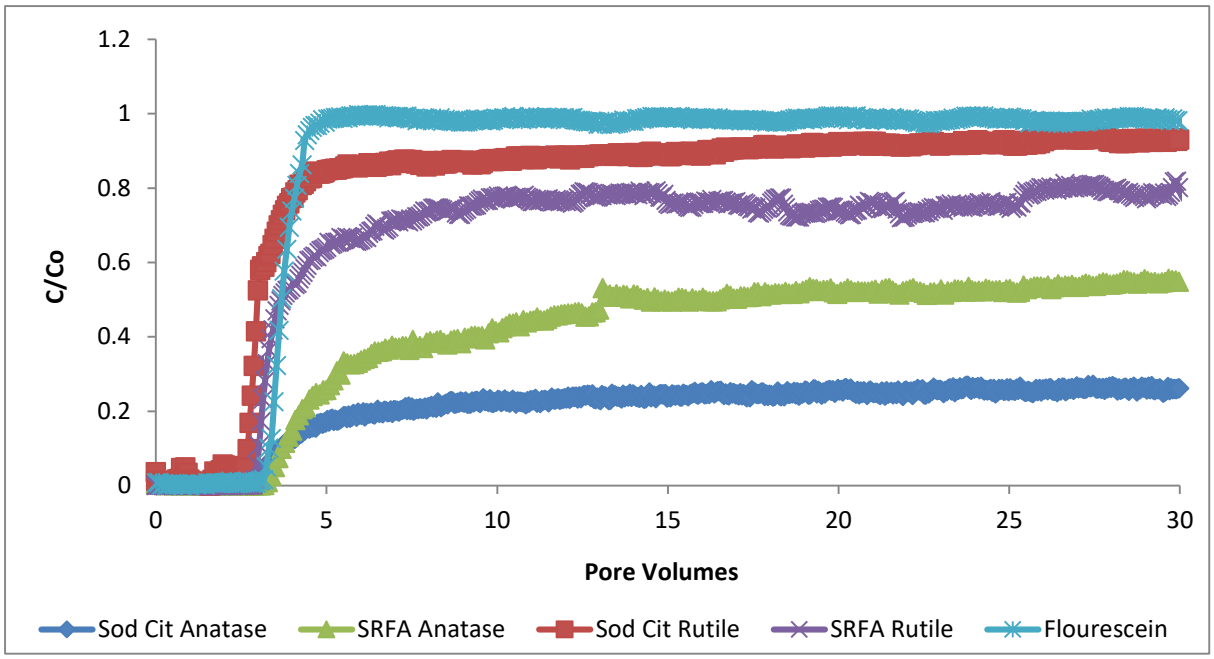

Figure 6.13: Comparison of sodium citrate and SRFA stabilized anatase and rutile through sandstone columns (Sod Cit Anatase = 0.09 cm/min, SRFA Anatase = 0.06 cm/min, Sod Cit Rutile = 0.04cm/min, SRFA Rutile = 0.04 cm/min, Fluorescein = 0.05 cm/min)

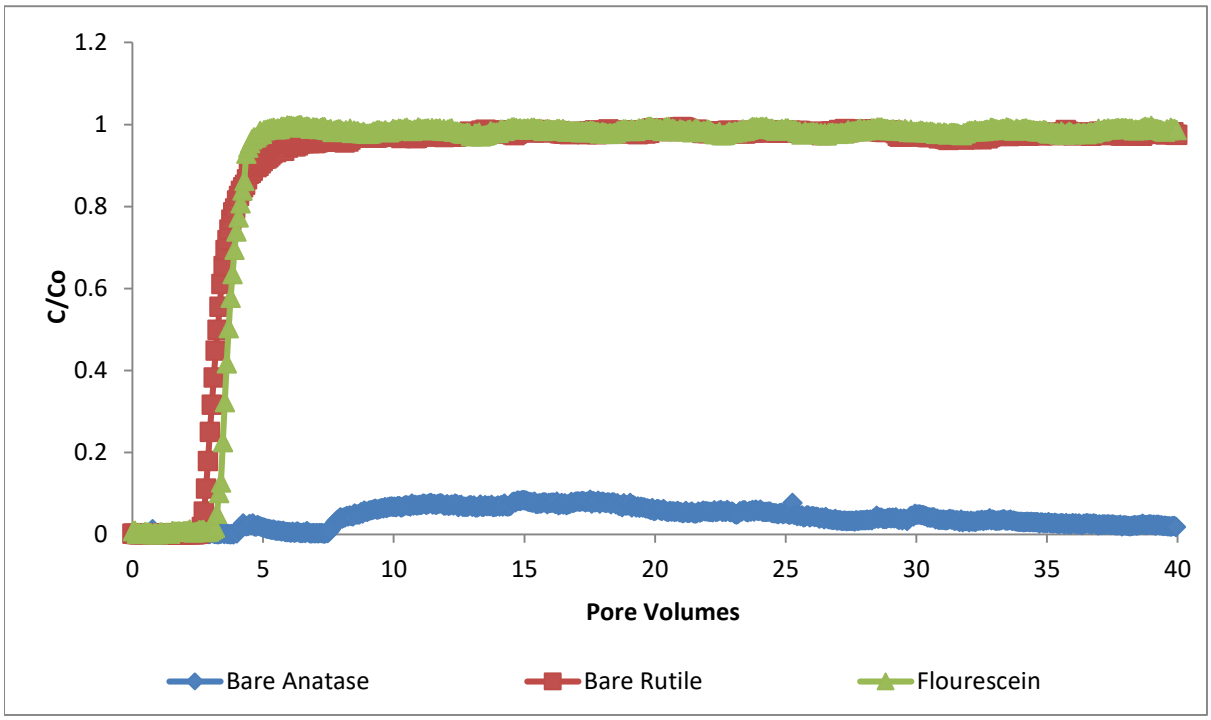

Figure 6.14: Comparison of bare anatase (0.04 cm/min) and rutile (0.05 cm/min) along with fluorescein (0.05 cm/min) through sandstone columns

Figure 6.14 shows the big contrast between the behaviour of bare anatase and rutile through sandstone cores. There is very little breakthrough for anatase, but complete

breakthrough for rutile. Mass balance analysis shows that 0 and 70.7% of the retained anatase and rutile ellipsoids were released through sandstone columns respectively.

In summary, these experiments have shown the following features:

1. C'/C_o of zero for bare anatase (Figure 6.14)
2. 100 % C'/C_o for bare rutile (Figure 6.13)
3. $0< C'/C_o<1$ for all the cases (Figure 6.13) except bare anatase
4. Breakthrough curves are tailed for all the cases
5. Mass balances show >40% release from glass bead columns except 0% bare anatase NPs (Table 6-4)
6. Anatase is not equal to rutile
7. Bare anatase is not equal to bare rutile

6.3.7 Explanation and discussions

6.3.7.1 Introduction

In summary the experiments have shown the following broad results:

1. Breakthrough of titania NPs is similar in style, though different in degree, in glass bead and sandstone columns;
2. The presence of different stabilizers affects mobility differently;
3. Anatase and rutile do not have the same mobility in the same stabilizers;
4. Tailing is common;
5. Ripening appears to occur for rutile under some conditions;
6. A large proportion of NPs retained in the columns are released on flushing.

These observations will be discussed in the following subsections.

For ease of reference, Table 6-5 repeats some of the main results from the experiments.

Table 6-6: C/Co and mass balances of bare vs stabilized anatase and rutile through (a) glass bead columns and (b) sandstone columns.

NP	Stabilizer	C'/C_o	pH	Retained as % total injected	Released by stabilizer flush as % injected	Released by DI water flush as % injected	Total released as % total injected	Total released as % retained
A	None	0	6.6	100	-	-	-	0
	Na Cit	0.74	7.4	26	6.64	14.39	21.03	80.9
	SRFA	0.76	8.8	24	13.58	9.35	22.93	95.5
R	None	0.98	8.7	2	-	2.07	2.07	103
	Na Cit	0.88	10.3	12	5.61	5.84	11.45	95.4
	SRFA	0.95	9.2	5	3.4	1.4	4.8	96

(a)

NP	Stabilizer	C'/C_o	pH	Retained as % total injected	Released by stabilizer flush as % injected	Released by DI water flush as % injected	Total released as % total injected	Total released as % retained
A	None	0	9.08	100	-	-	-	0
	Na Cit	0.31	10.4	69	3.24	11.77	15.01	22.6
	SRFA	0.59	6.3	41	13.27	4.01	17.28	42.1
R	None	0.97	6.7	3	-	2.12	2.12	70.7
	Na Cit	0.82	8.1	18	2.02	5.97	7.99	44.4
	SRFA	0.74	6.2	26	14.12	5.14	19.26	74.1

(b)

6.3.7.2 The similarity of breakthrough behaviour in glass bead and sandstone columns

Though differing in degree, the general style of breakthrough is similar in glass bead and sandstone columns, namely C'/Co is less than one and varies in the same order with the type of stabilizer present, and tailing is present. The values of C'/Co for the sandstone are slightly less than for the glass beads. This similarity suggests that the surface properties of the glass beads are similar to those of the sandstone and that the pore architecture of the sandstone has limited effect.

The zeta potential of the surface of very similar sandstones has been investigated in detail by Anderson (In Prep) (Amirbahman and Olson, 1993). Anderson (Amirbahman and Olson, 1993) (In Prep) used a new technique developed by Malvern Instruments called Single Surface Electroosmotic Flow Mapping (SS-EFM). Her results, extrapolated using

electrophoretic mobility measurements on sandstone fines, suggested that the zeta potentials of the sandstone surfaces, despite their mineralogical complexity, varied very little through a 60m sandstone sequence, with almost all values lying between -35 and -40 mV. This value compares with -37mV for glass (Stankus et al., 2010). The SS-EFM measurement is at a scale of a few millimetres and will not pick up changes in zeta potential below this scale. The similarity of the breakthrough curves for the two media suggests that the likely sub millimetre heterogeneity of the sandstone is not important. This argument is not to claim that zeta potential is the only control here but that possibly the surfaces of the GB and sandstones appear to be similar in terms of their initial, pre-injection, surface potentials.

The pore size of the glass beads is almost certainly less variable and has a minimum size much larger than the sandstone. Mercury injection pore size measurements have been made by Bloomfield et al. (2001) on UK Triassic sandstone samples similar to those used here, and they found that median pore throat diameters were around 20µm, but that perhaps 5% of pore throats are less than 100nm. The similarity of the breakthrough curves suggests that straining may not be an important part of the removal of titania NPs in the sandstones.

6.3.7.3 The presence of different stabilizers affects mobility differently

6.3.7.3.1 Introduction

It is obvious from the results obtained that different stabilizers enhance the NP mobility to different degrees as compared to bare NPs. These results are in line with those obtained from the stability (chapter 5) where SRFA and sodium citrate showed different stability and aggregation kinetics at different pHs and ionic strengths. Sodium citrate can be considered an example of an efficient stabilizer for TiO_2 NPs, and SRFA as representing natural humic and fulvic acids. Use of SRFA and sodium citrate surfactants during GB and sandstone column experiments changed the transport of NPs in two ways. Firstly, with use of surfactants the NP

surfaces were modified and remained stable for a period of time. Secondly, with the initial injection of NP-free surfactant, the surface of rock was being conditioned prior to NP injection. This might represent the condition at the tip of a pollution plume where the surfactant has travelled further than the NPs.

6.3.7.3.2 SRFA

The steric repulsion forces resulting from adsorbed SRFA on the surface of TiO_2 NPs gives high levels of steric protection providing steric barriers to aggregation and attachment of nanomaterials to the rock or glass bead surfaces. Hotze et al. (2010) confirmed similar sort of steric repulsion behaviour where DLVO forces alone are not sufficient to accurately predict the aggregation behaviour, rather another sort of imparted steric forces define whether the aggregation is temporary or permanent. Such additional forces are known as extended DLVO forces (XDLVO). Moreover, NOM and fulvic acid form covalent complexes on the metal NPs. However, they can also form intermolecular bridging connecting the collector (rock) surface to the NPs (Baalousha et al., 2013), or indeed NP to NP, hence tending to increase attachment or destabilize the suspension.

Generally, the greater C'/C_o of anatase NPs in SRFA than in both sodium citrate and pure water confirms the stability results reported in chapter 5 i.e. steric effects always dominate over bridging effects. SRFA has given an extended stability to the NPs by developing XDLVO forces which was not the case with the sodium citrate stabilizer.

6.3.7.3.3 Sodium citrate

In contrast, sodium citrate provides high levels of electrostatic repulsion as an ionic molecule. It is suggested that the sodium citrate provides increased stabilisation by electrostatic repulsion.

Generally, highly acidic pH gives more stabilization to the NPs suspension due to the presence of greater amount of H^+ ions in the system. This stability is further enhanced by the electrostatic effect of sodium citrate. It is already reported in chapter 5 that the pH of the NPs suspension has a pronounced effect on metal oxide nanoparticle stability. pH determines the zeta potential plane which is measured as the primary indicator of surface charge on NPs. This surface charge is altered with an increase or decrease in the pH. This change in pH and hence zeta potential can change agglomeration state, which influences the transport of NPs in a porous media. It is well documented that zeta potential values of ±30 mV can impart stability to NPs suspensions (Júnior and Baldo, 2014). This is because higher potentials of the same sign (either positive or negative) in the suspension system increases repulsion providing greater counter-balancing of the van der Waals forces and therefore enhancing stability (Hunter, 1981).

6.3.7.3.4 Bare

In case of bare rutile NPs there was relatively low zeta potential of the rutile was enough that rutile was mobile anyway in glass bead and sandstone. One other concept which comes in mind is no binding force on the surface of NPs so they passed relatively quickly through pores as compared to the stabilized NPs which have protecting shields which act as barriers and caused more resistance in movement (Macé et al., 2006). If this concept is true, then it should be same for bare anatase which should also move quickly through both systems. So clearly behaviour of bare rutile is not well understood and such behaviour is not documented either. The counter ion effect imparted by the alkoxide used during synthesis procedure is also important in determining overall stability of suspension. Such counter ion effect was present in rutile but absent in anatase because of the different surface properties of the polymorphs.

The bare rutile NPs were relatively stable in suspension when compared to bare anatase, having -43mV of zeta potential which is more negative than -37mV of anatase NPs. So rutile NPs were probably less likely to attach to the surfaces of the column medium, which they proved to be in both sandstone and glass bead media. Similar behaviour of predicted C'/C_o was observed recently by Anderson (2015) who noted a significant change in C'/C_o even with a slight change in zeta potential.

6.3.7.3.5 Conclusion

Overall, generally the differences in type of stabilization give rise to the differences in mobility of NPs. These differences are attributed to differences in electrostatic (provided by sodium citrate or the NP itself) and steric stabilization (provided by the SRFA).

6.3.7.4 Anatase and rutile do not have the same mobility in the same stabilizers

This is a very interesting finding as both stabilizers result in greater mobility for rutile than anatase in both glass beads and sandstone columns. It is suggested that this difference in mobility arises because of the different surface properties of the two polymorphs. It is already reported that isoelectric point is dependent on size and crystal structure (Suttiponparnit et al., 2011), which shows that difference in size, shape and crystal structure for both ~30 nm spherical anatase and 20x140 nm rutile ellipsoid might have a decisive role in the mobility of both NPs. It is already reported in literature that rutile NPs have always differences in IEP which is related to differences in coordination number and proportion of acidic and basic sites on the particle surface (Bullard and Cima, 2006).

It is true that without further experimental and modelling investigations, the likelihood of the effect of different surface properties cannot be determined, but it is well known that there are different behaviours of the surfaces as zeta potentials are lower for rutile than anatase.

Reason for a difference in transport of rutile may also be attributed to the different morphologies of anatase and rutile, where rutile is relatively more active as dense nanorods arrays and multilevel branched rutile NPs demonstrated enhanced chemical and field emission properties. It was reported that morphology, surface-related defects and oxygen species were responsible for the differences in behaviour (Sarkar et al., 2012).

As mentioned above, rutile ellipsoids have a width of 20±5 nm and average length of 120-140 nm and so exhibit a large aspect ratio as compared to spherical anatase NPs. The larger surface aspect ratio of rutile NPs provides greater opportunities to have steric and ionic shields around themselves to give them enhanced stability (Mukherjee et al., 2005, Macé et al., 2006). These protective shields are more efficient for ellipsoids than the protective shields for spherical NPs (Zhang, 2003), thus qualitatively explaining why rutile particles are more mobile than anatase particles.

The surface ionic or steric interactions can be affected by the spatial configuration of surfactants around the NPs that can act as shields that prevent or encourage the interaction of the nanorods with other nanomaterials or collector surfaces (Spaeth et al., 2011).

The transport of the anatase nanoparticles was significantly enhanced with SRFA compared with sodium citrate in the sandstone columns, though the two stabilizers performed similarly in the glass bead columns. For rutile, sodium citrate and SRFA performed similarly in both sandstone and glass bead columns. One possible reason for the difference in SRFA stabilization behaviour between anatase and rutile in the sandstone column experiments is that the high levels of steric protection. But this was not true for rutile ellipsoids.

NOM and fulvic acid form covalent complexes around the metal NPs as well as forming intermolecular bridging which act as a barrier on the collector surface to the NPs (Baalousha

et al., 2013). As mentioned earlier, rutile NPs size is approximately 20x140nm and molecule size of SRFA is well below than 10nm (<<100 kDa) (Haiber et al., 2001). This size range of SRFA and rutile NPs show that several 10s of SRFA molecules can adjust on the surface of rutile ellipsoids. In case of rutile the larger aspect ratio gives more available sites for the SRFA molecules to attach the rutile ellipsoids; a mechanism generally called molecular bridging. This bridging in certain cases imparts a reasonable amount of destabilization in the suspension by giving rise to larger agglomerates which eventually settle down.

In contrast sodium citrate provides high levels of electrostatic repulsion as an ionic molecule. It is suggested that the sodium citrate altered stabilisation by electrostatic repulsion to the rutile ellipsoids which have large aspect ratio.

The SRFA provides steric repulsion in addition to the electrostatic stability of both anatase and rutile NPs. It looks like dual action of SRFA which imparts negative charges to the NPs along with the steric stabilization as an additive effect.

In optimized conditions of SRFA stability negative SRFA attaches to positively charged TiO_2 NPs (Palomino et al., 2013). An increase or decrease in the SRFA concentration gives either inversion of surface charge or lack of required amount of required negative charges on the surface thus imparting destabilization. Overall stability of the suspension depends on the pH of the suspension as low and high pH values more surface charges prevent aggregation with increased number of charges. The aggregation is likely to occur at a pH near to pHzpc (Palomino et al., 2013).

In a nutshell from the above arguments we cannot resolve the reasons for greater effects of stabilizers on mobility of rutile compared with anatase without further experimental and modelling research. But it seems likely from simple geometric arguments that the reason is

probably less likely to do with particle-scale morphology but more likely to do with the interaction of the stabilizers with the particular surfaces which in turn modify surfaces for better transport.

6.3.7.5 Tailing is common

Tailing is usually caused by a physical non-equilibrium process usually involving a zone where flow is much slower than elsewhere in the porous medium and to and from which mass exchanges through diffusion, or through non-equilibrium attachment (Šimůnek and van Genuchten, 2008). Theoretically tailing should be more in sandstone as compared to glass bead columns. By comparing Figure 6.4 to Figure 6.11 it is obvious that although tailing is more in sandstone than in glass bead columns, it does occur in the glass bead columns too.

The fact that tailing is observed for both the glass bead and sandstone, and the fact that the fluorescein breakthroughs were much less tailed suggests that the tailing is not due to physical non-equilibrium but a process associated with the rock/particle interactions. This suggests that kinetic attachment and detachment processes need to be considered, suggesting that colloid filtration theory may well not be valid for these systems. To determine the possible types of process involved in the tailing process in glass bead and sandstone media, a numerical modelling investigation is recommended to determine whether kinetic attachment and detachment processes can describe the tailing consistently, and quantify the rates. Without such an investigation via numerical calculations followed by experimentation, further resolution is not possible. Rates determined may indicate processes involved, but even then the interpretation will be difficult; much more certain determination of process would be obtained if information could be obtained on concentrations within the columns, such as by use of imaging methods such as MRI, though this application of MRI is in its infancy.

6.3.7.6 A ripening appears to occur for rutile under some conditions

Ripening was only seen in the SRFA run using rutile and glass bead column. It shows continuous dropping of concentrations throughout the experiment. It was noted that pH of this run was usually higher than other glass bead runs at 9.2. This pH was the highest for any SRFA in both sandstone and glass bead columns. This high pH may well have some effect on the fulvic acid and hence mobility of rutile ellipsoids. Previous work on very dilute propylene glycol suspensions of titania in UK Triassic sandstone Tiller and O'Melia (1993) has also shown that ripening can occur (with a concomitant significant decrease in permeability); the pH values were similarly high in these experiments.

6.3.7.7 Release is limited

The mass balance data show that NP release is dependent on the media used. Glass bead media released more than 80% of retained NPs as a result of the sequential flushing using the stabilizing solution and DI water. It was observed that in the SRFA experiments a greater % of the retained NPs was released in both glass bead and sandstone columns. The release of retained NPs was less with sodium citrate flushing followed by increased release with DI water. For bare rutile the release is possibly related to the presence of secondary minima. SRFA imparts steric stabilization which limits the approach of NPs to the collector surfaces, and this may discourage attachment in the primary minimum. In the case of glass beads more NPs (almost 100% of that retained) were released with subsequent flushing with surfactant and DI water. The effectiveness of DI flushing on the total release is not possible to deduce as most of the NPs were already released with surfactant flushing.

Figure 6.15a illustrates the total release of NPs expressed as % injection, the results for the GB columns being plotted against those for the sst columns. It shows that the sandstone

columns release rather less than the GB columns. The relationship between the C'/Co values for the two media is linear, suggesting that glass beads are a reasonable analogue for the sandstone not just in terms of the form of the breakthrough curves, but also in terms of the particle release.

Figure 6.15b shows the total mass released as a percent of the injected mass following flushing with the stabilizing solution in the glass beads columns. Ignoring the case of bare anatase, flushing with the stabilizing solution releases 6-16% of total mass retained. The GB columns allow slightly more release than sandstone columns. Figure 6.15c shows the % release of NPs with DI water in the glass bead columns. Ignoring the case of bare anatase, flushing with DI water releases 2-14% of the injected mass.

Figure 6.15d shows a comparison of % release by DI water and solution in glass bead columns. For glass bead total release is nearly equal to total retention. Much of the retained mass in glass bead columns was released by the solution flush and hence as mentioned above, the results for the subsequent DI water flushes are not a very good indication of the effectiveness of DI flushing. At this stage we cannot really compare the actual effect of DI water due to lesser availability of NPs in second flush of DI water which was the case in all flushing. Total sandstone release was <100%, so more could have been released. However, there may still be a finite amount of retained particles that could not be removed by either solution or deionized water, so still may get different result if the order of flushing was reversed.

Figure 6.15e shows a comparison of % release by DI water and solution in sandstone columns. In this case total release is much less than total retention and hence the effectiveness of DI water release can be gauged. For the SRFA runs, more NPs are released by the SRFA

flush than the DI water flush (upper two points), but for the sodium citrate runs, more NPs are released by the DI water flush (lower 3 points).

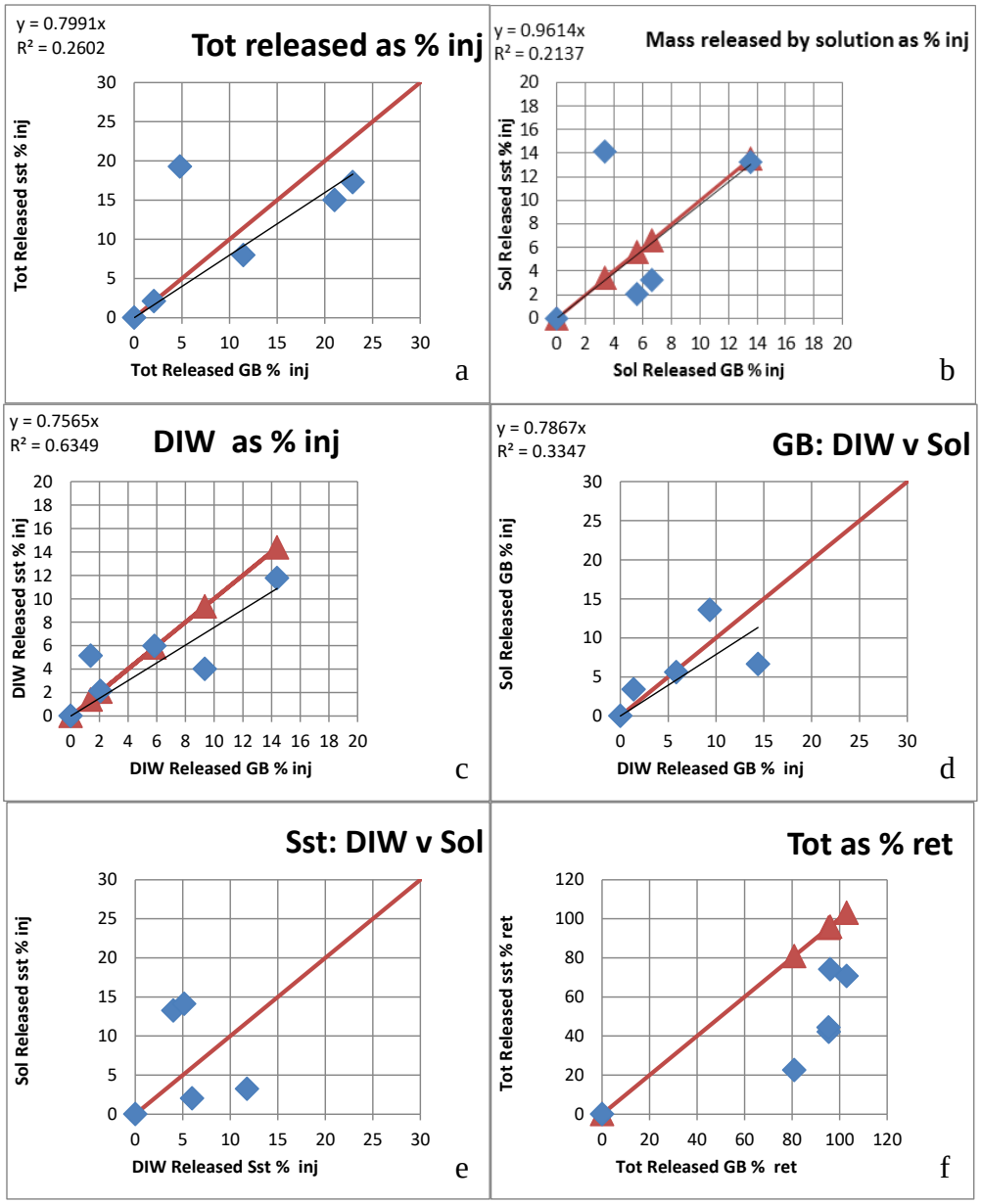

Figure 6.15: a) Total release of NMs as % injected mass b) Mass release by solution as percent injected (Yamago et al.) mass c) Release of DI waster as % injected mass d) DI water Vs solution in glass bead columns as % injected mass. e) DI water Vs solution in sandstone (sst) columns as % injected mass. f) Total released by glass bead Vs total released by sandstone columns as % retained (ret) mass.

Figure 6.15f shows a comparison of glass bead and sandstone overall retention, with values expressed as % retained. Glass bead columns (except bare anatase which gave 0%

release), released more than 80% as a result of two flushes, but the sandstone usually released much less.

6.4 Conclusions

The stabilized NPs with SRFA and sodium citrate were studied to understand their transport in porous media. It was evaluated that the overall mobility of the rutile ellipsoids is greater than the spherical anatase NPs. Bare anatase NPs gave no breakthrough and the NPs clogged both sandstone and glass bead columns; while bare rutile ellipsoids gave nearly 100% breakthrough curves. The breakthrough and release behaviour in the sandstone columns was similar to that in the glass beads columns, but overall retention of NPs was greater in the sandstone columns. In most of the cases for glass beads the C'/C_o values remained above 80% and more than 80% of retained NPs were released by subsequent flushing with NP-free stabilizing solution and deinoized water. Bare anatase showed difficulty in movement through both sandstone and glass bead media.

When compared glass bead with sandstone it might be concluded that surface properties are a little different as indicated by zeta potential values but these small differences can be significant in determining overall transport through glass bead and sandstone columns. From the results obtained it seems that pore architecture is not that important which suggest that straining is not that important and it was not seen either.

Both stabilizers i.e. have different effects on mobility of nanomaterials as SRFA gave steric while sodium citrate gave electrostatic stabilization. The stability of bare NPs depends on the zeta potential differences and even a minor difference in zeta potential can induce stabilization or destabilization within a NPs suspension system.

Rutile NPs gave greater breakthroughs as compared to anatase. It is concluded that surface properties are different as indicated by different zeta potential of anatase and rutile polymorphs. Morphology of both anatase and rutile is different but no much difference in total surface area, so bridging effect of stabilizer is less important in transport of both anatase and rutile. Overall reason for greater breakthroughs of rutile ellipsoids is still not well understood and needs further experimentation and modelling.

Tailing was seen in all runs and it is more physical in glass bead followed by sandstone columns while a little tailing is seen in fluorescein. This tailing behaviour shows probably non-equilibrium attachment processes which suggests that CFT not likely to be correct. As CFT behaviour was not completely studied nor reported in this thesis, this needs further investigation. Moreover, ripening of column was only seen with one high pH for rutile run in glass bead column.

The total release in case of glass bead columns was nearly 100% which was much greater than the total release from sandstone columns. Only 40% or less NPs were released from sandstone columns and rest of injected NPs were retained within the columns. Release of anatase with solution flush remained same in order of magnitude for both glass bead and sandstone columns while release of rutile with solution flush was different in sandstone and glass bead. SRFA gave greater release of NPs as compared to sodium citrate. For both sandstone and glass bead media SRFA proved a better flushing agent than sodium citrate. Deionized water released more mass than solution for sandstone except in case of SRFA flush.

From overall experimental results it is concluded that glass bead columns are analogous to sandstone columns, in style, though not in degree. So it is encouraging for laboratory experimentation. More release of NPs with SRFA flush is also important as it reflects the

ultimate fate and behaviour of TiO_2 NPs in natural environment which is rich in humic substances.

6.4.1.1 Implications

1. Even small drops in C'/Co below a value of 1 in columns of the sizes used here would result in severe attenuation of NP movement in porous media at field scale.
2. The SRFA used in this experiment is environmentally relevant because it is commonly found in soil and groundwater systems, and therefore the high C'/C_o observed during different experiments suggest that the fulvic acid may enhance mobility of nanoparticles in environment. As SRFA is a constituent of natural organic matter (Yamago et al.), it is predicted that the transport of NPs must be enhanced in natural environments with increase in overall stability of NPs. However, it would be very difficult to determine the role of indigenous SRFA molecules due to the complexity of natural systems and understanding about the interactions with the originally stabilizing solution(s) being also present.
3. The release mechanism is enhanced with SRFA flushing which means NOM in natural environments can enhance the movement of NPs through natural porous media, perhaps after any stabilizing solutions have been flushed out of the system. However previous research by different scientists (Gottschalk and Nowack, 2011, Petosa et al., 2010) emphasized greater release of NPs with DI than those observed with synthetic and natural groundwater.
4. In a nutshell, the stabilization process during manufacturing or post synthesis stabilization is an important parameter along with the chemistries and morphologies of the aquifer environment, for the transport of engineered nanomaterials. Also stabilization might be the case with release of NPs into the environment where

pollutants and/or natural humic substances may increase overall stability and hence mobility of NPs in groundwater.

5. From all of the experiments conducted during this research work, it is proved that glass bead columns are a reasonable though not perfect analogue and can be used for initial laboratory experiments to represent the complex porous media in real environment.

6.4.1.2 Recommendations

1. There is need of modelling of data for different aspects of NPs mobility in order to test out possible processes, and produce eventually a description that could be used for predication. A part of such modelling was conducted but not reported in this research work.
2. Studies on the flushing of columns after injection could help in understanding the total % release as an effect of the surfactants and/or surfactants. Columns should be flushed with DI water followed by surfactant solution or alternative washings with DI water and surfactants can help to understand the effect of flushing on total percent release. Moreover, SRFA flush can be followed by sodium citrate flush or vice versa and in some studies different surfactants might be mixed to tackle the complex natural systems.
3. It would be a great deal if concentrations could be checked against the distance travelled. That would enable the processes to be pinned down in better and precise way.
4. Effect of pH can be studied in detail and behaviour of different pH values on overall transport, release and retention might be studied in detail.
5. The aggregation kinetics of the NPs might be linked to the overall mobility in different media and effect of different ionic strengths especially different anion strength could be another landmark for this research work.

6. It is highly recommended to use the zetasizer for getting online particle size and zeta potential data during breakthrough. This will help in understanding the linkage of zeta potential with breakthrough and eventually with the overall interactions within the porous media columns.
7. Studies with different loadings of SRFA, humic acid, NOM and a mixture of all may help to understand the exact behaviour of NPs in complex environmental media.
8. The length of glass bead column and size of glass beads might be another parameter which can help in understanding the overall sticking coefficient of NPs and collector's surfaces.
9. In this research work, though effect of velocities was studied, there is still need of a proper investigation of effect of velocity on breakthrough with emphasis to horizontal and vertical layout of columns.

Chapter 7

Summary

The effects of different precursors, pHs, temperatures and alcohol concentrations on synthesis of TiO_2 nanoparticles have been studied. The data collected from all the synthesis experiments were varied and interesting. Some of the results obtained were as expected and were in line with the previous research work. However, few studies were interesting and not easy to interpret precisely and warranted further detailed research work. Overall this thesis gives a lot of beneficial results with breakthrough and advancement in experimentation and data collection. But there are many other aspects of relevant research work which need further experimentation. This chapter summarises the achievements, impact and future progression of the research work done to complete this PhD thesis.

The effect of pH was studied for nanopowder fabrication with titanium isopropoxide precursor at varied pH values from 1-11. A pH value of 4 proved to provide reasonably small anatase NPs. It was evaluated that NPs were in more dispersed and stable form at acidic pH values and morphology was changed from perfectly round NPs at acidic pH towards nanorods at highly basic pH values (9-10), when calcined at 700^{o}C. Titanium trichloride and tetrachloride were two other precursors which were used to fabricate NPs at room or near room temperature. Several alcohol and water concentrations were used to control the NPs morphology and phase. Various shapes of TiO_2 including spherical NPs with shape factor of 0.9 or more, nanocubes, nanorods and ellipsoids were synthesised with different mixture alcohols and water ratios. The research work in this section of thesis is very precise and gives a different understanding to the materials scientist for nanomaterials growth with respect to control on morphology, specifically effect of pH and alcohol water ratios help to understand the growth kinetics. This needs further

investigation in the area of pH control for alcohol water synthesis methodology as only two pH values, pH3.8 and pH4.0 were studied for rutile and anatase growth respectively. This can be further extended to study the effect of range of pH values on alcohol and water mixture synthesis methodology.

Couple of synthesized NPs were checked for their stability with 5 different surfactants; PEG, PVP, SDS, SRFA and sodium citrate. The stability of anatase spherical attenuated as sodium citrate, SRFA, PVP, PEG and SDS while this attenuation was SRFA, sodium citrate, PEG, SDS and PVP for rutile ellipsoids. SRFA and sodium citrate at 0.3% weight concentration proved to be the best stabilising agents without any change in the hydrodynamic diameter over a period of 2 weeks. These two types of NPs stabilized with two different types of surfactants i.e. SRFA and sodium citrate were further used for aggregation kinetics and transport studies through natural and artificial porous media. This aspect of research was important as it gave a better understanding of nanoparticles stability specifically with respect to their behaviour in natural environments. SRFA stabilization and its further use in aggregation kinetics studies and transport through different packed and loose media gave a breakthrough in new type of research work where coated and stabilized nanoparticles were studied for their behaviour in natural environments. There are many aspects of this research work which can easily be further studied. For example, the effect of nanoparticles size was not studied and a detailed study on nanoparticles size can be planned. Furthermore, type of nanoparticles, a mixture of nanoparticles, type and loading of surfactants, salinity of media, duration of exposure, use of other type of natural organic matter and interaction with a mixed or more complex media etc. could be other possible ways to extend this research work.

The aggregation kinetic studies showed that rutile ellipsoids behaved well against different mono and divalent cations. It has been observed in this study that SRFA stabilized

NMs proved to be slightly less stable in either mono or divalent cations as compared to sodium citrate stabilized NMs of same kind. In comparison CCC's observed for sodium citrate stabilized NMs were significantly higher than SRFA stabilized NMs, showing that sodium citrate is a better stabilizing agent than SRFA. TEM analysis of aggregated samples in slow and fast regime of aggregation showed different morphologies of aggregates which were analysed with fractal dimension analysis. Most of the aggregating salts gave a fractal dimension of more than 1.5 which means presence of perfect aggregates after addition of different salts. In this part of research work the idea of aggregation kinetics studies for stabilized nanoparticles was new and novel. Four different types of mono and divalent cations were used for their aggregation behaviour. Although this work gave a better understanding of the effect of cations on the aggregation kinetics of stabilized different shaped nanoparticles, this research work can easily be extended to further studies on behaviour of anions. Other possible options for further investigation in this area might be the type, size and other shapes of nanoparticles along with a better control on pH of the media. Studies on mixture of nanoparticles, mixture of salts and a blend of different surfactants can give a better understanding of the nanoparticles behaviour in natural environments.

The stabilized NPs with SRFA and sodium citrate were studied for porous media column transport by using glass bead as an artificial and sandstone as more complex natural environmental media. The mobility of the rutile ellipsoids is greater than spherical anatase. Bare anatase NPs gave no breakthrough and the NPs clogged both the sandstone and glass bead columns; while bare rutile ellipsoids gave nearly 100% breakthrough curves. There was no significant trend in the behaviour of transport for sandstones and glass beads except retention of NPs is more in sandstone columns than in glass bead columns. It was observed that glass beads gave almost double breakthroughs as compared to sandstone columns. TiO_2 aggregation

kinetics is important in their transport as mobility of stabilized NPs is higher than that of bare anatase NPs. In most of the cases for glass beads the C'/C_o values remained above 80% and after retention NPs release gave more than 80% of retained NPs. Only 40% or less NPs were released from sandstone columns and rest of injected NPs were retained within the columns. For both sandstone and glass bead media SRFA proved a better flushing agent than sodium citrate. Stabilized anatase showed no difference in mobility as compared to stabilized rutile but bare rutile NPs behaved entirely different from bare anatase. Bare anatase showed difficulty in movement through both sandstone and glass bead media. This was the most interesting study because there is a lack of understanding on the transport of stabilized and different shaped nanomaterials through porous media. The data obtained from this work showed a clear advancement in the techniques used for such complex data acquisition. There in an improvement in glass bead packing methodology and a new method of nanoparticles transport through porous media is introduced. The results obtained are also different from all those which are previously reported so far in the literature. This gave a breakthrough in the understanding of stabilized nanomaterials transport through porous media. Clearly this work gives a better understanding of nanomaterials behaviour in natural environments specifically their movement in soil and in the aquifer. Although this research work has a better impact on current research work on nanoparticles transport, this is only a small part of study and it can be extended to many big projects of related research work. For example, this research work was aimed at only one type of glass bead which can be further extended to different type of beads with different sizes, shapes and composition. Only few types of sand stone cores were used with more or less similar core size, but definitely different types of sandstone with different porosity, grain structure, pore size distribution and size can be used for further investigation. In current research work only two types of stabilising agents were used and pH was not studied in much detail, so this can be further investigated to more types of stabilizing agents, acidic and basic

pH ranges and a mixture of stabilizing agents for a better understanding with respect to complex environmental media. Transport in soils with different chemical and mechanical properties would be a very interesting area to do further investigation. Different types of nanoparticles, different shapes and morphologies, nano-hybrids or a mixture of nanoparticles could be other possible ways to extend this research work further. One last area which needs further investigation is to study the nanoparticles transport at different pressure levels to get understanding of nanoparticles transport in deep aquifer zone where pressure is relatively higher than atmospheric pressure.

In a nutshell, this research work gave a breakthrough in understanding the nanomaterials synthesis approaches, their stability and transport in natural environments. New methodologies are developed; to engineer nanoparticles with desired morphologies, to make TEM grids, to study aggregation kinetics and to study the nanoparticles transport through porous media. Alcohol water mixing methodology might be very beneficial to do further research to control other types of nanomaterials. The standard operating procedures for nanoparticles transport can give future perspective students an easy way to conduct experiments. Sandwich TEM grid making technique gives an even distribution of nanoparticles on the surface of grid which avoids the effect of improper drying of grid. This technique will solve many TEM related issues. As explained in individual paragraphs of this summary chapter, this research has a good impact on future research work and can give many new areas of investigation in nanomaterials synthesis, stability, aggregation kinetics and their transport in natural environmental media. The results obtained can help the regulatory authorities to make regulations for nanomaterials use in different domestic products and it gives a breakthrough for further investigation in this field.

Chapter 8

Literature Cited

ACHER, A., FISCHER, E., TURNHEIM, R. & MANOR, Y. 1997. Ecologically friendly wastewater disinfection techniques. *Water research,* 31**,** 1398-1404.

ADÁN, C., MARTÍNEZ-ARIAS, A., FERNÁNDEZ-GARCÍA, M. & BAHAMONDE, A. 2007. Photocatalytic degradation of ethidium bromide over titania in aqueous solutions. *Applied Catalysis B: Environmental,* 76**,** 395-402.

AGRAFIOTIS, C. & TSETSEKOU, A. 2000. The effect of powder characteristics on washcoat quality. Part I: Alumina washcoats. *Journal of the European Ceramic Society,* 20**,** 815-824.

AGRIOS, A. & PICHAT, P. 2005. State of the art and perspectives on materials and applications of photocatalysis over TiO_2. *Journal of Applied Electrochemistry,* 35**,** 655-663.

AITKEN, R. J., CREELY, K. S., TRAN, C. L., HEALTH, G. B., EXECUTIVE, S. & ., I. O. O. M. 2004. *Nanoparticles: An Occupational Hygiene Review*, HSE Books.

AITKEN, R. J., M. Q. CHAUDHRY, ET AL. 2006. Manufacture and use of nanomaterials:current status in the UK and global trends. *Occupational Medicine,* 56**,** 300-306.

AKHTAR, M. K., PRATSINIS, S. E. & MASTRANGELO, S. V. 1992. Dopants in Vapor-Phase Synthesis of Titania Powders. *Journal of the American Ceramic Society,* 75**,** 3408-3416.

AKHTAR, M. K., PRATSINIS, S. E. & MASTRANGELO, S. V. 1994. VAPOUR PHASE SYNTHESIS OF Al-DOPED TITANIA POWDERS. *Journal of materials research,* 9**,** 1241-1249.

ALAGARASI, A. 2011. Introduction to nanomaterials. *Book Chapter***,** 1-76.

ALEXANDRESCU, R., DUMITRACHE, F., MORJAN, I., SANDU, I., SAVOIU, M., VOICU, I., FLEACA, C. & PITICESCU, R. 2004. TiO_2 nanosized powders by $TiCl_4$ laser pyrolysis. *Nanotechnology,* 15**,** 537.

ALKILANY, A. M. & MURPHY, C. J. 2009. Gold Nanoparticles with a Polymerizable Surfactant Bilayer: Synthesis, Polymerization, and Stability Evaluation†. *Langmuir,* 25**,** 13874-13879.

ALVARO, M., CARBONELL, E., GARCIA, H., LAMAZA, C. & NARAYANA PILLAI, M. 2004. Ship-in-a-bottle synthesis of 2,4,6-triphenylthiapyrylium cations encapsulated in zeolites Y and beta: a novel robust photocatalyst. *Photochemical & Photobiological Sciences,* 3**,** 189-193.

AMIRBAHMAN, A. & OLSON, T. M. 1993. Transport of humic matter-coated hematite in packed beds. *Environmental Science & Technology,* 27**,** 2807-2813.

AMMANN, A. A. 2007. Inductively coupled plasma mass spectrometry (ICP MS): a versatile tool. *Journal of Mass Spectrometry,* 42**,** 419-427.

ANDERSON, B. J. 2015. *Manufactured nanoparticles: assessing the mobility of a future class of containment in groundwaters.* University of Birmingham.

ANI, J. K., SAVITHRI, S., SURENDER, G., LATHA, K. M., BADARINATH, K., LEE, B. U., YERMAKOV, M., GRINSHPUN, S. A., LUO, C.-H. & YUAN, C.-S. 2005. Characteristics of Titania Nanoparticles Synthesized Through Low Temperature Aerosol Process. *Aerosol and Air Quality Research,* 5.

ARMELAO, L., BARRECA, D., BOTTARO, G., GASPAROTTO, A., MACCATO, C., MARAGNO, C., TONDELLO, E., ŠTANGAR, U. L., BERGANT, M. & MAHNE, D. 2007. Photocatalytic and antibacterial activity of TiO_2 and Au/TiO_2 nanosystems. *Nanotechnology,* 18**,** 375709.

ARNALL, A. H. 2003. Future technologies, today's choices, nanotechnology, artificial intelligence and robotics a technical, political and institutional map of emerging technologies. *London, G.B. Greenpeace Environmental Trust***,** 69p.

AU, K.-K., PENISSON, A. C., YANG, S. & O'MELIA, C. R. 1999. Natural organic matter at oxide/water interfaces: complexation and conformation. *Geochimica et Cosmochimica Acta,* 63**,** 2903-2917.

BAALOUSHA, M. 2009. Aggregation and disaggregation of iron oxide nanoparticles: Influence of particle concentration, pH and natural organic matter. *Science of The Total Environment,* 407**,** 2093-2101.

BAALOUSHA, M., MANCIULEA, A., CUMBERLAND, S., KENDALL, K. & LEAD, J. R. 2008. Aggregation and surface properties of iron oxide nanoparticles: Influence of ph and natural organic matter. *Environmental Toxicology and Chemistry,* 27**,** 1875-1882.

BAALOUSHA, M., NUR, Y., RÖMER, I., TEJAMAYA, M. & LEAD, J. R. 2013. Effect of monovalent and divalent cations, anions and fulvic acid on aggregation of citrate-coated silver nanoparticles. *Science of The Total Environment,* 454–455**,** 119-131.

BAIER, G., BAKI, A., TOMCIN, S., MAILÄNDER, V., ALEXANDRINO, E., WURM, F. & LANDFESTER, K. 2014. Stabilization of Nanoparticles Synthesized by Miniemulsion Polymerization Using "Green" Amino-Acid Based Surfactants. *Macromolecular Symposia,* 337**,** 9-17.

BALIKDJIAN, J., DAVIDSON, A., LAUNAY, S., ECKERT, H. & CHE, M. 2000. Sintering and phase transformation of V-loaded anatase materials containing bulk and surface V species. *The Journal of Physical Chemistry B,* 104**,** 8931-8939.

BANFIELD, J. F., BISCHOFF, B. L. & ANDERSON, M. A. 1993. TiO_2 accessory minerals: coarsening, and transformation kinetics in pure and doped synthetic nanocrystalline materials. *Chemical Geology,* 110**,** 211-231.

BARNARD, A. S., ZAPOL, P. & CURTISS, L. A. 2004. Modeling the Morphology and Phase Stability of TiO_2 Nanocrystals in Water. *Journal of Chemical Theory and Computation,* 1**,** 107-116.

BEHNAJADY, M. A., ALAMDARI, M. E. & MODIRSHAHLA, N. 2013. Investigation of the effect of heat treatment process on characteristics and photocatalytic activity of TiO_2-uv100 nanoparticles. *Environment Protection Engineering,* 39.

BERGAMASCHI, E. 2009. Occupational exposure to nanomaterials: present knowledge and future development. *Nanotoxicology,* 3**,** 194-201.

BERNE, B. J. & PECORA, R. 2000. *Dynamic Light Scatterin,* New York., Dover Publications.

BESSEKHOUAD, Y., ROBERT, D. & WEBER, J. V. 2004. Bi_2S_3/TiO_2 and CdS/TiO_2 heterojunctions as an available configuration for photocatalytic degradation of organic pollutant. *Journal of Photochemistry and Photobiology A: Chemistry,* 163**,** 569-580.

BLOOMFIELD, J., GOODDY, D., BRIGHT, M. & WILLIAMS, P. 2001. Pore-throat size distributions in Permo-Triassic sandstones from the United Kingdom and some implications for contaminant hydrogeology. *Hydrogeology Journal,* 9**,** 219-230.

BLOUNT, M. C., KIM, D. H. & FALCONER, J. L. 2001. Transparent Thin-Film TiO_2 Photocatalysts with High Activity. *Environmental Science & Technology,* 35**,** 2988-2994.

BOJINOVA, A., KRALCHEVSKA, R., POULIOS, I. & DUSHKIN, C. 2007. Anatase/rutile TiO_2 composites: Influence of the mixing ratio on the photocatalytic degradation of Malachite Green and Orange II in slurry. *Materials Chemistry and Physics,* 106**,** 187-192.

BONCAGNI, N. T., OTAEGUI, J. M., WARNER, E., CURRAN, T., REN, J. & FIDALGO DE CORTALEZZI, M. M. 2009. Exchange of TiO_2 Nanoparticles between Streams and Streambeds. *Environmental Science & Technology,* 43**,** 7699-7705.

BOXALL, A. B., TIEDE, K. & CHAUDHRY, Q. 2007. Engineered nanomaterials in soils and water: how do they behave and could they pose a risk to human health? *Nanomedicine,* 2**,** 919-927.

BRINKER, C., WALLACE, S., RAMAN, N., SEHGAL, R., SAMUEL, J. & CONTAKES, S. 2002. Sol-Gel Processing of Amorphous Nanoporous Silicas: Thin Films and Bulk. *In:* PINNAVAIA, T. & THORPE, M. (eds.) *Access in Nanoporous Materials.* Springer US.

BRINKER, C. J. & DUNPHY, D. R. 2006. Morphological control of surfactant-templated metal oxide films. *Current Opinion in Colloid & Interface Science,* 11**,** 126-132.

BRINKER, C. J. A. S., G. W. 1990. Sol-Gel Science: The Physics and Chemistry of Sol-Gel Processing. *Academic Press, San Diego, CA.*

BROWN, D. M., WILSON, M. R., MACNEE, W., STONE, V. & DONALDSON, K. 2001. Size-Dependent Proinflammatory Effects of Ultrafine Polystyrene Particles: A Role for Surface Area and Oxidative Stress in the Enhanced Activity of Ultrafines. *Toxicology and Applied Pharmacology,* 175**,** 191-199.

BULLARD, J. W. & CIMA, M. J. 2006. Orientation Dependence of the Isoelectric Point of TiO_2 (Rutile) Surfaces. *Langmuir,* 22**,** 10264-10271.

BURNSIDE, S. D., SHKLOVER, V., BARBÉ, C., COMTE, P., ARENDSE, F., BROOKS, K. & GRÄTZEL, M. 1998. Self-Organization of TiO_2 Nanoparticles in Thin Films. *Chemistry of Materials,* 10**,** 2419-2425.

BUZEA, C., PACHECO, I. & ROBBIE, K. 2007a. Nanomaterials and nanoparticles: Sources and toxicity. *Biointerphases,* 2**,** MR17-MR71.

BUZEA, C., PACHECO, I. I. & ROBBIE, K. 2007b. Nanomaterials and nanoparticles: sources and toxicity. *Biointerphases,* 2**,** MR17-MR71.

BYUN, K.-T., SEO, K. W., SHIM, I.-W. & KWAK, H.-Y. 2008. Syntheses of ZnO and ZnO-coated TiO_2 nanoparticles in various alcohol solutions at multibubble sonoluminescence (MBSL) condition. *Chemical Engineering Journal,* 135**,** 168-173.

CAO, T., LI, Y., WANG, C., SHAO, C. & LIU, Y. 2011. One-step nonaqueous synthesis of pure phase TiO_2 nanocrystals from $TiCl_4$ in butanol and their photocatalytic properties. *J. Nanomaterials,* 2011**,** 1-6.

CAO, Y., YANG, W., CHEN, Y., DU, H. & YUE, P. 2004. Effect of chemisorbed surface species on the photocatalytic activity of TiO_2 nanoparticulate films. *Applied surface science,* 236**,** 223-230.

CAPPELLETTI, M., MUGGLETON, N. & WALSH, V. 2009. Quantity without numbers and numbers without quantity in the parietal cortex. *NeuroImage,* 46**,** 522-529.

CARLSON, C. 2006. In vitro toxicity assessment of silver nanoparticles in rat alveolar macrophages *Wright State University*.

CAROLE, S. & ET AL. 2009. Dispersion and stability of TiO_2 nanoparticles synthesized by laser pyrolysis in aqueous suspensions. *Journal of Physics: Conference Series,* 170**,** 012013.

CASTRO LÓPEZ, C. A., REYES GÓMEZ, S. E., CENTENO HURTADO, A. & GIRALDO DUARTE, S. A. 2011. Effect of the synthesis variables of TiO_2 on the photocatalytic activity towards the degradation of water pollutants. *Revista Facultad de Ingeniería Universidad de Antioquia***,** 49-56.

CHAE, S. Y., PARK, M. K., LEE, S. K., KIM, T. Y., KIM, S. K. & LEE, W. I. 2003. Preparation of size-controlled TiO2 nanoparticles and derivation of optically transparent photocatalytic films. *Chemistry of materials,* 15**,** 3326-3331.

CHEN, B., ZHANG, H., DUNPHY-GUZMAN, K. A., SPAGNOLI, D., KRUGER, M. B., MUTHU, D. V. S., KUNZ, M., FAKRA, S., HU, J. Z., GUO, Q. Z. & BANFIELD, J. F. 2009. Size-dependent elasticity of nanocrystalline titania. *Physical Review B,* 79**,** 125406.

CHEN, G., LIU, X. & SU, C. 2011a. Transport and retention of TiO_2 rutile nanoparticles in saturated porous media under low-ionic-strength conditions: Measurements and mechanisms. *Langmuir,* 27**,** 5393-5402.

CHEN, G., LIU, X. & SU, C. 2012. Distinct effects of humic acid on transport and retention of TiO_2 rutile nanoparticles in saturated sand columns. *Environmental science & technology,* 46**,** 7142-7150.

CHEN, G., LUO, G., YANG, X., SUN, Y. & WANG, J. 2004. Anatase-TiO_2 nano-particle preparation with a micro-mixing technique and its photocatalytic performance. *Materials Science and Engineering A,* 380**,** 320-325.

CHEN, J., XIU, Z., LOWRY, G. V. & ALVAREZ, P. J. J. 2011b. Effect of natural organic matter on toxicity and reactivity of nano-scale zero-valent iron. *Water Research,* 45**,** 1995-2001.

CHEN, K. L. & ELIMELECH, M. 2007. Influence of humic acid on the aggregation kinetics of fullerene (C_{60}) nanoparticles in monovalent and divalent electrolyte solutions. *Journal of Colloid and Interface Science,* 309**,** 126-134.

CHEN, K. L. & ELIMELECH, M. 2008. Interaction of Fullerene (C_{60}) Nanoparticles with Humic Acid and Alginate Coated Silica Surfaces: Measurements, Mechanisms, and Environmental Implications. *Environmental Science & Technology,* 42**,** 7607-7614.

CHEN, K. L., MYLON, S. E. & ELIMELECH, M. 2006. Aggregation Kinetics of Alginate-Coated Hematite Nanoparticles in Monovalent and Divalent Electrolytes. *Environmental Science & Technology,* 40**,** 1516-1523.

CHEN, Y.-F., LEE, C.-Y., YENG, M.-Y. & CHIU, H.-T. 2003. The effect of calcination temperature on the crystallinity of TiO_2 nanopowders. *Journal of Crystal Growth,* 247**,** 363-370.

CHENG, Q., LI, C., PAVLINEK, V., SAHA, P. & WANG, H. 2006. Surface-modified antibacterial TiO_2/Ag^+ nanoparticles: Preparation and properties. *Applied Surface Science,* 252**,** 4154-4160.

CHIANG, K., LIM, T. M., TSEN, L. & LEE, C. C. 2004. Photocatalytic degradation and mineralization of bisphenol A by TiO2 and platinized TiO_2. *Applied Catalysis A: General,* 261**,** 225-237.

CHIBOWSKI, S., PASZKIEWICZ, M. & KRUPA, M. 2000. Investigation of the influence of the polyvinyl alcohol adsorption on the electrical properties of Al_2O_3–solution interface, thickness of the adsorption layers of PVA. *Powder Technology,* 107**,** 251-255.

CHO, C. H., KIM, D. K. & KIM, D. H. 2003. Photocatalytic activity of monodispersed spherical TiO_2 particles with different crystallization routes. *Journal of the American Ceramic Society,* 86**,** 1138-1145.

CHOWDHURY, I., CWIERTNY, D. M. & WALKER, S. L. 2012. Combined factors influencing the aggregation and deposition of nano-TiO_2 in the presence of humic acid and bacteria. *Environmental science & technology,* 46**,** 6968-6976.

CHOWDHURY, I., HONG, Y., HONDA, R. J. & WALKER, S. L. 2011. Mechanisms of TiO_2 nanoparticle transport in porous media: Role of solution chemistry, nanoparticle concentration, and flowrate. *Journal of Colloid and Interface Science,* 360**,** 548-555.

CHRISTENSON, H. K. 1984. DLVO (Derjaguin-Landau-Verwey-Overbeek) theory and solvation forces between mica surfaces in polar and hydrogen-bonding liquids. *Journal of the Chemical Society, Faraday Transactions 1: Physical Chemistry in Condensed Phases,* 80**,** 1933-1946.

CHU, W., CHOY, W. & SO, T. 2007. The effect of solution pH and peroxide in the TiO_2-induced photocatalysis of chlorinated aniline. *Journal of hazardous materials,* 141**,** 86-91.

CHUNG, C. J., LIN, H. I. & HE, J. L. 2007. Antimicrobial efficacy of photocatalytic TiO_2 coatings prepared by arc ion plating. *Surface and Coatings Technology,* 202**,** 1302-1307.

COLVIN, V. L. 2003. The potential environmental impact of engineered nanomaterials. *Nature biotechnology,* 21**,** 1166-1170.

CROMER, D. T. & HERRINGTON, K. 1955. The Structures of Anatase and Rutile. *Journal of the American Chemical Society,* 77**,** 4708-4709.

CRYSTAL, A. 2013a. Crystal Structure Gallery. *Downloaded from http://staff.aist.go.jp/nomura-k/common/STRUCIMAGES/Anatase.gif on 28/10/2013*.

CRYSTAL, B. 2013b. Image downloaded from http://staff.aist.go.jp/nomura-k/common/STRUCIMAGES/TiO2-Brookite.gif on 28/10/2013.

CRYSTAL, R. 2013c. Image downlaoded from http://staff.aist.go.jp/nomura-k/common/STRUCIMAGES/Rutile.gif on 28/10/2013.

CULLITY, B. D. & STOCK, S. R. 2001. *Elements of X-ray Diffraction*, Prentice hall Upper Saddle River, NJ.

D. H. NAPPER, D., A. S. 1986. Polymeric stabilization of colloidal dispersions. *British Polymer Journal,* 18**,** 278-278.

DAI, S., WU, Y., SAKAI, T., DU, Z., SAKAI, H. & ABE, M. 2010. Preparation of Highly Crystalline TiO_2 Nanostructures by Acid-assisted Hydrothermal Treatment of Hexagonal-structured Nanocrystalline Titania/Cetyltrimethyammonium Bromide Nanoskeleton. *Nanoscale Research Letters,* 5**,** 1829-1835.

DARLINGTON, T. K., NEIGH, A. M., SPENCER, M. T., GUYEN, O. T. N. & OLDENBURG, S. J. 2009. Nanoparticle characteristics affecting environmental fate and transport through soil. *Environmental Toxicology and Chemistry,* 28**,** 1191-1199.

DEMYDOV, D. V. 2006. *Nanosized alkaline earth metal titanates: effects of size on photocatalytic and dielectric properties*, ProQuest.

DOMÈNECH GARCIA, B., BASTOS ARRIETA, J., ALONSO GONZÁLEZ, A., MACANÀS DE BENITO, J., MUÑOZ TAPIA, M. & MURAVIEV, D. N. 2012. Bifunctional polymer-metal nanocomposite ion exchange materials.

DOMINGOS, R. F., TUFENKJI, N. & WILKINSON, K. J. 2009. Aggregation of Titanium Dioxide Nanoparticles: Role of a Fulvic Acid. *Environmental Science & Technology,* 43**,** 1282-1286.

DOONG, R.-A., CHANG, S.-M., HUNG, Y.-C. & KAO, I.-L. 2007. Preparation of highly ordered titanium dioxide porous films: Characterization and photocatalytic activity. *Separation and Purification Technology,* 58**,** 192-199.

DUNNIVANT, F. M., SCHWARZENBACH, R. P. & MACALADY, D. L. 1992. Reduction of substituted nitrobenzenes in aqueous solutions containing natural organic matter. *Environmental Science & Technology,* 26**,** 2133-2141.

DUNPHY GUZMAN, K. A., FINNEGAN, M. P. & BANFIELD, J. F. 2006. Influence of Surface Potential on Aggregation and Transport of Titania Nanoparticles. *Environmental Science & Technology,* 40**,** 7688-7693.

DUVAL, J. F. L., LEERMAKERS, F. A. M. & VAN LEEUWEN, H. P. 2004. Electrostatic Interactions between Double Layers: Influence of Surface Roughness, Regulation, and Chemical Heterogeneities. *Langmuir,* 20**,** 5052-5065.

DYSART, B. C. & HINES, W. W. 1969. *Control of water quality in a complex natural system*.

ECKELMAN, M. J., MAUTER, M. S., ISAACS, J. A. & ELIMELECH, M. 2012. New Perspectives on Nanomaterial Aquatic Ecotoxicity: Production Impacts Exceed Direct Exposure Impacts for Carbon Nanotoubes. *Environmental Science & Technology,* 46**,** 2902-2910.

EDGINGTON, A. J., ROBERTS, A. P., TAYLOR, L. M., ALLOY, M. M., REPPERT, J., RAO, A. M., MAO, J. & KLAINE, S. J. 2010. The influence of natural organic matter on the toxicity of multiwalled carbon nanotubes. *Environmental Toxicology and Chemistry,* 29**,** 2511-2518.

EDWARD, J. T. 1970. Molecular volumes and the Stokes-Einstein equation. *Journal of Chemical Education,* 47**,** 261.

EIDEN-ASSMANN, S., WIDONIAK, J. & MARET, G. 2003. Synthesis and Characterization of Porous and Nonporous Monodisperse Colloidal TiO_2 Particles. *Chemistry of Materials,* 16**,** 6-11.

ELIMELECH, M., CHEN, J. Y. & KUZNAR, Z. A. 2003. Particle Deposition onto Solid Surfaces with Micropatterned Charge Heterogeneity: The “Hydrodynamic Bump” Effect. *Langmuir,* 19**,** 6594-6597.

ELIMELECH, M., NAGAI, M., KO, C.-H. & RYAN, J. N. 2000. Relative Insignificance of Mineral Grain Zeta Potential to Colloid Transport in Geochemically Heterogeneous Porous Media. *Environmental Science & Technology,* 34**,** 2143-2148.

ELIMELECH, M. & O'MELIA, C. R. 1990. Effect of particle size on collision efficiency in the deposition of Brownian particles with electrostatic energy barriers. *Langmuir,* 6**,** 1153-1163.

ELIMELECH, M. G., J.; JIA, X.; WILLIAMS. R.A 1995. Particle Deposition and Aggregation: Measurement, Modelling and Simulation. *Boston: Butterworth-Heinemann*.

ENUSTUN, B. V. & TURKEVICH, J. 1963. Coagulation of Colloidal Gold. *Journal of the American Chemical Society,* 85**,** 3317-3328.

EU 2011. Commission recommendation of 18 October 2011 on the definition of nanomaterial *Official Journal L,* 275**,** 38-40.

FANG, C., BHATTARAI, N., SUN, C. & ZHANG, M. 2009a. Functionalized Nanoparticles with Long-Term Stability in Biological Media. *Small,* 5**,** 1637-1641.

FANG, J., SHAN, X.-Q., WEN, B., LIN, J.-M. & OWENS, G. 2009b. Stability of titania nanoparticles in soil suspensions and transport in saturated homogeneous soil columns. *Environmental Pollution,* 157**,** 1101-1109.

FARN, R. J. 2008. *Chemistry and technology of surfactants*, John Wiley & Sons.

FARRÉ, M., GAJDA-SCHRANTZ, K., KANTIANI, L. & BARCELÓ, D. 2009. Ecotoxicity and analysis of nanomaterials in the aquatic environment. *Analytical and Bioanalytical Chemistry,* 393**,** 81-95.

FATISSON, J., QUEVEDO, I. R., WILKINSON, K. J. & TUFENKJI, N. 2012. Physicochemical characterization of engineered nanoparticles under physiological conditions: Effect of culture media components and particle surface coating. *Colloids and Surfaces B: Biointerfaces,* 91**,** 198-204.

FEDERICI, G., SHAW, B. J. & HANDY, R. D. 2007. Toxicity of titanium dioxide nanoparticles to rainbow trout (Oncorhynchus mykiss): Gill injury, oxidative stress, and other physiological effects. *Aquatic Toxicology,* 84**,** 415-430.

FEIGENBAUM, D., NSAMIRISI, A., SINCLAIR-DESGAGNE, B. 2004. Les Nanotechnologies: leurs bénéfices et leurs risques potentiels. *Montréal, CIRANO***,** 45p.

FENDLER, J. H. 2008. *Nanoparticles and nanostructured films*, Wiley. com.

FENG, Q., HIRASAWA, M. & YANAGISAWA, K. 2001. Synthesis of crystal-axis-oriented $BaTiO_3$ and anatase platelike particles by a hydrothermal soft chemical process. *Chemistry of materials,* 13**,** 290-296.

FIGGEMEIER, E., KYLBERG, W., CONSTABLE, E., SCARISOREANU, M., ALEXANDRESCU, R., MORJAN, I., SOARE, I., BIRJEGA, R., POPOVICI, E., FLEACA, C., GAVRILA-FLORESCU, L. & PRODAN, G. 2007. Titanium dioxide nanoparticles prepared by laser pyrolysis: Synthesis and photocatalytic properties. *Applied Surface Science,* 254**,** 1037-1041.

FINDLAY, A. D., THOMPSON, D. W. & TIPPING, E. 1996. The aggregation of silica and haematite particles dispersed in natural water samples. *Colloids and Surfaces A: Physicochemical and Engineering Aspects,* 118**,** 97-105.

FOSTIER, A. H., PEREIRA, M. D. S. S., RATH, S. & GUIMARÃES, J. R. 2008. Arsenic removal from water employing heterogeneous photocatalysis with TiO_2 immobilized in PET bottles. *Chemosphere,* 72**,** 319-324.

FRANCHI, A. & O'MELIA, C. R. 2003. Effects of Natural Organic Matter and Solution Chemistry on the Deposition and Reentrainment of Colloids in Porous Media. *Environmental Science & Technology,* 37**,** 1122-1129.

FRENCH, R. A., JACOBSON, A. R., KIM, B., ISLEY, S. L., PENN, R. L. & BAVEYE, P. C. 2009. Influence of Ionic Strength, pH, and Cation Valence on Aggregation Kinetics of Titanium Dioxide Nanoparticles. *Environmental Science & Technology,* 43**,** 1354-1359.

FUJISHIMA, A. 1972. Electrochemical photolysis of water at a semiconductor electrode. *nature,* 238**,** 37-38.

FUKUSHI, K. & SATO, T. 2005. Using a Surface Complexation Model To Predict the Nature and Stability of Nanoparticles. *Environmental Science & Technology,* 39**,** 1250-1256.

GAMER, A. O., LEIBOLD, E. & VAN RAVENZWAAY, B. 2006. The in vitro absorption of microfine zinc oxide and titanium dioxide through porcine skin. *Toxicology in Vitro,* 20**,** 301-307.

GARVIE, R. 1978. Stabilization of the tetragonal structure in zirconia microcrystals. *The Journal of Physical Chemistry,* 82**,** 218-224.

GARZELLA, C., COMINI, E., TEMPESTI, E., FRIGERI, C. & SBERVEGLIERI, G. 2000. TiO_2 thin films by a novel sol–gel processing for gas sensor applications. *Sensors and Actuators B: Chemical,* 68**,** 189-196.

GERVAIS, C., SMITH, M. E., POTTIER, A., JOLIVET, J. P. & BABONNEAU, F. 2001. Solid-State 47,49Ti NMR Determination of the Phase Distribution of Titania Nanoparticles. *Chemistry of Materials,* 13**,** 462-467.

GODINEZ, I. G. & DARNAULT, C. J. G. 2011. Aggregation and transport of nano-TiO_2 in saturated porous media: Effects of pH, surfactants and flow velocity. *Water Research,* 45**,** 839-851.

GONZÁLEZ-MOZUELOS, P. & DE LA CRUZ, M. O. 2009. Asymmetric charge renormalization for nanoparticles in aqueous media. *Physical Review E,* 79**,** 031901.

GOTTSCHALK, F. & NOWACK, B. 2011. The release of engineered nanomaterials to the environment. *Journal of Environmental Monitoring,* 13**,** 1145-1155.

GOTTSCHALK, F., SONDERER, T., SCHOLZ, R. W. & NOWACK, B. 2009. Modeled environmental concentrations of engineered nanomaterials (TiO_2, ZnO, Ag, CNT, fullerenes) for different regions. *Environmental Science & Technology,* 43**,** 9216-9222.

GRASS, R. N., TSANTILIS, S. & PRATSINIS, S. E. 2006. Design of high-temperature, gas-phase synthesis of hard or soft TiO_2 agglomerates. *AIChE Journal,* 52**,** 1318-1325.

GREENWOOD, R. 2003. Review of the measurement of zeta potentials in concentrated aqueous suspensions using electroacoustics. *Advances in Colloid and Interface Science,* 106**,** 55-81.

GRESWELL, R. B., RAHMAN, S. H., CUTHBERT, M. O. & TELLAM, J. H. 2010. An inexpensive flow-through laser nephelometer for the detection of natural colloids and manufactured nanoparticles. *Journal of Hydrology,* 388**,** 112-120.

GRZMIL, B., KIC, B. & RABE, M. 2004. Inhibition of the anatase–rutile phase transformation with addition of K_2O, P_2O_5, and Li_2O. *Chem. Pap,* 58**,** 410-414.

GU, B., SCHMITT, J., CHEN, Z., LIANG, L. & MCCARTHY, J. F. 1994. Adsorption and desorption of natural organic matter on iron oxide: mechanisms and models. *Environmental Science & Technology,* 28**,** 38-46.

GUILLARD, C., BEAUGIRAUD, B., DUTRIEZ, C., HERRMANN, J.-M., JAFFREZIC, H., JAFFREZIC-RENAULT, N. & LACROIX, M. 2002. Physicochemical properties and photocatalytic activities of TiO_2 films prepared by sol–gel methods. *Applied Catalysis B: Environmental,* 39**,** 331-342.

HAHN, M. W. & O'MELIA, C. R. 2003. Deposition and Reentrainment of Brownian Particles in Porous Media under Unfavorable Chemical Conditions: Some Concepts and Applications. *Environmental Science & Technology,* 38**,** 210-220.

HAIBER, S., HERZOG, H., BURBA, P., GOSCINIAK, B. & LAMBERT, J. 2001. Two-Dimensional NMR Studies of Size Fractionated Suwannee River Fulvic and Humic Acid Reference. *Environmental Science & Technology,* 35**,** 4289-4294.

HAINES, J. & LÉGER, J. M. 1993. X-ray diffraction study of TiO_2 up to 49 GPa. *Physica B: Condensed Matter,* 192**,** 233-237.

HALL-STOODLEY, L., COSTERTON, J. W. & STOODLEY, P. 2004. Bacterial biofilms: from the Natural environment to infectious diseases. *Nat Rev Micro,* 2**,** 95-108.

HANDY, R., OWEN, R. & VALSAMI-JONES, E. 2008a. The ecotoxicology of nanoparticles and nanomaterials: current status, knowledge gaps, challenges, and future needs. *Ecotoxicology,* 17**,** 315-325.

HANDY, R. D., OWEN, R. & VALSAMI-JONES, E. 2008b. The ecotoxicology of nanoparticles and nanomaterials: current status, knowledge gaps, challenges, and future needs. *Ecotoxicology,* 17**,** 315-325.

HEARNE, G. R., ZHAO, J., DAWE, A. M., PISCHEDDA, V., MAAZA, M., NIEUWOUDT, M. K., KIBASOMBA, P., NEMRAOUI, O., COMINS, J. D. & WITCOMB, M. J. 2004. Effect of grain size on structural transitions in anatase TiO_2: A Raman spectroscopy study at high pressure. *Physical Review B,* 70**,** 134102.

HEHLEN, M. P., SHEIK-BAHAE, M. & EPSTEIN, R. I. 2014. Chapter 265 - Solid-State Optical Refrigeration. *In:* JEAN-CLAUDE, G. B. & VITALIJ, K. P. (eds.) *Handbook on the Physics and Chemistry of Rare Earths.* Elsevier.

HEURTAULT, B., SAULNIER, P., PECH, B., PROUST, J.-E. & BENOIT, J.-P. 2003. Physico-chemical stability of colloidal lipid particles. *Biomaterials,* 24**,** 4283-4300.

HIEMENZ, P. C. & RAJAGOPALAN, R. 1997. *Principles of Colloid and Surface Chemistry, revised and expanded*, CRC Press.

HIRNER, A. 2006. Speciation of alkylated metals and metalloids in the environment. *Analytical and Bioanalytical Chemistry,* 385**,** 555-567.

HOGG, R., HEALY, T. W. & FUERSTENAU, D. W. 1966. Mutual coagulation of colloidal dispersions. *Transactions of the Faraday Society,* 62**,** 1638-1651.

HORIE, M., FUJITA, K., KATO, H., ENDOH, S., NISHIO, K., KOMABA, L. K., NAKAMURA, A., MIYAUCHI, A., KINUGASA, S., HAGIHARA, Y., NIKI, E., YOSHIDA, Y. & IWAHASHI, H. 2012. Association of the physical and chemical properties and the cytotoxicity of metal oxide nanoparticles: metal ion release, adsorption ability and specific surface area. *Metallomics,* 4**,** 350-360.

HOTZE, E. M., PHENRAT, T. & LOWRY, G. V. 2010. Nanoparticle Aggregation: Challenges to Understanding Transport and Reactivity in the Environment All rights reserved. No part of this periodical may be reproduced or transmitted in any form or by any means, electronic or mechanical, including photocopying, recording, or any information storage and retrieval system, without permission in writing from the publisher. *J. Environ. Qual.,* 39**,** 1909-1924.

HOUK, R. S., FASSEL, V. A., FLESCH, G. D., SVEC, H. J., GRAY, A. L. & TAYLOR, C. E. 1980. Inductively coupled argon plasma as an ion source for mass spectrometric determination of trace elements. *Analytical Chemistry,* 52**,** 2283-2289.

HU, Y., TSAI, H. L. & HUANG, C. L. 2003. Phase transformation of precipitated TiO_2 nanoparticles. *Materials Science and Engineering: A,* 344**,** 209-214.

HUBER, U., STOECKLI, F. & HOURIET, J.-P. 1978. A generalization of the Dubinin-Radushkevich equation for the filling of heterogeneous micropore systems in strongly activated carbons. *Journal of Colloid and Interface Science,* 67**,** 195-203.

HUNTER, R. J. 1981. Chapter 8 - Influence of More Complex Adsorbates on Zeta Potential. *In:* HUNTER, R. J. (ed.) *Zeta Potential in Colloid Science.* Academic Press.

HUYNH, K. A. & CHEN, K. L. 2011. Aggregation Kinetics of Citrate and Polyvinylpyrrolidone Coated Silver Nanoparticles in Monovalent and Divalent Electrolyte Solutions. *Environmental Science & Technology,* 45**,** 5564-5571.

ISLEY, S. L. & PENN, R. L. 2006. Relative brookite and anatase content in sol-gel-synthesized titanium dioxide nanoparticles. *The Journal of Physical Chemistry B,* 110**,** 15134-15139.

ISMAGILOV, Z. R., SHIKINA, N. V., BESSUDNOVA, E. V., KORNEEV, D. V., ISHCHENKO, A. V., CHESALOV, Y. A., VLADIMIROVA, A. & RYABCHIKOVA, E. I. 2012. The effect of chemical treatment conditions of titanium dioxide sols on their dispersion and cytotoxic properties. *CHEMICAL ENGINEERING,* 27.

IVANOVA, T., HARIZANOVA, A., KOUTZAROVA, T. & VERTRUYEN, B. 2013. Optical and structural characterization of TiO_2 films doped with silver nanoparticles obtained by sol–gel method. *Optical Materials,* 36**,** 207-213.

IWASAKI, T., SLADE, J. & STANLEY, W. E. 1937. Some notes on sand filtration [with discussion]. *Journal (American Water Works Association),* 29**,** 1591-1602.

JIANG, J. K., OBERDORSTER, G. & BISWAS, P. 2009. Characterization of size, surface charge, and agglomeration state of nanoparticle dispersions for toxicological studies. *Journal of Nanoparticle Research,* 11**,** 77-89.

JIANG, X., HERRICKS, T. & XIA, Y. 2003. Monodispersed spherical colloids of titania: synthesis, characterization, and crystallization. *Advanced Materials,* 15**,** 1205-1209.

JIN, C., TANG, Y., YANG, F., LI, X., XU, S., FAN, X., HUANG, Y. & YANG, Y. 2011. Cellular Toxicity of TiO_2 Nanoparticles in Anatase and Rutile Crystal Phase. *Biological Trace Element Research,* 141**,** 3-15.

JÚNIOR, J. A. A. & BALDO, J. B. 2014. The Behavior of Zeta Potential of Silica Suspensions. *New Journal of Glass and Ceramics,* 4**,** 29.

KAEGI, R., ULRICH, A., SINNET, B., VONBANK, R., WICHSER, A., ZULEEG, S., SIMMLER, H., BRUNNER, S., VONMONT, H. & BURKHARDT, M. 2008. Synthetic TiO_2 nanoparticle emission from exterior facades into the aquatic environment. *Environmental Pollution,* 156**,** 233-239.

KALSIN, A. M., FIALKOWSKI, M., PASZEWSKI, M., SMOUKOV, S. K., BISHOP, K. J. M. & GRZYBOWSKI, B. A. 2006. Electrostatic Self-Assembly of Binary Nanoparticle Crystals with a Diamond-Like Lattice. *Science,* 312**,** 420-424.

KANEL, S. & CHOI, H. 2007. Transport characteristics of surface-modified nanoscale zero-valent iron in porous media. *Water Science & Technology,* 55**,** 157-162.

KATAOKA, S., GURAU, M. C., ALBERTORIO, F., HOLDEN, M. A., LIM, S.-M., YANG, R. D. & CREMER, P. S. 2004. Investigation of Water Structure at the TiO_2/Aqueous Interface. *Langmuir,* 20**,** 1662-1666.

KE, D., LIU, H., PENG, T., LIU, X. & DAI, K. 2008. Preparation and photocatalytic activity of WO_3/TiO_2 nanocomposite particles. *Materials Letters,* 62**,** 447-450.

KELLER, A. A., WANG, H., ZHOU, D., LENIHAN, H. S., CHERR, G., CARDINALE, B. J., MILLER, R. & JI, Z. 2010. Stability and Aggregation of Metal Oxide Nanoparticles in Natural Aqueous Matrices. *Environmental Science & Technology,* 44**,** 1962-1967.

KERNER, D. 1993. Chemical processing of advanced materials. By L. L. Hench, J. K. West, Wiley, Chichester 1992, 1048 pp., hardback, £ 75, ISBN 0-471-54201-6. *Advanced Materials,* 5**,** 682-682.

KIM, C. S., NAKASO, K., XIA, B., OKUYAMA, K. & SHIMADA, M. 2005a. A new observation on the phase transformation of TiO_2 nanoparticles produced by a CVD method. *Aerosol science and technology,* 39**,** 104-112.

KIM, E. K. & WALKER, H. W. 2001. Effect of cationic polymer additives on the adsorption of humic acid onto iron oxide particles. *Colloids and Surfaces A: Physicochemical and Engineering Aspects,* 194**,** 123-131.

KIM, J.-H., FUJITA, S. & SHIRATORI, S. 2006. Fabrication and characterization of TiO_2 thin film prepared by a layer-by-layer self-assembly method. *Thin solid films,* 499**,** 83-89.

KIM, J., SHAN, W., DAVIES, S. H. R., BAUMANN, M. J., MASTEN, S. J. & TARABARA, V. V. 2009. Interactions of Aqueous NOM with Nanoscale TiO_2: Implications for Ceramic Membrane Filtration-Ozonation Hybrid Process. *Environmental Science & Technology,* 43**,** 5488-5494.

KIM, S. J., LEE, N. H., OH, H. J., YOON, C. R., QAMAR, M., CZOSKA, A., PARK, K. & LEE, K. 2007. Preparation of titanium oxide nanotube by hydrothermal process. *Solid State Phenomena,* 124**,** 1165-1168.

KIM, T., LEE, C.-H., JOO, S.-W. & LEE, K. 2008. Kinetics of gold nanoparticle aggregation: Experiments and modeling. *Journal of Colloid and Interface Science,* 318**,** 238-243.

KIM, T. K., LEE, M. N., LEE, S. H., PARK, Y. C., JUNG, C. K. & BOO, J. H. 2005b. Development of surface coating technology of TiO_2 powder and improvement of photocatalytic activity by surface modification. *Thin Solid Films,* 475**,** 171-177.

KLAINE, S. J., ALVAREZ, P. J., BATLEY, G. E., FERNANDES, T. F., HANDY, R. D., LYON, D. Y., MAHENDRA, S., MCLAUGHLIN, M. J. & LEAD, J. R. 2008a. Nanomaterials in the environment: behavior, fate, bioavailability, and effects. *Environmental Toxicology and Chemistry,* 27**,** 1825-1851.

KLAINE, S. J., ALVAREZ, P. J. J., BATLEY, G. E., FERNANDES, T. F., HANDY, R. D., LYON, D. Y., MAHENDRA, S., MCLAUGHLIN, M. J. & LEAD, J. R. 2008b. Nanomaterials in the environment: Behavior, fate, bioavailability, and effects. *Environmental Toxicology and Chemistry,* 27**,** 1825-1851.

KOBAYASHI, M., JUILLERAT, F., GALLETTO, P., BOWEN, P. & BORKOVEC, M. 2005. Aggregation and Charging of Colloidal Silica Particles: Effect of Particle Size. *Langmuir,* 21**,** 5761-5769.

KONRADI, R. & RÜHE, J. 2005. Interaction of Poly(methacrylic acid) Brushes with Metal Ions: Swelling Properties. *Macromolecules,* 38**,** 4345-4354.

KOZLOVA, E. A. & VORONTSOV, A. V. 2007. Influence of mesoporous and platinum-modified titanium dioxide preparation methods on photocatalytic activity in liquid and gas phase. *Applied Catalysis B: Environmental,* 77**,** 35-45.

KRETZSCHMAR, R. & SCHÄFER, T. 2005. Metal Retention and Transport on Colloidal Particles in the Environment. *Elements,* 1**,** 205-210.

KRIVEC, M., SEGUNDO, R. A., FARIA, J. L., SILVA, A. M. T. & DRAŽIĆ, G. 2013. Low-temperature synthesis and characterization of rutile nanoparticles with amorphous surface layer for photocatalytic degradation of caffeine. *Applied Catalysis B: Environmental,* 140–141**,** 9-15.

KRUG, H. F. & WICK, P. 2011. Nanotoxicology: an interdisciplinary challenge. *Angewandte Chemie International Edition,* 50**,** 1260-1278.

KUMAR, R. V. & RAZA, G. 2009. Photocatalytic disinfection of water with Ag–TiO_2 nanocrystalline composite. *Ionics,* 15**,** 579-587.

KUNG, W., GONZALEZ-MOZUELOS, P. & DE LA CRUZ, M. O. 2010. Nanoparticles in aqueous media: crystallization and solvation charge asymmetry. *Soft Matter,* 6.

LAB, J. 2013. The Element Titanium. *The Periodic Table of Elements, It's Elemental.,* http://education.jlab.org/itselemental/ele022.html.

LABILLE, J., FENG, J., BOTTA, C., BORSCHNECK, D., SAMMUT, M., CABIE, M., AUFFAN, M., ROSE, J. & BOTTERO, J.-Y. 2010. Aging of TiO_2 nanocomposites used in sunscreen. Dispersion and fate of the degradation products in aqueous environment. *Environmental Pollution,* 158**,** 3482-3489.

LAKHWANI, S. & RAHAMAN, M. 1999. Adsorption of polyvinylpyrrolidone (PVP) and its effect on the consolidation of suspensions of nanocrystalline CeO_2 particles. *Journal of Materials Science,* 34**,** 3909-3912.

LAKSHMI, B. B., PATRISSI, C. J. & MARTIN, C. R. 1997. Sol−Gel Template Synthesis of Semiconductor Oxide Micro- and Nanostructures. *Chemistry of Materials,* 9**,** 2544-2550.

LATHAM, A. H. & WILLIAMS, M. E. 2006. Versatile Routes toward Functional, Water-Soluble Nanoparticles via Trifluoroethylester−PEG−Thiol Ligands. *Langmuir,* 22**,** 4319-4326.

LENHART, J. J. & HONEYMAN, B. D. 1999. Uranium(VI) sorption to hematite in the presence of humic acid. *Geochimica et Cosmochimica Acta,* 63**,** 2891-2901.

LEVCHENKO, A. A., LI, G., BOERIO-GOATES, J., WOODFIELD, B. F. & NAVROTSKY, A. 2006. TiO_2 Stability Landscape: Polymorphism, Surface Energy, and Bound Water Energetics. *Chemistry of Materials,* 18**,** 6324-6332.

LI, G., LI, L., BOERIO-GOATES, J. & WOODFIELD, B. F. 2003. Grain-growth kinetics of rutile TiO_2 nanocrystals under hydrothermal conditions. *Journal of materials research,* 18**,** 2664-2669.

LI, Q. & ELIMELECH, M. 2006. Synergistic effects in combined fouling of a loose nanofiltration membrane by colloidal materials and natural organic matter. *Journal of Membrane Science,* 278**,** 72-82.

LI, X., LENHART, J. J. & WALKER, H. W. 2010. Dissolution-Accompanied Aggregation Kinetics of Silver Nanoparticles. *Langmuir,* 26**,** 16690-16698.

LIAO, Y., QUE, W., JIA, Q., HE, Y., ZHANG, J. & ZHONG, P. 2012. Controllable synthesis of brookite/anatase/rutile TiO_2 nanocomposites and single-crystalline rutile nanorods array. *Journal of Materials Chemistry,* 22**,** 7937-7944.

LIDIA, A. & ET AL. 2007. Photocatalytic and antibacterial activity of TiO_2 and Au/TiO_2 nanosystems. *Nanotechnology,* 18**,** 375709.

LIN, D., TIAN, X., WU, F. & XING, B. 2010. Fate and Transport of Engineered Nanomaterials in the Environment All rights reserved. No part of this periodical may be reproduced or transmitted in any form or by any means, electronic or mechanical, including photocopying, recording, or any information storage and retrieval system, without permission in writing from the publisher. *J. Environ. Qual.,* 39**,** 1896-1908.

LIN, L., HU, C., WANG, Z. & HAO, Z. 2004. Photocatalytic degradation of ethylene over titania-based photocatalysts]. *Huan jing ke xue= Huanjing kexue/[bian ji, Zhongguo ke xue yuan huan jing ke xue wei yuan hui" Huan jing ke xue" bian ji wei yuan hui.],* 25**,** 105.

LINSE, S., CABALEIRO-LAGO, C., XUE, W.-F., LYNCH, I., LINDMAN, S., THULIN, E., RADFORD, S. E. & DAWSON, K. A. 2007. Nucleation of protein fibrillation by nanoparticles. *Proceedings of the National Academy of Sciences,* 104**,** 8691-8696.

LIU, S., YU, J. & JARONIEC, M. 2011a. Anatase TiO_2 with dominant high-energy {001} facets: Synthesis, properties, and applications. *Chemistry of Materials,* 23**,** 4085-4093.
LIU, X., CHEN, G. & SU, C. 2011b. Effects of material properties on sedimentation and aggregation of titanium dioxide nanoparticles of anatase and rutile in the aqueous phase. *Journal of Colloid and Interface Science,* 363**,** 84-91.
LIU, Y., CHOI, H., DIONYSIOU, D. & LOWRY, G. V. 2005. Trichloroethene Hydrodechlorination in Water by Highly Disordered Monometallic Nanoiron. *Chemistry of Materials,* 17**,** 5315-5322.
LIU, Y., WANG, H., LI, H., ZHAO, W., LIANG, C., HUANG, H., DENG, Y. & SHEN, H. 2011c. Length-controlled synthesis of oriented single-crystal rutile TiO_2 nanowire arrays. *Journal of Colloid and Interface Science,* 363**,** 504-510.
LIVAGE, J., HENRY, M. & SANCHEZ, C. 1988. Sol-gel chemistry of transition metal oxides. *Progress in Solid State Chemistry,* 18**,** 259-341.
LJUBAS, D. 2005. Solar photocatalysis—a possible step in drinking water treatment. *Energy,* 30**,** 1699-1710.
LONDON, F. 1937. The general theory of molecular forces. *Transactions of the Faraday Society,* 33**,** 8b-26.
LUE, J. T. 2007. Physical Properties of Nanomaterials. *Encyclopedia of Nanoscience and Nanotechnology, American scientific publishers*.
LUO, H., WANG, C. & YAN, Y. 2003. Synthesis of mesostructured titania with controlled crystalline framework. *Chemistry of materials,* 15**,** 3841-3846.
MACÉ, C., DESROCHER, S., GHEORGHIU, F., KANE, A., PUPEZA, M., CERNIK, M., KVAPIL, P., VENKATAKRISHNAN, R. & ZHANG, W.-X. 2006. Nanotechnology and groundwater remediation: A step forward in technology understanding. *Remediation Journal,* 16**,** 23-33.
MALVERN 2014. Dynamic light scattering. *http://www.malvern.com/labeng/technology/dynamic_light_scattering/classical_90_degree_scattering.htm*.
MANDZY, N., GRULKE, E. & DRUFFEL, T. 2005. Breakage of TiO_2 agglomerates in electrostatically stabilized aqueous dispersions. *Powder Technology,* 160**,** 121-126.
MARTYANOV, I. N. & KLABUNDE, K. J. 2004. Comparative study of TiO_2 particles in powder form and as a thin nanostructured film on quartz. *Journal of Catalysis,* 225**,** 408-416.
MASALA, O. & SESHADRI, R. 2004. SYNTHESIS ROUTES FOR LARGE VOLUMES OF NANOPARTICLES. *Annual Review of Materials Research,* 34**,** 41-81.
MATIJEVIC, E. 1985. Production of Monodispersed Colloidal Particles. *Annual Review of Materials Science,* 15**,** 483-516.
MATOS, J., LAINE, J. & HERRMANN, J. M. 2001. Effect of the Type of Activated Carbons on the Photocatalytic Degradation of Aqueous Organic Pollutants by UV-Irradiated Titania. *Journal of Catalysis,* 200**,** 10-20.
MCCOLM, I. J. 1995. Special ceramics for modern applications: which? why? how? *In:* TERPSTRA, R. A., PEX, P. P. A. C. & VRIES, A. H. (eds.) *Ceramic Processing.* Springer Netherlands.
MI, J.-L., JOHNSEN, S., CLAUSEN, C., HALD, P., LOCK, N., SØ, L. & IVERSEN, B. B. 2013. Highly controlled crystallite size and crystallinity of pure and iron-doped anatase-TiO_2 nanocrystals by continuous flow supercritical synthesis. *Journal of Materials Research,* 28**,** 333-339.
MIDDLEMAS, S., FANG, Z. Z. & FAN, P. 2013. A new method for production of titanium dioxide pigment. *Hydrometallurgy,* 131–132**,** 107-113.
MILLS, A., DAVIES, R. H. & WORSLEY, D. 1993. Water purification by semiconductor photocatalysis. *Chem. Soc. Rev.,* 22**,** 417-425.
MIRKIN, C. A., LETSINGER, R. L., MUCIC, R. C. & STORHOFF, J. J. 1996. A DNA-based method for rationally assembling nanoparticles into macroscopic materials. *Nature,* 382**,** 607-609.
MITRANO, D. M., BARBER, A., BEDNAR, A., WESTERHOFF, P., HIGGINS, C. P. & RANVILLE, J. F. 2012. Silver nanoparticle characterization using single particle ICP-MS (SP-ICP-MS) and asymmetrical

flow field flow fractionation ICP-MS (AF4-ICP-MS). *Journal of Analytical Atomic Spectrometry,* 27**,** 1131-1142.

MO, S.-D. & CHING, W. Y. 1995. Electronic and optical properties of three phases of titanium dioxide: Rutile, anatase, and brookite. *Physical Review B,* 51**,** 13023-13032.

MOHAMMED, B. 2009. Aggregation and disaggregation of iron oxide nanoparticles: Influence of particle concentration, pH and natural organic matter. *Science of The Total Environment,* 407**,** 2093-2101.

MOLDOVAN, M., KRUPP, E. M., HOLLIDAY, A. E. & DONARD, O. F. X. 2004. High resolution sector field ICP-MS and multicollector ICP-MS as tools for trace metal speciation in environmental studies: a review. *Journal of Analytical Atomic Spectrometry,* 19**,** 815-822.

MORRISON, I. D. & ROSS, S. 2002. *Colloidal dispersions: suspensions, emulsions, and foams*, Wiley-Interscience New York.

MORSY, S. M. 2014. Role of Surfactants in Nanotechnology and Their Applications. *Int. J. Curr. Microbiol. App. Sci,* 3**,** 237-260.

MOSLEY, L. M., HUNTER, K. A. & DUCKER, W. A. 2003. Forces between Colloid Particles in Natural Waters. *Environmental Science & Technology,* 37**,** 3303-3308.

MUELLER, N. C. & NOWACK, B. 2008. Exposure Modeling of Engineered Nanoparticles in the Environment. *Environmental Science & Technology,* 42**,** 4447-4453.

MUKHERJEE, A., RAICHUR, A. M. & MODAK, J. M. 2005. Dissolution studies on TiO2 with organics. *Chemosphere,* 61**,** 585-588.

MÜLLER, M., MACKEBEN, S. & MÜLLER-GOYMANN, C. C. 2004. Physicochemical characterisation of liposomes with encapsulated local anaesthetics. *International journal of pharmaceutics,* 274**,** 139-148.

MYLON, S. E., CHEN, K. L. & ELIMELECH, M. 2004. Influence of Natural Organic Matter and Ionic Composition on the Kinetics and Structure of Hematite Colloid Aggregation: Implications to Iron Depletion in Estuaries. *Langmuir,* 20**,** 9000-9006.

MYLON, S. E., RINCIOG, C. I., SCHMIDT, N., GUTIERREZ, L., WONG, G. C. L. & NGUYEN, T. H. 2009. Influence of Salts and Natural Organic Matter on the Stability of Bacteriophage MS2. *Langmuir,* 26**,** 1035-1042.

NAPPER, D. H. 1970. Colloid Stability. *Product R&D,* 9**,** 467-477.

NAVARRO, D. A. G., WATSON, D. F., AGA, D. S. & BANERJEE, S. 2009. Natural Organic Matter-Mediated Phase Transfer of Quantum Dots in the Aquatic Environment. *Environmental Science & Technology,* 43**,** 677-682.

NAVROTSKY, A. & KLEPPA, O. J. 1967. Enthalpy of the Anatase-Rutile Transformation. *Journal of the American Ceramic Society,* 50**,** 626-626.

NIAN, J.-N. & TENG, H. 2006. Hydrothermal Synthesis of Single-Crystalline Anatase TiO_2 Nanorods with Nanotubes as the Precursor. *The Journal of Physical Chemistry B,* 110**,** 4193-4198.

NMSU 2014. Electric double layer. *New Mexico State University website article, a*[*http://web.nmsu.edu/~snsm/classes/chem435/Lab14/double_layer.html*](http://web.nmsu.edu/~snsm/classes/chem435/Lab14/double_layer.html).

NNI 2013. Definition of nanotechnology view on 12th October, 2013 on NNI website. [*http://www.nano.gov/nanotech-101/what/definition*](http://www.nano.gov/nanotech-101/what/definition).

NOWACK, B. & BUCHELI, T. D. 2007. Occurrence, behavior and effects of nanoparticles in the environment. *Environmental Pollution,* 150**,** 5-22.

NOWACK, B., RANVILLE, J. F., DIAMOND, S., GALLEGO-URREA, J. A., METCALFE, C., ROSE, J., HORNE, N., KOELMANS, A. A. & KLAINE, S. J. 2012. Potential scenarios for nanomaterial release and subsequent alteration in the environment. *Environmental Toxicology and Chemistry,* 31**,** 50-59.

O'REGAN, B. & GRfiTZELI, M. 1991. A low-cost, high-efficiency solar cell based on dye-sensitized. *nature,* 353**,** 24.

OBERDÖRSTER, G., OBERDÖRSTER, E. & OBERDÖRSTER, J. 2005. Nanotoxicology: An Emerging Discipline Evolving from Studies of Ultrafine Particles. *Environ Health Perspect,* 113.

OGWU, A. A., PLACIDO, F., ADEMOSU, O., MOH, S., CROSSAN, E. & BOUQUEREL, E. 2005. An extended Derjaguin-Landau-Verwey-Overbeek theory approach to determining the surface energy of copper oxide thin films prepared by reactive magnetron sputtering. *Metallurgical and Materials Transactions A,* 36**,** 2435-2439.

OH, S. H., KIM, D. J., HAHN, S. H. & KIM, E. J. 2003. Comparison of optical and photocatalytic properties of TiO_2 thin films prepared by electron-beam evaporation and sol–gel dip-coating. *Materials Letters,* 57**,** 4151-4155.

OSTIGUY, C., LAPOINTE, G., MENARD, L., CLOUTIER, Y., TROTTIER, M., BOUTIN, M., ANTOUN, M. & NORMAND, C. 2006. Nanoparticles: Actual knowledge about occupational health and safety risks and prevention measures. Montreal, CN: Institut de recherche Robert-Sauvé en santé et en sécurité du travail.

OTHMAN, S. H., RASHID, S. A., GHAZI, T. I. M. & ABDULLAH, N. 2012. Dispersion and stabilization of photocatalytic TiO_2 nanoparticles in aqueous suspension for coatings applications. *J. Nanomaterials,* 2012**,** 2-2.

OTTOFÜLLING, S. 2010. *Engineered nanoparticles in the environment.* uniwien.

OZAWA, T., IWASAKI, M., TADA, H., AKITA, T., TANAKA, K. & ITO, S. 2005. Low-temperature synthesis of anatase–brookite composite nanocrystals: the junction effect on photocatalytic activity. *Journal of Colloid and Interface Science,* 281**,** 510-513.

PAAL 2014. Minimizing Liquid Contaminants in Natural Gas Liquids. *http://www.pall.com/main/fuels-and-chemicals/literature-library-details.page?id=5207*.

PALOMINO, D., YAMUNAKE, C., COUSTUMER, P. L. & STOLL, S. 2013. Stability of TiO_2 Nanoparticles in Presence of Fulvic Acids. Importance of pH. *Journal of Colloid Science and Biotechnology,* 2**,** 62-69.

PAZ, Y., LUO, Z., RABENBERG, L. & HELLER, A. 1995. Photooxidative self-cleaning transparent titanium dioxide films on glass. *Journal of Materials Research,* 10**,** 2842-2848.

PELLEY, A. J. & TUFENKJI, N. 2008. Effect of particle size and natural organic matter on the migration of nano- and microscale latex particles in saturated porous media. *Journal of Colloid and Interface Science,* 321**,** 74-83.

PETOSA, A. R., JAISI, D. P., QUEVEDO, I. R., ELIMELECH, M. & TUFENKJI, N. 2010. Aggregation and Deposition of Engineered Nanomaterials in Aquatic Environments: Role of Physicochemical Interactions. *Environmental Science & Technology,* 44**,** 6532-6549.

PIEROTTI, R. & ROUQUEROL, J. 1985. Reporting physisorption data for gas/solid systems with special reference to the determination of surface area and porosity. *Pure Appl Chem,* 57**,** 603-619.

PODA, A. R., BEDNAR, A. J., KENNEDY, A. J., HARMON, A., HULL, M., MITRANO, D., RANVILLE, J. & STEEVENS, J. 2011. Characterization of silver nanoparticles using flow-field flow fractionation interfaced to inductively coupled plasma mass spectrometry. *Journal of Chromatography A,* 1218**,** 4219-4225.

POOKMANEE, P., RUJIJANAGUL, G., ANANTA, S., HEIMANN, R. B. & PHANICHPHANT, S. 2004. Effect of sintering temperature on microstructure of hydrothermally prepared bismuth sodium titanate ceramics. *Journal of the European Ceramic Society,* 24**,** 517-520.

POPOV, A., PRIEZZHEV, A., LADEMANN, J. & MYLLYLÄ, R. 2005. TiO_2 nanoparticles as an effective UV-B radiation skin-protective compound in sunscreens. *Journal of Physics D: Applied Physics,* 38**,** 2564.

PUETZ, J., GASPARRO, G. & AEGERTER, M. A. 2003. Liquid film spray deposition of transparent conducting oxide coatings. *Thin Solid Films,* 442**,** 40-43.

QAMAR, M., YOON, C. R., OH, H. J., LEE, N. H., PARK, K., KIM, D. H., LEE, K. S., LEE, W. J. & KIM, S. J. 2008. Preparation and photocatalytic activity of nanotubes obtained from titanium dioxide. *Catalysis Today,* 131**,** 3-14.

RAKHI, R. B., SETHUPATHI, K. & RAMAPRABHU, S. 2008. Synthesis and hydrogen storage properties of carbon nanotubes. *International Journal of Hydrogen Energy,* 33**,** 381-386.

RANADE, M., NAVROTSKY, A., ZHANG, H. Z., BANFIELD, J. F., ELDER, S. H., ZABAN, A., BORSE, P. H., KULKARNI, S. K., DORAN, G. S. & WHITFIELD, H. J. 2002. Energetics of nanocrystalline TiO_2. *Abstracts of Papers of the American Chemical Society,* 223**,** 148-GEOC.

RAO, C. N. R., MÜLLER, A. & CHEETHAM, A. K. 2006. *The chemistry of nanomaterials*, Wiley. com.

RAY, S. J., ANDRADE, F., GAMEZ, G., MCCLENATHAN, D., ROGERS, D., SCHILLING, G., WETZEL, W. & HIEFTJE, G. M. 2004. Plasma-source mass spectrometry for speciation analysis: state-of-the-art. *Journal of Chromatography A,* 1050**,** 3-34.

RENGARAJ, S., VENKATARAJ, S., YEON, J.-W., KIM, Y., LI, X. Z. & PANG, G. K. H. 2007. Preparation, characterization and application of Nd-TiO_2 photocatalyst for the reduction of Cr(VI) under UV light illumination. *Applied Catalysis B: Environmental,* 77**,** 157-165.

REYES-CORONADO, D., RODRÍGUEZ-GATTORNO, G., ESPINOSA-PESQUEIRA, M. E., CAB, C., COSS, R. D. & OSKAM, G. 2008. Phase-pure TiO_2 nanoparticles: anatase, brookite and rutile. *Nanotechnology,* 19**,** 145605.

RICHARDS, L. A., RICHARDS, B. S. & SCHÄFER, A. I. 2011. Renewable energy powered membrane technology: Salt and inorganic contaminant removal by nanofiltration/reverse osmosis. *Journal of Membrane Science,* 369**,** 188-195.

RÖMER, I., WHITE, T. A., BAALOUSHA, M., CHIPMAN, K., VIANT, M. R. & LEAD, J. R. 2011. Aggregation and dispersion of silver nanoparticles in exposure media for aquatic toxicity tests. *Journal of Chromatography A,* 1218**,** 4226-4233.

SALMI, M., TKACHENKO, N., VEHMANEN, V., LAMMINMÄKI, R.-J., KARVINEN, S. & LEMMETYINEN, H. 2004. The effect of calcination on photocatalytic activity of TiO_2 particles: femtosecond study. *Journal of Photochemistry and Photobiology A: Chemistry,* 163**,** 395-401.

SARKAR, D., GHOSH, C. K. & CHATTOPADHYAY, K. K. 2012. Morphology control of rutile TiO_2 hierarchical architectures and their excellent field emission properties. *CrystEngComm,* 14**,** 2683-2690.

SAW, S. H., WANG, K., YONG, T. & RAMAKRISHNA, S. 2007. Polymeric Nanofibers in Tissue Engineering. *Nanotechnologies for the Life Sciences.* Wiley-VCH Verlag GmbH & Co. KGaA.

SAYES, C. M., WAHI, R., KURIAN, P. A., LIU, Y., WEST, J. L., AUSMAN, K. D., WARHEIT, D. B. & COLVIN, V. L. 2006. Correlating Nanoscale Titania Structure with Toxicity: A Cytotoxicity and Inflammatory Response Study with Human Dermal Fibroblasts and Human Lung Epithelial Cells. *Toxicological Sciences,* 92**,** 174-185.

SCHEFFER, A., ENGELHARD, C., SPERLING, M. & BUSCHER, W. 2008. ICP-MS as a new tool for the determination of gold nanoparticles in bioanalytical applications. *Analytical and Bioanalytical Chemistry,* 390**,** 249-252.

SCHENKEL, J. & KITCHENER, J. 1960. A test of the Derjaguin-Verwey-Overbeek theory with a colloidal suspension. *Transactions of the Faraday Society,* 56**,** 161-173.

SEO, J.-W., CHUNG, H., KIM, M.-Y., LEE, J., CHOI, I.-H. & CHEON, J. 2007. Development of Water-Soluble Single-Crystalline TiO2 Nanoparticles for Photocatalytic Cancer-Cell Treatment. *Small,* 3**,** 850-853.

SERPONE, N., DONDI, D. & ALBINI, A. 2007. Inorganic and organic UV filters: Their role and efficacy in sunscreens and suncare products. *Inorganica Chimica Acta,* 360**,** 794-802.

SIEGEL, R. W., HU, E., ROCO, M. C., COX, D. M. & GORONKIN, H. 1998. Nanostructure Science and Technology. A Worldwide Study.

SIFONTES, A. B., ROSALES, M., MÉNDEZ, F. J., OVIEDO, O. & ZOLTAN, T. 2013. Effect of Calcination Temperature on Structural Properties and Photocatalytic Activity of Ceria Nanoparticles Synthesized Employing Chitosan as Template. *Journal of Nanomaterials,* 2013.

ŠIMŮNEK, J. & VAN GENUCHTEN, M. T. 2008. Modeling Nonequilibrium Flow and Transport Processes Using HYDRUS

in any form or by any means, electronic or mechanical, including photocopying, recording, or any information storage and retrieval system, without permission in writing from the publisher. *Vadose Zone J.,* 7**,** 782-797.

SINGH, R. & NALWA, H. S. 2011. Medical applications of nanoparticles in biological imaging, cell labeling, antimicrobial agents, and anticancer nanodrugs. *Journal of biomedical nanotechnology,* 7**,** 489-503.

SINGH, S. & NALWA, H. S. 2007. Nanotechnology and Health Safety; Toxicity and Risk Assessments of Nanostructured Materials on Human Health. *Journal of Nanoscience and Nanotechnology,* 7**,** 3048-3070.

SMITH, S. J., STEVENS, R., LIU, S., LI, G., NAVROTSKY, A., BOERIO-GOATES, J. & WOODFIELD, B. F. 2009. Heat capacities and thermodynamic functions of TiO_2 anatase and rutile: Analysis of phase stability. *American Mineralogist,* 94**,** 236-243.

SPAETH, J. R., KEVREKIDIS, I. G. & PANAGIOTOPOULOS, A. Z. 2011. Dissipative particle dynamics simulations of polymer-protected nanoparticle self-assembly. *The Journal of Chemical Physics,* 135**,** -.

SPERLING, R. A. & PARAK, W. J. 2010. Surface modification, functionalization and bioconjugation of colloidal inorganic nanoparticles. *Philosophical Transactions of the Royal Society A: Mathematical, Physical and Engineering Sciences,* 368**,** 1333-1383.

SPURR, R. A. & MYERS, H. 1957. Quantitative analysis of anatase-rutile mixtures with an X-ray diffractometer. *Analytical Chemistry,* 29**,** 760-762.

STANJEK, H. & HÄUSLER, W. 2004. Basics of X-ray Diffraction. *Hyperfine interactions,* 154**,** 107-119.

STANKUS, D. P., LOHSE, S. E., HUTCHISON, J. E. & NASON, J. A. 2010. Interactions between Natural Organic Matter and Gold Nanoparticles Stabilized with Different Organic Capping Agents. *Environmental Science & Technology,* 45**,** 3238-3244.

SU, W.-Y., FU, X.-Z., WEI, K.-M., ZHANG, H., LIN, H., WANG, X. & LI, D. 2001. Spectrum studies on titania photocatalysts]. *Guang pu xue yu guang pu fen xi= Guang pu,* 21**,** 32.

SUGIMOTO, T. & ZHOU, X. 2002. Synthesis of Uniform Anatase TiO_2 Nanoparticles by the Gel-Sol Method: 2. Adsorption of OH^- Ions to $Ti(OH)_4$ Gel and TiO_2 Particles. *Journal of Colloid and Interface Science,* 252**,** 347-353.

SUGIMOTO, T., ZHOU, X. & MURAMATSU, A. 2003. Synthesis of uniform anatase TiO_2 nanoparticles by gel-sol method: 3. Formation process and size control. *Journal of Colloid and Interface Science,* 259**,** 43-52.

SUTTIPONPARNIT, K., JIANG, J., SAHU, M., SUVACHITTANONT, S., CHARINPANITKUL, T. & BISWAS, P. 2010. Role of Surface Area, Primary Particle Size, and Crystal Phase on Titanium Dioxide Nanoparticle Dispersion Properties. *Nanoscale Research Letters,* 6**,** 1-8.

SUTTIPONPARNIT, K., JIANG, J., SAHU, M., SUVACHITTANONT, S., CHARINPANITKUL, T. & BISWAS, P. 2011. Role of Surface Area, Primary Particle Size, and Crystal Phase on Titanium Dioxide Nanoparticle Dispersion Properties. *Nanoscale Res Lett,* 6**,** 27.

SWAMY, V., KUZNETSOV, A., DUBROVINSKY, L. S., CARUSO, R. A., SHCHUKIN, D. G. & MUDDLE, B. C. 2005. Finite-size and pressure effects on the Raman spectrum of nanocrystalline anatase TiO_{2}. *Physical Review B,* 71**,** 184302.

TABOADA-SERRANO, P., VITHAYAVEROJ, V., YIACOUMI, S. & TSOURIS, C. 2005. Surface Charge Heterogeneities Measured by Atomic Force Microscopy†. *Environmental Science & Technology,* 39**,** 6352-6360.

TALAPIN, D. V., ROGACH, A. L., HAASE, M. & WELLER, H. 2001. Evolution of an Ensemble of Nanoparticles in a Colloidal Solution: Theoretical Study. *The Journal of Physical Chemistry B,* 105**,** 12278-12285.

TANG, J., REDL, F., ZHU, Y., SIEGRIST, T., BRUS, L. E. & STEIGERWALD, M. L. 2005. An organometallic synthesis of TiO2 nanoparticles. *Nano letters,* 5**,** 543-548.

TAVERNER, C. 2014. Structural Chemistry; Crystallography and Theoratical Chemistry. www.gh.wits.ac.za/craig/diagrams/bragg.gif.

TELEKI, A., WENGELER, R., WENGELER, L., NIRSCHL, H. & PRATSINIS, S. E. 2008. Distinguishing between aggregates and agglomerates of flame-made TiO_2 by high-pressure dispersion. *Powder Technology,* 181**,** 292-300.

THIO, B. J. R., ZHOU, D. & KELLER, A. A. 2011. Influence of natural organic matter on the aggregation and deposition of titanium dioxide nanoparticles. *Journal of Hazardous Materials,* 189**,** 556-563.

THOMAS, K. & SAYRE, P. 2005. Research strategies for safety evaluation of nanomaterials, Part I: evaluating the human health implications of exposure to nanoscale materials. *Toxicological Sciences,* 87**,** 316-321.

THOTTOLI, A. & ACHUTHANUNNI, A. 2013. Effect of polyvinyl alcohol concentration on the ZnS nanoparticles and wet chemical synthesis of wurtzite ZnS nanoparticles. *Journal of Nanostructure in Chemistry,* 3**,** 31.

TILLER, C. L. & O'MELIA, C. R. 1993. Natural organic matter and colloidal stability: Models and measurements. *Colloids and Surfaces A: Physicochemical and Engineering Aspects,* 73**,** 89-102.

TOURINHO, P. S., VAN GESTEL, C. A. M., LOFTS, S., SVENDSEN, C., SOARES, A. M. V. M. & LOUREIRO, S. 2012. Metal-based nanoparticles in soil: Fate, behavior, and effects on soil invertebrates. *Environmental Toxicology and Chemistry,* 31**,** 1679-1692.

TUFENKJI, N. & ELIMELECH, M. 2004. Deviation from the Classical Colloid Filtration Theory in the Presence of Repulsive DLVO Interactions. *Langmuir,* 20**,** 10818-10828.

TUFENKJI, N. & ELIMELECH, M. 2005. Breakdown of Colloid Filtration Theory: Role of the Secondary Energy Minimum and Surface Charge Heterogeneities. *Langmuir,* 21**,** 841-852.

TURKEVICH, J. 1985. Colloidal gold. Part I. *Gold Bulletin,* 18**,** 86-91.

VAN OVERSCHELDE, O., SNYDERS, R. & WAUTELET, M. 2007. Crystallisation of TiO_2 thin films induced by excimer laser irradiation. *Applied Surface Science,* 254**,** 971-974.

VELIKOVSKÁ, P. & MIKULÁŠEK, P. 2007. The influence of Cl^-, SO_4^{2-} and PO_4^{3-} ions on the ζ-potential and microfiltration of titanium dioxide dispersions. *Separation and Purification Technology,* 58**,** 295-298.

VENZ, P., KLOPROGGE, J. & FROST, R. 2000. Chemically modified titania hydrolysates: Physical properties. *Langmuir,* 16**,** 4962-4968.

VERWEY, E. E. J. W., OVERBEEK, J. T. G. & OVERBEEK, J. T. J. T. G. 1999. *Theory of the stability of lyophobic colloids*, DoverPublications. com.

VERWEY, E. J. W. 1947. Theory of the Stability of Lyophobic Colloids. *The Journal of Physical and Colloid Chemistry,* 51**,** 631-636.

VORKAPIC, D. & MATSOUKAS, T. 1998. Effect of Temperature and Alcohols in the Preparation of Titania Nanoparticles from Alkoxides. *Journal of the American Ceramic Society,* 81**,** 2815-2820.

VRIJ, A. 1976. Polymers at interfaces and the interactions in colloidal dispersions. *Pure Appl. Chem,* 48**,** 471.

WALKER, H. W. & BOB, M. M. 2001. Stability of particle flocs upon addition of natural organic matter under quiescent conditions. *Water Research,* 35**,** 875-882.

WAMKAM, C. T., OPOKU, M. K., HONG, H. & SMITH, P. 2011. Effects of pH on heat transfer nanofluids containing ZrO2 and TiO2 nanoparticles. *Journal of Applied Physics,* 109**,** 024305-024305-5.

WANG, C.-Y., BAHNEMANN, D. W. & DOHRMANN, J. K. 2000. A novel preparation of iron-doped TiO_2 nanoparticles with enhanced photocatalytic activity. *Chemical Communications***,** 1539-1540.

WANG, C., DENG, Z.-X., ZHANG, G., FAN, S. & LI, Y. 2002. Synthesis of nanocrystalline TiO_2 in alcohols. *Powder Technology,* 125**,** 39-44.

WANG, H., YANG, R., YANG, L. & TAN, W. 2009. Nucleic Acid Conjugated Nanomaterials for Enhanced Molecular Recognition. *ACS Nano,* 3**,** 2451-2460.

WANG, J., MISHRA, A. K., ZHAO, Q. & HUANG, L. 2013. Size effect on thermal stability of nanocrystalline anatase TiO_2. *Journal of Physics D: Applied Physics,* 46**,** 255303.

WANG, M., WOO, K.-D., KIM, I.-Y., WOONG, K. & SUI, Z. 2007a. Separation of Fe^{3+} during hydrolysis of TiO_2^+ by addition of EDTA. *Hydrometallurgy,* 89**,** 319-322.

WANG, S.-H., CHEN, T.-K., RAO, K. K. & WONG, M.-S. 2007b. Nanocolumnar titania thin films uniquely incorporated with carbon for visible light photocatalysis. *Applied Catalysis B: Environmental,* 76**,** 328-334.

WANG, Y., GAO, B., MORALES, V., TIAN, Y., WU, L., GAO, J., BAI, W. & YANG, L. 2012. Transport of titanium dioxide nanoparticles in saturated porous media under various solution chemistry conditions. *Journal of Nanoparticle Research,* 14**,** 1-9.

WASHINGTON, U. O. 2014. Bragg's Law and Diffraction: How waves reveal the atomic structure of crystals? . *www.bmsc.washington.edu/people/merritt/bc530/bragg*.

WIKIPEDIA 2016. Hydrothermal Synthesis. *http://en.wikipedia.org/wiki/Hydrothermal_synthesis*.

WILSKA, S. 1954. An X-ray diffraction study to determine the effect of the method of preparation upon the crystal structure of TiO_2. *Acta chem. scand,* 8**,** 1796-1801.

WU, C.-H., CHANG-CHIEN, G.-P. & LEE, W.-S. 2004. Photodegradation of polychlorinated dibenzo-p-dioxins: comparison of photocatalysts. *Journal of Hazardous Materials,* 114**,** 191-197.

WU, N., WEI, H. & ZHANG, L. 2011. Efficient Removal of Heavy Metal Ions with Biopolymer Template Synthesized Mesoporous Titania Beads of Hundreds of Micrometers Size. *Environmental Science & Technology,* 46**,** 419-425.

WUILLOUD, R. G. & ALTAMIRANO, J. C. 2006. Speciation Analysis of Non-Metallic Elements Using Plasma-Based Atomic Spectrometry for Detection. *Current Analytical Chemistry,* 2**,** 353-377.

XU, H., LI, M. & JUN, Z. 2013. Preparation, characterization, and photocatalytic studies on anatase nano-TiO2 at internal air lift circulating photocatalytic reactor. *Materials Research Bulletin,* 48**,** 3144-3148.

XU, J.-H., DAI, W.-L., LI, J., CAO, Y., LI, H., HE, H. & FAN, K. 2008. Simple fabrication of thermally stable apertured N-doped TiO_2 microtubes as a highly efficient photocatalyst under visible light irradiation. *Catalysis Communications,* 9**,** 146-152.

YAMAGO, S., TOKUYAMA, H., NAKAMURA, E., KIKUCHI, K., KANANISHI, S., SUEKI, K., NAKAHARA, H., ENOMOTO, S. & AMBE, F. 1995. In vivo biological behavior of a water-miscible fullerene: 14C labeling, absorption, distribution, excretion and acute toxicity. *Chemistry & Biology,* 2**,** 385-389.

YANG, H., SHI, R., ZHANG, K., HU, Y., TANG, A. & LI, X. 2005. Synthesis of WO_3/TiO_2 nanocomposites via sol–gel method. *Journal of Alloys and Compounds,* 398**,** 200-202.

YANG, J., MEI, S. & FERREIRA, J. M. F. 2001. Hydrothermal Synthesis of Nanosized Titania Powders: Influence of Tetraalkyl Ammonium Hydroxides on Particle Characteristics. *Journal of the American Ceramic Society,* 84**,** 1696-1702.

YANG, N., HAO, Z., FENGXIA, D., XUELI, L., JIE, W. & BAI, Y. 2010. Direct synthesis of polymerizable surfactant-stabilized nanoparticles: the macromolecular monomers for fabricating nanoparticle–polymer composites. *Nanotechnology,* 21**,** 285604.

YANG, P., LU, C., HUA, N. & DU, Y. 2002. Titanium dioxide nanoparticles co-doped with Fe^{3+} and Eu^{3+} ions for photocatalysis. *Materials Letters,* 57**,** 794-801.

YANG, Y., LI, X.-J., CHEN, J.-T. & WANG, L.-Y. 2004. Effect of doping mode on the photocatalytic activities of Mo/TiO_2. *Journal of Photochemistry and Photobiology A: Chemistry,* 163**,** 517-522.

YOON, S., LEE, E.-S. & MANTHIRAM, A. 2012. Microwave-Solvothermal Synthesis of Various Polymorphs of Nanostructured TiO2 in Different Alcohol Media and Their Lithium Ion Storage Properties. *Inorganic Chemistry,* 51**,** 3505-3512.

YU, J. C., YU, J. & ZHAO, J. 2002. Enhanced photocatalytic activity of mesoporous and ordinary TiO_2 thin films by sulfuric acid treatment. *Applied Catalysis B: Environmental,* 36**,** 31-43.

ZHANG, W.-X. 2003. Nanoscale Iron Particles for Environmental Remediation: An Overview. *Journal of Nanoparticle Research,* 5**,** 323-332.

ZHANG, Y., CHEN, Y., WESTERHOFF, P. & CRITTENDEN, J. 2009. Impact of natural organic matter and divalent cations on the stability of aqueous nanoparticles. *Water Research,* 43**,** 4249-4257.

ZHANG, Y., TANG, Z.-R., FU, X. & XU, Y.-J. 2010. TiO2−Graphene Nanocomposites for Gas-Phase Photocatalytic Degradation of Volatile Aromatic Pollutant: Is TiO_2−Graphene Truly Different from Other TiO2−Carbon Composite Materials? *ACS Nano,* 4**,** 7303-7314.

ZHANG, Y. W., TANG, M., JIN, X., LIAO, C. S. & YAN, C. H. 2003. Polymeric adsorption behavior of nanoparticulate yttria stabilized zirconia and the deposition of as-formed suspensions on dense Al_2O_3 ="http://pub2web.metastore.ingenta.com/ns/">2</sub>O₃ substrates. *Solid State Sciences,* 5**,** 435-440.

ZHANG, Z., WANG, C.-C., ZAKARIA, R. & YING, J. Y. 1998. Role of particle size in nanocrystalline TiO_2-based photocatalysts. *The Journal of Physical Chemistry B,* 102**,** 10871-10878.

ZHAO, W., MA, W., CHEN, C., ZHAO, J. & SHUAI, Z. 2004. Efficient Degradation of Toxic Organic Pollutants with Ni_2O_3/TiO_2-xBx under Visible Irradiation. *Journal of the American Chemical Society,* 126**,** 4782-4783.

ZHAO, X., ZHAO, Q., YU, J. & LIU, B. 2008. Development of multifunctional photoactive self-cleaning glasses. *Journal of Non-Crystalline Solids,* 354**,** 1424-1430.

ZHU, H. Y., LAN, Y., GAO, X., RINGER, S. P., ZHENG, Z., SONG, D. Y. & ZHAO, J.-C. 2005. Phase transition between nanostructures of titanate and titanium dioxides via simple wet-chemical reactions. *Journal of the American Chemical Society,* 127**,** 6730-6736.

ZLAMAL, M., MACAK, J. M., SCHMUKI, P. & KRÝSA, J. 2007. Electrochemically assisted photocatalysis on self-organized TiO_2 nanotubes. *Electrochemistry Communications,* 9**,** 2822-2826.